11-4-2003

Analysis of Flow in a Spray Nozzle With Emphasis on Exiting Jet Free Surface

Ryan M. Mead
University of South Florida

Analysis of Flow in a Spray Nozzle

With Emphasis on Exiting Jet Free Surface

by

Ryan M. Mead

A thesis submitted in partial fulfillment
of the requirements for the degree of
Master of Science in Mechanical Engineering
Department of Mechanical Engineering
College of Engineering
University of South Florida

Major Professor: Muhammad M. Rahman, Ph.D.
Roger A. Crane, Ph.D.
Autar K. Kaw, Ph.D.

Date of Approval:
November 4, 2003

Keywords: spray cooling, cone angle, mixing length, liquid-gas interface, atomizer

Table of Contents

List of Tables

List of Figures

Analysis of Flow in a Spray Nozzle
With Emphasis on Exiting Jet Free Surface

Ryan Mead

Abstract

A conical nozzle with two separate inlets within its top plate is analyzed. One of the inlets is in the center of the top plate, which is free to rotate, whereas the other inlet is positioned away from the center. The fluid entering through the outer inlet slot causes the top plate of the nozzle to spin. Several fluids including FC-77, FC-72, FC-87, and Methanol running at different flow rates were investigated to observe the effect that their particular properties have on the geometry of the fluid's free surface exiting the nozzle. Another variation performed was the geometry of the nozzle. The outer inlet slot was positioned at various radial distances along the top plate. For this nozzle, the top plate remained stationary and swirling was introduced to the fluid at the inlets. It was observed that the faster flow rates caused an increase in the free surface height and cone angle. For the various radial locations of the outer inlet slot, it was noted that a position at approximately 75% of the nozzle radius produced the largest free surface height. The largest cone angle was produced when the outer inlet slot was positioned at the edge of the nozzle top plate. Another factor that increased the radial height and cone angle of the free surface was the working fluid used in the study. A larger Reynolds number produced a larger cone angle and larger free surface height (while a smaller Reynolds number produced a less significant cone angle and free surface height).

1

Introduction

Spray-cooling is commonly used throughout the industry for heat transfer applications due to the high heat transfer coefficients that they provide. They are frequently used to anneal metals, cool effluents from pulp and paper mills, cool fission and fusion components, as well as cooling combustion walls and turbine blades.

Another emerging application is the cooling of electronics. Cooling electronic circuit integration is a vital part in maintaining the efficiency and reliability of the circuitry. Undesirably high temperatures can severely strain the operational safety and effectiveness of the electronics. By spraying fluid on a plate that is shielding electronic sources, it is possible to carry heat away through the fluid and maintain an acceptable temperature. However, before determining the heat transfer properties of the system, it is important to determine the geometry of the spray exiting the swirl-atomizer used to emit the fluid. Prediction of nozzle performance for design and analysis is critical in aiding designers to meet strict performance requirements. For instance, the cone angle of a particular spray would be an important number to determine. A larger cone angle would mean that the spray would be covering a greater surface area, and thus cooling a larger portion of the electronics. Another important factor is how wide the spray becomes after it exits the nozzle, or the radial height of the free surface. Again, a greater radial height would signal that more surface are is being introduced to the spray. An increase in these two factors would provide better cooling for the electronics.

It has been recognized that a change in the geometry of the nozzle results in a change in geometry of the exiting spray. Jeng et al. (1998) performed experiments on 15 different nozzle geometries with four different flow rates. They used the Arbitrary-Langrangian-Eulerian (ALE) method to calculate the position of the free surface. The finite element predictions were in good agreement with their experiments. They concluded that the geometry of the nozzle had a significant effect on the parameters of the exiting free surface that they were investigating.

The idea that the nozzle geometry plays a major role in the nozzle performance was reiterated by Dumouchel et al. (1993). They applied numerical analysis to the velocity field throughout a swirl spray nozzle, and more specifically, at the nozzle orifice. They found that the conical liquid sheet produced at the nozzle's orifice was mainly dependent on the shape of the nozzle. Also in agreement with this statement is Sakman et al. (2000). They studied the length-to-diameter ratio of the swirl chamber and orifice, stating that an increase in the length-do-diameter ratio for both the swirl chamber and orifice resulted in a decrease in the cone angle. However, an increase in the length-to-diameter ratio for the swirl chamber produced an increase in film thickness; an increase in the length-to-diameter ratio for the orifice resulted in a decrease in the film thickness.

Miller and Ellis (2000) investigated spray nozzles for agricultural uses, mainly focusing on spray characteristics and droplet size. They concluded that the interaction between the physical properties of the spray liquid and the characteristics of the spray formed was a function of the nozzle design. While some of the changes in spray formation could be related to the dynamic surface tension of the spray liquid, there was

evidence to show that there were other physical parameters that influenced spray formation. Som and Biswas (1986) agreed, stating that the pertinent governing parameters regarding the spray dispersion included the liquid velocity, liquid viscosity, liquid surface tension, the density of the ambient atmosphere, as well as the geometrical dimensions of the nozzle.

Some other investigations were performed that observed the effect some parameters had on the free surface position and the cone angle of the fluid exiting the nozzle. Datta and Som (2000) studied ways to provide theoretical predictions of the cone angle produced by swirl spray pressure nozzles using numerical computations of the flow. They found that an increase in the fluid flow rate created a sharp increase in the cone angle of the fluid exiting the swirl nozzle. Rothe and Block (1977) examined the effect that the pressure of the ambient environment to which the fluid is being sprayed had on the shape of the liquid sheet. Their work, which agrees with many other studies, found that an increase in ambient pressure and nozzle pressure drop created an increase in contraction of the liquid sheet emanating from the nozzle. However, an increase in nozzle diameter aided in decreasing the amount of contraction.

Gavaises and Arcoumanis (2001) state that an accurate estimation of the nozzle flow exit conditions are significant in the calculation of sprays ejected from the nozzle. Therefore, it is important to know the conditions at the location where the fluid exits the nozzle in order to truthfully predict the position of the free surface, as well as other interesting variables. After the free surface of the fluid has been modeled correctly, the heat transfer potential can then be evaluated. Ciofalo et al. (1999) performed

experiments with full cone swirl atomizers onto a heated wall. They confirmed that the heat transfer coefficient and maximum heat flux was dependent of the mass flux of the spray, as well as the droplet velocity.

For this problem, two different-sized conical nozzles with two inlet slots and one outlet were analyzed. The top plate for both of the nozzles housed the two inlet slots – one inlet was in the center of the top plate, whereas the outer inlet slot was positioned at the edge of the top plate. Several different nozzle geometries were examined, as well as several different fluids such as FC-77, FC-72, FC-87, and Methanol. Each of these fluids was run at various flow rates ranging from 1.262×10^{-7} m^3/s to 5.678×10^{-7} m^3/s in the smaller nozzle. For a larger nozzle that was studied, only FC-77 and FC-72 were analyzed at flow rates of 1.262×10^{-6} m^3/s, 2.524×10^{-6} m^3/s, and 3.785×10^{-6} m^3/s.

For the smaller nozzle that was studied, an investigation into the effect of the location of the outer inlet slot was performed. The outer inlet slot was moved throughout the range of the top plate to observe any changes in the performance of the nozzle. What was analyzed during each trial was the height of the free surface formed by the fluid exiting the nozzle. From this data, the cone angle of the spray could easily be calculated. As mentioned earlier, the radial height of the free surface along with the cone angle of the spray exiting the nozzle are important for later aspects of this project. Future studies will use the data collected in this investigation to analyze the heat transfer characteristics of these fluids as they are used to cool electronics. Therefore, a larger radial height and cone angle of the free surface is beneficial, because this would indicate that a greater

fraction of the electronics would be cooled. This is significant for efficiency, and consequently, the cost of the design.

However, the trouble with accurately predicting the flow exiting the nozzle deals mainly with tracking the fluid/air interface. Commercially available software, FIDAP, which utilized the Galerkin finite element method, was used to solve for the position of the free surface. For the cases where the flow within the nozzle was deemed turbulent, the mixing length model was employed in FIDAP. This was done so that the Newton-Raphson solution method could be used to solve the flow problem.

Nomenclature

Arabic Symbols

A	Total area [m^2]
B	Damping constant [non-dim]
C_p	Coefficient of pressure [non-dim]
Ca	Cavitation number [non-dim]
f	Friction factor [non-dim]
g	Gravitational constant [m/s^2]
h_f	Head loss [m]
L	Length of nozzle [m]
L_f	Length of free surface [m]
l	Mixing length [m]
$\dot{m}$	Mass flow rate, ρQ [kg/s]
$\dot{m}_{in}$	Mass flow rate in [kg/s]
$\dot{m}_{out}$	Mass flow rate out [kg/s]
$\dot{M}_r$	Radial component of momentum [kg m/s^2]
$\dot{M}_z$	Axial component of momentum [kg m/s^2]
$\dot{M}_\theta$	Theta component of momentum [kg m/s^2]
$\dot{M}$	Resultant vector of momentum [kg m/s^2]

n	Unit normal vector [non-dim]
p	Pressure [N/m^2]
ΔP	Inlet to outlet pressure drop [$kg/m\ s^2$]
Q	Volumetric flow rate [m^3/s]
r	Radial coordinate [m]
R	Radial distance to nozzle wall [m]
R_1	Radial distance of central inlet [m]
R_2	Radial distance to outer inlet slot [m]
R_3	Radial distance to outside of outer inlet slot [m]
Re	Reynolds number, $2\rho Ur/\mu$ [non-dim]
R_{out}	Radius of the nozzle outlet [m]
R_{top}	Radius of the top plate [m]
U	Average velocity at the nozzle exit, [m/s]
V_{in}	Inlet velocity [m/s]
V_{out}	Outlet velocity [m/s]
v_r	Radial velocity component [m/s]
v_z	Axial velocity component [m/s]
v_θ	Theta velocity component [m/s]
v^*	Friction velocity [m/s]
y_n	Normal distance from a node to the wall [m]
y_n^+	Non-dimensional scale for y_n [non-dim]
z	Axial coordinate [m]

Greek Symbols

δ	Radius of free surface height [m]
ϕ	Cone angle [degrees]
κ	Von Karman constant [non-dim]
ρ	Density [kg/m^3]
μ	Absolute viscosity [kg/m s]
ν	Kinematic viscosity [m^2/s]
ν_t	Momentum eddy viscosity [m^2/s]
σ	Surface tension or surface stress [kg/s^2]
Ω	Angular velocity of the top plate [rad/s]

Subscripts

atm	Atmospheric
avg	Average
i	Unit vector direction
j	Unit vector direction
min	Minimum
sat	Saturation

3

Mathematical Model

Consider the axi-symmetric conical nozzle as shown in Figures 2 and 3 (pages 21 and 22). The top of the nozzle contains four inlets – one at the center and three outer inlets spaced equidistant from each other around the top plate, which are drilled at a 45 degree angle. To model this flow in two dimensions, the three outer inlets are modeled as a single inlet along the entire outer edge of the nozzle. The fluid entering the nozzle through the outer inlet at a 45 degree angle causes the top plate to rotate around the z-axis. This causes the fluid to have a swirling effect within the nozzle. To determine the rate at which the exiting fluid causes the disc to rotate, the angular momentum theorem is applied. These calculations were done for a three-dimensional geometry, whereas the problem is simulated as two-dimensional. According to White (1999), a control volume analysis can be useful to the angular momentum relation:

$$\mathbf{M} = \frac{d\mathbf{H}}{dt} \tag{1}$$

where **M** is the net moment about the center of mass of the system, **H** is the angular moment of the system about its center of mass, and t is time. Since this system involves non-rigid fluid particles that each has a different velocity, the theory of mass moment of inertia has to be abandoned. For this system, the instantaneous angular momentum has to be calculated by integrating H over the entire elemental masses, dm. To calculate the angular momentum about a point O, the following equation is used:

$$\mathbf{H}_O = \int_{system} (\mathbf{r} \times \mathbf{V}) dm \tag{2}$$

where **r** is the position vector from O to the elemental mass dm, and **V** is the velocity of that elemental mass. Applying the Reynolds transport theorem to Equation (2) reveals:

$$\left.\frac{d\mathbf{H}_O}{dt}\right|_{system} = \frac{d}{dt}\left[\int_{CV} (\mathbf{r} \times \mathbf{V}) \rho \, d^\circ V\right] + \int_{CS} (\mathbf{r} \times \mathbf{V}) \rho (\mathbf{V_r} \cdot \mathbf{n}) \, dA \tag{3}$$

where $\rho \, d^\circ V$ is the differential mass of the fluid and $\mathbf{V_r} \cdot \mathbf{n}$ is the relative normal velocity component. From the angular momentum theorem, Equation (3) must be equal to the sum of all the moments about point O which is exerted on the control volume. Therefore,

$$\frac{d\mathbf{H}_O}{dt} = \sum \mathbf{M}_O = \sum (\mathbf{r} \times \mathbf{F})_O \tag{4}$$

where $\mathbf{M}_O$ are the moments about point O, and **F** are the forces applied to the system. In this situation, the sum of the moments is to be taken at the center of the disc, point O.

$$\sum \mathbf{M}_O = -\mathbf{T}_O \cdot \mathbf{j} = (\mathbf{r} \times \mathbf{V}_{out}) \cdot \dot{m}_{out} - (\mathbf{r} \times \mathbf{V}_{in}) \cdot \dot{m}_{in} \tag{5}$$

where $\mathbf{T}_O$ is the retarding torque, and $\dot{m}$ is the mass flow rate of the system. For this study, the retarding torque, $\mathbf{T}_O$, is considered to be negligible, and therefore is set to zero. Applying the conditions of this system to the angular momentum theorem results in:

$$\dot{m}_{in} = \dot{m}_{out} = \rho \cdot Q \tag{6}$$

$$V_{in} = \left(\frac{-Q}{A}\right)\mathbf{j} \tag{7}$$

$$V_{out} = \left[\left(\frac{-Q}{A}\right) \cdot \cos(45)\right]\mathbf{j} + \left[\left(\frac{Q}{A}\right) \cdot \cos(45) - r \cdot \Omega\right]\mathbf{k} \tag{8}$$

$$\mathbf{r}\times\mathbf{V}_{out}=\left[r^2\cdot\Omega-r\cdot\left(\frac{Q}{A}\right)\cdot\cos(45)\right]\mathbf{j}+\left[r\cdot\left(\frac{Q}{A}\right)\cdot\cos(45)\right]\mathbf{k} \tag{9}$$

$$\mathbf{r}\times\mathbf{V}_{in}=\left[-r\cdot\left(\frac{Q}{A}\right)\right]\mathbf{k} \tag{10}$$

where Q is the volumetric flow rate of the fluid, Ω is the angular velocity of the disc, and A is the total inlet area. Since the disk is rotating solely about the j-axis, and it is fixed with respect to the other axes, then only the 'j-terms' of the cross products are of interest. Therefore,

$$\sum\mathbf{M}_O=0=\rho\cdot Q\cdot\left[r^2\cdot\Omega-r\cdot\left(\frac{Q}{A}\right)\cdot\cos(45)\right] \tag{11}$$

$$r^2\cdot\Omega=r\cdot\left(\frac{Q}{A}\right)\cdot\cos(45) \tag{12}$$

$$\Omega=Q\cdot\left(\frac{\cos(45)}{A\cdot r}\right) \tag{13}$$

For the dimensions of the conical nozzle, we can calculate the total inlet area, A, and the position vector, r.

$$A=2\cdot\pi\cdot({R_{top}}^2-{R_2}^2)\cdot\cos(45)+\pi\cdot(R_1)^2 \tag{14}$$

$$r=R_{top} \tag{15}$$

Hence, for the smaller nozzle:

$$\Omega=\left(1.852\times10^9\cdot\frac{1}{\mathrm{m}^3}\right)\cdot Q \tag{16}$$

where Q is the volumetric flow rate given in m^3/sec. As for the larger nozzle, the spinning rate is obtained from the following equation.

$$\Omega = \left(2.248 \times 10^6 \cdot \frac{1}{m^3} \right) \cdot Q \tag{17}$$

where, again, Q is the volumetric flow rate given in m^3/sec. The following is a table that lists several flow rates of interest, along with its corresponding angular velocity, Ω.

Table 1: Angular velocity for given flow rate in the smaller nozzle

Inlet Flow Rate Q [m^3/s]	Angular Velocity Ω [rad/sec]
1.262 x 10^{-7}	233.67
2.524 x 10^{-7}	467.34
4.416 x 10^{-7}	817.84
5.678 x 10^{-7}	1051.50

Table 2: Angular velocity for given flow rate in the larger nozzle

Inlet Flow Rate Q [m^3/s]	Angular Velocity Ω [rad/sec]
1.262 x 10^{-6}	2.837
2.524 x 10^{-6}	5.675
3.785 x 10^{-6}	8.512

Next, the actual fluid mechanics of the problem must be solved. If the fluid is considered to be incompressible, the equations describing the conservation of mass and momentum in cylindrical coordinates can be expressed as (Burmeister, 1993):

$$\frac{\partial v_r}{\partial r} + \frac{v_r}{r} + \frac{\partial v_z}{\partial z} = 0 \tag{18}$$

$$v_r\left(\frac{\partial v_r}{\partial r}\right) - \frac{{v_\theta}^2}{r} + v_z\left(\frac{\partial v_r}{\partial z}\right) = -\frac{1}{\rho}\frac{\partial p}{\partial r} + (\nu + \nu_t)\left[\frac{1}{r}\frac{\partial}{\partial r}\left(r\frac{\partial v_r}{\partial r}\right) + \frac{\partial^2 v_r}{\partial {z^2}} - \frac{v_r}{{r^2}}\right] \tag{19}$$

$$v_r\left(\frac{\partial v_\theta}{\partial r}\right) + \frac{v_r v_\theta}{r} + v_z\left(\frac{\partial v_\theta}{\partial z}\right) = (\nu + \nu_t)\left[\frac{1}{r}\frac{\partial}{\partial r}\left(r\frac{\partial v_\theta}{\partial r}\right) + \frac{\partial^2 v_\theta}{\partial {z^2}} - \frac{v_\theta}{{r^2}}\right] \tag{20}$$

$$v_r\left(\frac{\partial v_z}{\partial r}\right) + v_z\left(\frac{\partial v_z}{\partial z}\right) = -g - \frac{1}{\rho}\frac{\partial p}{\partial z} + (\nu + \nu_t)\left[\frac{1}{r}\frac{\partial}{\partial r}\left(r\frac{\partial v_z}{\partial r}\right) + \frac{\partial^2 v_z}{\partial {z^2}}\right] \tag{21}$$

Now, the turbulence within the fluid must be considered. For the larger nozzle, all of the flow rates resulted in laminar flow. However, for the smaller nozzle, only the flow rates of 1.262 x 10^{-6} m^3/s and 2.524 x 10^{-6} m^3/s resulted in laminar flow. For the remaining flow rates, the mixing length model was used for simulation of turbulence in this problem. The mixing length turbulence model is a zero-equation model which uses the following relationship to determine the turbulent viscosity.

$$\nu_t = l^2 \cdot \left| v_r \cdot \frac{\partial \bar{v}_r}{\partial r} \right| \tag{22}$$

$$l = \kappa \cdot y_n \cdot \left[1 - \exp\left(\frac{-{y_n}^+}{B}\right)\right] \tag{23}$$

where κ is the Von Karman constant ($\kappa = 0.4$), y_n is the normal distance from the node to the wall ${y_n}^+$ is a scale used to non-dimensionalize the problem, and B is the damping constant. The Van Driest damping factor is located within the brackets [ ].

$${y_n}^+ = \frac{y_n \cdot v^*}{\nu} \tag{24}$$

where v^* is the friction velocity.

The previous equations are subject to the following boundary conditions:

$$\text{At } z = 0, \quad 0 \le r \le 1.00 \cdot 10^{-3}: \quad v_r = 0, \quad v_z = v_{in}, \quad v_\theta = 0 \tag{25}$$

$$\text{At } z = 0, \quad 1.00 \cdot 10^{-3} \le r \le 5.43 \cdot 10^{-3}: \quad v_r = 0, \quad v_z = 0 \tag{26}$$

$$\text{At } z = 0, \ 5.43 \cdot 10^{-3} \le r \le 7.43 \cdot 10^{-3}: \ v_r = -v_{in} \sin 45, \quad v_z = v_{in} \cos 45, \quad v_\theta = 0 \tag{27}$$

$$\text{At } 0 \le z \le L, \quad r = R: \quad v_r = 0, \quad v_z = 0, \quad v_\theta = 0 \tag{28}$$

$$\text{At } r = 0, \quad 0 \le z \le L: \quad v_r = 0, \quad v_\theta = 0, \quad \frac{\partial v_z}{\partial z} = 0 \tag{29}$$

$$\text{At } z = L + L_f, \ 0 \le r \le \delta: \quad p = 0 \tag{30}$$

$$\text{At } r = \delta, \ L \le z \le L + L_f: \quad \frac{d\delta}{dz} = \frac{v_r}{v_z}, \quad p = p_{atm} - \left[\frac{\sigma \dfrac{d^2\delta}{dz^2}}{\left[1 + \left(\dfrac{d\delta}{dz} \right)^2 \right]^{3/2}} \right], \quad \frac{\partial v_t}{\partial n} = 0 \tag{31}$$

For the instance where the outer inlet slot on the smaller nozzle was varied, Equation 25 through Equation 27 of the boundary conditions became:

$$\text{At } z = 0, \quad 0 \le r \le 1.00 \cdot 10^{-3}: \quad v_r = 0, \quad v_z = v_{in}, \quad v_\theta = 0 \tag{32}$$

$$\text{At } z = 0, \quad 1.00 \cdot 10^{-3} \le r \le R_2: \quad v_r = 0, \quad v_z = 0, \quad v_\theta = 0 \tag{33}$$

$$\text{At } z = 0, \quad R_2 \le r \le R_3: \quad v_r = 0, \quad v_z = v_{in}, \quad v_\theta = v_{in} \tag{34}$$

$$\text{At } z = 0, \quad R_3 \le r \le R: \quad v_r = 0, \quad v_z = 0, \quad v_\theta = 0 \tag{35}$$

Also for the instance where the outer inlet slot on the smaller nozzle was varied, R_1 remained constant at 1.00×10^{-3} m and four cases for R_2 was chosen. The outer radial dimension for the outer inlet slot, R_3, was then calculated. The outer inlet was simulated as a continuous slot around the nozzle. In actuality, there are three separate outer inlets, each having the same area as the central inlet. Therefore, R_3 was determined so that the continuous slot had three times the area of the central inlet. Therefore the inlet velocity would be the flow rate divided by the sum of the inlet areas. Since all four inlets have the same area, the total area can be taken as four times the area of the central inlet. The following equations show how R_3 and the inlet velocity were determined.

$$R_3^2 - R_2^2 = 3 \cdot R_1^2 \tag{36}$$

$$V_{in} = \frac{Q}{4 \cdot \pi \cdot R_1^2} \tag{37}$$

Often, due to limitations in computer resources it is necessary to simulate a given flow problem in a truncated computational domain. In such situations, a boundary condition must be supplied at the boundary, typically an outlet boundary ($z = L + L_f$), of the truncated computational domain. In most situations, the stress-free boundary condition that arises naturally from the application of the finite element method to the flow equations is quite adequate. However, in certain situations the natural outflow boundary condition is not suitable. This occurs when there is a free surface involved with the problem. The problem arises from the presence of the pressure term in the expression for the normal stress. At the outlet boundary, the surface stress vector on the boundary of a fluid element is defined in FIDAP by:

$$\sigma_i = \sigma_{ij} \cdot n_j \tag{38}$$

$$\sigma_{ij} = -p \cdot \delta_{ij} + \mu \cdot \left(v_{ij} + v_{ji}\right) \tag{39}$$

where σ_{ij} is the stress tensor and n_j is the unit normal vector at the boundary. The normal component of the stress vector is given in FIDAP by:

$$\sigma_n = \sigma_i \cdot n_i = -p + \mu \cdot \left(v_{ij} + v_{ji}\right) \cdot n_e \cdot n_j \tag{40}$$

It is also desired to determine if cavitation is present at the location where the pressure is a minimum in the nozzle. Cavitation occurs when the pressure of the liquid falls below the saturation pressure for that particular fluid. When this happens, the fluid begins to evaporate causing tiny bubbles to form on the boundary surface, which will eventually erode and destroy the system. The cavitation number is found by:

$$Ca = \frac{p_{\min} - p_{sat}}{0.5 \cdot \rho \cdot U^2} \tag{41}$$

Next, it is important to know the average value for each component of velocity within the system. With the average component of velocity it is easy to calculate the average component of momentum for the fluid. The equations to accomplish this are given for the radial component of velocity and momentum.

$$V_{r,avg} = \frac{1}{A} \cdot \int_0^R V_r \cdot dA \tag{42}$$

$$\dot{M}_{r,avg} = \dot{m} \cdot V_{r,avg} \tag{43}$$

where the axial and theta components of velocity and momentum are calculated in the same manner.

The pressure coefficient can be calculated for each case. A larger pressure coefficient usually means that there is a large pressure drop. However, the pressure coefficient is also dependent on the velocity, as well as the density, of the fluid.

$$C_p = \frac{\Delta p}{0.5 \cdot \rho \cdot U^2} \tag{44}$$

To assure that the pressure drops from the inlet to the outlet of the nozzles are in accordance with what they should be, Bernoulli's equation was used to calculate them. Theses calculated values were then compared to the values obtained from FIDAP. The pressure drop obtained using Bernoulli's equation must be larger than the values produced by FIDAP. Bernoulli's equation is given by:

$$\Delta p = \rho \cdot \left[\left(\frac{{V_{out}}^2 - {V_{in}}^2}{2} \right) + g \cdot (z_2 - z_1) + g \cdot h_f \right] \tag{45}$$

where g is the gravitational constant, and h_f is the head loss due to friction. This value is given by:

$$h_f = f \cdot \left(\frac{z_2 - z_1}{2 \cdot r} \right) \cdot \left(\frac{{V_{out}}^2}{2 \cdot g} \right) \tag{46}$$

where f is the friction factor found in the Moody chart (White, 1999).

4

Numerical Computation

The governing equations, along with the boundary and initial conditions were solved using the finite-element method. The fluid region was divided into a number of quadrilateral elements. After the Galerkin formulation was used to separate the governing equations, the Newton-Raphson method was used to solve the ensuing algebraic equations. For the turbulent flows, the mixing length turbulence model was employed so that the Newton-Raphson method could be utilized. The equations for the conservation of mass and conservation of momentum were then solved simultaneously. For this free surface problem, calculations were performed for each time step until steady state conditions were attained. The results observed were the results that occurred at steady state. A variable time step was instituted to ensure efficiency due to large variations in the beginning and small variations toward the arrival of steady state conditions.

In order to ensure that an accurate solution was obtained, the number of elements that were used to mesh the geometry had to be deemed adequate. This was done by performing computations for several combinations of elements in the axial and radial directions covering the nozzle geometry. The velocity profiles at the nozzle outlet for these simulations are plotted in Figure 1. It was noted that the numerical solution became grid independent when the number of elements in the axial and radial directions were greater than 172 and 32, respectively. Computations with a 172x32 grid produced results

that were identical up to four significant figures to the values produced by a grid of 248x48. In order to conserve computer time while maintaining accuracy, a grid size of 172x32 was used for all of the final compuations. The quantitative difference in grid independence can be calculated using the following equation:

$$V = C + \frac{D}{N^e} \tag{47}$$

where N is the number of elements along an axis, and C, D, and e were constants to be evaluated. V is the velocity at a given radial coordinate along the outlet of the nozzle. Equation (47) has three unknowns at three sets of velocities taken at three different grid sizes. The result is a set of non-linear equations with three variables. An initial value of e is assumed, and after performing a number of iterations, a correct value for e is determined. By definition the value of e must be greater than one. At the radial coordinate of r = 4.8 x 10^{-5} m, e was found to be 8.056. After replacing e into Equation (47), the values of C and D were determined to be 851.7149598 and 7.1324174 x 10^{16}, respectively. To obtain a percent error for the various computations, the following equation was used.

$$\left|\frac{V - C}{C}\right| \times 100 \tag{48}$$

It was seen that at r = 4.8 x 10^{-5} m, the percent error for the grid involving 80 elements in the axial direction and 16 elements in the radial direction was approximately 3.906%. At the same radial location, the percent error for the 172x32 grid was calculated to be 8.206 x 10^{-3} %, whereas the percent error for the 248x48 grid was determined to be 4.33 x 10^{-4} %. It is easily seen that these two grids produce nearly identical results. This

calculation is also backed up by Figure 1 in which the velocity profile at the outlet of the nozzle is plotted for the various grid sizes.

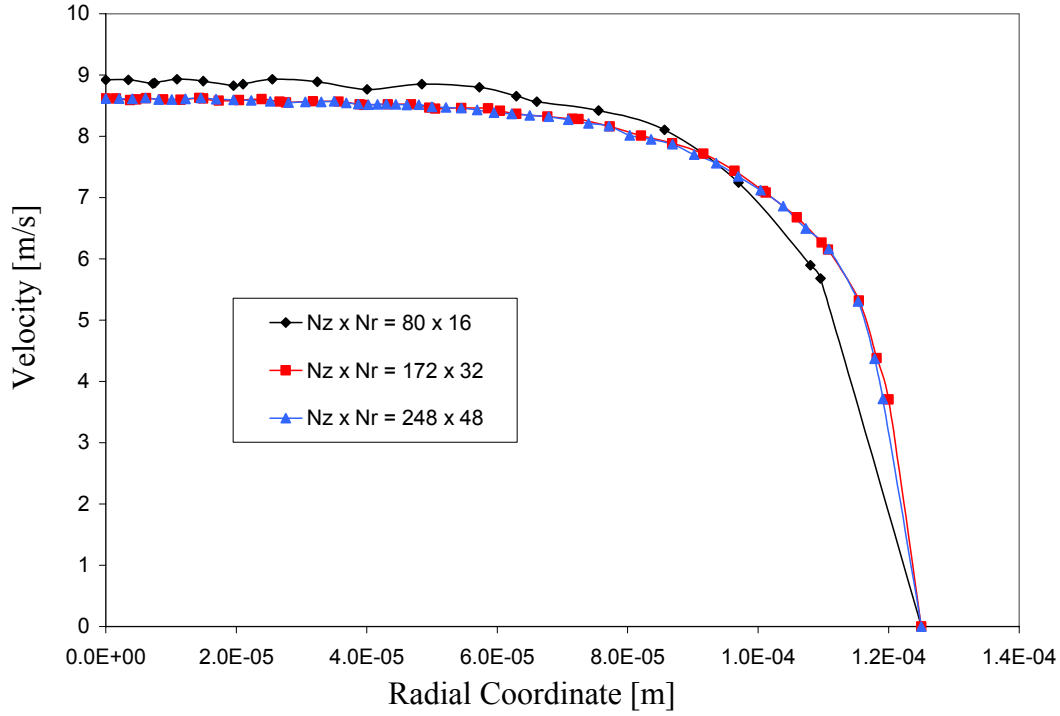

Figure 1: Velocity profile for various grid sizes

5

Results and Discussion

Computations were performed with two different general nozzle sizes. Figure 2 shows the dimensions of the larger nozzle, while Figure 3 shows the dimensions of the smaller nozzle. For the larger nozzle, two fluids (FC-77 and FC-72) were tested at three different flow rates (1.262 x 10^{-6} m^3/s, 2.524 x 10^{-6} m^3/s, and 3.785 x 10^{-6} m^3/s). For the smaller nozzle, FC-77 and FC-72 were used in addition with FC-87 and methanol. These fluids were tested through a range of inlet flow rates that varied from 1.262 x 10^{-7} m^3/s to about 5.678 x 10^{-7} m^3/s. The inlet velocities were calculated so that the velocity of the fluid entering the center hole was equal to that of the fluid entering through the outer slot.

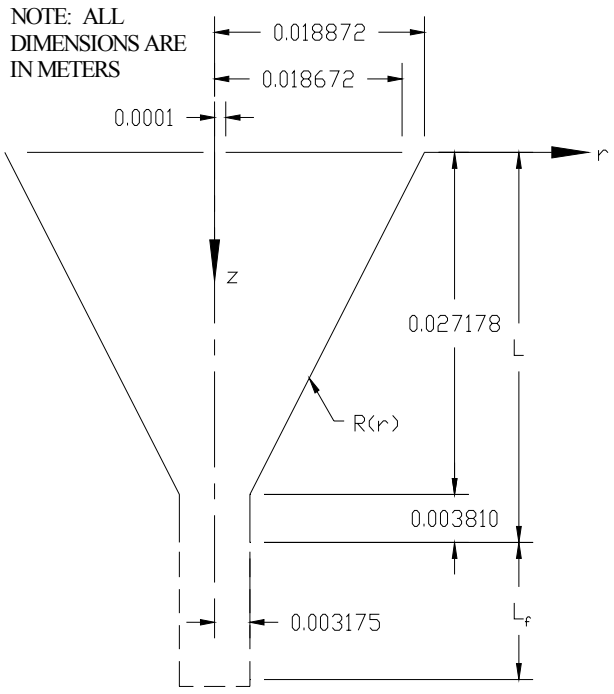

Figure 2: Dimensioned schematic for larger nozzle

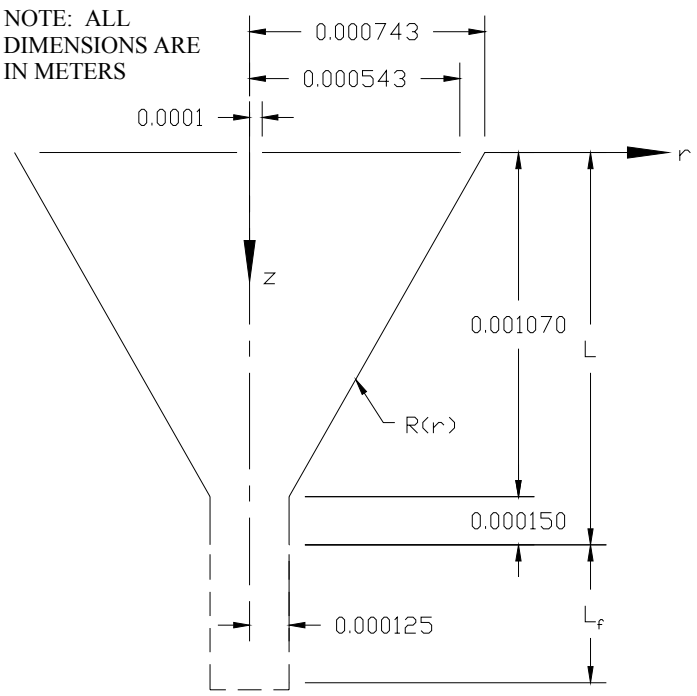

Figure 3: Dimensioned schematic of smaller nozzle

5.1 Large Nozzle

The larger nozzle is to be analyzed first. The inlet flow entering through the outer slot causes the top plate to rotate at a calculated rate. Table 3 depicts the spinning rate of the top plate as a result of the corresponding inlet flow rate in the larger nozzle. As would be expected, the increase in flow rate results in an increased spinning rate.

Table 3: Calculated spinning rate for given flow rate in larger nozzle

Inlet Flow Rate Q [m^3/s]	Spinning Rate Ω [rad/sec]
1.262×10^{-6}	2.837
2.524×10^{-6}	5.674
3.785×10^{-6}	8.512

As was mentioned previously, the fluid velocity through the center inlet and the outer slot are equal. Since the fluid enters the nozzle through the outer slot at a 45 degree angle, the axial component of the velocity is equal to the total velocity multiplied by the cosine of 45 degrees, and the radial velocity is equal to the total velocity multiplied by the negative sine of 45 degrees. Table 4 shows the inlet flow rates with the equivalent inlet velocities. All of the flow rates were determined to be laminar in the nozzle.

Table 4: Inlet velocities for the given flow rates in the larger nozzle

Inlet Flow Rate Q [m^3/s]	Center Hole V_{in} [m/s]	Axial Component for Outer Slot V_z [m/s]	Radial Component for Outer Slot V_r [m/s]
1.262×10^{-6}	0.0757	0.0535	-0.0535
2.524×10^{-6}	0.1513	0.1070	-0.1070
3.785×10^{-6}	0.2270	0.1605	-0.1605

Table 5 shows the Reynolds number calculated at the nozzle exit for each fluid and each flow rate used with the large nozzle. The Reynolds number for FC-72, which plays an important role in the shape of the free surface, is almost twice the value used for FC-77. This is because the viscosity of FC-72 is approximately half of that for FC-77.

Table 5: Reynolds number for each fluid and each flow rate

Inlet Flow Rate Q [m^3/s]	Working Fluid	Reynolds Number at Nozzle Outlet [non-dim]
1.262×10^{-6}	FC-77	316
	FC-72	664
2.524×10^{-6}	FC-77	632
	FC-72	1328
3.785×10^{-6}	FC-77	949
	FC-72	1992

5.1.1 Large Nozzle – FC-77

The first fluid that was tested in the larger nozzle was FC-77. This fluid has a density of 1780 kg/m^3, a viscosity of 1.424x10^{-3} kg/ms, and a surface tension of 0.015 N/m. Figure 4 shows the velocity vector plot for FC-77 with an inlet flow rate of 1.262 x 10^{-6} m^3/s. For this case, the top plate is spinning at a rate of 2.837 rad/sec. For each case the radial free surface heights, as well as the cone angles, were analyzed to provide information for future projects concentrating on heat transfer characteristics involving these sprays. As can be observed from the velocity vector plot, the free surface of the spray exiting the nozzle tends to rise as the axial distance increases.

For this particular trial, the initial free surface height was 3.175 x 10^{-3} m and the final free surface height reached 3.427 x 10^{-3} m, which caused a cone angle of 11.75 degrees. The maximum velocity experienced was 0.0757 m/s, at each of the inlets. This is because a smaller area should have a greater velocity due to the conservation of momentum, which states that the inlet flow rate must be equal to the outlet flow rate.

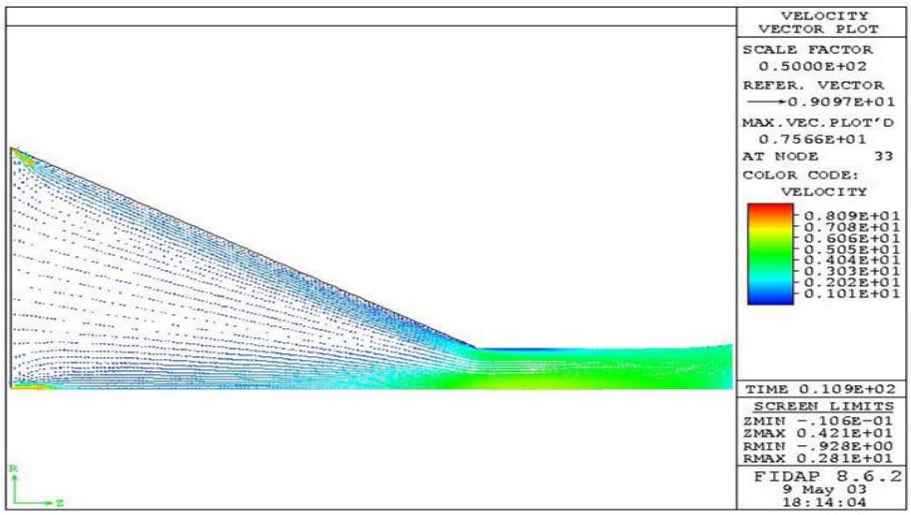

Figure 4: Velocity vector plot for FC-77 (Q = 1.262 x 10^{-6} m^3/s). Units are cm/s.

The pressure contour plot for this case is shown in Figure 5. The inlet-to-outlet pressure drop for this trial was 3.06 Pa, which is excellent. It is ideal to have a minimum pressure drop from the inlet of the nozzle to the outlet of the nozzle, so as to allow the fluid to flow freely through the nozzle. It was noted that the larger nozzle produced a much smaller pressure drop than did the smaller nozzle. As will be seen later in the paper, the smaller nozzle forces the fluid to move very fast through the throat and essentially the outlet of the nozzle, which causes a decrease in the pressure at that location. Therefore, the slower moving fluid in the larger nozzle allows the pressure at the outlet to remain at a greater value causing a minute pressure drop.

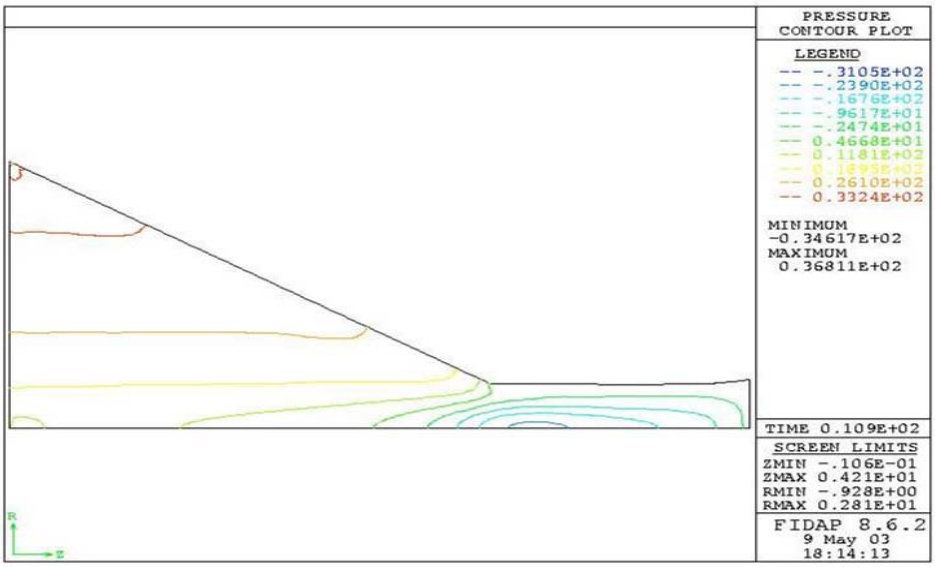

Figure 5: Pressure contour plot for FC-77 (Q = 1.262 x 10^{-6} m^3/s). Units are gm/cm s^2 (x10^1 Pa).

Next, Figure 6 shows the results of the velocity vector plot for FC-77 with an inlet flow rate of 2.524 x 10^{-6} m^3/s. This flow rate results in the top plate spinning at 5.674 rad/sec. The maximum velocity was discovered to be 0.1513 m/s, and similar to the previous trial, was located at the two nozzle inlets. Again, the initial free surface height

was 3.175 x 10^{-3} m and the final free surface height was 3.409 x 10^{-3} m. The phenomenon also resulted in a cone angle of 11.75 degrees. This result was counter-intuitive in the sense that it the final free surface height for 2.524 x 10^{-6} m^3/s was less than that of 1.262 x 10^{-6} m^3/s. It was concluded that this was a numerical error within the computing program itself.

The pressure contour plot for this case is shown in Figure 7. The maximum pressure was found to be 16.45 Pa, and the minimum pressure was found to be -8.99 Pa. The inlet-to-outlet pressure drop for this scenario was 12.72 Pa, which is greater than that of the previous trial. All of the pressure contour plots for the larger nozzle reveal that the pressure is at a maximum in the area of the outer inlet slot, and then decreases as the axis of symmetry and the outlet of the nozzle are approached.

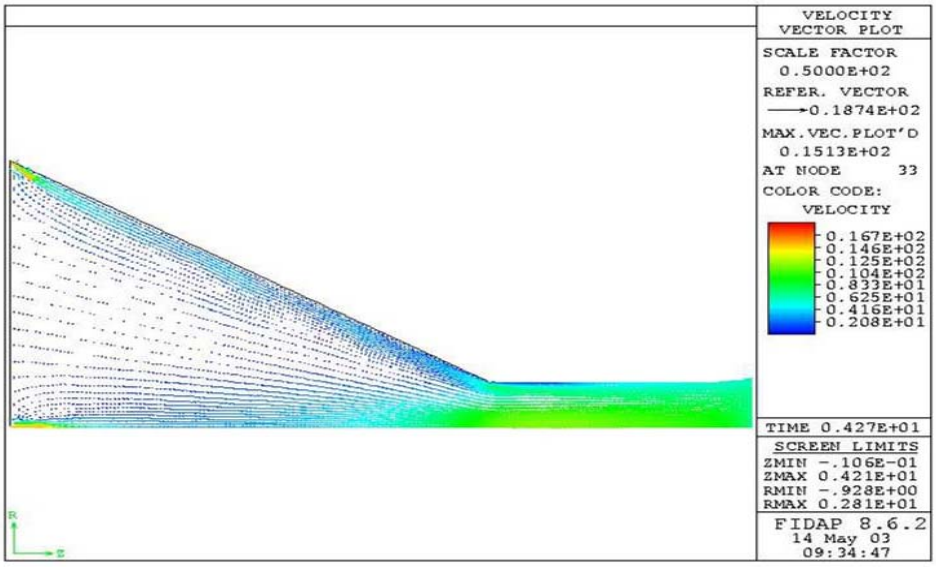

Figure 6: Velocity vector plot for FC-77 (Q = 2.524 x 10^{-6} m^3/s). Units are cm/s.

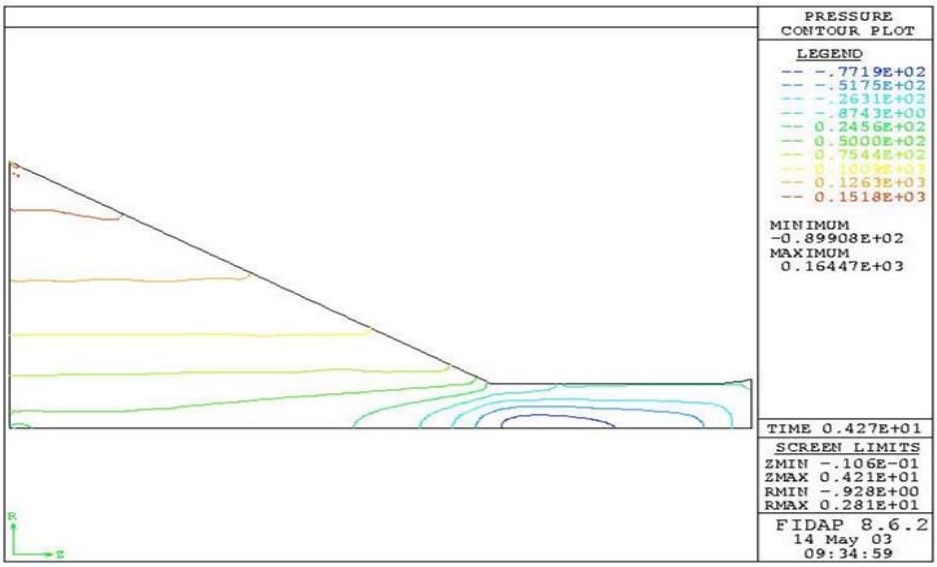

Figure 7: Pressure contour plot for FC-77 (Q = 2.524 x 10^{-6} m^3/s). Units are gm/cm s^2 (x10^1 Pa).

The velocity vector plot for an inlet flow rate of 3.785 x 10^{-6} m^3/s is shown in Figure 8. For this case, the top plate was spinning at a rate of 8.512 rad/sec due to an inlet velocity of 0.227 m/s. Identical to the other two cases, the maximum velocity in the nozzle is located at the inlets and equal to the inlet velocity. Also identical to the other two cases, the initial free surface height was 3.175 x 10^{-3} m; however, the final free surface height rose to 3.540 x 10^{-3} m with a cone angle of 15.00 degrees. This was to be expected, since an increase in flow rate results in a faster moving fluid, which should result in a larger cone angle.

Figure 9 illustrates the pressure contour plot for this case. The maximum and minimum pressures calculated for this case were 42.59 Pa and -18.77 Pa. The inlet-to-outlet pressure drop was determined to be about 33.74 Pa, which is quite higher than the previous two cases. Also, similar to the other trials, the pressure is a maximum at the outer inlet slot and gradually wanes towards the axis of symmetry and the nozzle outlet.

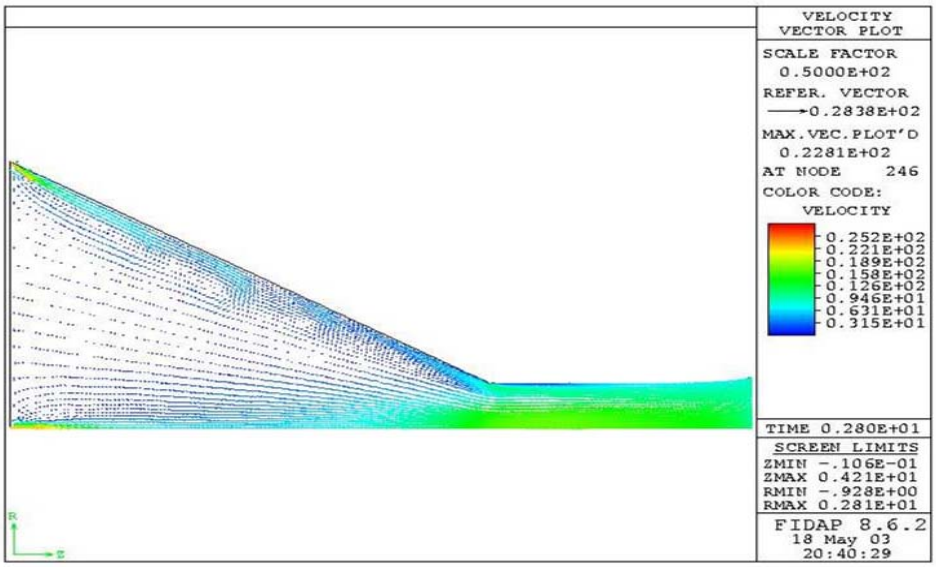

Figure 8: Velocity vector plot for FC-77 (Q = 3.785 x 10^{-6} m^3/s). Units are cm/s.

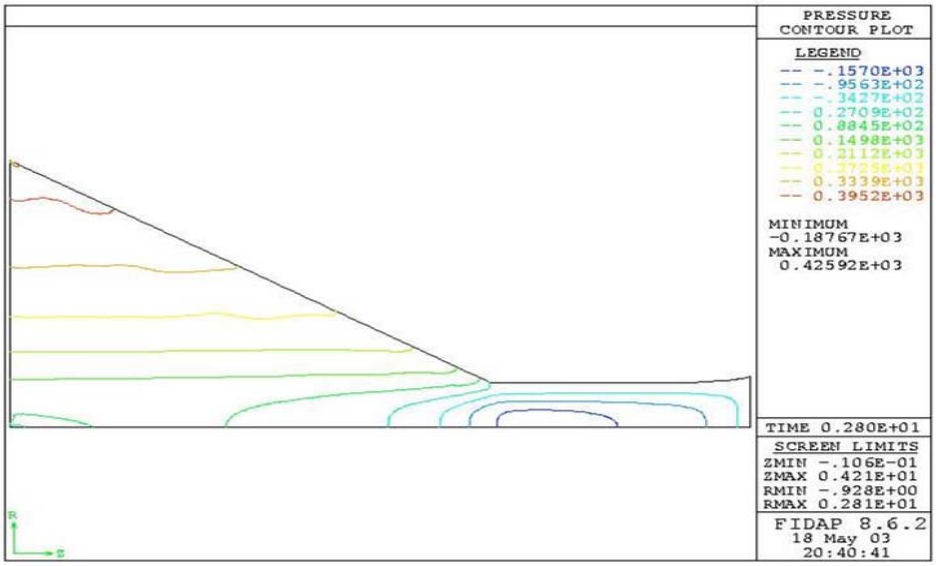

Figure 9: Pressure contour plot for FC-77 (Q = 3.785 x 10^{-6} m^3/s). Units are gm/cm s^2 (x10^1 Pa).

Figure 10 shows the free surface profile for FC-77 at the previous flow rates. It was noted that the flow rate of 3.785 x 10^{-6} m^3/s produced the greatest radial height of the free surface, whereas 1.262 x 10^{-6} m^3/s and 2.524 x 10^{-6} m^3/s produced similar radial heights.

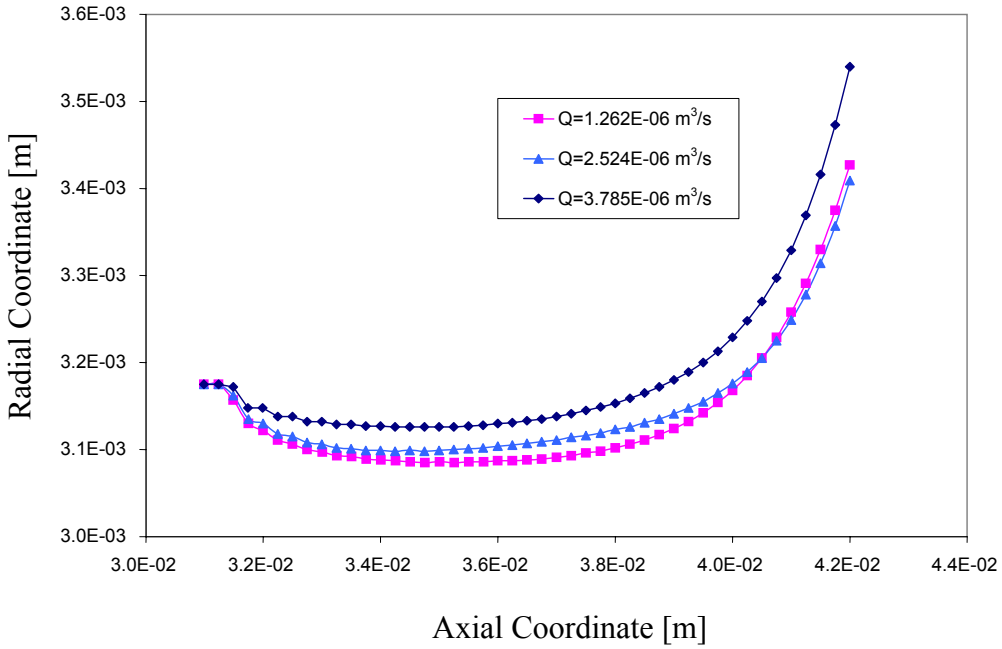

Figure 10: Free surface profile for FC-77 at various inlet flow rates

A dimensionless free surface profile is shown in Figure 11 based on the Reynolds number calculated at the nozzle exit. It was observed that a higher Reynolds number provided a greater radial free surface height and a larger cone angle.

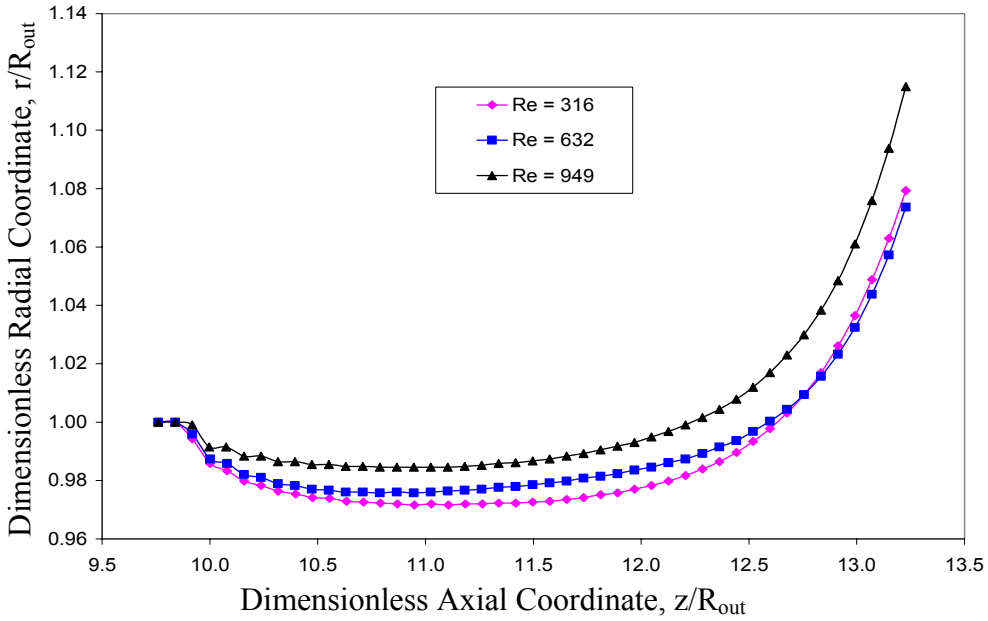

Figure 11: Dimensionless free surface profile for FC-77 (large nozzle)

5.1.2 Large Nozzle – FC-72

The above analysis was for the larger nozzle using FC-77 as the working fluid. Now, the larger nozzle with FC-72 introduced as the working fluid shall be discussed. FC-72 has a density of 1680 kg/m^3, a viscosity of 6.4 x 10^{-4} kg/ms, and a surface tension of 0.010 N/m. Similar to the investigation involving FC-77, this investigation is to include trials involving 1.262 x 10^{-6} m^3/s, 2.524 x 10^{-6} m^3/s, and 3.785 x 10^{-6} m^3/s as the various inlet flow rates. The inlet velocities for each case are the same as the previous cases, which in turn result in the same spinning rates for the top plate. Therefore, the maximum velocities, as well as the location of these velocities, are also the same as the previous cases where FC-77 was used as the working fluid. Again, the radial free surface heights, as well as the cone angles were analyzed. A larger free surface height and larger cone angle would be beneficial for this problem, since it is desired to yield a spray that covers a maximum surface area.

Figure 12 shows the velocity vector plot for 1.262 x 10^{-6} m^3/s as the inlet flow rate. With the initial free surface height remaining at 3.175 x 10^{-3} m, the final free surface height reached 3.691 x 10^{-3} m. This is slightly greater than the final free surface height obtained for FC-77. The cone angle for this case was calculated to be about 18.16 degrees, which is also greater than the value that resulted from FC-77 as the working fluid. For this same case, Figure 13 shows the pressure contour plot. The maximum and minimum pressures obtained in the nozzle were 4.13 Pa and -2.93 Pa, respectively. The inlet-to-outlet pressure drop for this instance was 3.88 Pa. It was noted that for both working fluids, as the inlet flow rate increased, so did the inlet-to-outlet pressure drop.

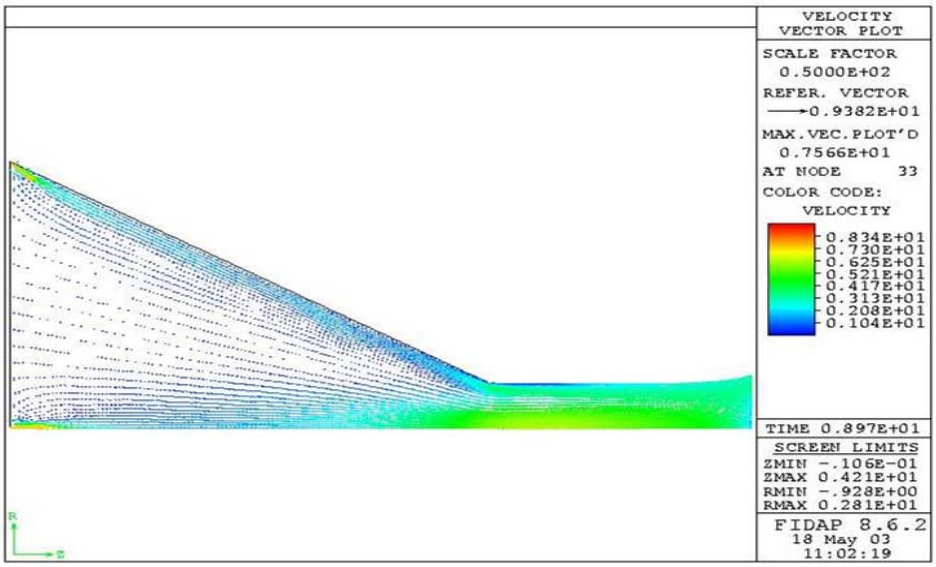

Figure 12: Velocity vector plot for FC-72 (Q = 1.262 x 10^{-6} m^3/s). Units are cm/s.

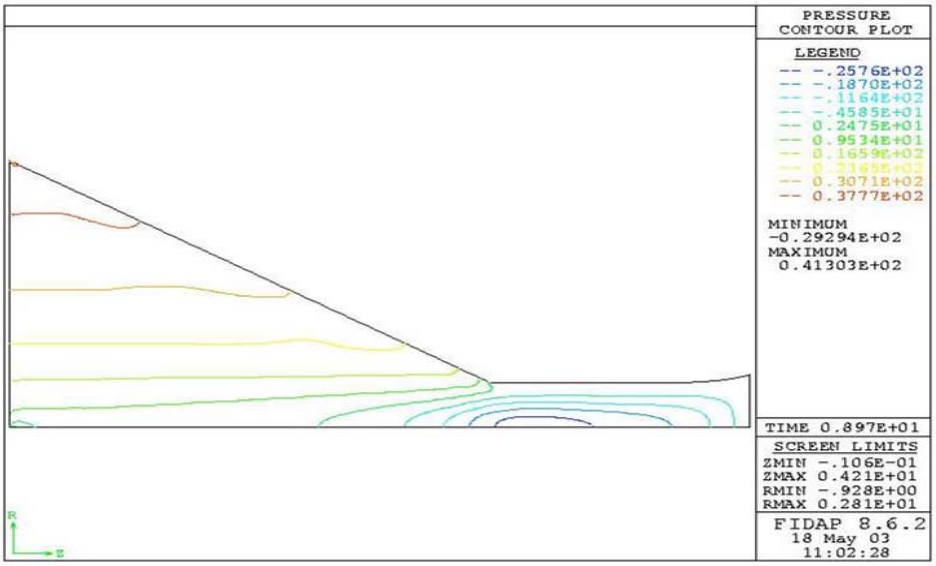

Figure 13: Pressure contour plot for FC-72 (Q = 1.262 x 10^{-6} m^3/s). Units are gm/cm s^2 (x10^1 Pa).

The inlet flow rate of 2.524 x 10^{-6} m^3/s was observed next. Figure 14 shows the velocity vector plot, which revealed that the maximum velocity was again located at the nozzle inlets. The free surface of the spray exiting the nozzle increased to 3.775 x 10^{-3} m from an original height of 3.175 x 10^{-3} m, which meant a cone angle of 20.61 degrees was

present. Figure 15 shows the pressure contour plot for this case. The maximum pressure observed in the nozzle was 20.57 Pa and the minimum pressure was -9.06 Pa. The inlet-to-outlet pressure drop was determined to be 14.81 Pa, which is greater than the pressure drop for the same inlet flow rate using FC-77 as the working fluid.

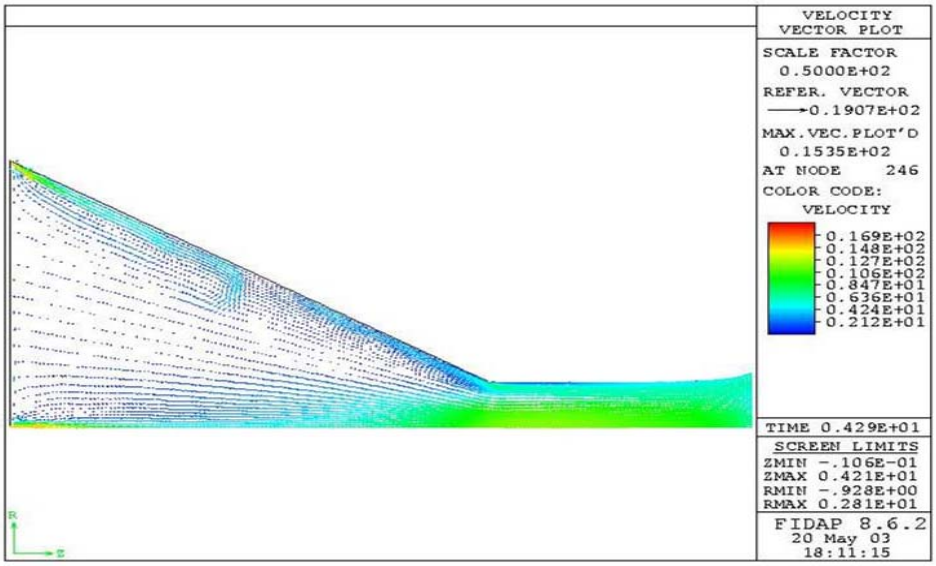

Figure 14: Velocity vector plot for FC-72 (Q = 2.524 x 10^{-6} m^3/s). Units are cm/s.

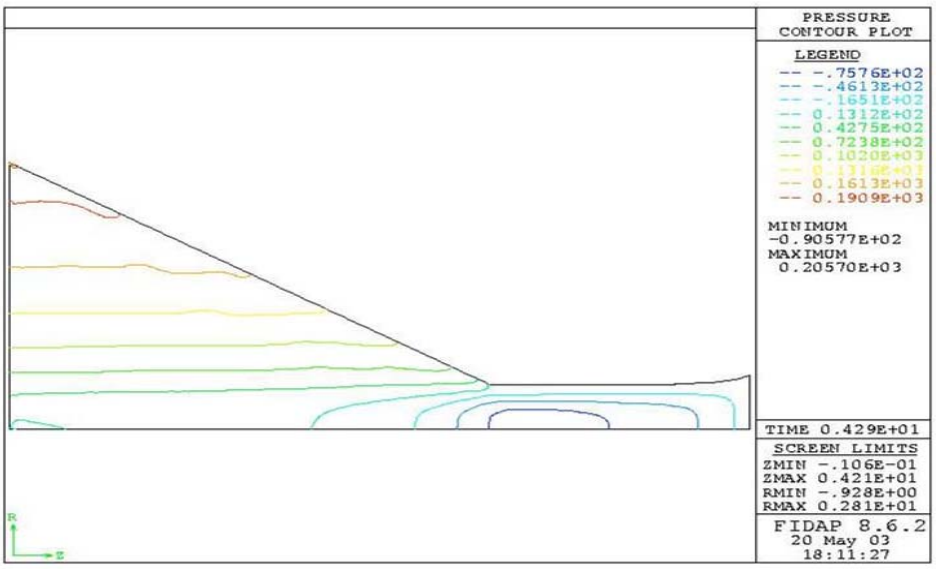

Figure 15: Pressure contour plot for FC-72 (Q = 2.524 x 10^{-6} m^3/s). Units are gm/cm s^2 (x10^1 Pa).

Figure 16 and Figure 17 show the velocity vector plot and pressure contour plot for 3.785 x 10^{-6} m^3/s used as the inlet flow rate. The vector velocity plot continues to support the fact that greater flow rates result in a greater free surface height. For this case, the free surface height increased from 3.175 x 10^{-3} m to a height of 4.049 x 10^{-3} m. The cone angle for this situation was determined to be 26.75 degrees, which was the highest value obtained for the larger nozzle. The pressure contour plot shows that the maximum pressure within the nozzle was 52.90 Pa, and the minimum pressure was -23.93 Pa. The inlet-to-outlet pressure drop was calculated as 38.41 Pa. Comparing the two working fluids that were studied, it was observed that although both of the fluids resulted in similar pressure drops, FC-72 was noted to result in an increased pressure drop for each inlet flow rate.

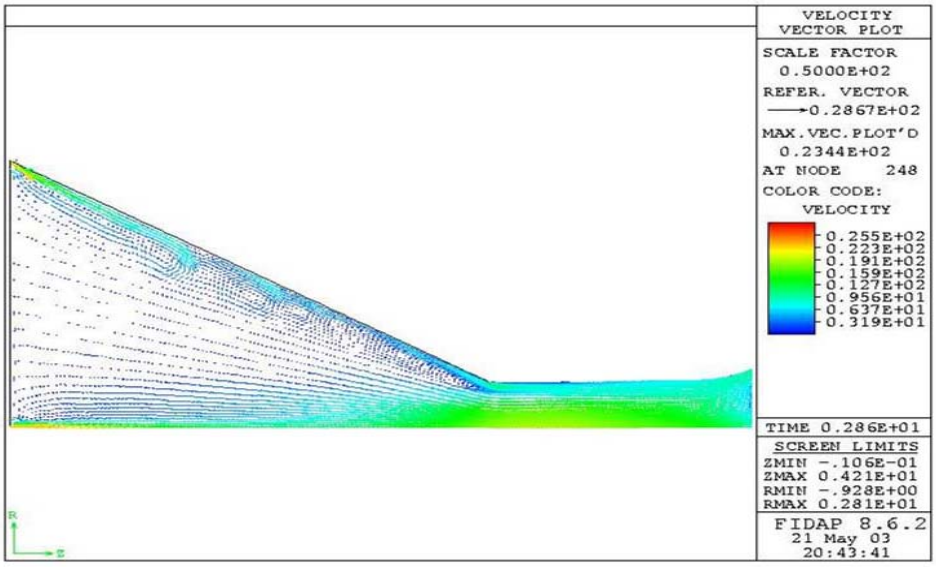

Figure 16: Velocity vector plot for FC-72 (Q = 3.785 x 10^{-6} m^3/s). Units are cm/s.

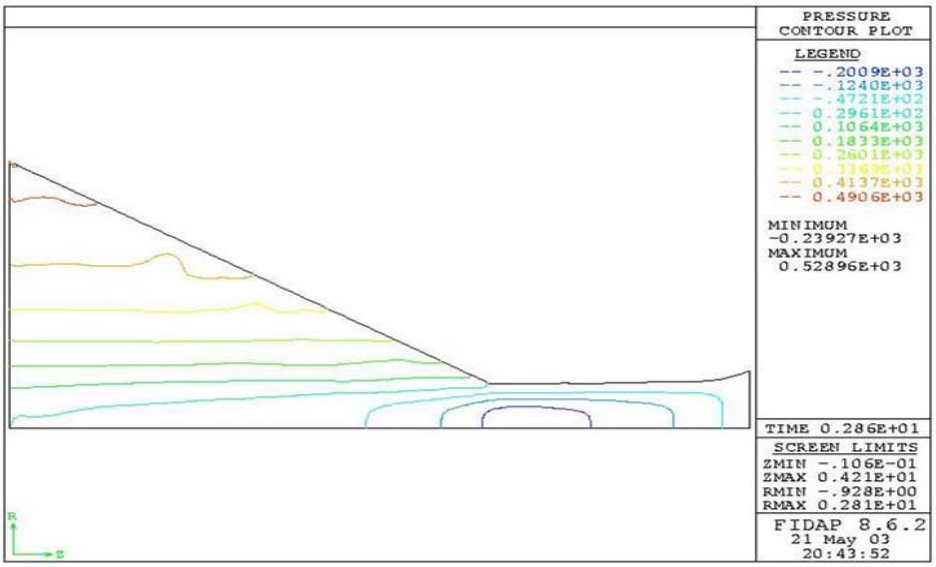

Figure 17: Pressure contour plot for FC-72 (Q = 3.785 x 10^{-6} m^3/s). Units are gm/cm s^2 (x10^1 Pa).

Figure 18 shows the free surface profile obtained for each flow rate when FC-72 was used as the working fluid. Again, the inlet flow rate of 3.785 x 10^{-6} m^3/s produced the greatest free surface height.

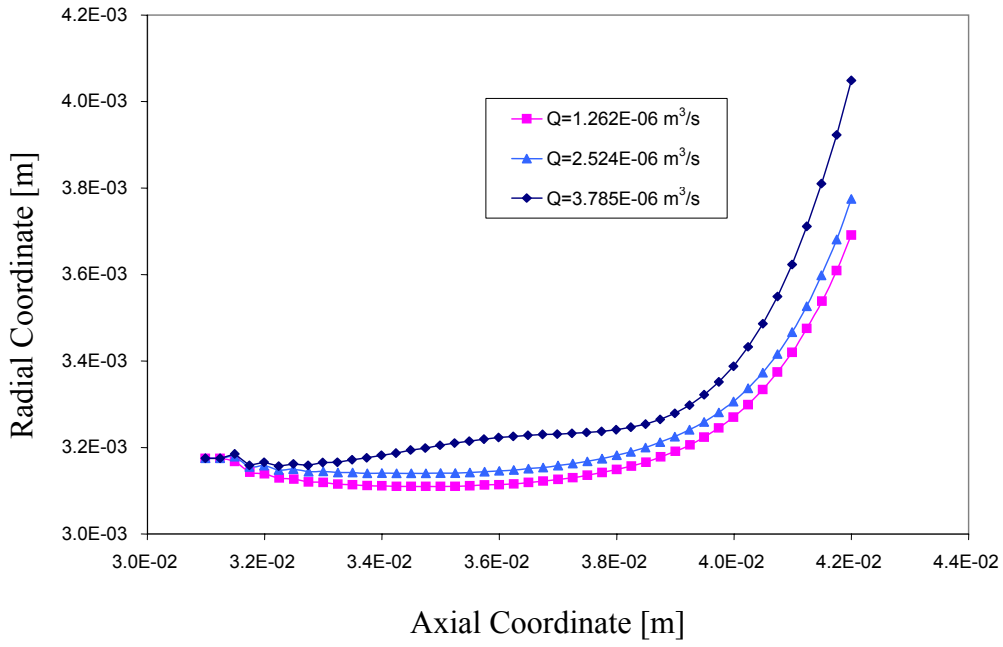

Figure 18: Free surface profile for FC-72 at various flow rates

Figure 19 shows the dimensionless plot for the free surface profile with FC-72 used as the working fluid. Similar to the same plot involving FC-77, this figure shows that a higher Reynolds number produces a greater radial height for the free surface, as well as a larger cone angle, which will be important values for future investigations.

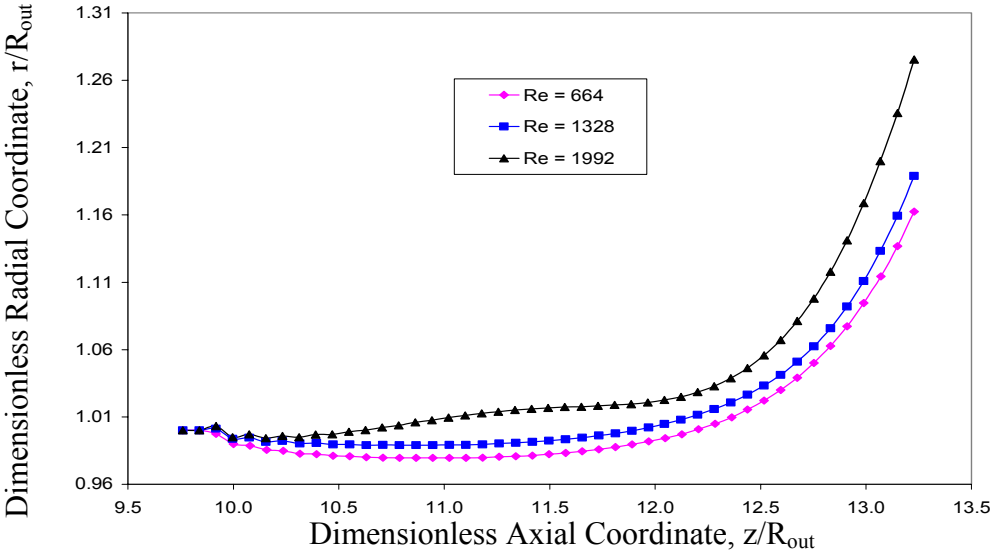

Figure 19: Dimensionless free surface profile for FC-72 (large nozzle)

In summary of the results for the larger nozzle, Tables 6 – 8 compare the pressure drop, final free surface height, and cone angle respectively, for the two working fluids. For this problem, it is advantageous to have a large final free surface height and a large cone angle. Since these sprays are going to be used to cool electronics, a larger value for these factors results in a cooling process that is more efficient. It was also observed that an increase in the Reynolds number produced a larger free surface height and a larger cone angle. As the inlet velocity increased, so did the values for these variables. Also, as the viscosity decreased, these values increased. This is because a fluid with lower viscosity has lower shear stress, which allows the fluid to flow more freely.

Table 6: Inlet-to-outlet pressure drop for each working fluid and each inlet flow rate

Inlet Flow Rate Q [m^3/s]	FC-77	FC-72
1.262×10^{-6}	3.06 Pa	3.88 Pa
2.524×10^{-6}	12.72 Pa	14.81 Pa
3.785×10^{-6}	33.74 Pa	38.41 Pa

Table 7: Final free surface height for each working fluid and each flow rate

Inlet Flow Rate Q [m^3/s]	FC-77	FC-72
1.262×10^{-6}	3.427×10^{-3} m	3.691×10^{-3} m
2.524×10^{-6}	3.409×10^{-3} m	3.775×10^{-3} m
3.785×10^{-6}	3.540×10^{-3} m	4.409×10^{-3} m

Table 8: Cone angle for each working fluid and each flow rate

Inlet Flow Rate Q [m^3/s]	Working Fluid	Cone Angle [deg]
1.262×10^{-6}	FC-77	11.75
	FC-72	18.16
2.524×10^{-6}	FC-77	11.75
	FC-72	20.61
3.785×10^{-6}	FC-77	15.00
	FC-72	26.75

5.2 Small Nozzle

The next variation analyzed involved using a smaller nozzle. For this design, the central nozzle inlet remained the same size, whereas the other nozzle dimensions decreased. For this nozzle, FC-77 was used as the working fluid for inlet flow rates of

1.262×10^{-7} m^3/s, 2.524×10^{-7} m^3/s, 4.416×10^{-7} m^3/s, and 5.678×10^{-7} m^3/s. FC-72 was also used, but with flow rates of only 4.416×10^{-7} m^3/s, and 5.678×10^{-7} m^3/s. For this nozzle geometry, no cone angles were produced, so therefore, none were reported. This smaller nozzle was also subject to some additional alterations, which will be discussed later in the paper. Similar to the large nozzle, and for the same reasons, the free surface height and cone angle were analyzed for each variation as necessary.

First, since the nozzle dimensions are much smaller than the larger nozzle, the velocity of the fluid through the inlets needs to be large to produce the required flow rates. This large velocity in turn results in a very large spinning rate for the top plate of the nozzle. Although the geometry of this nozzle is different than that of the larger nozzle tested, the velocities through the nozzle inlets are calculated in the same manner. The velocity through the central hole is equivalent to the velocity entering through the outer slot at a 45 degree angle. Table 9 and Table 10 depict the spinning rate and inlet velocities, respectively, for the various inlet flow rates.

Table 9: Calculated spinning rate for given flow rate in smaller nozzle

Inlet Flow Rate Q [m^3/s]	Spinning Rate Ω [rad/sec]
1.262×10^{-7}	233.67
2.524×10^{-7}	467.34
4.416×10^{-7}	817.84
5.678×10^{-7}	1051.50

Table 10: Inlet velocities for the given flow rates in the smaller nozzle

Inlet Flow Rate Q [m^3/s]	Center Hole V_{in} [m/s]	Axial Component for Outer Slot V_z [m/s]	Radial Component for Outer Slot V_r [m/s]
1.262×10^{-7}	0.2455	0.1736	-0.1736
2.524×10^{-7}	0.4911	0.3472	-0.3472
4.416×10^{-7}	0.8594	0.6077	-0.6077
5.678×10^{-7}	1.1049	0.7813	-0.7813

Table 11 shows the Reynolds number calculated at the nozzle exit for each fluid and each flow rate used with the small nozzle. It can again be seen that FC-72 produces a Reynolds number almost twice as much as FC-77. This is because their densities are very similar, but the viscosity of FC-72 is approximately half of that for FC-77.

Table 11: Reynolds number for each fluid and each flow rate

Inlet Flow Rate Q [m^3/s]	Working Fluid	Reynolds Number at Nozzle Outlet [non-dim]
1.262×10^{-7}	FC-77	803
	FC-72	--
2.524×10^{-7}	FC-77	1607
	FC-72	--
4.416×10^{-7}	FC-77	2812
	FC-72	5904
5.678×10^{-7}	FC-77	3615
	FC-72	7591

5.2.1 Small Nozzle – FC-77

Figure 20 shows the velocity vector plot for FC-77 as the working fluid flowing at 1.262×10^{-7} m^3/s. For this flow rate, the top plate was spinning at 233.67 rad/sec. Also

for this flow rate, the flow throughout the nozzle was determined to be laminar. The maximum velocity was found to be around 3.25 m/s, located in the throat of the nozzle. Unlike the larger nozzle, the smaller dimensions of this nozzle force the fluid through the throat of the nozzle at a much faster rate than when it enters the through the inlets. The free surface began at an initial height of 1.250×10^{-4} m, but decreased to a final height of 1.202×10^{-4} m.

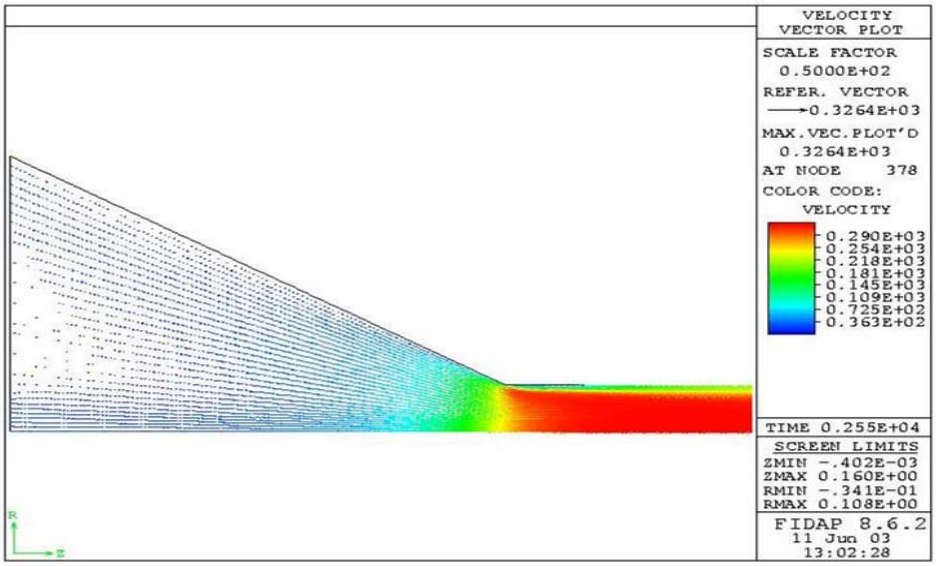

Figure 20: Velocity vector plot for FC-77 ($Q = 1.262 \times 10^{-7}$ m^3/s). Units are cm/s.

Figure 21 and Figure 22 show the pressure and streamline contour plots, respectively. The maximum pressure within the nozzle was found to be 9.48×10^3 Pa, while the minimum pressure was -1.47×10^3 Pa. The inlet-to-outlet pressure drop was calculated to be about 6.28×10^3 Pa. The streamline contour plot shows that most of the fluid entering the outer slot flows along the nozzle wall toward the outlet, while some of that fluid initially flowed toward the center of the nozzle. The fluid entering through the

central inlet flows slightly outward in the radial direction as it moved toward the outlet. Still, some of the entering fluid was swirling next to the rotating top plate.

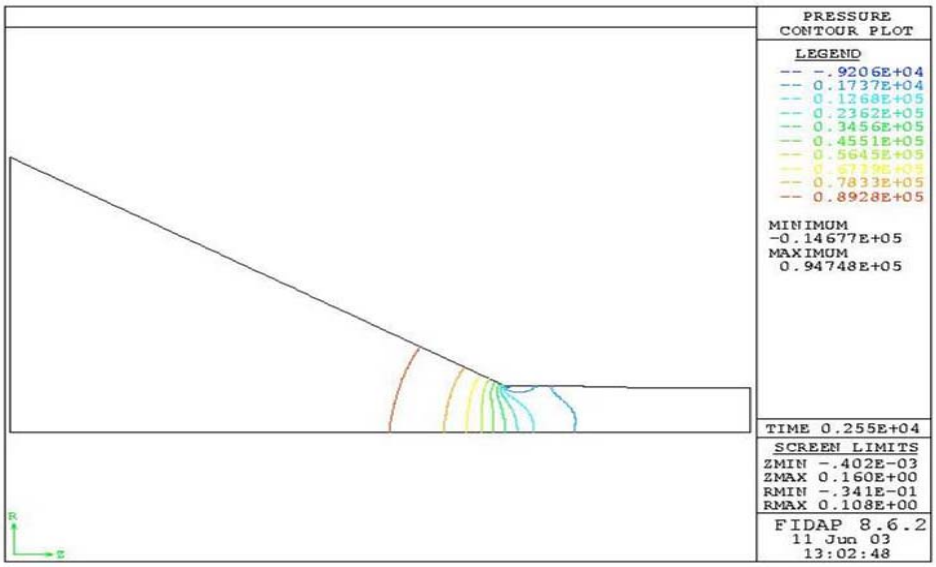

Figure 21: Pressure contour plot for FC-77 (Q = 1.262 x 10^{-7} m^3/s). Units are gm/cm s^2 (x10^1 Pa).

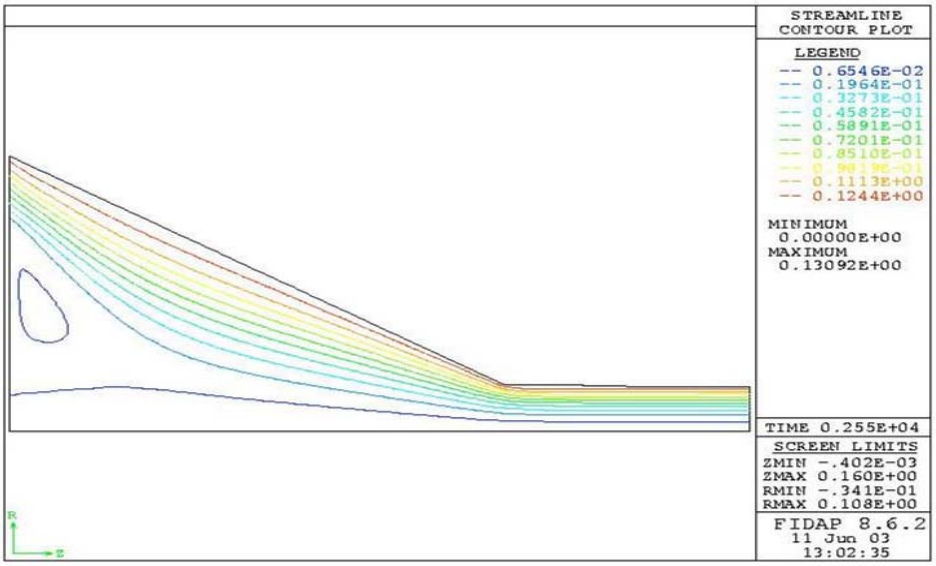

Figure 22: Streamline contour plot for FC-77 (Q = 1.262 x 10^{-7} m^3/s)

The next flow rate that was used with FC-77 as the fluid was 2.524 x 10^{-7} m^3/s. For this trial, the top plate was rotating at 467.34 rad/sec. The velocity vector plot for

this scenario is shown in Figure 23. The maximum velocity within the nozzle was found to be about 6.57 m/s. The free surface of the liquid exiting the nozzle began at a height of 1.250 x 10^{-4} m, and steadily declined to a final height of 1.210 x 10^{-4} m. In Figure 23, it is observed that as the fluid enters the throat of the nozzle, the velocity of the fluid near the wall and the outer portion of the free surface have lower velocities than elsewhere in the flow. This phenomenon is due to the boundary condition of zero velocity at the nozzle walls.

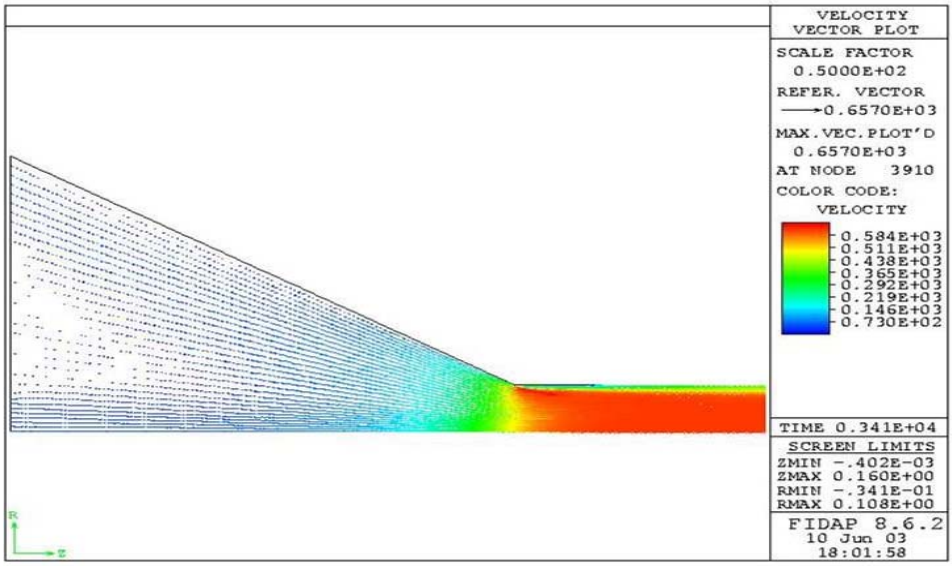

Figure 23: Velocity vector plot for FC-77 (Q = 2.524 x 10^{-7} m^3/s). Units are cm/s.

Figure 24 and Figure 25 show the pressure contour plot and the streamline contour plot for this case. The maximum pressure was found to be 3.48 x 10^4 Pa, whereas the minimum pressure was found to be -8.75 x 10^3 Pa. The pressure drop from the inlet to the outlet of the nozzle was calculated to be approximately 2.29 x 10^4 Pa. Similar to the other cases, the streamline contour plot shows that most of the fluid that enters through the outer slot follows the nozzle wall to the outlet, while some of the fluid

move toward the center of the nozzle as it flows to the outlet. The fluid that enters through the central inlet has almost a purely axial flow, while a portion of the fluid in the nozzle is caught swirling near the top plate.

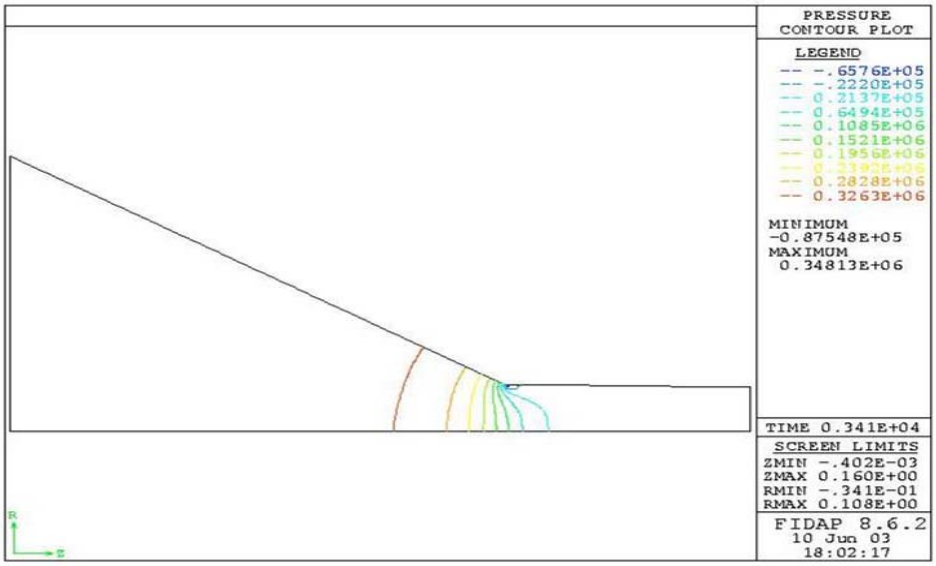

Figure 24: Pressure contour plot for FC-77 (Q = 2.524 x 10^{-7} m^3/s). Units are gm/cm s^2 (x10^1 Pa).

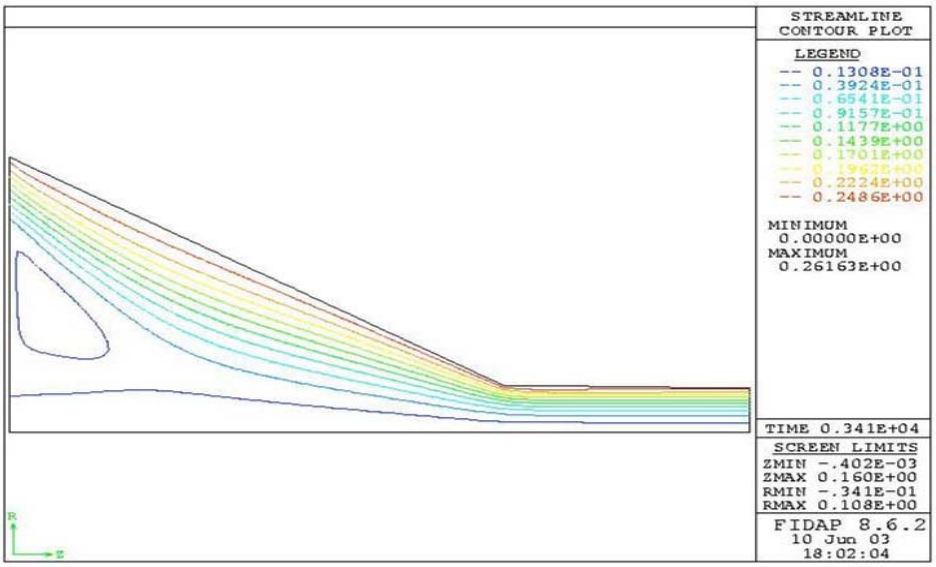

Figure 25: Streamline contour plot for FC-77 (Q = 2.524 x 10^{-7} m^3/s)

Figure 26 reveals the velocity vector plot for the case where 4.416 x 10^{-7} m^3/s is used as the inlet flow rate with FC-77 as the working fluid. This resulted in the top plate of the nozzle spinning at 817.84 rad/sec. The maximum velocity was found to be around 11.20 m/s, and was also located in the throat of the nozzle. The free surface began at a height of 1.250 x 10^{-4} m, decreased to a height 1.217 x 10^{-4} m, then increased back to a height of 1.220 x 10^{-4} m. This flow was determined to be turbulent, and the mixing length turbulence model was employed for this case.

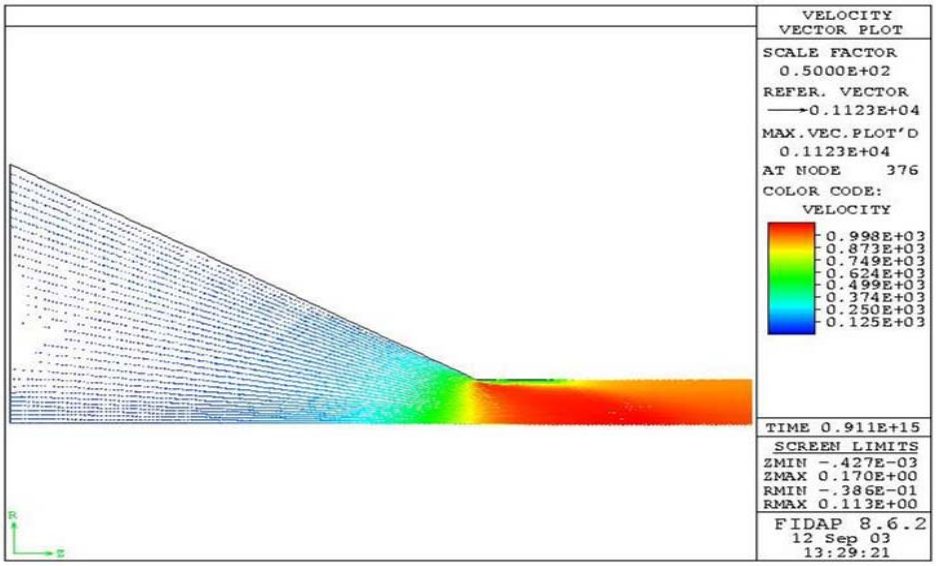

Figure 26: Velocity vector plot for FC-77 (Q = 4.416 x 10^{-7} m^3/s). Units are cm/s.

Figure 27 shows the pressure contour plot for this case. The maximum and minimum pressures plotted were determined to be 1.29 x 10^5 Pa and -2.69 x 10^4 Pa, respectively. The inlet-to-outlet pressure drop was calculated to be 1.19 x 10^5 Pa. The streamline contour plot is depicted in Figure 28. It shows that most of the fluid entering through the outer inlet slot follows the outer nozzle wall as it makes it way towards the outlet. The fluid entering through the central inlet moves slightly outward in the radial

direction before heading toward the outlet. However, for this flow rate, there is no portion of the fluid swirling at the top plate. For this case, the top plate is rotating faster than the previous cases, which essentially pushes the fluid down the nozzle, thus eliminating the portion of fluid shown in the previous streamline plots.

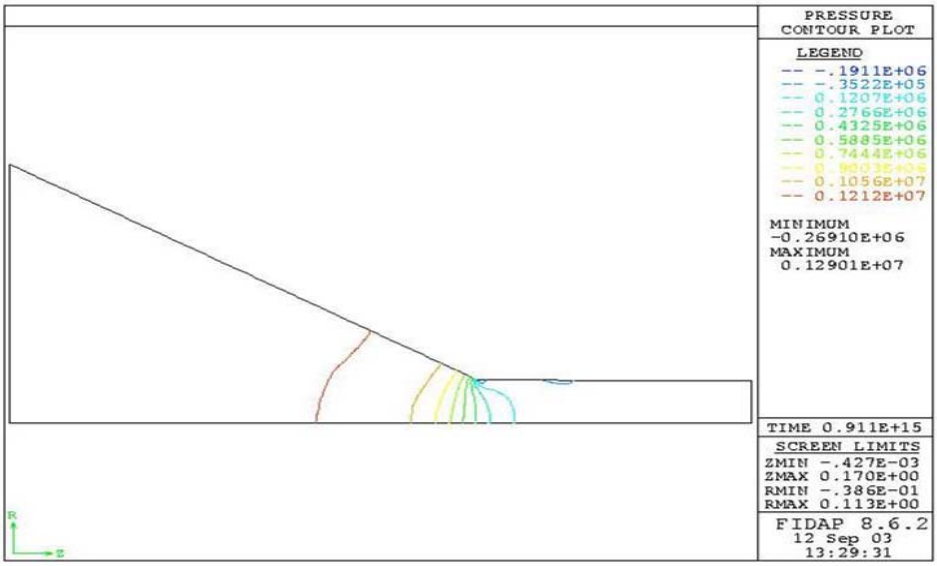

Figure 27: Pressure contour plot for FC-77 (Q = 4.416 x 10^{-7} m^3/s). Units are gm/cm s^2 (x10^1 Pa).

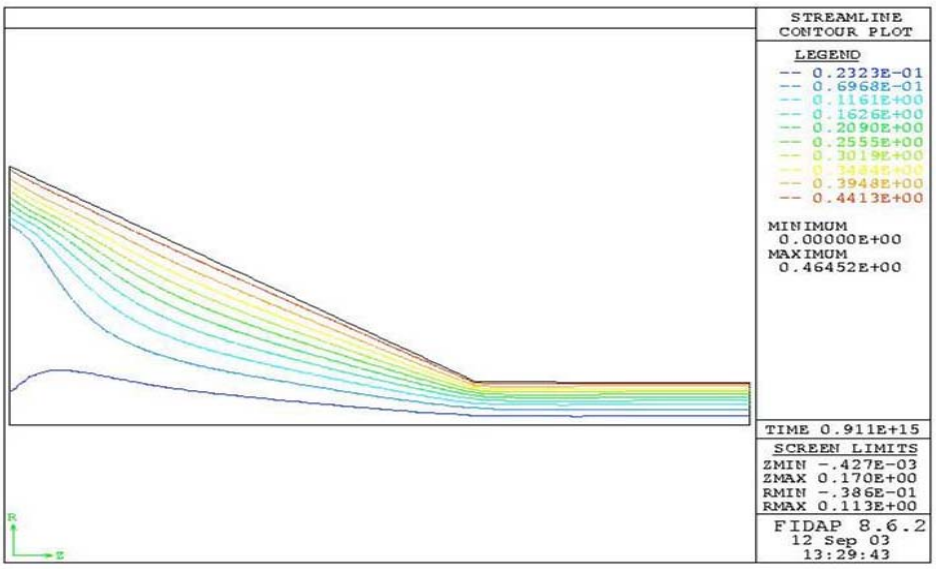

Figure 28: Streamline contour plot for FC-77 (Q = 4.416 x 10^{-7} m^3/s)

The velocity vector plot for FC-77 traveling at 5.678 x 10^{-7} m^3/s, which increased the spinning rate of the top plate to 1051.5 rad/sec, is shown in Figure 29. This was also found to be turbulent, and again, the mixing length turbulence model was used. The maximum velocity, like the other trials, was found to be in the throat of the nozzle, and equivalent to about 14.30 m/s. Also similar to the previous trial, the free surface height started at 1.250 x 10^{-4} m, declined to 1.217 x 10^{-4} m, then rose to 1.221 x 10^{-4} m. It was observed from this data, that the inlet flow rate had very little effect on the free surface height; however, out of all of the variations, the inlet flow rate affected the free surface height and the cone angle the most.

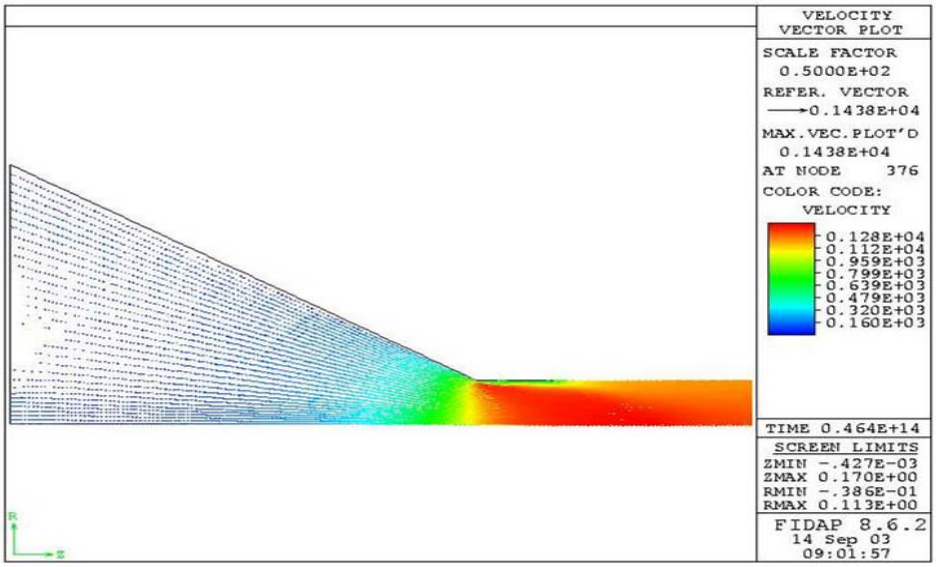

Figure 29: Velocity vector plot for FC-77 (Q = 5.678 x 10^{-7} m^3/s). Units are cm/s.

Figure 30 and Figure 31 show the pressure and streamline contour plots for this situation. The maximum pressure was determined to be 2.11 x 10^5 Pa, whereas the minimum pressure was determined to be -4.62 x 10^4 Pa. The two extremes were located at the inlet and outlet of the nozzle, respectively. The pressure drop from inlet to outlet

was calculated to be 1.95 x 10^5 Pa. The streamline plot shows that the fluid flows in a fairly straight path toward the nozzle outlet. Most of the fluid entering through the outer inlet slot flows along the nozzle wall, while the fluid entering through the central inlet flows along the line of symmetry.

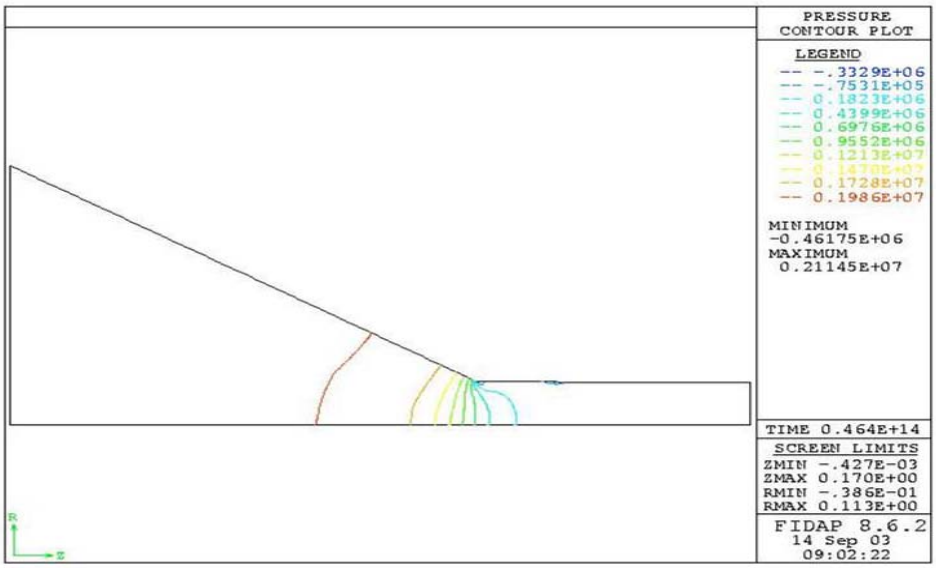

Figure 30: Pressure contour plot for FC-77 (Q = 5.678 x 10^{-7} m^3/s). Units are gm/cm s^2 (x10^1 Pa).

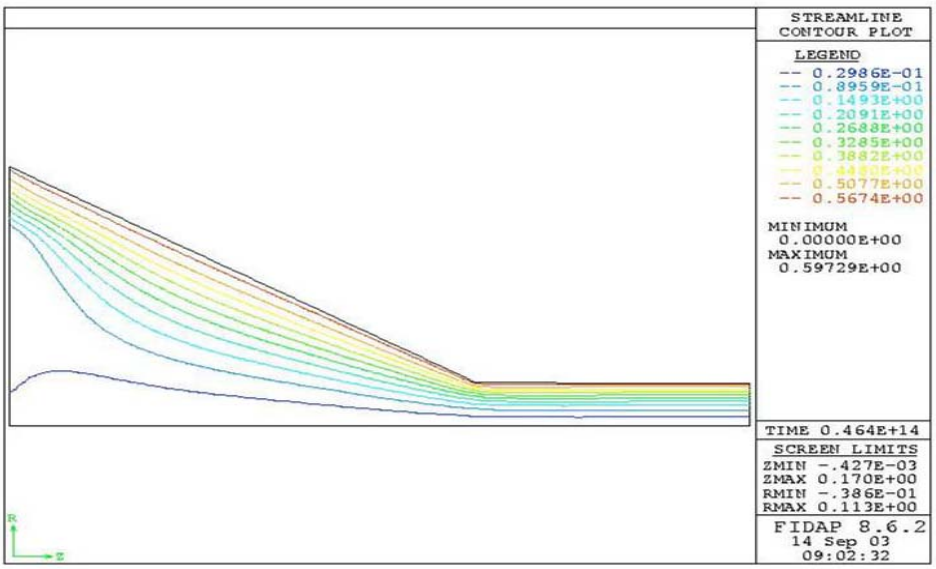

Figure 31: Streamline contour plot for FC-77 (Q = 5.678 x 10^{-7} m^3/s).

Figure 32 and Figure 33 depict the profile of the free surface obtained when the working fluid was FC-77. It was noted that the inlet flow rate had little effect on the height of the free surface; however, 5.678 x 10^{-7} m^3/s produced a slightly greater height.

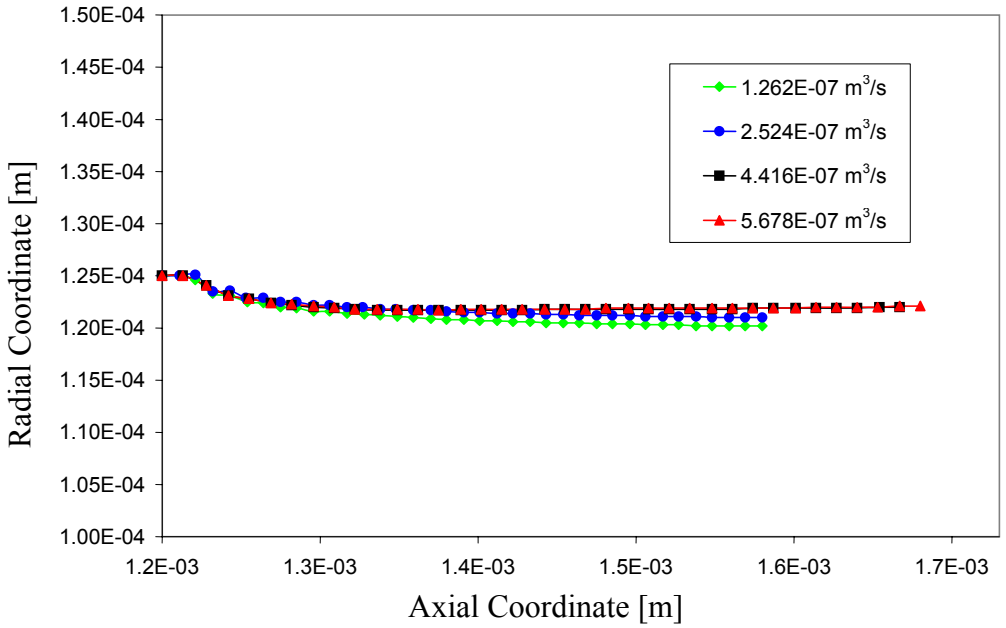

Figure 32: Free surface profile for FC-77 at various flow rates

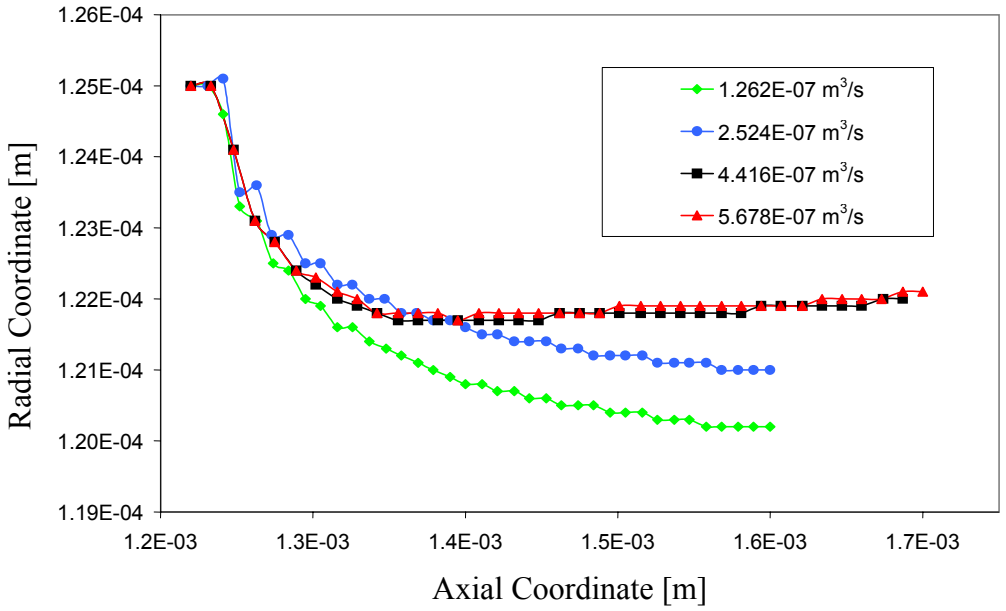

Figure 33: Magnified free surface profile for FC-77 at various flow rates

Figure 34 shows the dimensionless free surface profile for FC-77 with respect to the Reynolds number. As was expected, it was shown that a higher Reynolds number produced a greater height for the free surface. Since FC-77 was the only fluid analyzed for this plot, the greater Reynolds number is solely a product of a larger velocity. Therefore, it is reasonable to state that a larger velocity produces a larger radial free surface height. However, it was observed that for the cases when the Reynolds number was 2812 and 3615, the height did not vary a significant amount.

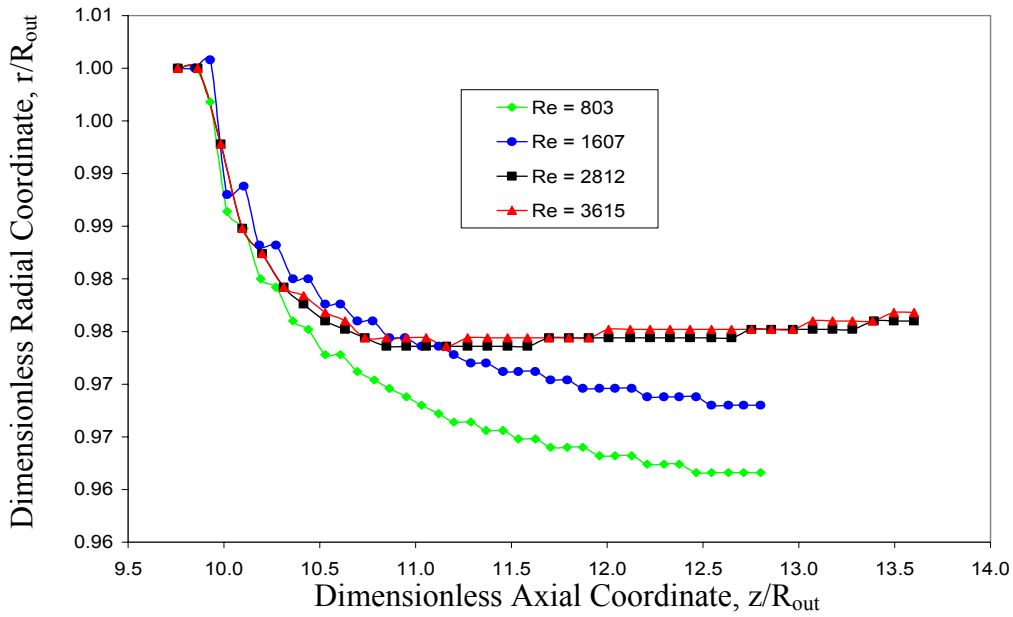

Figure 34: Dimensionless free surface profile for FC-77 (small nozzle)

5.2.2 Small Nozzle – FC-72

Next, FC-72 was substituted as the working fluid, and trials were run for inlet flow rates of 4.416×10^{-7} m^3/s and 5.678×10^{-7} m^3/s. The top plate of the nozzle is still being simulated as a spinning disc. The case using FC-72 at 4.416×10^{-7} m^3/s through the nozzle inlets was analyzed first. Similar to the case involving FC-77 as the working

fluid, this flow rate caused the top plate to spin at 233.67 rad/sec. Figure 35 shows the velocity vector plot for this variation. The maximum velocity was found to be approximately 11.10 m/s. The free surface of the fluid exiting the nozzle began at a height of 1.250 x 10^{-4} m, decreased to 1.218 x 10^{-4} m, and then increased to a final height of 1.222 x 10^{-4} m.

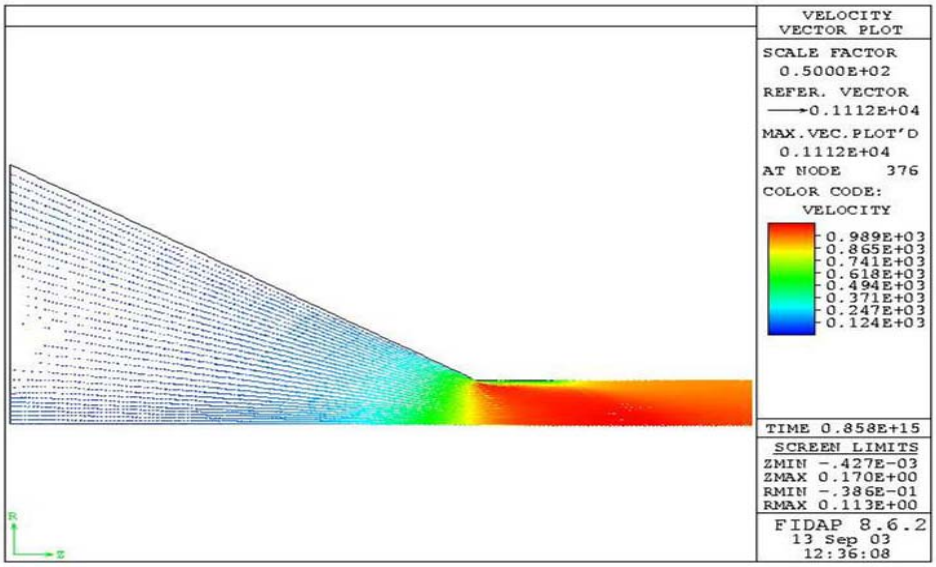

Figure 35: Velocity vector plot for FC-72 (Q = 4.416 x 10^{-7} m^3/s). Units are cm/s.

Figure 36 and Figure 37 show the pressure and streamline contour plots for this case, respectively. The maximum pressure within the nozzle was found to be approximately 1.19 x 10^5 Pa, whereas the minimum pressure was about -2.77 x 10^4 Pa. The pressure drop from the inlet of the nozzle to the outlet was calculated to be about 1.10 x 10^5 Pa. The streamline plot shows results similar to the others obtained thus far. This particular nozzle geometry allows the fluid to flow in the same manner regardless of the working fluid or the inlet flow rate.

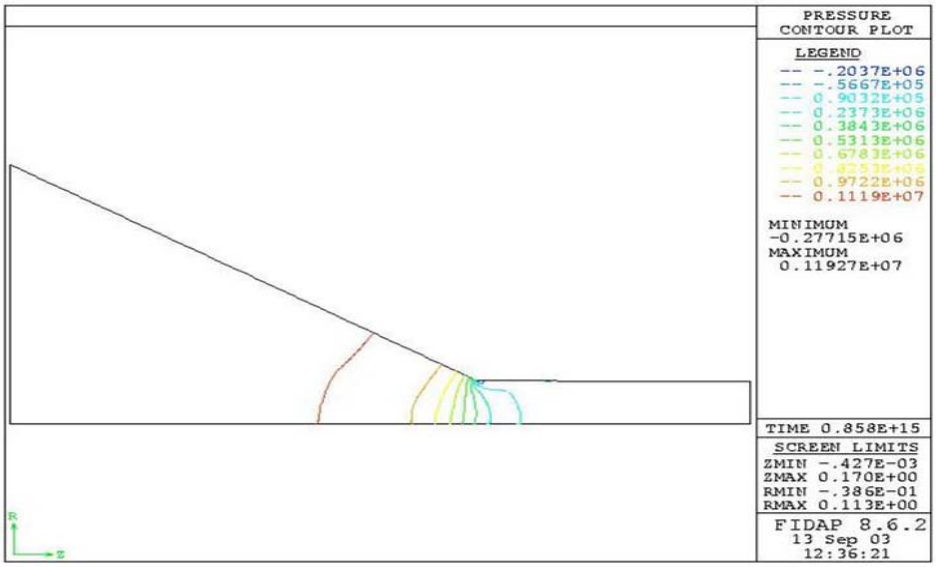

Figure 36: Pressure contour plot for FC-72 (Q = 4.416 x 10^{-7} m^3/s). Units are gm/cm s^2 (x10^1 Pa).

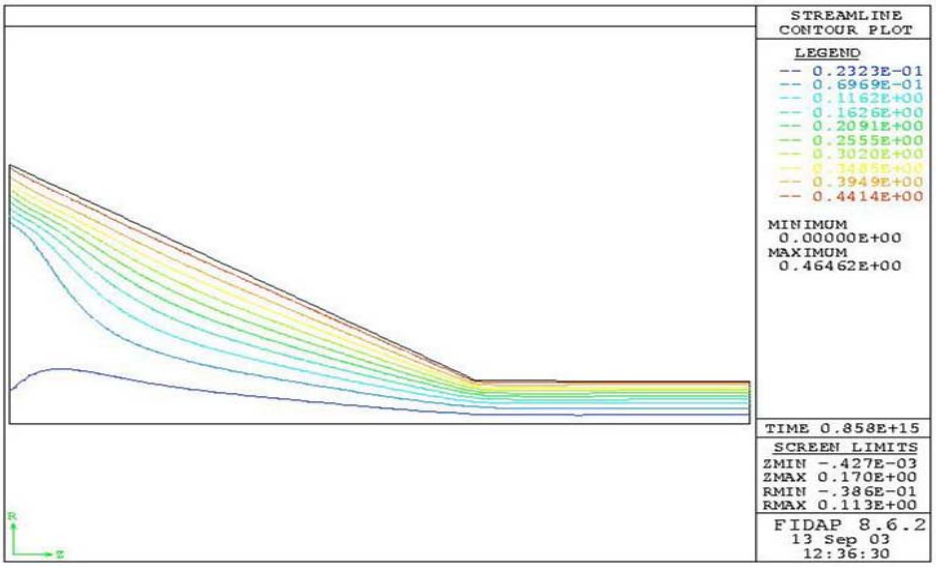

Figure 37: Streamline contour plot for FC-72 (Q = 4.416 x 10^{-7} m^3/s).

Next, the inlet flow rate of FC-72 was increased to 5.678 x 10^{-7} m^3/s. The velocity vector plot for this situation is shown in Figure 38. The maximum velocity was again located in the throat of the nozzle, and had a value of about 14.25 m/s. The free

surface for this case initiated at a height of 1.250 x 10^{-4} m, declined to 1.220 x 10^{-4} m, before increasing to a final radial height of 1.223 x 10^{-4} m. It was noted that throughout the various inlet flow rates, FC-72 produced a greater radial height for the free surface over FC-77.

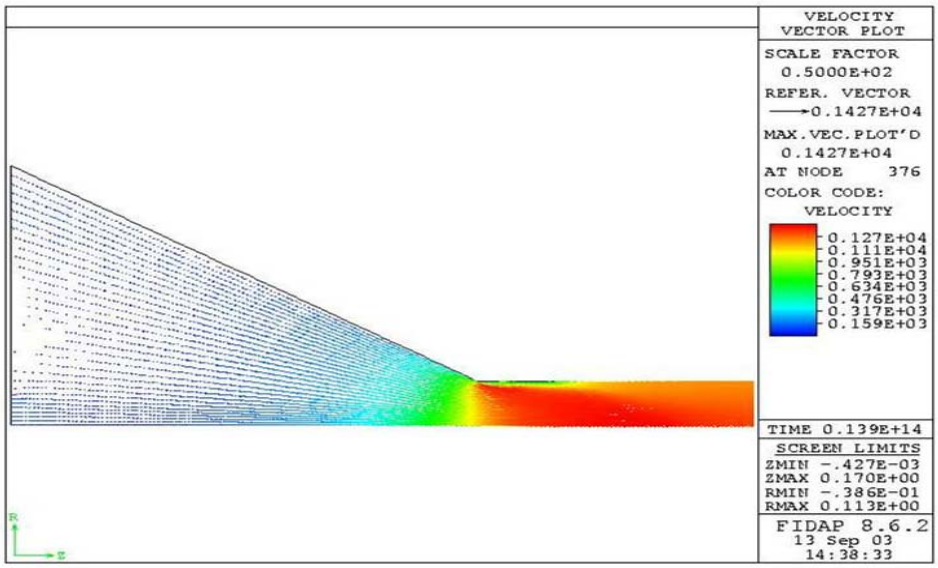

Figure 38: Velocity vector plot for FC-72 (Q = 5.678 x 10^{-7} m^3/s). Units are cm/s.

Figure 39 and Figure 40 show the pressure and streamline contour plot for this situation. The maximum pressure within the nozzle was found to be 1.96 x 10^5 Pa, while the minimum pressure was found to be about -4.66 x 10^4 Pa. The maximum pressure was present at the nozzle inlet, whereas the minimum pressure was located at the throat of the nozzle. The inlet-to-outlet pressure drop of the system was calculated to be approximately 1.81 x 10^5 Pa. The streamline contour plot shows that most of the fluid entering through the outer inlet slot follows the nozzle wall as it flows toward the inlet. However, some of that fluid does flow toward the line of symmetry of the nozzle as it

flows toward the outlet. The fluid entering through the central inlet travels in an axial path through the nozzle.

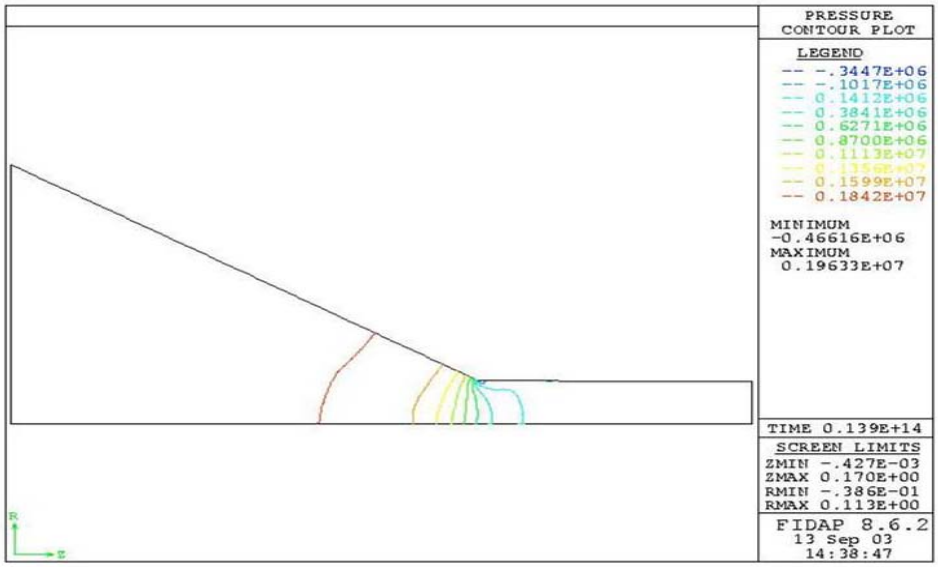

Figure 39: Pressure contour plot for FC-72 (Q = 5.678 x 10^{-7} m^3/s). Units are gm/cm s^2 (x10^1 Pa).

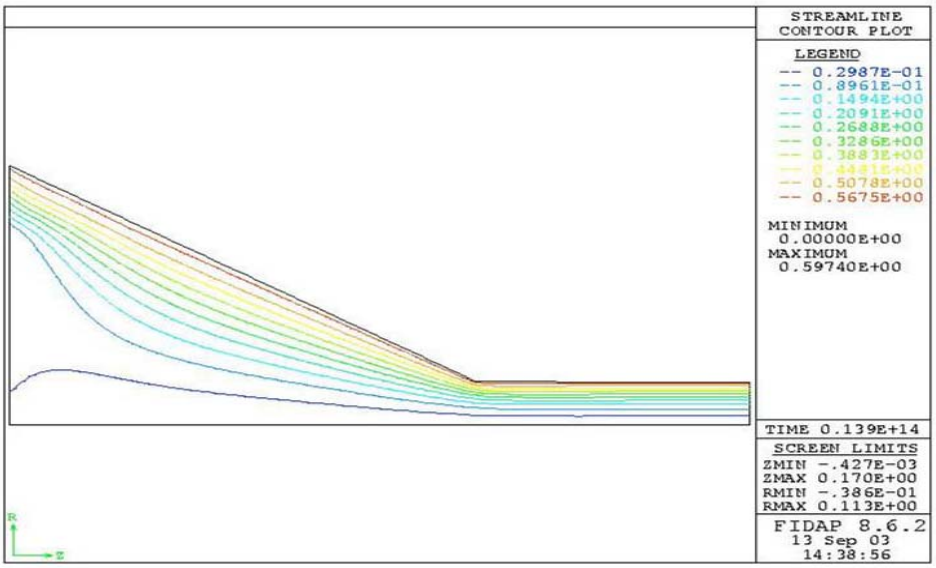

Figure 40: Streamline contour plot for FC-72 (Q = 5.678 x 10^{-7} m^3/s).

The profile of the free surface obtained when FC-72 was used as the working fluid is displayed in Figure 41 and Figure 42. It was noted that the inlet flow rate had a

very minute effect on the radial height of the free surface. However, a flow rate of 5.678 x 10^{-7} m^3/s did produce a slightly greater radial height.

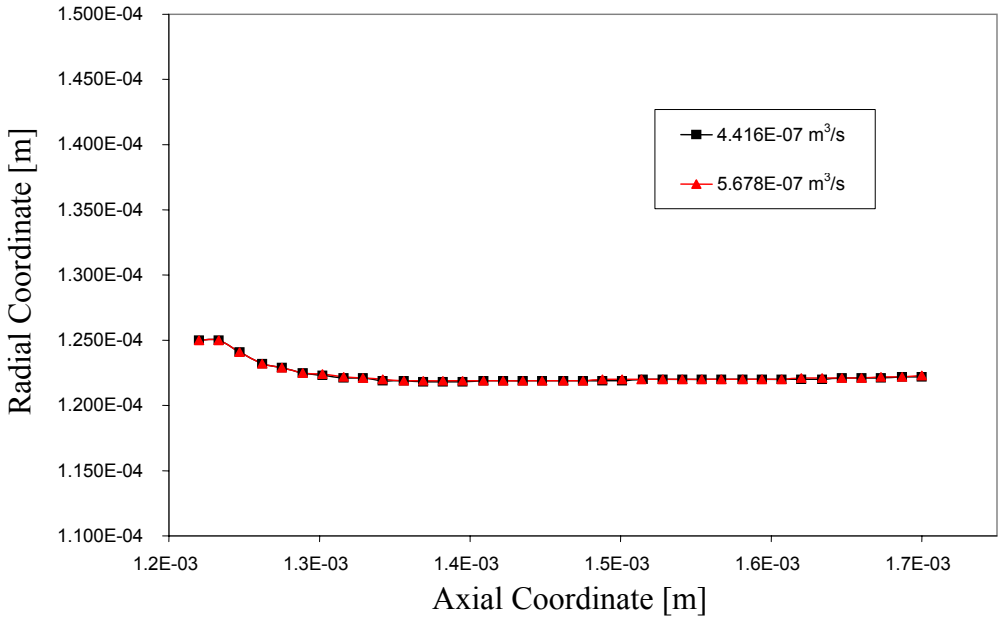

Figure 41: Free surface profile for FC-72 at various flow rates

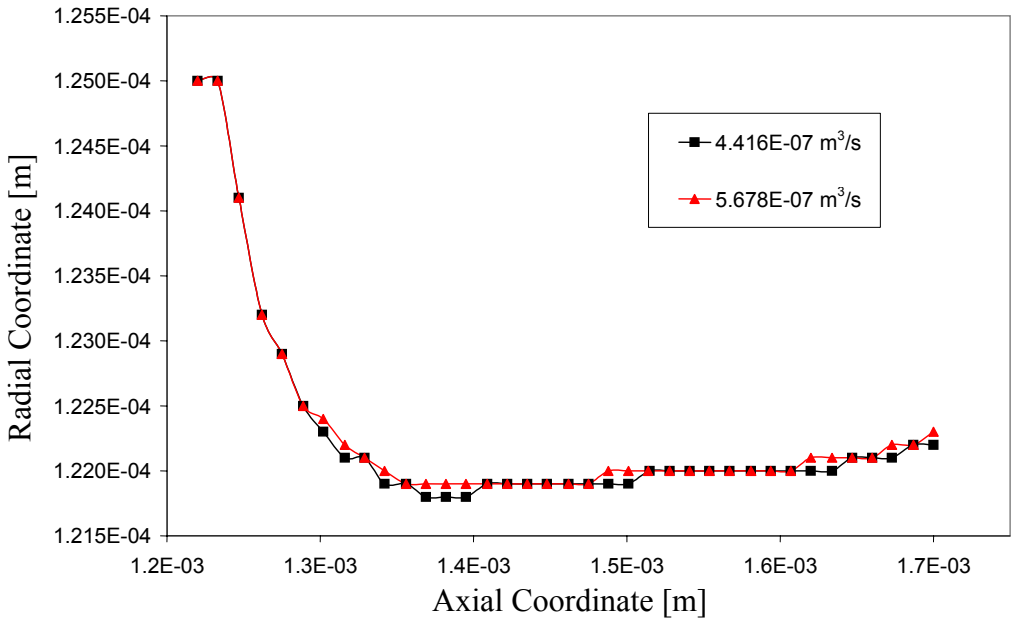

Figure 42: Magnified free surface profile for FC-72 at various flow rates

The dimensionless free surface profile based on the Reynolds number for FC-72 is shown in Figure 43. It can be seen that the free surface heights for the two Reynolds numbers are not much different. However, similar to all of the other cases, a greater Reynolds number produced a greater value for the final radial free surface height. It was noted that FC-72 produced a larger free surface height than FC-77. Since FC-72 has a viscosity almost half of that for FC-77, a larger Reynolds number is present for FC-72. Therefore, not only is the free surface height a function of velocity, but also of viscosity. A fluid with a lower viscosity has a lower shear stress. This permits the fluid to flow in a more free manner, which allows for an increase in the final height of the free surface.

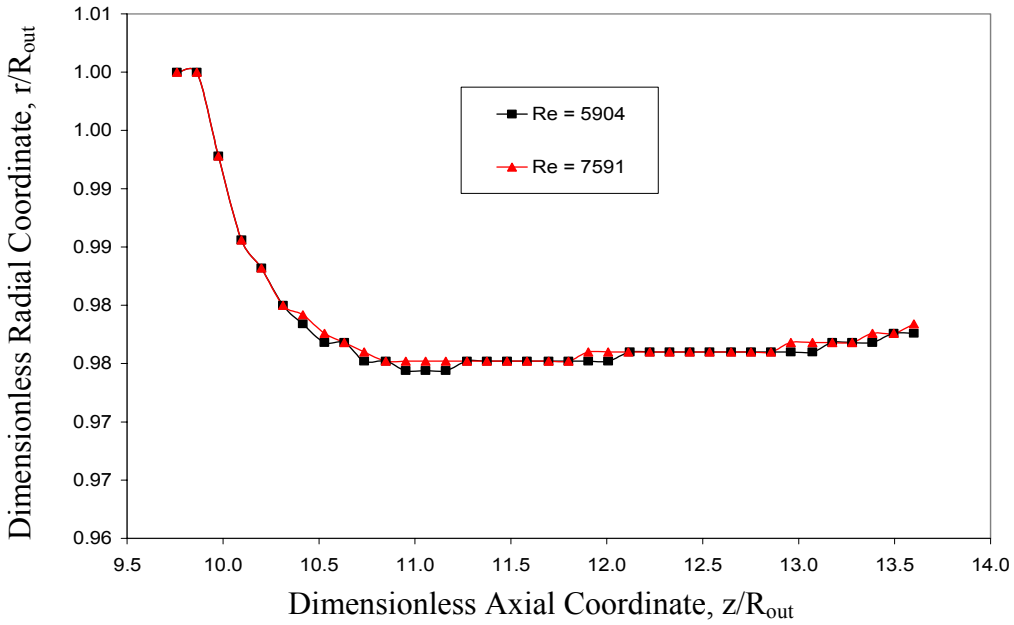

Figure 43: Dimensionless free surface profile for FC-72 (small nozzle)

5.2.3 Cavitation

Cavitation is a phenomenon that occurs when the pressure of the liquid falls below the saturated pressure of that particular liquid corresponding to the temperature of

that liquid. When this happens, the fluid begins to evaporate, which causes tiny bubbles to form at the location where the pressure is below the critical point. These bubbles will eventually erode and destroy the boundary of the nozzle. Table 12 shows the value of the cavitation number for each fluid and each flow rate for this nozzle geometry. It was observed that only FC-77 with an inlet flow rate of 1.262×10^{-7} m^3/s (Re = 803) and FC-72 with an inlet flow rate of 4.416×10^{-7} m^3/s (Re = 5904) caused cavitation. There was no cavitation found to be present in any of the other cases that were investigated thus far.

Table 12: Cavitation number for FC-77 and FC-72 in the small nozzle

Working Fluid	Saturation Pressure P_{sat} [Pa]	Reynolds Number Re [non-dim]	Minimum Pressure P_{min} [Pa]	Pressure Difference $P_{min} - P_{sat}$ [Pa]	Cavitation Number Ca [non-dim]
FC-77	5.62×10^3	803	1470	-4150	-0.353
		1607	8750	3130	0.067
		2812	26900	21280	0.148
		3615	46200	40580	0.170
FC-72	30.9×10^3	5904	27700	-3200	-0.024
		7591	46600	15700	0.070

5.2.4 Varied Nozzle Height

Another variation of the nozzle geometry was performed with FC-77 as the working fluid and 4.416×10^{-7} m^3/s as the inlet flow rate. The length of the nozzle, L, was changed from 1.22×10^{-3} m to 1.05×10^{-3} m. However, the slope of the outer wall remained the same, which caused the radius of the nozzle outlet to increase from 1.25×10^{-4} m to 2.23×10^{-4} m. The velocity vector plot for this case is depicted in Figure 44. The top plate of the nozzle was still spinning at the same calculated rate, which was

233.67 rad/sec. The maximum velocity was determined to be 3.55 m/s within the throat of the nozzle. The free surface of the fluid exiting the nozzle began at a height of 2.230 x 10^{-4} m, and decreased to a height of 2.151 x 10^{-4} m.

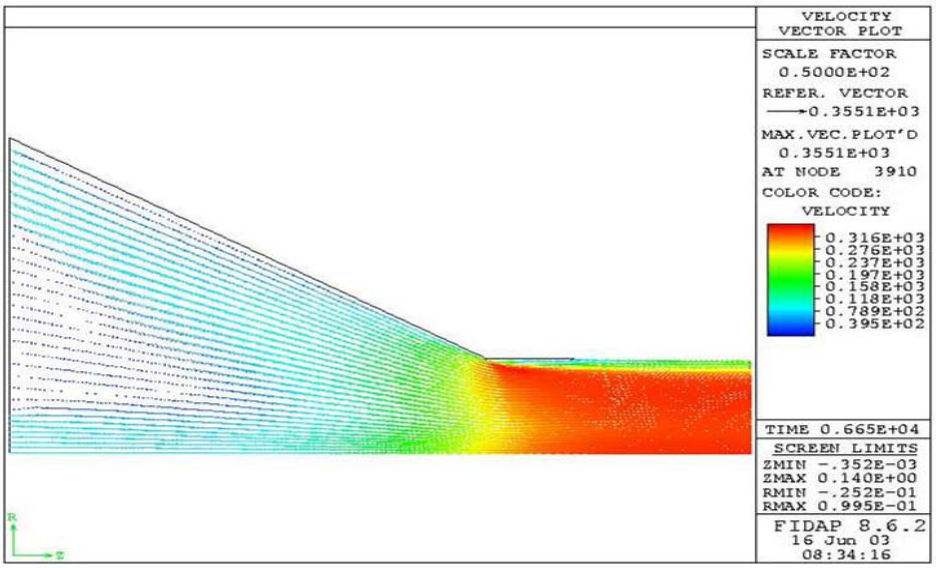

Figure 44: Velocity vector plot for FC -77 (Q = 4.416 x 10^{-7} m^3/s, L = 1.05 x 10^{-3} m). Units are cm/s.

Figure 45 and Figure 46 show the pressure and streamline contour plots for the case involving the shortened nozzle. The maximum and minimum pressure plotted was 9.90 x 10^3 Pa and -3.22 x 10^3 Pa, respectively. Again, the maximum value was located at the inlet of the nozzle, and the minimum value was located at the throat of the nozzle. The resulting inlet-to-outlet pressure drop was calculated to be 5.85 x 10^3 Pa, which is much less than the other trial involving the longer nozzle with FC-77 flowing at 4.416 x 10^{-7} m^3/s. The streamline contour plot shows that the fluid entering the central inlet has almost a purely axial flow, whereas most of the flow entering through the outer slot flows along the outer nozzle wall toward the outlet. Also, a large portion of the fluid inside the nozzle is swirling next to the rotating top plate.

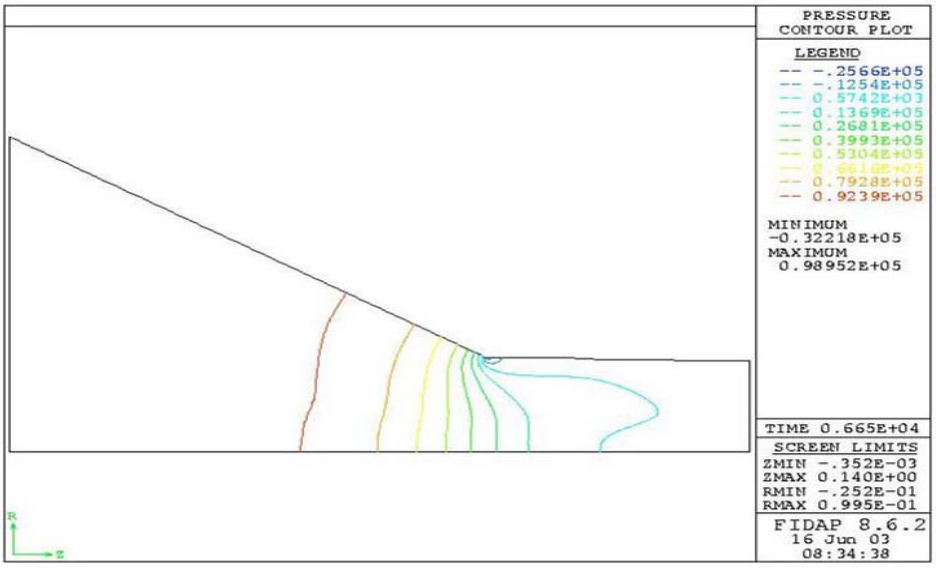

Figure 45: Pressure contour plot for FC-77 (Q = 4.416 x 10^{-7} m^3/s, L = 1.05 x 10^{-3} m). Units are gm/cm s^2 (x10^1 Pa).

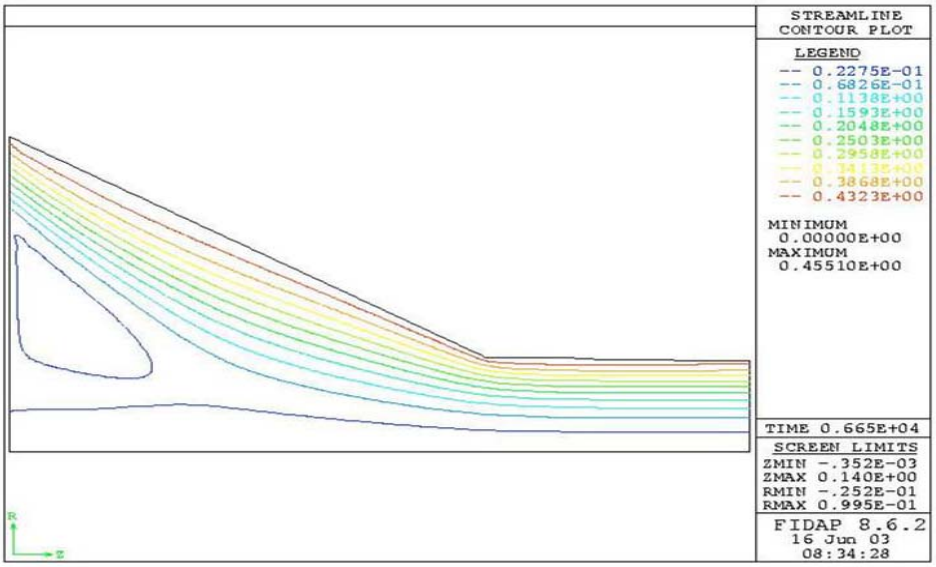

Figure 46: Streamline contour plot for FC-77 (Q = 4.416 x 10^{-7} m^3/s, L = 1.05 x 10^{-3} m)

5.2.5 Extended Free Surface

To ensure that a variation in the length of the free surface did not affect the final position of the free surface, a trial was run with an extended free surface length. For this

study, it was increased from a length of 4.8 x 10^{-4} m to 7.8 x 10^{-4} m. It was found that the variation in length did not alter the position of the free surface. Figure 47 shows the free surface profile for this situation. The profiles for the longer free surfaces are in very good comparison to the profiles involving the shorter free surface lengths.

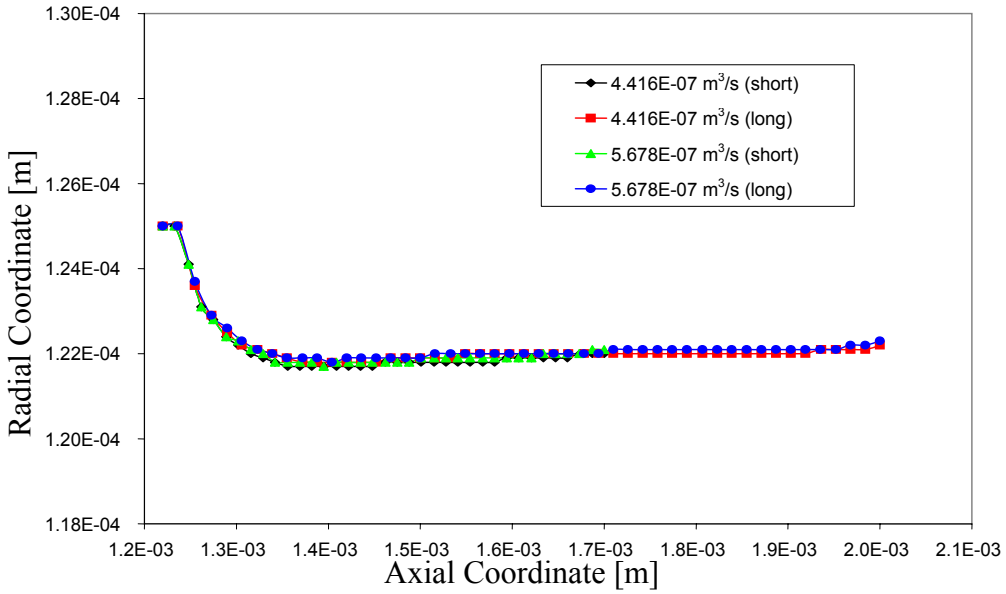

Figure 47: Free surface profile for varied free surface length

5.2.6 Initial Mesh with Upward Slope

To assure that the program was obtaining the correct free surface position of the fluid exiting the nozzle, the initial mesh of the free surface was given an upward slope. Figure 48 shows the mesh plot of this particular system. After the program was complete, it was observed that this case produced the same final position of the free surface as did the situation with an initially horizontal free surface. Therefore, it was noted that the initial free surface position did not affect the outcome that was produced. However, another mesh was created to reiterate this point.

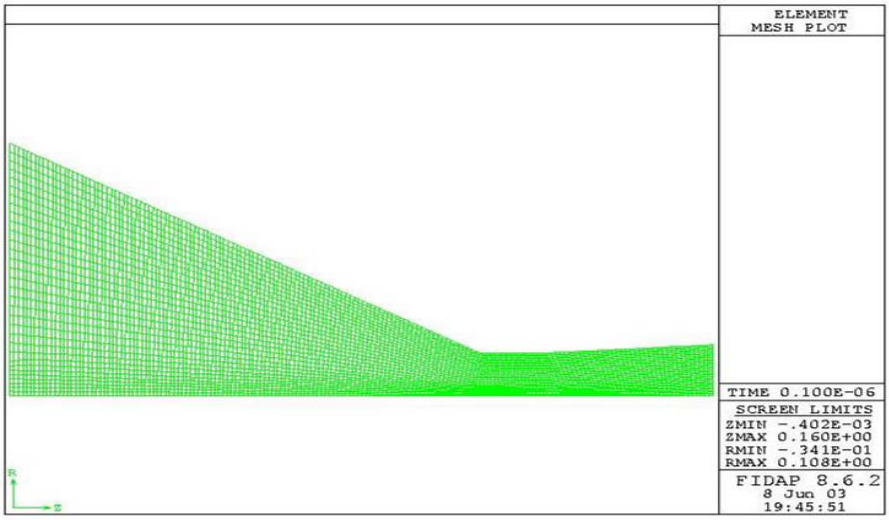

Figure 48: Mesh plot of nozzle with initial upward slope of the free surface.

5.2.7 Initial Mesh with Downward Slope

For this trial, the mesh of the free surface was initially set with a downward slope. Figure 49 shows this mesh plot. Again, this produced no effect on the final free surface position that was created. The final free surface had the same position as did the free surface obtained with an initial horizontal profile, along with an initial upward slope.

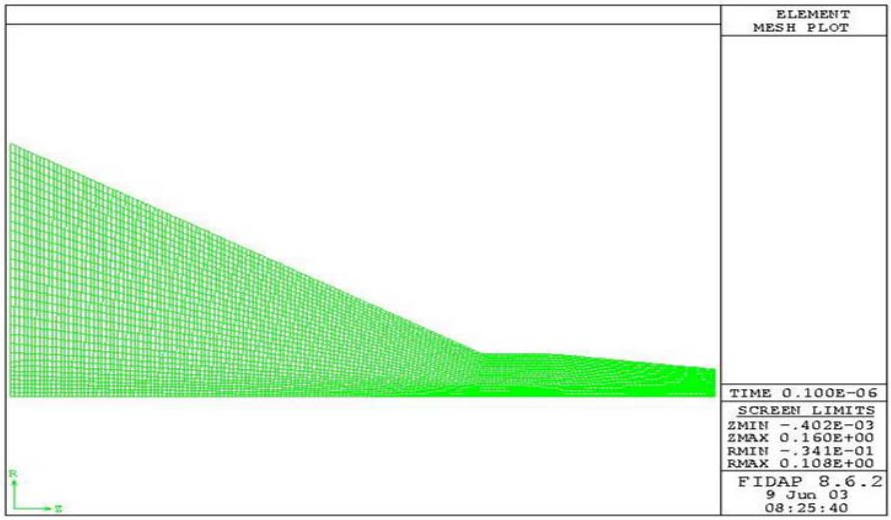

Figure 49: Mesh plot of nozzle with initial downward slope of the free surface.

5.2.8 Varying Outer Slot Location

Next, additional adjustments were made to the operating system, and the results that were produced were analyzed. The investigation of the spray exiting the nozzle involved altering the geometry of the nozzle. The most significant variation in the geometry was the location of the outer inlet slot on the nozzle. Figure 50 shows a schematic of the nozzle and the placement of the outer inlet slot. The radius for the center inlet, R_1, remained constant at 1.00 x 10^{-4} m, and then a value was chosen for R_2. The location of R_3 was then bounded by Equation 36.

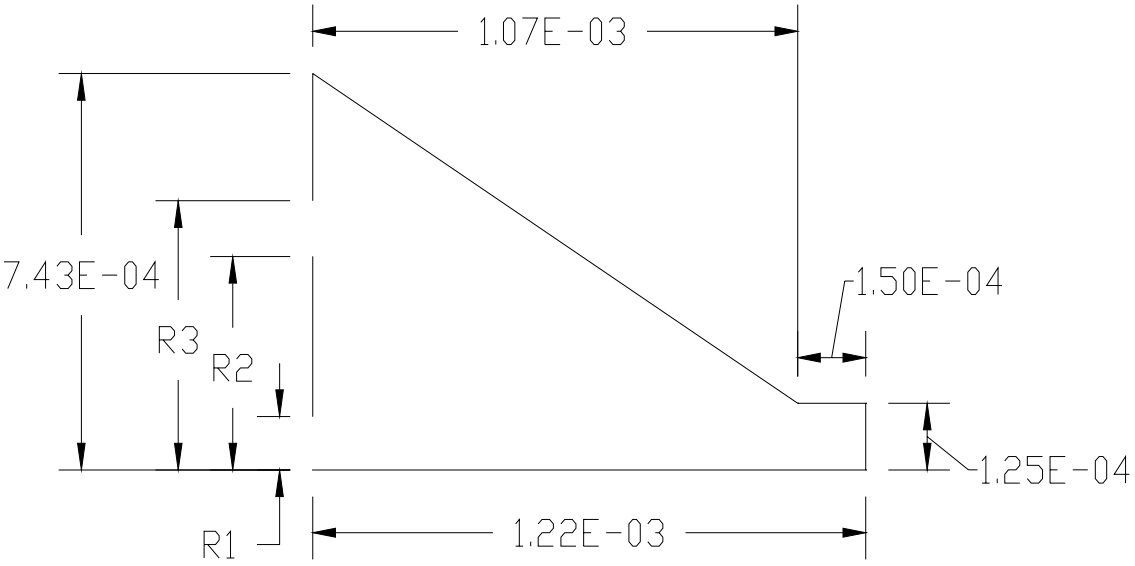

Figure 50: Schematic of nozzle with varying outer slot radii. All dimensions are in meters.

Four different values for R_2 were used in this study, with each variation subject to different fluids at different flow rates. Table 13 lists the values of R_2 that were used and the corresponding value of R_3.

Table 13: Values of R_1, R_2, and R_3 used in the investigation

R_1	R_2	R_3
1.00×10^{-4} m	2.50×10^{-4} m	3.04×10^{-4} m
1.00×10^{-4} m	4.00×10^{-4} m	4.36×10^{-4} m
1.00×10^{-4} m	5.50×10^{-4} m	5.77×10^{-4} m
1.00×10^{-4} m	7.20×10^{-4} m	7.43×10^{-4} m

The inlet velocity was then determined by Equation 37. The axial velocity is equal to V_{in} for both the center hole and the outer slot, whereas the outer slot has an additional theta velocity also equal to V_{in}. For this part of the investigation, the top plate of the nozzle remained stationary and swirl was introduced at the inlets. These problems were treated as turbulent, and the mixing length model was employed in FIDAP. This was done so that the Newton-Raphson method could be used. The following table illustrates the different inlet flow rates and the inlet velocities that they produce.

Table 14: Inlet velocities for the given flow rates

Inlet Flow Rate Q $[m^3/s]$	Inlet Velocity for Center Hole V_z [m/s]	Axial Component of Inlet Velocity for Outer Slot V_z [m/s]	Theta Component of Inlet Velocity for Outer Slot V_θ [m/s]
4.416×10^{-7}	3.514	3.514	3.514
5.678×10^{-7}	4.519	4.519	4.519

5.2.8.1 R_2 Equal to 2.50×10^{-4} m

As was mentioned previously, this study involved the use of different fluids, as well as different flow rates. The different fluids used were FC-77, FC-72, FC-87, and

methanol. All of these fluids were chosen because of their compatibility with electronics, and the possibility of being used as a cooling agent for these electronics. The first geometry that was observed was where R_2 was 2.50 x 10^{-4} m. This was first observed with FC-77 as the working fluid. Figure 51 shows the vector velocity plot for this geometry with an inlet flow rate of 4.416 x 10^{-7} m^3/s. The maximum velocity was found to be approximately 8.75 m/s located within the throat of the nozzle. An important value is the final height of the free surface. For this case, the free surface began at a height of 1.250 x 10^{-4} m, gradually decreased to 1.215 x 10^{-4} m, but then rose again to end at a height of 1.239 x 10^{-4} m. This free surface produced a cone angle determined to be 1.51 degrees, which was the lowest value observed for this particular nozzle geometry.

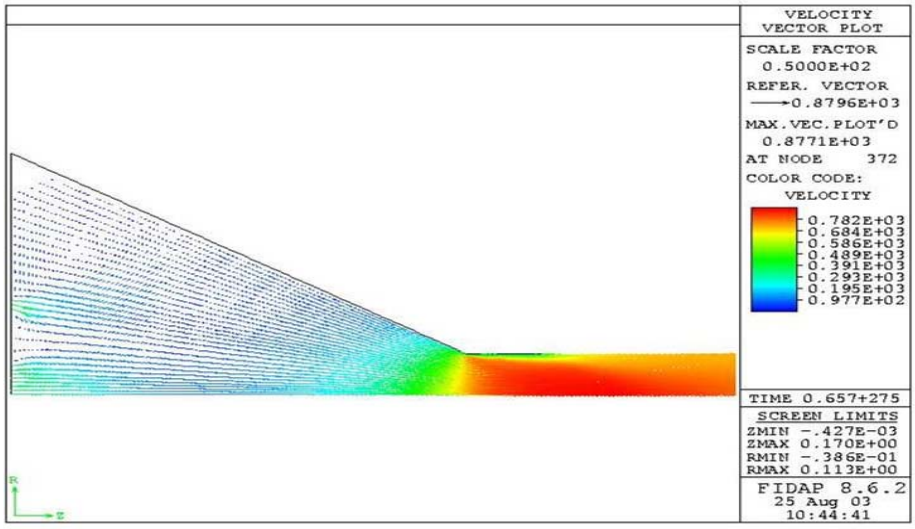

Figure 51: Velocity vector plot for FC-77 (Q = 4.416 x 10^{-7} m^3/s, R_2 = 2.5 x 10^{-4} m). Units are cm/s.

Figure 52 and Figure 53 show the pressure and streamline contour plots, respectively, for the same case involving FC-77 with a flow rate of 4.416 x 10^{-7} m^3/s. The pressure drop from the inlet to the outlet was calculated to be 7.25 x 10^4 Pa. As with all of the cases, the fluid increases speed in the throat of the nozzle, this in turn caused the

pressure at that area to decrease. The streamline contour plot shows that as the fluid enters through the outer slot, some of the fluid begins to swirl at the top of the nozzle before it follows the outer wall towards the outlet. The fluid entering through the center hole briefly moves toward the outer wall, then flows in the direction of the outlet.

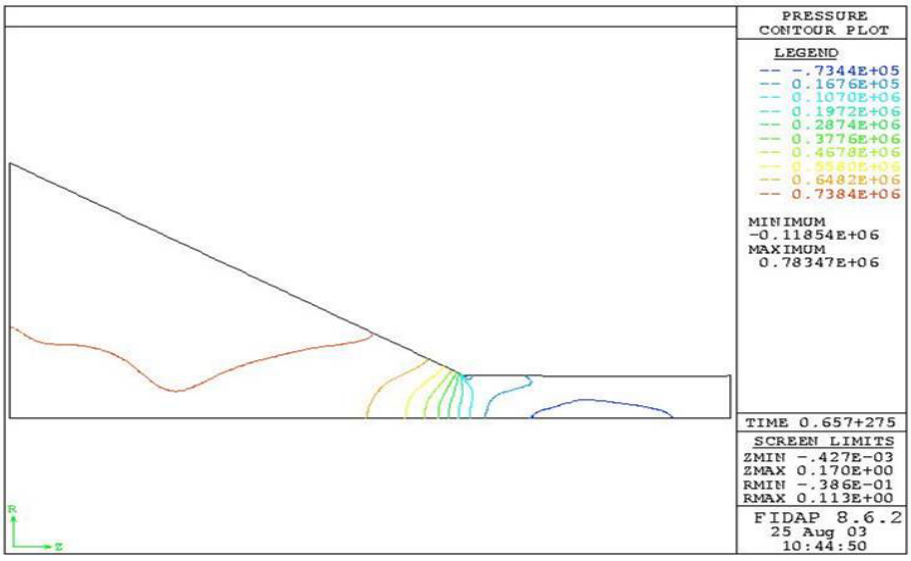

Figure 52: Pressure contour plot for FC-77 ($Q = 4.416 \times 10^{-7}$ m^3/s, $R_2 = 2.5 \times 10^{-4}$ m). Units are g/cm s^2 ($x10^1$ Pa).

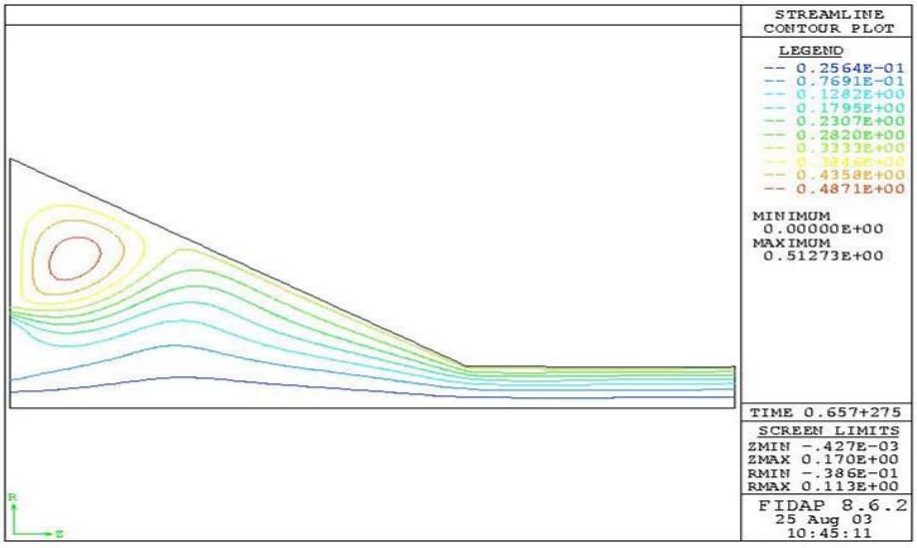

Figure 53: Streamline contour plot for FC-77 ($Q = 4.416 \times 10^{-7}$ m^3/s, $R_2 = 2.5 \times 10^{-4}$ m)

Next, the inlet flow rate of the FC-77 was increased to 5.678 x 10^{-7} m^3/s and used in the nozzle having the same geometry as the above case. Figure 54 shows the vector velocity plot for this trial. The maximum velocity was again located in the throat of the nozzle; however, its value has increased to 11.25 m/s. The height of the free surface began at 1.250 x 10^{-4} m, declined to 1.215 x 10^{-4} m, then increased to 1.243 x 10^{-4} m. This value is greater than that when the lesser flow rate was used. The cone angle for this case was calculated as about 1.73 degrees. It was expected that a faster moving fluid would provide a greater free surface height, as well as a greater cone angle.

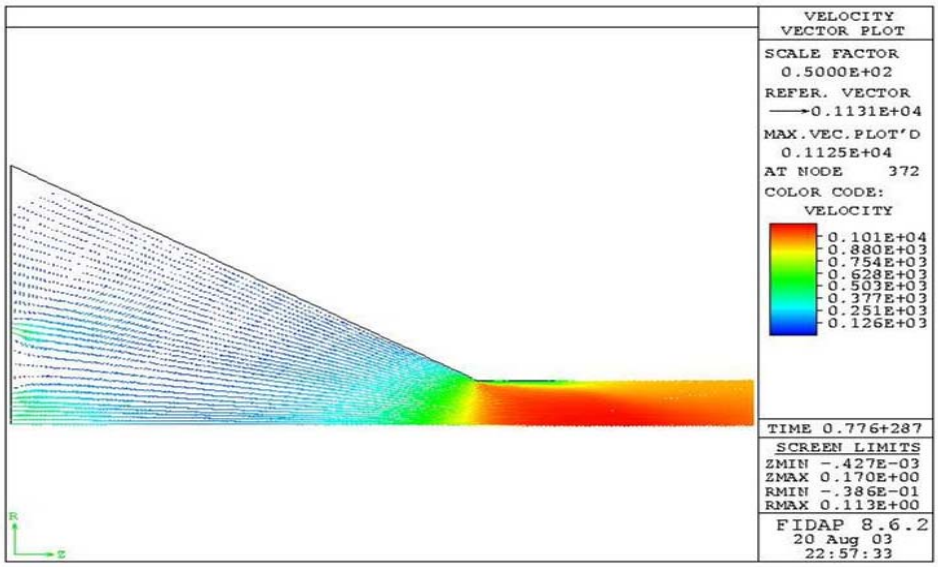

Figure 54: Vector velocity plot for FC-77 (Q = 5.678 x 10^{-7} m^3/s, R_2 = 2.5 x 10^{-4} m). Units in cm/s.

Figure 55 shows the pressure contour plot for this case. The inlet-to-outlet pressure drop was determined to be 1.04 x 10^5 Pa. Again, there was high pressure towards the inlets of the nozzle, and then it decreased as the outlet was approached. Figure 56 details the streamline contour plot. It shows that the fluid is behaving the same way it did with 4.416 x 10^{-7} m^3/s as the inlet flow rate. After entering the inlets, the fluid

tends to go towards the outer wall of the nozzle before making its way to the outlet. Again, some of the fluid begins to swirl in the top part of the nozzle.

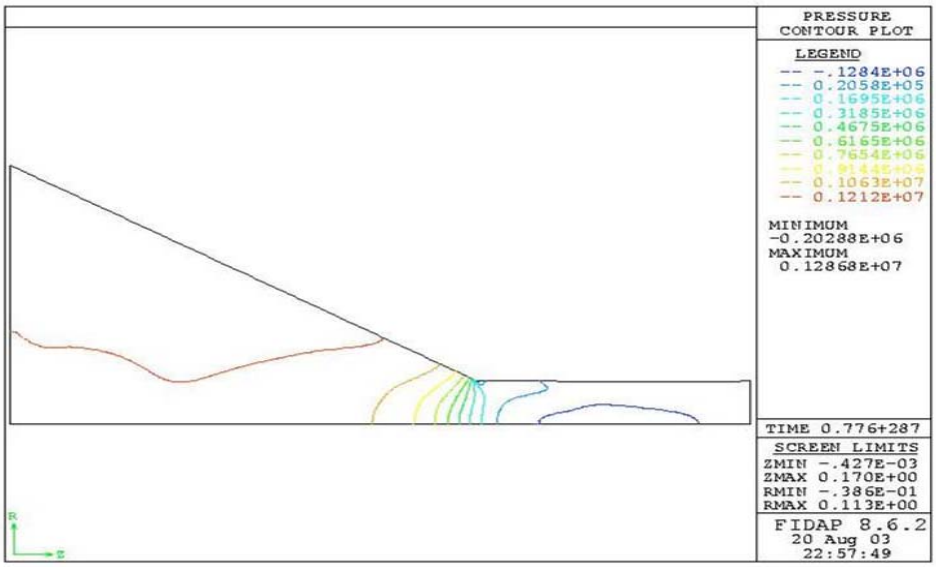

Figure 55: Pressure contour plot for FC-77 ($Q = 5.678 \times 10^{-7}$ m^3/s, $R_2 = 2.5 \times 10^{-4}$ m). Units are gm/cm s^2 ($x10^1$ Pa).

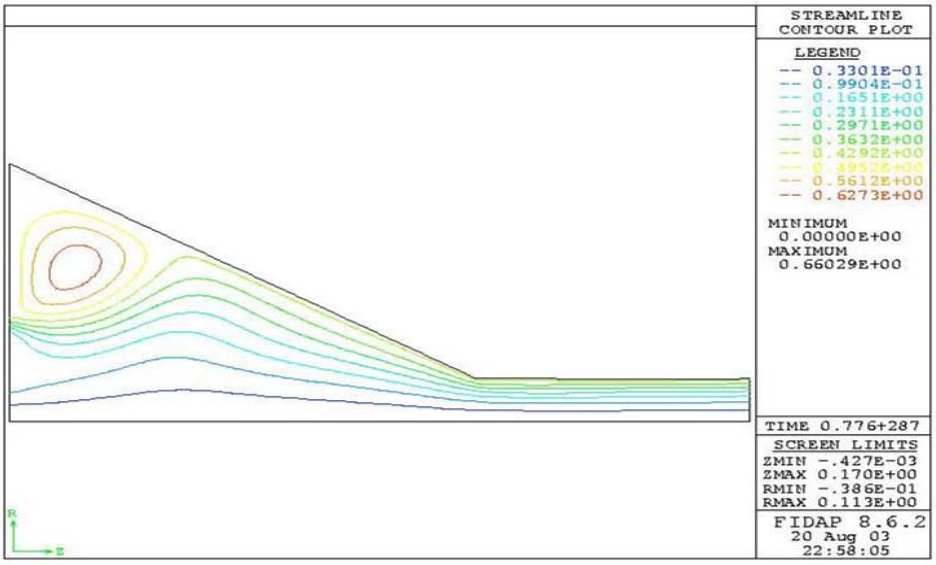

Figure 56: Streamline contour plot for FC-77 ($Q = 5.678 \times 10^{-7}$ m^3/s, $R_2 = 2.5 \times 10^{-4}$ m)

The next variation performed with this geometry was changing the working fluid to FC-72. This fluid has a lower density, lower viscosity, and a lower surface tension than FC-77. The first case to be examined involved was an inlet flow rate of 4.416 x 10^{-7} m^3/s. Figure 57 shows the velocity vector plot for this scenario. The maximum velocity was about 8.72 m/s within the throat of the nozzle. The free surface height began at 1.250 x 10^{-4} m, gradually decreased to 1.216 x 10^{-4} m, and then increased to a final radial height of 1.248 x 10^{-4} m. The cone angle calculated for this scenario was determined to be 2.05 degrees.

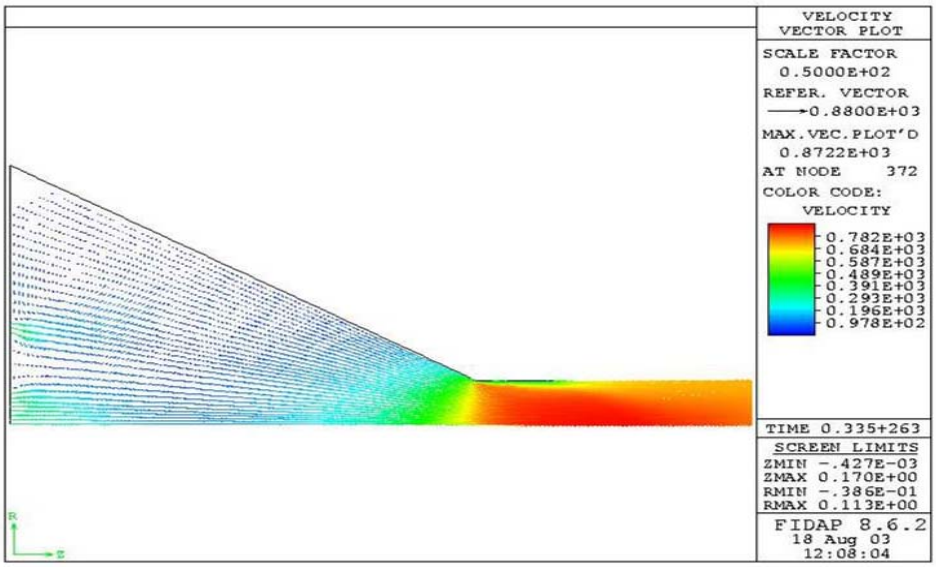

Figure 57: Velocity vector plot for FC-72 (Q = 4.416x 10^{-7} m^3/s, R_2 = 2.5 x 10^{-4} m) . Units are cm/s.

The pressure contour plot is depicted in Figure 58. The inlet-to-outlet pressure drop is extremely similar to the pressure drop found with FC-77 as the working fluid. The pressure drop for this case was found to be about 7.23 x 10^4 Pa. Figure 59 shows the streamline contour plot. This streamline plot is also similar to the trial with FC-77 as the working fluid. It shows that as the fluid enters the nozzle, a portion of it begins to swirl

in the top region, whereas the rest of the fluid moves towards the outer wall as it proceeds to the outlet.

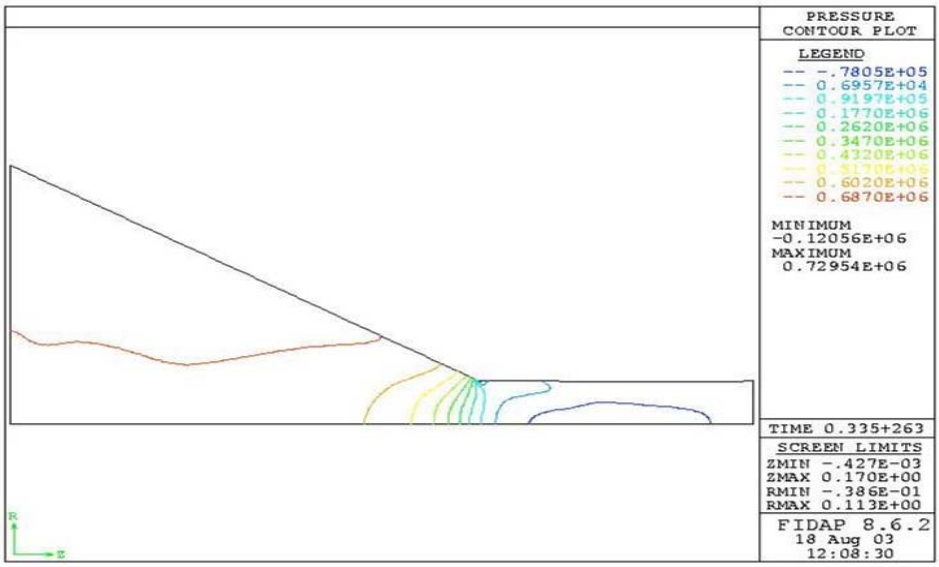

Figure 58: Pressure contour plot for FC-72 ($Q = 4.416 \times 10^{-7}$ m^3/s, $R_2 = 2.5 \times 10^{-4}$ m). Units are gm/cm s^2 ($x10^1$ Pa).

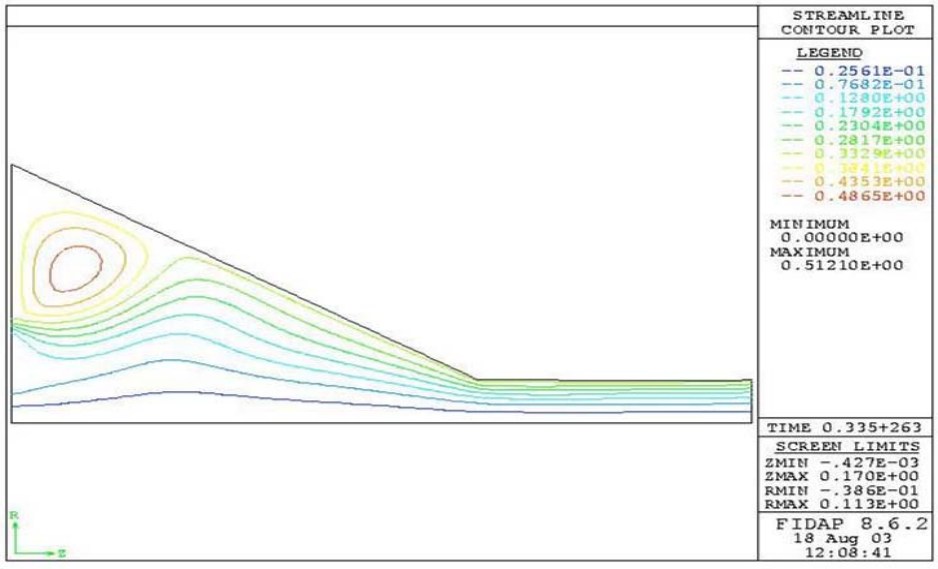

Figure 59: Streamline contour plot for FC-72 ($Q = 4.416 \times 10^{-7}$ m^3/s, $R_2 = 2.5 \times 10^{-4}$ m)

The next variation in the study executed with the nozzle geometry having R_2 equal to 2.50 x 10^{-4} m is using FC-72 as the working fluid with an inlet flow rate of 5.678 x 10^{-7} m^3/s. Figure 60 shows the velocity vector plot for this particular case. The maximum velocity was found to be about 11.21 m/s, which is very fast. The initial free surface height was 1.250 x 10^{-4} m. After exiting the nozzle, the fluid decreased to a height of 1.217 x 10^{-4} m, before gradually increasing to a final height of 1.251 x 10^{-4} m, which resulted in a cone angle of approximately 2.27 degrees.

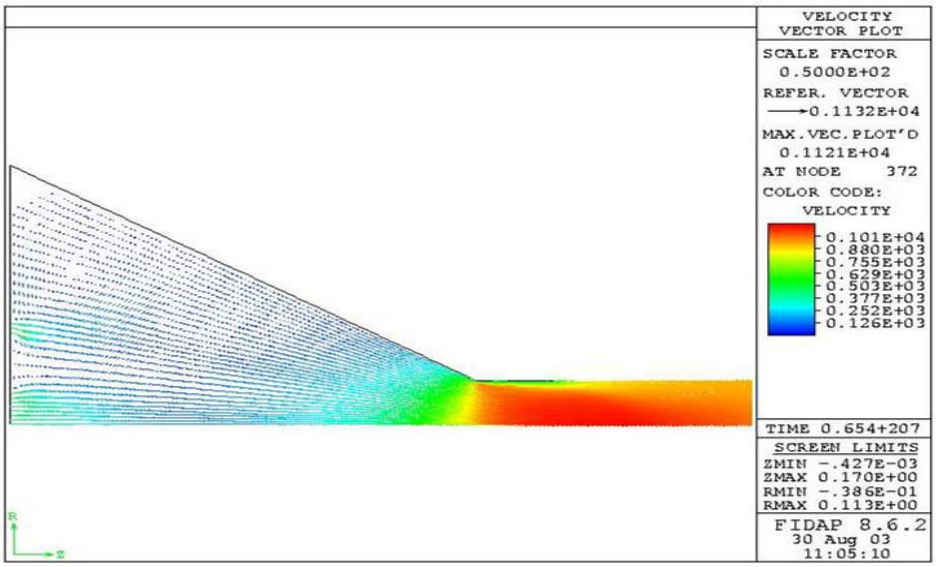

Figure 60: Velocity vector plot for FC-72 (Q = 5.678 x 10^{-7} m^3/s, R_2 = 2.5 x 10^{-4} m). Units are cm/s.

Figure 61 shows the pressure contour plot for this case. The maximum pressure found was 1.20 x 10^5 Pa, whereas the minimum pressure was found to be -2.04 x 10^4 Pa. The pressure drop from the inlet to the outlet of the nozzle was calculated to be approximately 9.85 x 10^4 Pa, which is very similar to the value obtained for FC-77 with an inlet flow rate of 5.678 x 10^{-7} m^3/s. A streamline contour plot for FC-72 traveling at 5.678 x 10^{-7} m^3/s is shown in Figure 62. The movement of the fluid through the nozzle is

observed to be very similar for all of the trials. After the fluid enters the nozzle through the outer slot, it moves toward the outer wall, then down towards the outlet. The fluid entering through the center hole briefly flows toward the outer wall before moving to the outlet of the nozzle.

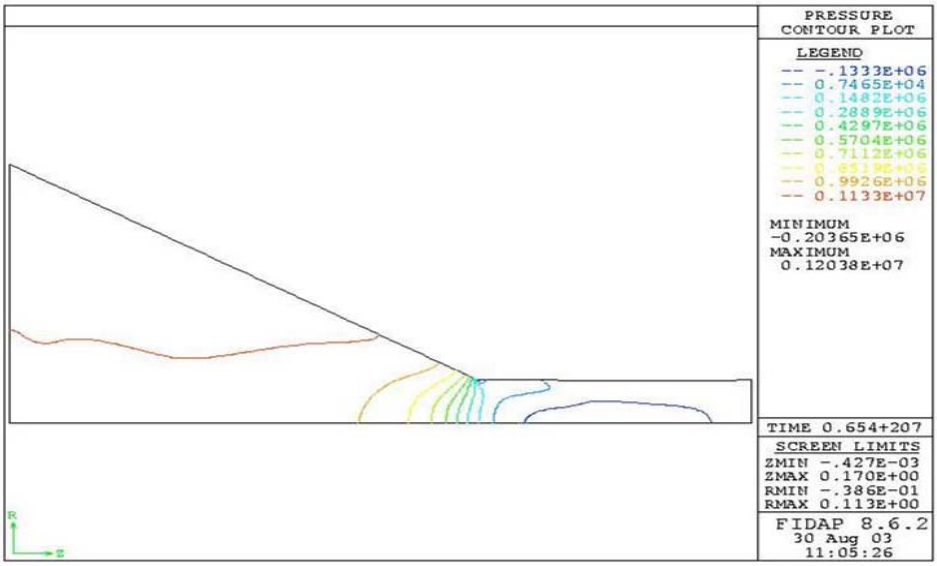

Figure 61: Pressure contour plot for FC-72 ($Q = 5.678 \times 10^{-7}$ m^3/s, $R_2 = 2.5 \times 10^{-4}$ m). Units are gm/cm s^2 ($x10^1$ Pa).

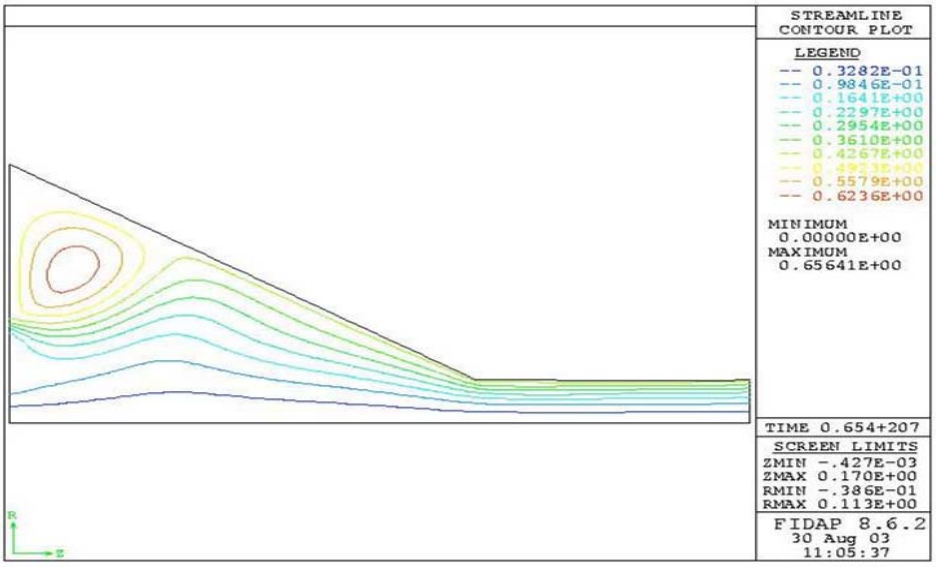

Figure 62: Streamline contour plot for FC-72 ($Q = 5.678 \times 10^{-7}$ m^3/s, $R_2 = 2.5 \times 10^{-4}$ m)

Next, FC-87 was used as the working fluid with 4.416 x 10^{-7} m^3/s as the inlet flow rate. Figure 63 shows the velocity vector plot for this situation. The maximum velocity was again located in the throat of the nozzle and had a value of about 8.75 m/s. Beginning at a height of 1.250 x 10^{-4} m, the free surface dipped to a minimum height of 1.217 x 10^{-4} m before rising again to a final height of 1.251 x 10^{-4} m, which caused a cone angle of 2.27 degrees to be present. This proved to be the largest value of the free surface height and cone angle where the parameters included R_2 equal to 2.50 x 10^{-4} m and the inlet flow rate equal to 4.416 x 10^{-7} m^3/s.

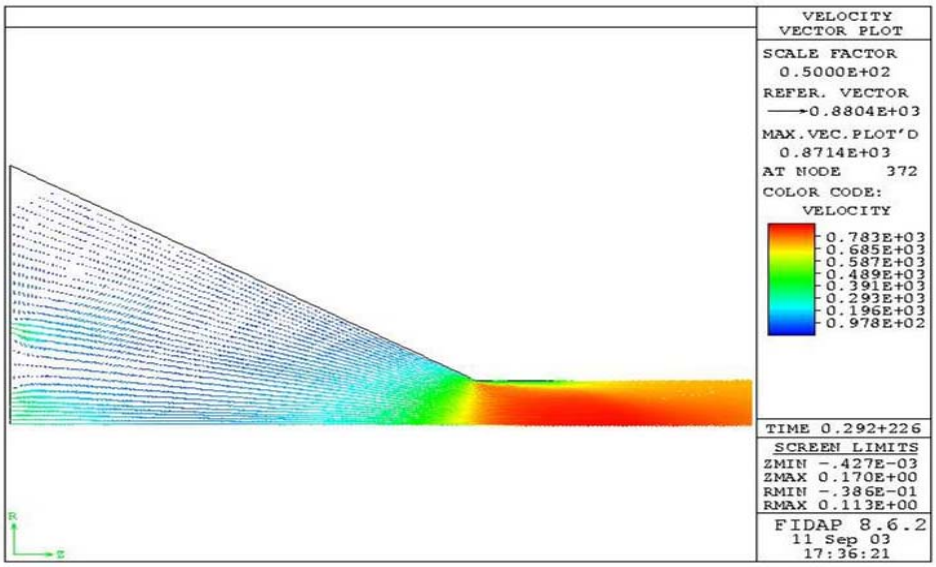

Figure 63: Velocity vector plot for FC-87 (Q = 4.416 x 10^{-7} m^3/s, R_2 = 2.5 x 10^{-4} m). Units are cm/s.

The pressure and streamline contour plots are shown in Figure 64 and Figure 65. The maximum pressure within the nozzle was determined to be 7.06 x 10^4 Pa, whereas the minimum pressure was found to be -1.21 x 10^4 Pa. The pressure drop from the inlet to the outlet of the nozzle was calculated as 7.18 x 10^4 Pa. The streamline contour plot shows that the fluid entering through the outer inlet slot flows toward the line of

symmetry, and then flows toward the outer wall as it moves through the nozzle. A pocket of swirling fluid formed just to the outside of the outer inlet slot. A portion of the fluid entering through that slot got caught in that pocket. The fluid entering through the central inlet flowed almost purely in the axial direction to the outlet of the nozzle.

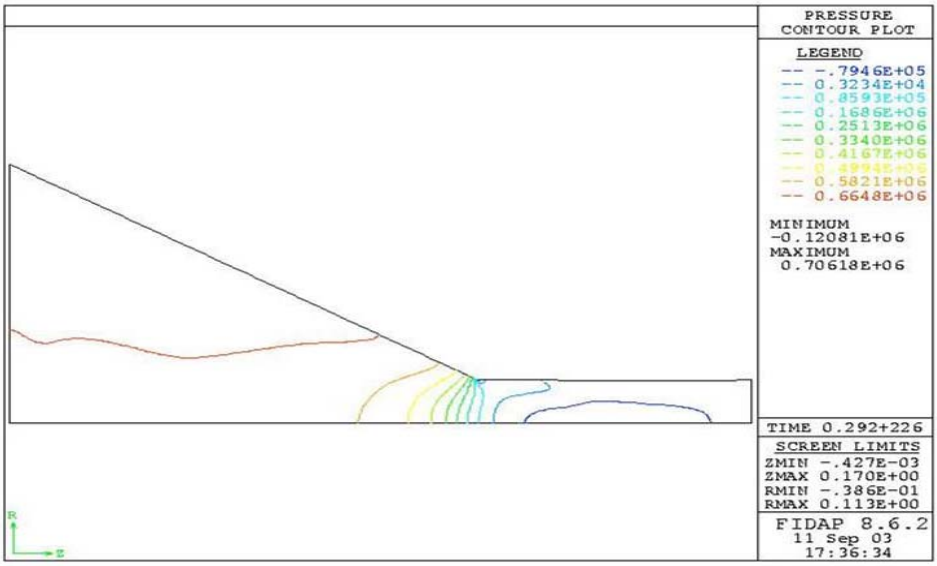

Figure 64: Pressure contour plot for FC-87 (Q = 4.416 x 10^{-7} m^3/s, R_2 = 2.5 x 10^{-4} m). Units are gm/cm s^2 (x10^1 Pa).

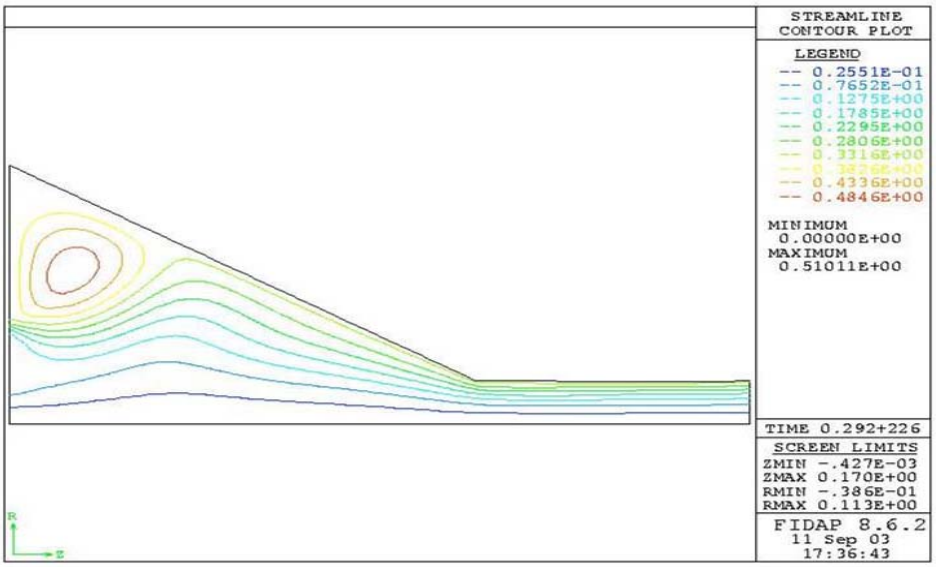

Figure 65: Streamline contour plot for FC-87 (Q = 4.416 x 10^{-7} m^3/s, R_2 = 2.5 x 10^{-4} m)

Still using FC-87 as the working fluid, the flow rate was increased to 5.678 x 10^{-7} m^3/s. The velocity vector plot for this scenario is shown in Figure 66. The maximum velocity within the nozzle was found to be approximately 11.20 m/s. The free surface began at a radial height of 1.250 x 10^{-4} m, decreased to 1.217 x 10^{-4} m, and then increased to a final height of 1.253 x 10^{-4} m. The cone angle for these parameters was calculated as 2.38 degrees. Again, this fluid produced the greatest radial height of the free surface, as well as the greatest cone angle for the studies including similar parameters.

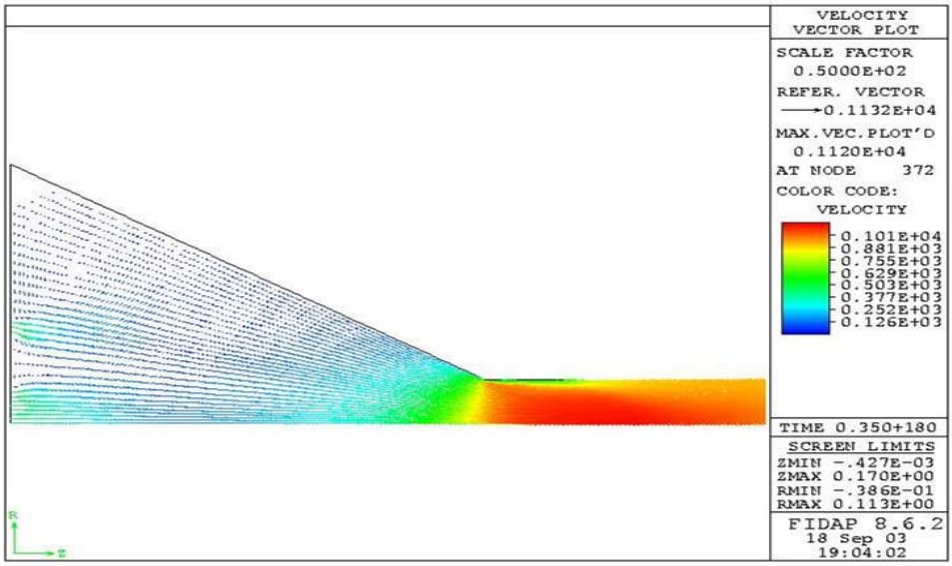

Figure 66: Velocity vector plot for FC-87 (Q = 5.678 x 10^{-7} m^3/s, R_2 = 2.5 x 10^{-4} m). Units are cm/s.

Figure 67 and Figure 68 show the pressure contour plot and the streamline contour plot, respectively. The maximum pressure within the nozzle was found to be 1.17 x 10^5 Pa, while the minimum pressure was found to be -2.07 x 10^4 Pa. The inlet-to-outlet pressure drop was then calculated to be about 1.19 x 10^5 Pa. This value is slightly larger than the values obtained from the other fluids. The streamline contour plot shows results that are similar to all of the streamline plots for this nozzle geometry. Some of the

fluid entering through the outer inlet slot began to swirl near the top plate of the nozzle, while the rest of the fluid flowed toward the outer wall before heading toward the outlet.

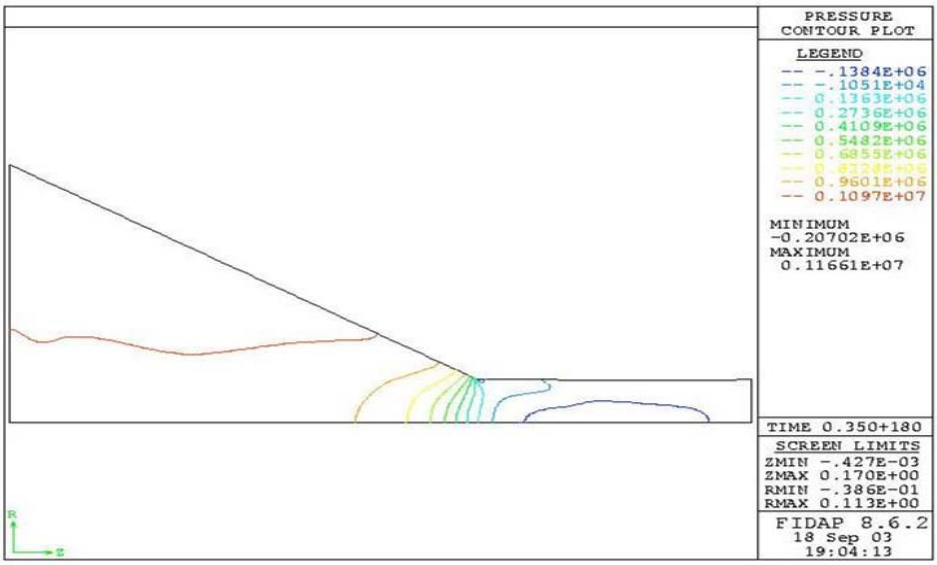

Figure 67: Pressure contour plot for FC-87 ($Q = 5.678 \times 10^{-7}$ m^3/s, $R_2 = 2.5 \times 10^{-4}$ m). Units are gm/cm s^2 ($x10^1$ Pa).

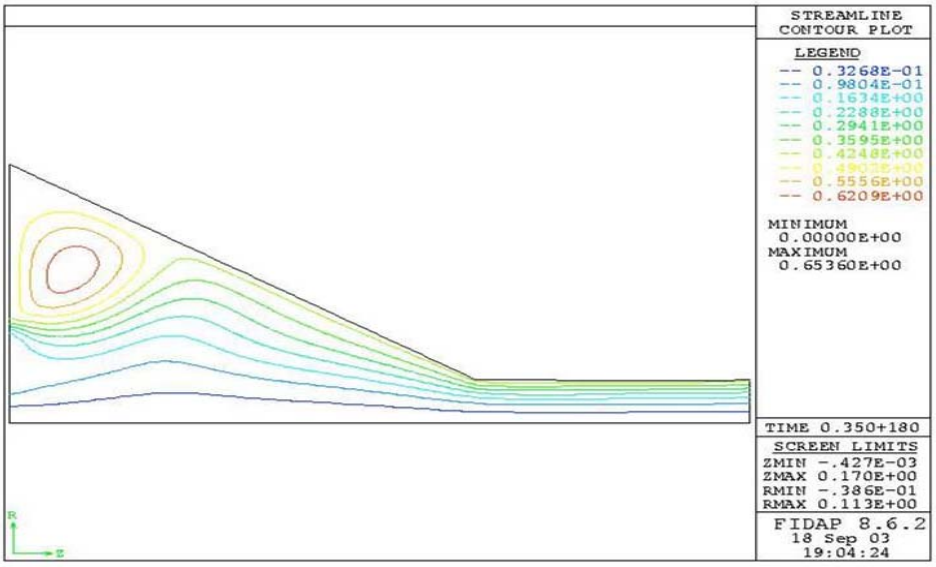

Figure 68: Streamline contour plot for FC-87 ($Q = 5.678 \times 10^{-7}$ m^3/s, $R_2 = 2.5 \times 10^{-4}$ m)

The final variations performed on this particular nozzle geometry involved Methanol as the working fluid. This fluid is the least dense fluid used in the investigation, but it has the greatest surface tension out of all of the fluids that were studied. Figure 69 shows the velocity vector plot for Methanol with an inlet flow rate of 4.416×10^{-7} m^3/s. Again, the maximum velocity within the nozzle occurred at the location of the throat and had a magnitude of about 8.75 m/s. The radial height of the free surface was initially at 1.250×10^{-4} m before it decreased to about 1.216×10^{-4} m, and then rose again to a final height of 1.241×10^{-4} m, which produced a cone angle of only 1.62 degrees.

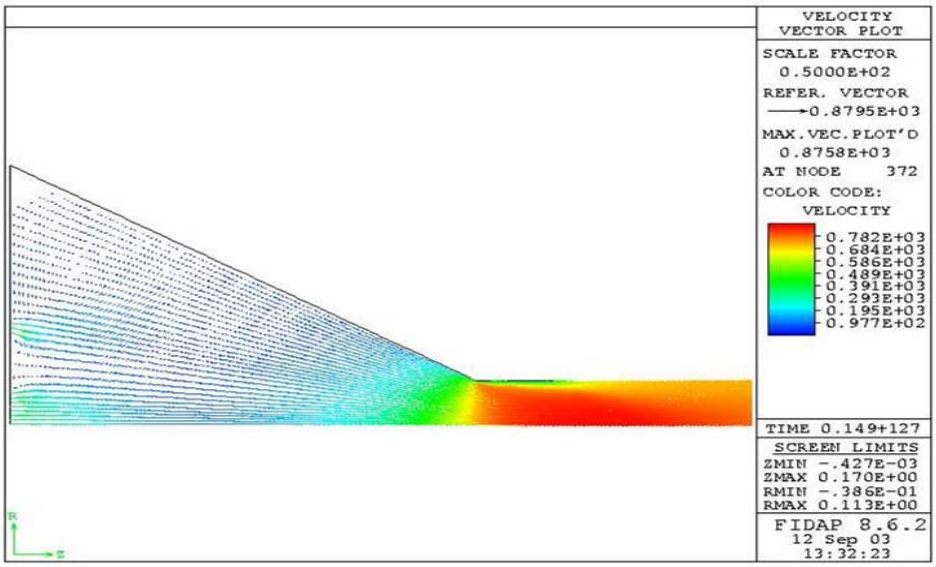

Figure 69: Velocity vector plot for Methanol ($Q=4.416 \times 10^{-7}$ m^3/s, $R_2 = 2.5 \times 10^{-4}$ m). Units are cm/s.

Figure 70 and Figure 71 show the pressure contour plot and the streamline contour plot for this situation. The maximum pressure within the nozzle was found to be 3.44×10^4 Pa, while the minimum pressure was -5.34×10^3 Pa. These values are much smaller than any of the other trials. The pressure drop was then calculated to be about

3.44 x 10^4 Pa, which is about half of that for the other trials using the same flow rate and nozzle geometry. The streamline contour plot shows results very similar to the other trials. The fluid entering through the central inlet flows axially toward the outlet, whereas the fluid entering through the outer inlet slot first flows toward the nozzle wall.

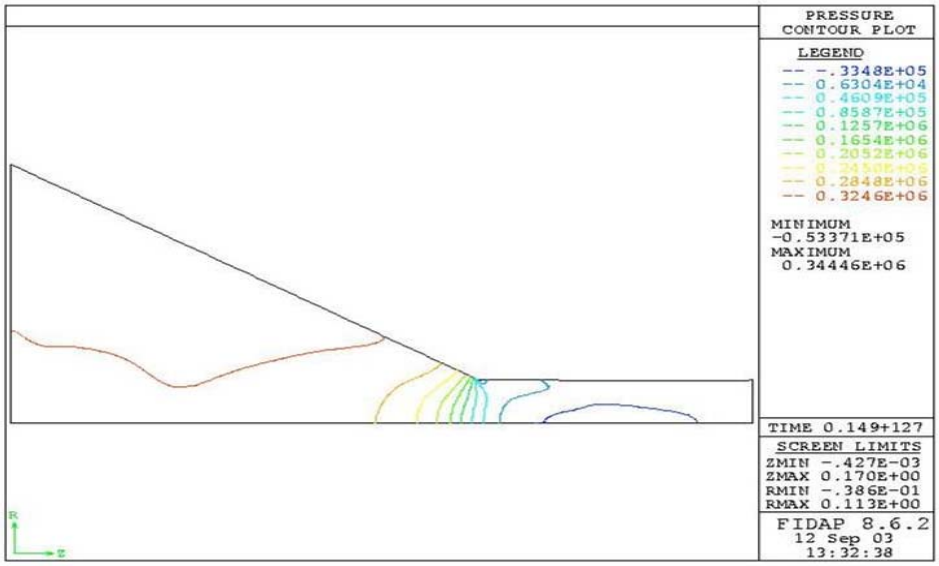

Figure 70: Pressure contour plot for Methanol (Q = 4.416 x 10^{-7} m^3/s, R_2 = 2.5 x 10^{-4} m). Units are gm/cm s^2 (x10^1 Pa).

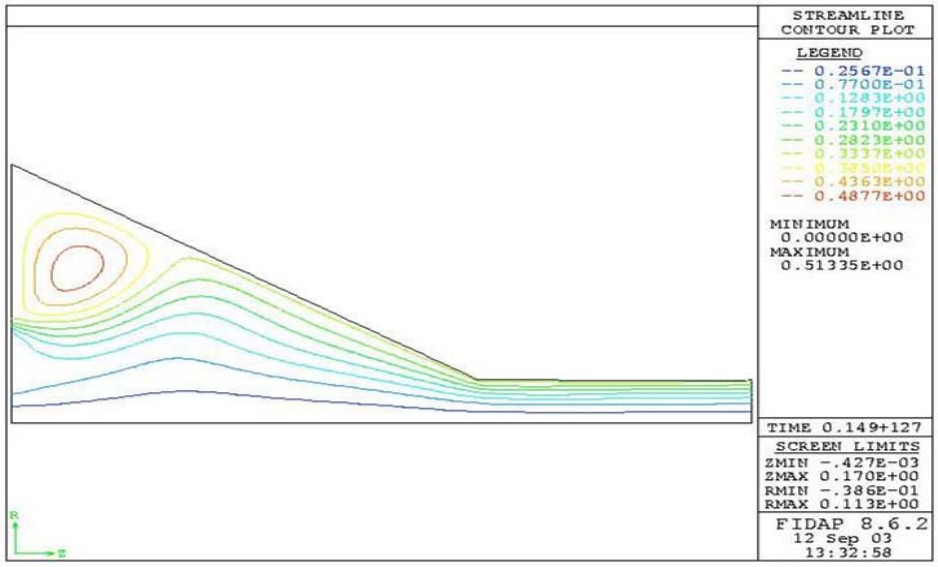

Figure 71: Streamline contour plot for Methanol (Q = 4.416 x 10^{-7} m^3/s, R_2 = 2.5 x 10^{-4} m)

Finally, the last variation for this nozzle geometry included Methanol as the working fluid with an inlet flow rate of 5.678 x 10^{-7} m^3/s. Figure 72 shows the velocity vector plot for this situation. Similar to the other cases, the maximum velocity had a value of about 11.25 m/s and was located in the throat of the nozzle. The free surface of the fluid exiting the nozzle began at a height of 1.250 x 10^{-4} m, decreased to 1.216 x 10^{-4} m, and then increased to a height of 1.245 x 10^{-4} m. A cone angle of 1.95 degrees was observed for this particular study.

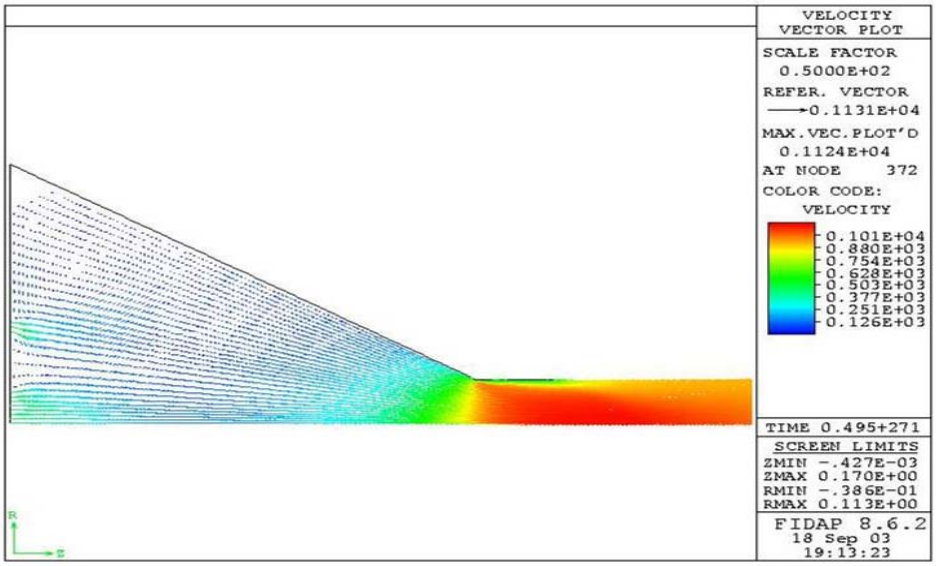

Figure 72: Vector velocity plot for Methanol (Q=5.678 x 10^{-7} m^3/s, R_2 = 2.5 x 10^{-4} m). Units are cm/s.

The pressure contour plot and streamline contour plot for this case are shown in Figures 73 and 74. The maximum pressure was found to be about 5.66 x 10^4 Pa, while the minimum pressure was found to be -9.08 x 10^3 Pa. The pressure drop from the inlet of the nozzle to the outlet of the nozzle was calculated as 5.11 x 10^4 Pa. Similar to the case involving 4.416 x 10^{-7} m^3/s as the inlet flow rate, this pressure drop is about half of that for the other cases involving the same nozzle geometry and inlet flow rate. The

streamline plot shows that the fluid entering through the central inlet has almost pure axial motion as it flows toward the outlet. The fluid entering through the outer inlet slot flows around a swirling pocket as it moved to the nozzle wall, and then toward the outlet.

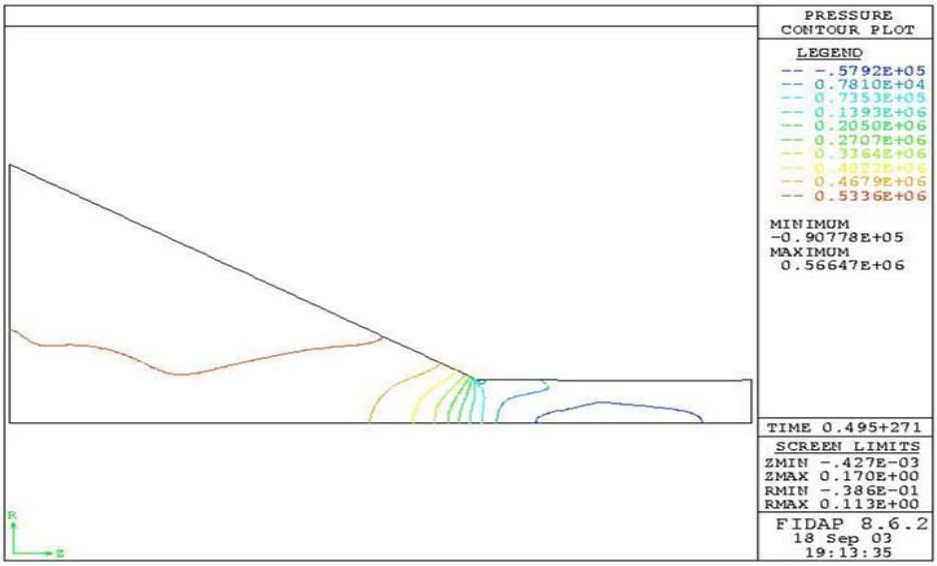

Figure 73: Pressure contour plot for Methanol (Q = 5.678 x 10^{-7} m^3/s, R_2 = 2.5 x 10^{-4} m). Units are gm/cm s^2 (x10^1 Pa).

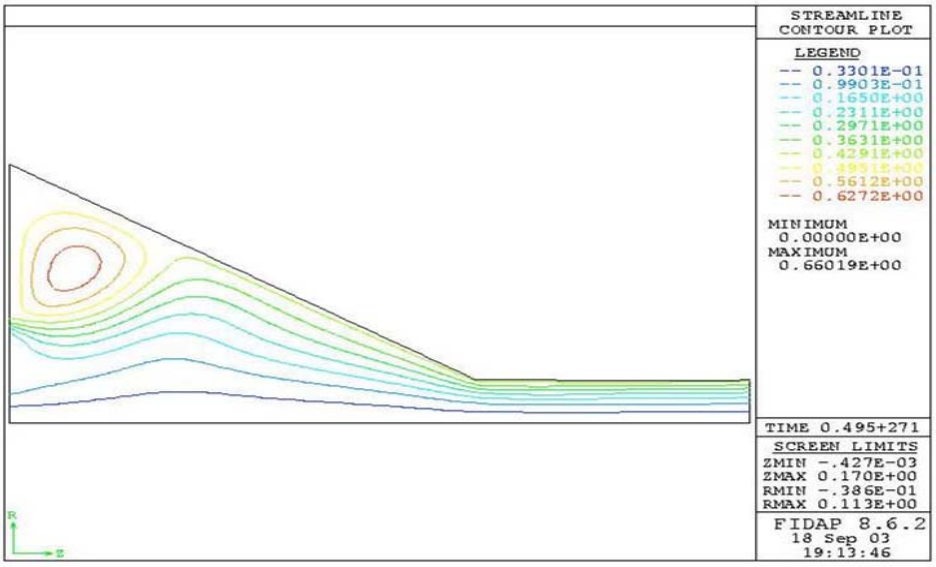

Figure 74: Streamline contour plot for Methanol (Q = 5.678 x 10^{-7} m^3/s, R_2 = 2.5 x 10^{-4} m)

Figure 75 and Figure 76 show the free surface profile for all of the fluids entering at 4.416 x 10^{-7} m^3/s for this nozzle geometry. It was noted that FC-87 produced the highest free surface position with a height of 1.251 x 10^{-4} m.

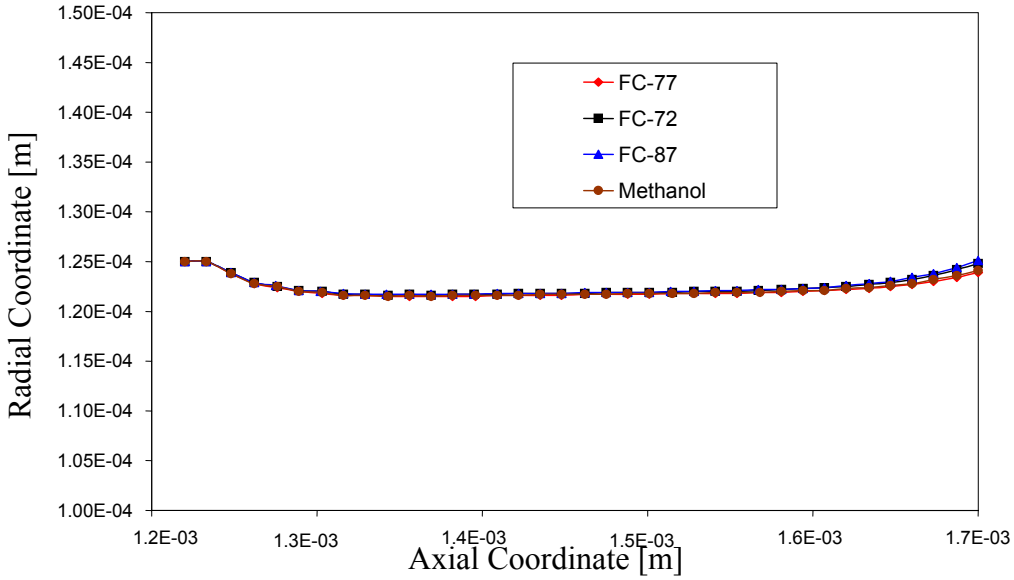

Figure 75: Free surface profile for all fluids (Q = 4.416 x 10^{-7} m^3/s, R_2 = 2.5 x 10^{-4} m)

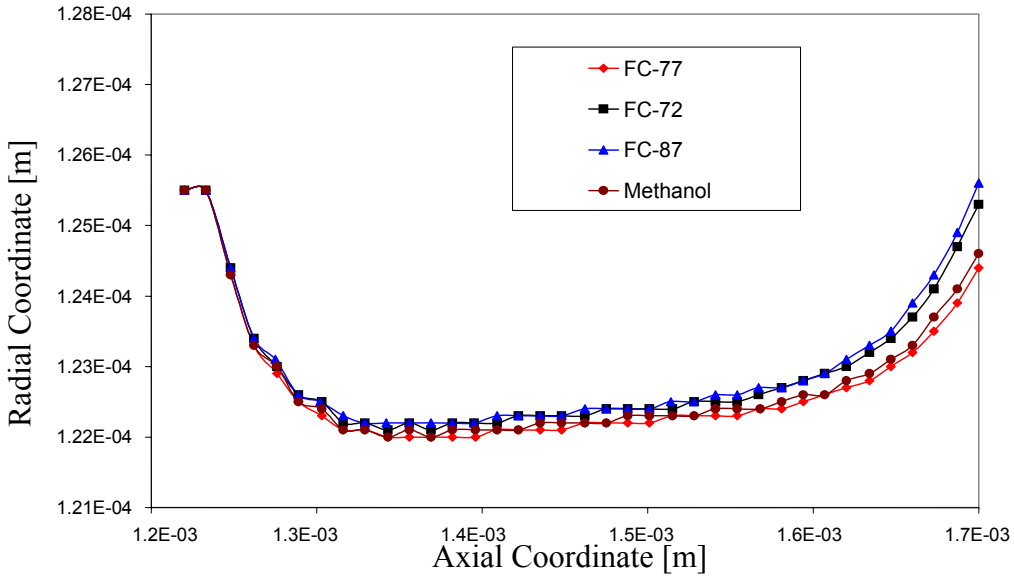

Figure 76: Magnified free surface profile for all fluids (Q = 4.416 x 10^{-7} m^3/s, R_2 = 2.5 x 10^{-4} m)

Figure 77 and Figure 78 show the free surface profile for all of the fluids entering at 5.678 x 10^{-7} m^3/s for this nozzle geometry. Again, it was observed that FC-87 produced the highest free surface position with a height of 1.253 x 10^{-4} m.

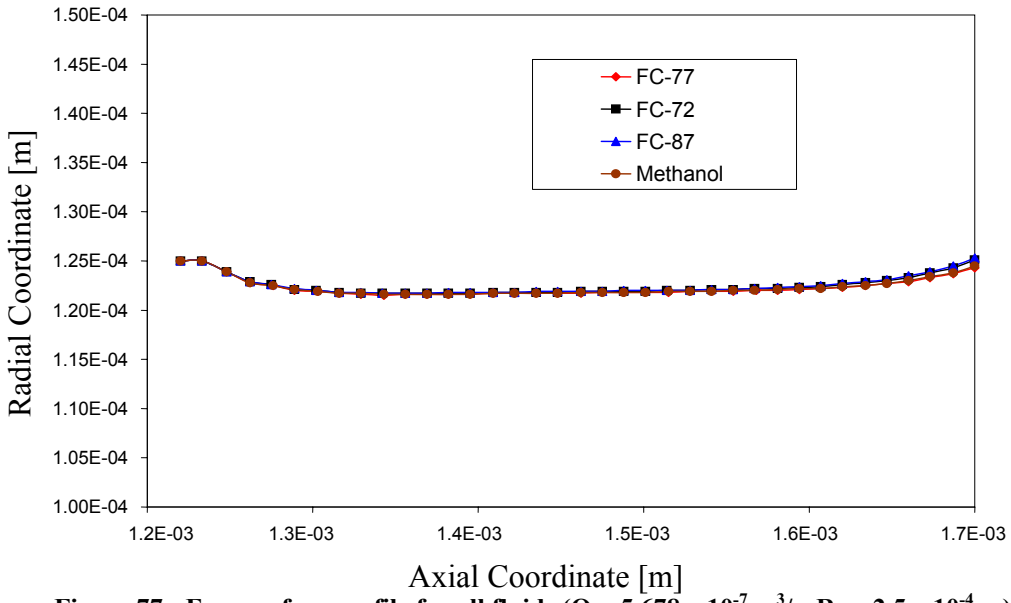

Figure 77: Free surface profile for all fluids (Q = 5.678 x 10^{-7} m^3/s, R_2 = 2.5 x 10^{-4} m)

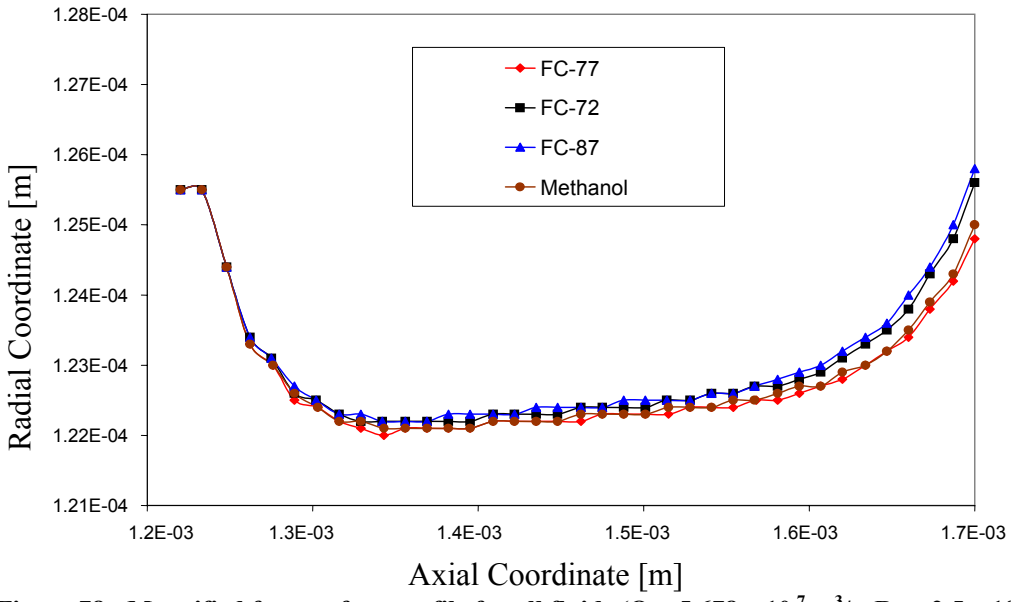

Figure 78: Magnified free surface profile for all fluids (Q = 5.678 x 10^{-7} m^3/s, R_2 = 2.5 x 10^{-4} m)

Figure 79 and Figure 80 show the dimensionless free surface profile for this nozzle geometry based on the Reynolds number produced for each fluid at each flow rate. It is noted that the larger Reynolds number produced the greatest free surface height.

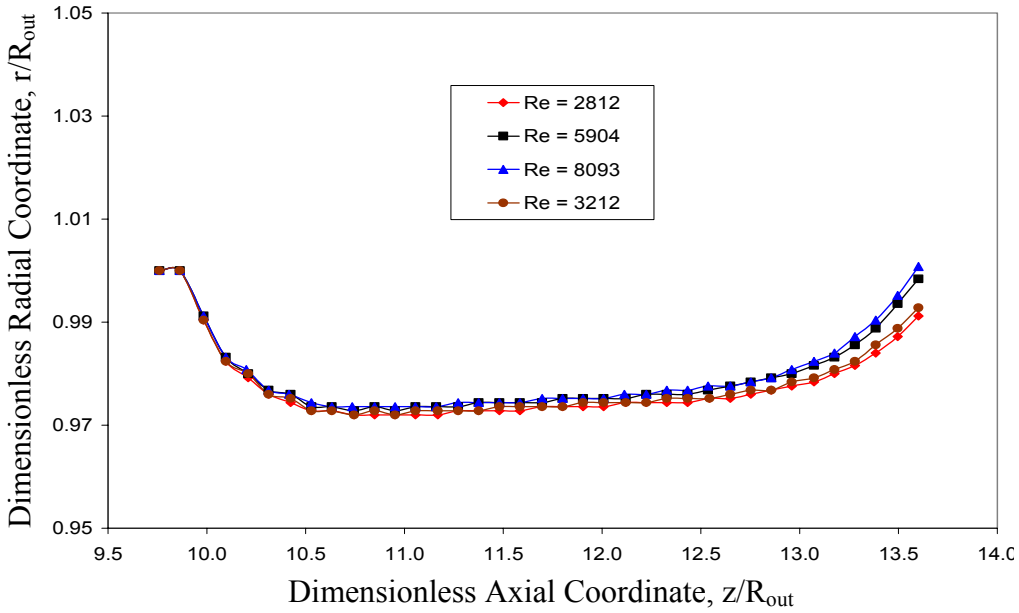

Figure 79: Dimensionless free surface profile for all fluids ($Q = 4.416 \times 10^{-7}$ m^3/s, $R_2 = 2.5 \times 10^{-4}$ m)

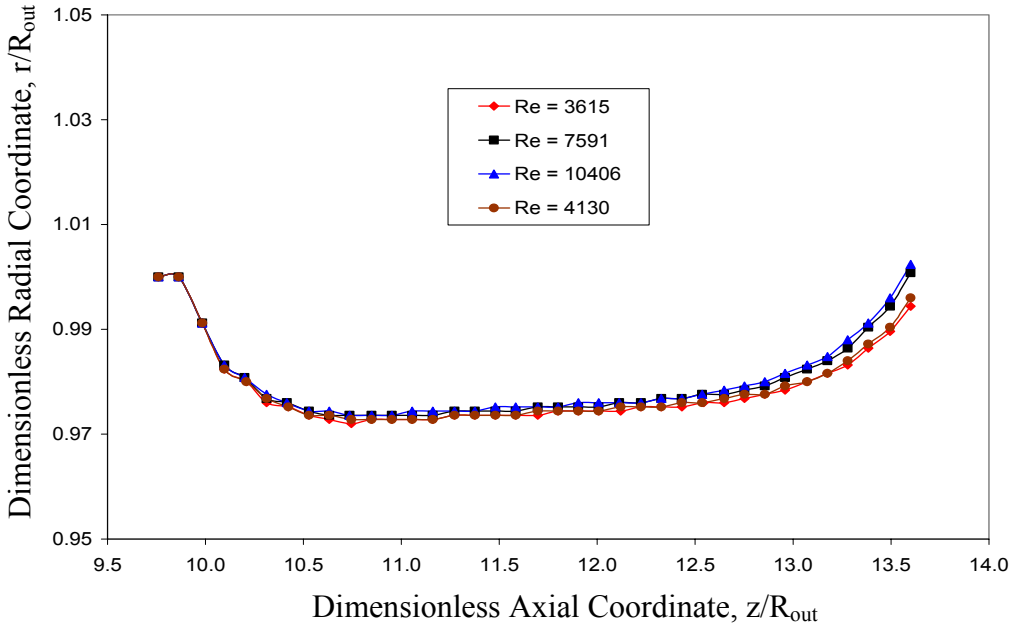

Figure 80: Dimensionless free surface profiles for all fluids ($Q = 5.678 \times 10^{-7}$ m^3/s, $R_2 = 2.5 \times 10^{-4}$ m)

5.2.8.2 R_2 Equal to 4.00 x 10^{-4} m

The next geometry that was used was when R_2 was equal to 4.00 x 10^{-4} m and R_3 was equal to 4.36 x 10^{-4} m. The same fluids and flow rates were used as the previous geometry. First, the case of FC-77 with an inlet flow rate of 5.678 x 10^{-7} m^3/s was analyzed. Figure 81 shows the vector velocity plot for this particular scenario. The maximum velocity was found to be 8.83 m/s located within the throat of the nozzle. The free surface began at a height of 1.250 x 10^{-4} m, decreased to 1.216 x 10^{-4} m, but then rose to a final height 1.245 x 10^{-4} m. The cone angle was found to be 1.84 degrees. This value is slightly more than the height when R_2 was equal to 2.50 x 10^{-4} m.

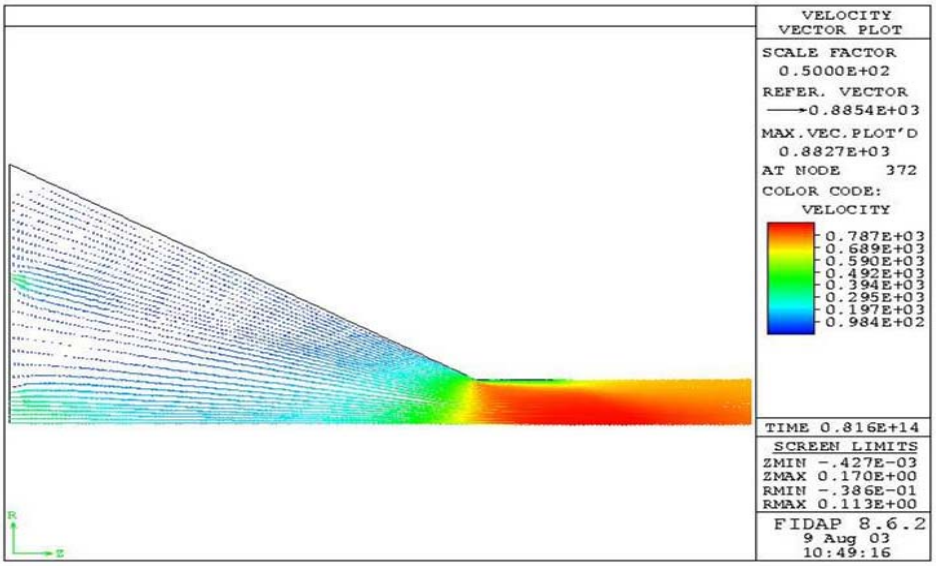

Figure 81: Velocity vector plot for FC-77 (Q = 4.416 x 10^{-7} m^3/s, R_2 = 4.0 x 10^{-4} m). Units are cm/s.

Figure 82 and Figure 83 show the pressure contour plot and streamline contour plot, respectively. Again, the pressure decreases from the inlet to the outlet as the velocity of the fluid increases. The pressure drop from the inlet to the outlet was determined to be 7.93 x 10^4 Pa. The streamline contour plot illustrates the path of the

fluid as it flows through the nozzle. After entering the nozzle, a portion of the fluid begins to swirl near the top, while the rest of the fluid flows toward the outer wall, and eventually, the outlet. However, since the location of the outer slot has moved more towards the out edge of the nozzle, the portion of the fluid that is swirling has decreased.

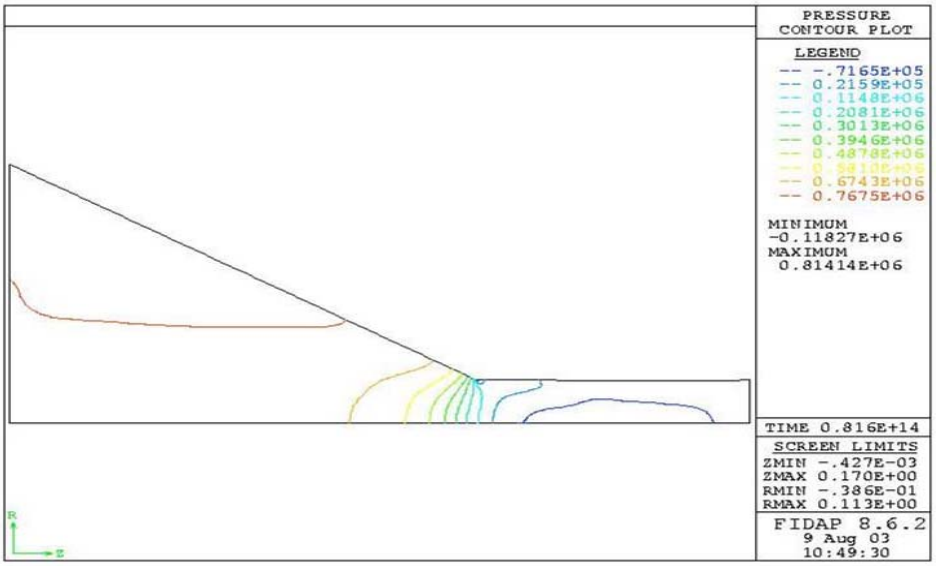

Figure 82: Pressure contour plot for FC-77 (Q = 4.416 x 10^{-7} m^3/s, R_2 = 4.0 x 10^{-4} m). Units are gm/cm s^2 (x10^1 Pa).

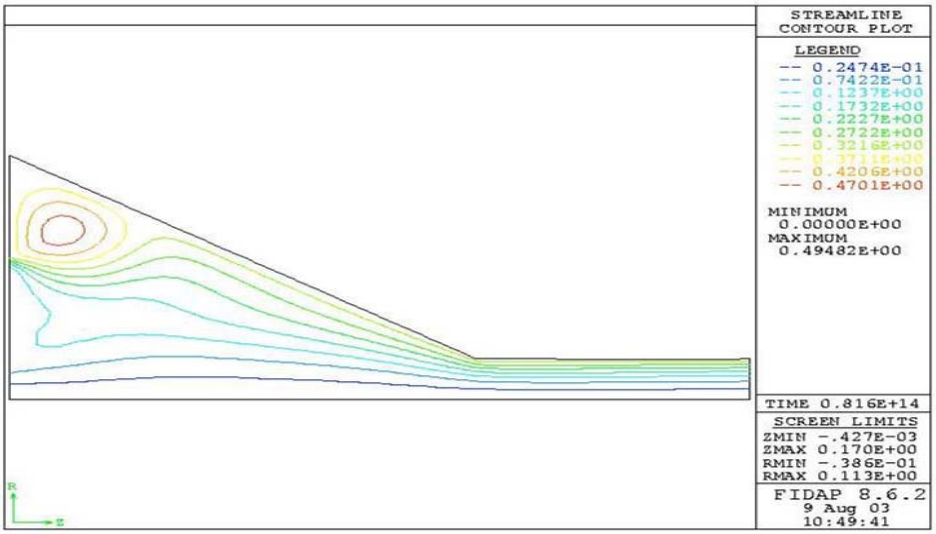

Figure 83: Streamline contour plot for FC-77 (Q = 4.416 x 10^{-7} m^3/s, R_2 = 4.0 x 10^{-4} m)

The inlet flow rate of the FC-77 was then increased to 5.678 x 10^{-7} m^3/s. The velocity vector plot for this case is shown in Figure 84. The maximum velocity was found to be in the throat of the nozzle with a value of about 11.33 m/s. The free surface is initially at a height of 1.250 x 10^{-4} m, and then gradually decreases to 1.216 x 10^{-4} m, before rising to a height of 1.249 x 10^{-4} m. It was noted that for both flow rates, this geometry with the outer slot located further away from the center, has produced a more pronounced free surface profile than the previous geometry. The cone angle for this situation increased to a value of 2.05 degrees.

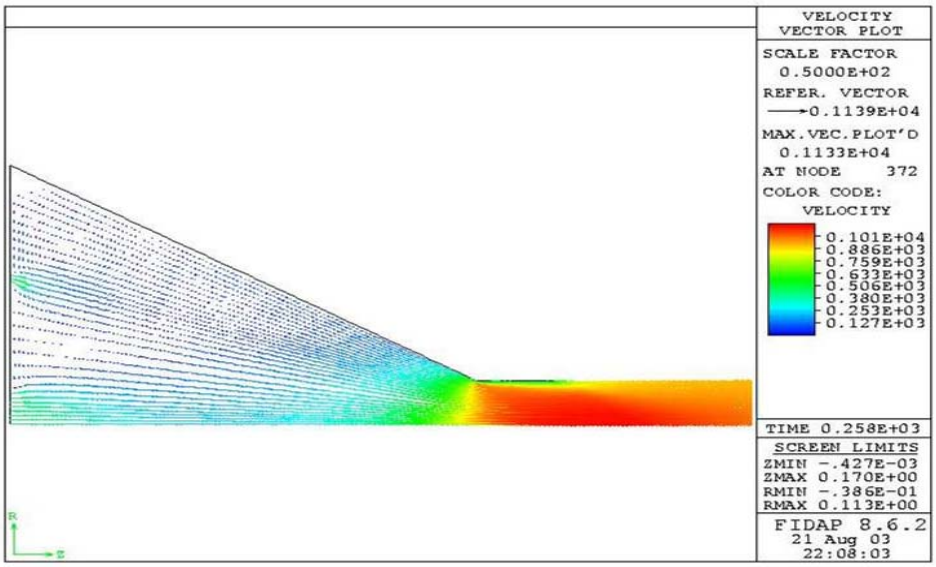

Figure 84: Velocity vector plot for FC-77 (Q = 5.678 x 10^{-7} m^3/s, R_2 = 4.0 x 10^{-4} m). Units are cm/s.

The pressure contour plot is shown in Figure 85. The inlet-to-outlet pressure drop was calculated as 1.20 x 10^5 Pa, which is slightly greater than when 4.416 x 10^{-7} m^3/s was used as the flow rate. The maximum pressure was 1.34 x 10^5 Pa, and the minimum pressure was -2.11 x 10^4 Pa. Figure 86 shows the streamline contour plot for this case. The fluid behaves the same with this flow rate as it did when 4.416 x 10^{-7} m^3/s was used

as the flow rate. Most of the fluid entering the nozzle through the outer slot flow toward the outer wall before moving to the outlet; but some of the fluid moves toward the center of the nozzle before heading to the outlet. There is also still a portion of the fluid which begins to swirl in the top region of the nozzle.

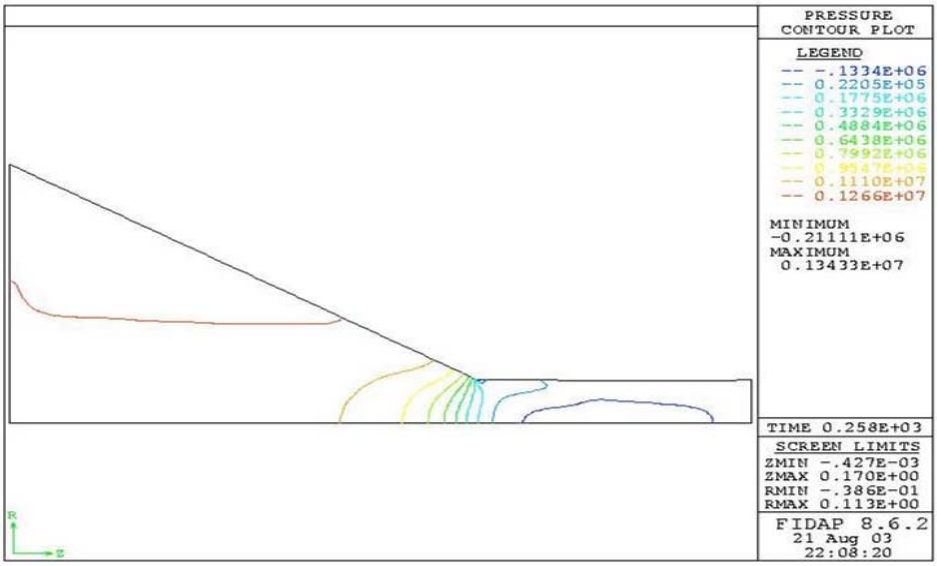

Figure 85: Pressure contour plot for FC-77 (Q = 5.678 x 10^{-7} m^3/s, R_2 = 4.0 x 10^{-4} m). Units are gm/cm s^2 (x10^1 Pa).

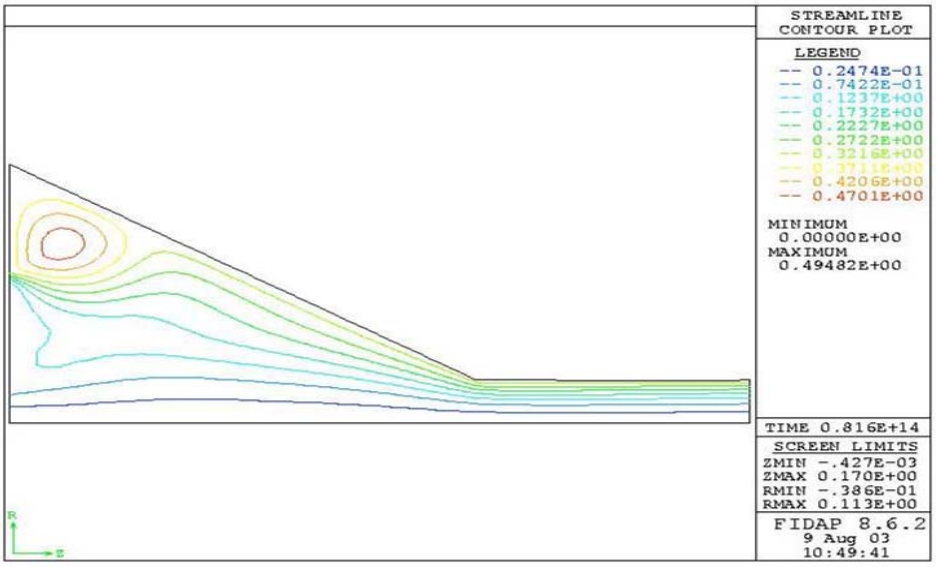

Figure 86: Streamline contour plot for FC-77 (Q = 5.678 x 10^{-7} m^3/s, R_2 = 4.0 x 10^{-4} m)

The next study involves the use of the same geometry and flow rates, but with FC-72 as the working fluid. Figure 87 shows the vector velocity plot for FC-72 as the working fluid traveling at 4.416 x 10^{-7} m^3/s. The maximum velocity within the nozzle was found to be about 8.79 m/s. The fluid exiting the nozzle began at a height of 1.250 x 10^{-4} m. This free surface then began to decline to a height of 1.217 x 10^{-4} m before rising to a final height of 1.256 x 10^{-4} m, which formed a cone angle of 2.48 degrees. This is greater than the values obtained from either flow rate using FC-77 as the working fluid.

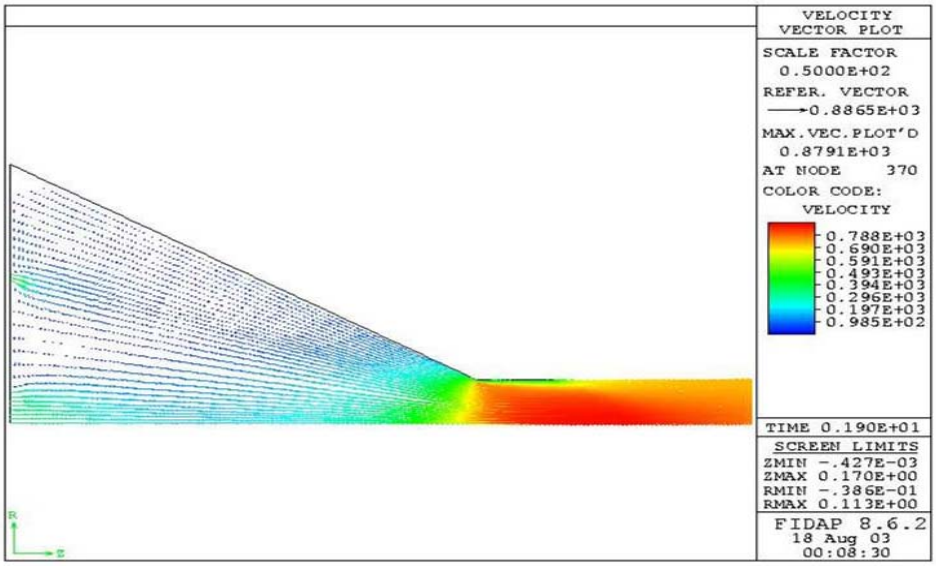

Figure 87: Velocity vector plot for FC-72 (Q = 4.416 x 10^{-7} m^3/s, R_2 = 4.0 x 10^{-4} m). Units are cm/s.

Figure 88 shows the pressure contour plot for this case. The maximum pressure was found to be 7.66 x 10^4 Pa, whereas the minimum pressure was found to be approximately -1.39 x 10^4 Pa. The pressure drop from the inlet to the outlet was also calculated and determined to be 5.43 x 10^4 Pa, which is less than the value obtained with FC-77 as the working fluid. The streamline contour plot for this situation is shown in Figure 89. This graphic shows that the fluid is moving along the same paths with this

geometry, independent of the flow rate. Most of the fluid entering through the inlets moves toward the outer wall as it moves through the nozzle, while a fraction of the fluid begins to swirl.

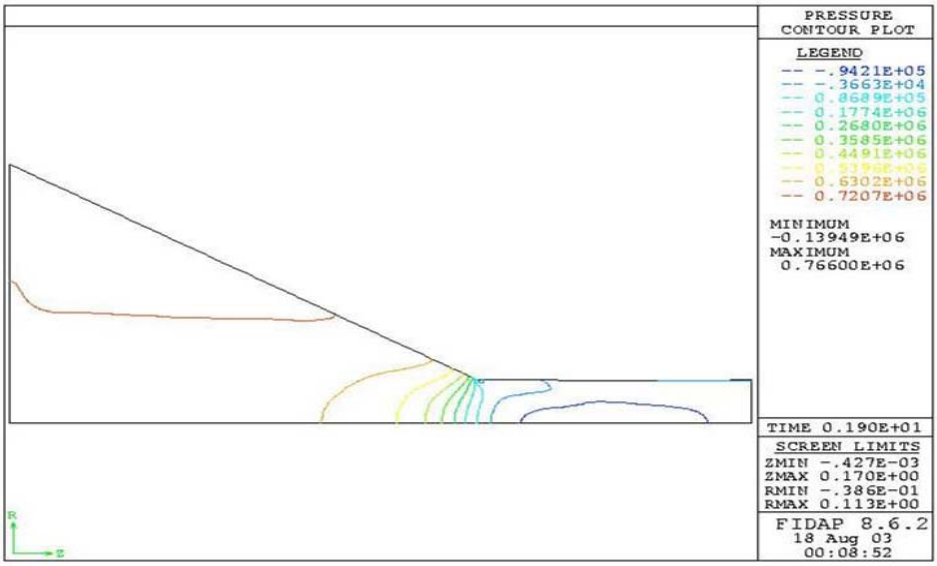

Figure 88: Pressure contour plot for FC-72 ($Q = 4.416 \times 10^{-7}$ m^3/s, $R_2 = 4.0 \times 10^{-4}$ m). Units are gm/cm s^2 ($x10^1$ Pa).

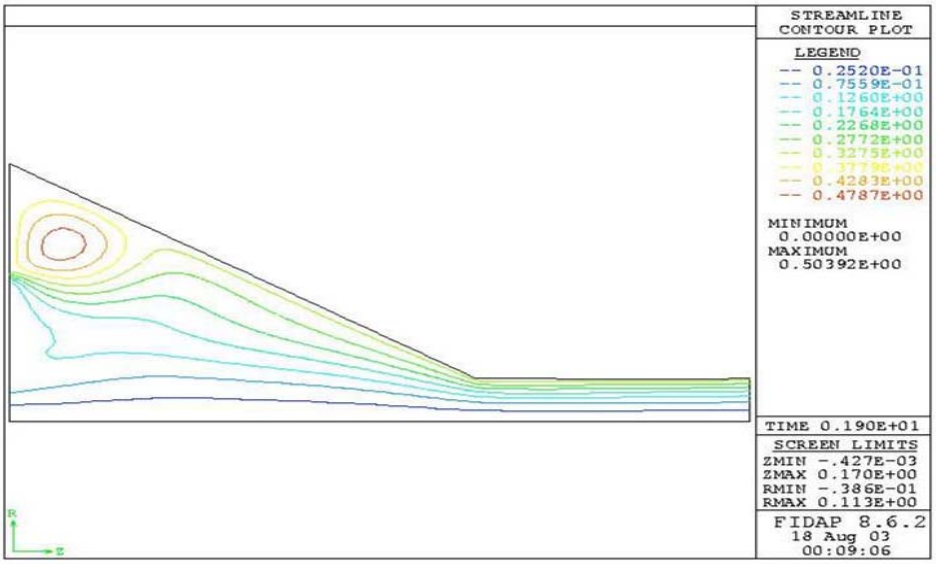

Figure 89: Streamline contour plot for FC-72 ($Q = 4.416 \times 10^{-7}$ m^3/s, $R_2 = 4.0 \times 10^{-4}$ m)

The next variation for this geometry was using FC-72 as the working fluid and increasing the inlet flow rate to 5.678 x 10^{-7} m^3/s. This flow rate provided an axial inlet velocity of 4.519 m/s to both the center inlet and outer slot. The outer slot also maintained a theta velocity component, which was also equal to 4.519 m/s. Figure 90 shows the velocity vector plot for this case. The maximum velocity in the nozzle was located in the throat and found to have a value of 11.30 m/s. The free surface height began at 1.250 x 10^{-4} m, decreased to 1.218 x 10^{-4} m, then increased to 1.259 x 10^{-4} m. The resulting cone angle was calculated as 2.70 degrees.

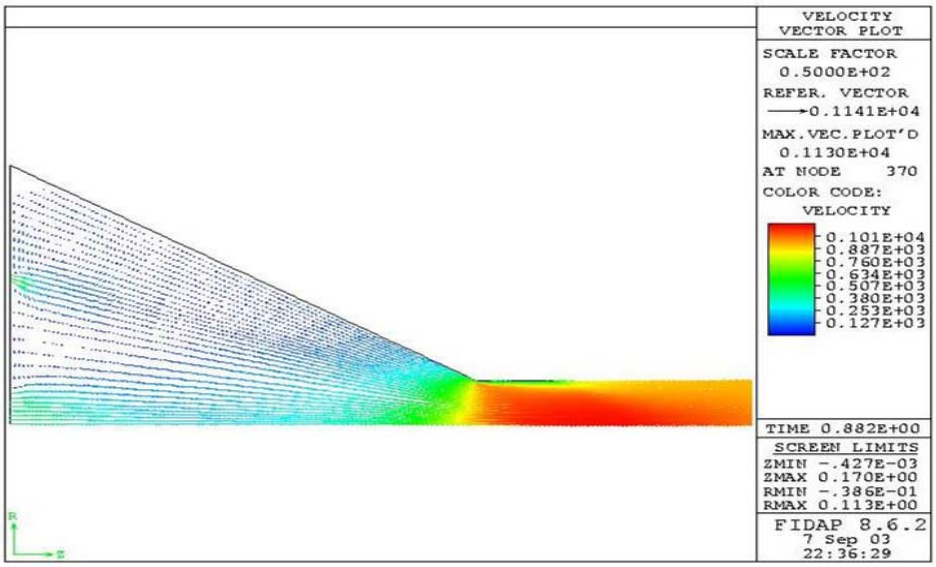

Figure 90: Velocity vector plot for FC-72 (Q = 5.678 x 10^{-7} m^3/s, R_2 = 4.0 x 10^{-4} m). Units are cm/s.

The pressure contour plot is shown in Figure 91. The maximum pressure was determined to be 1.27 x 10^5 Pa, whereas the minimum pressure was determined to be -2.43 x 10^4 Pa. The inlet-to-outlet pressure drop was calculated as 1.02 x 10^5 Pa, which is just slightly larger than for FC-77 under the same parameters. Figure 92 shows the streamline contour plot. It shows the same image as the rest of the trial involving the

nozzle where R_2 is equal to 4.00 x 10^{-4} m. Most of the fluid that enters the nozzle through the outer slot flows toward the outer wall before going to the outlet. The fluid entering through the center inlet moves to in the radial direction briefly before going towards the outlet, with some of the fluid swirling in the top portion of the nozzle.

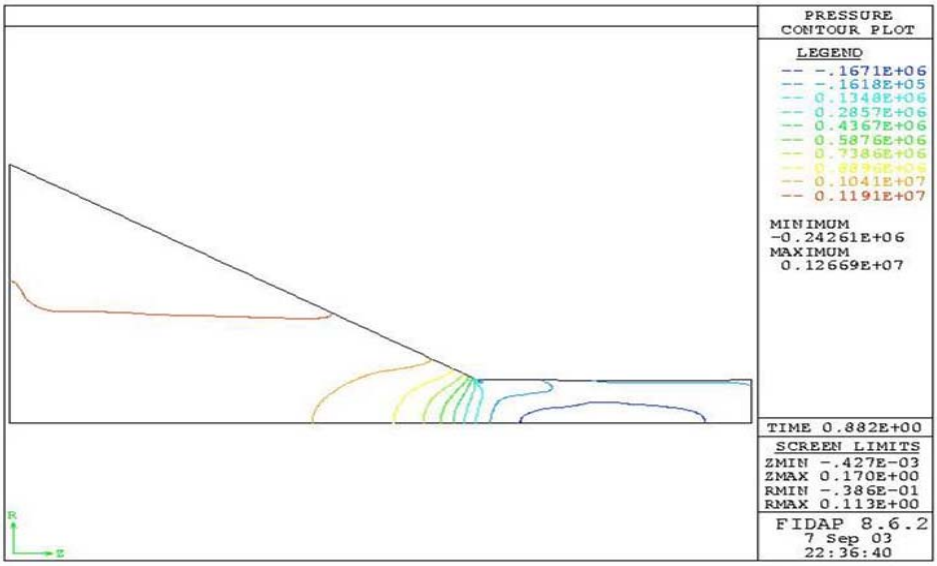

Figure 91: Pressure contour plot for FC-72 (Q = 5.678 x 10^{-7} m^3/s, R_2 = 4.0 x 10^{-4} m). Units are gm/cm s^2 (x10^1 Pa).

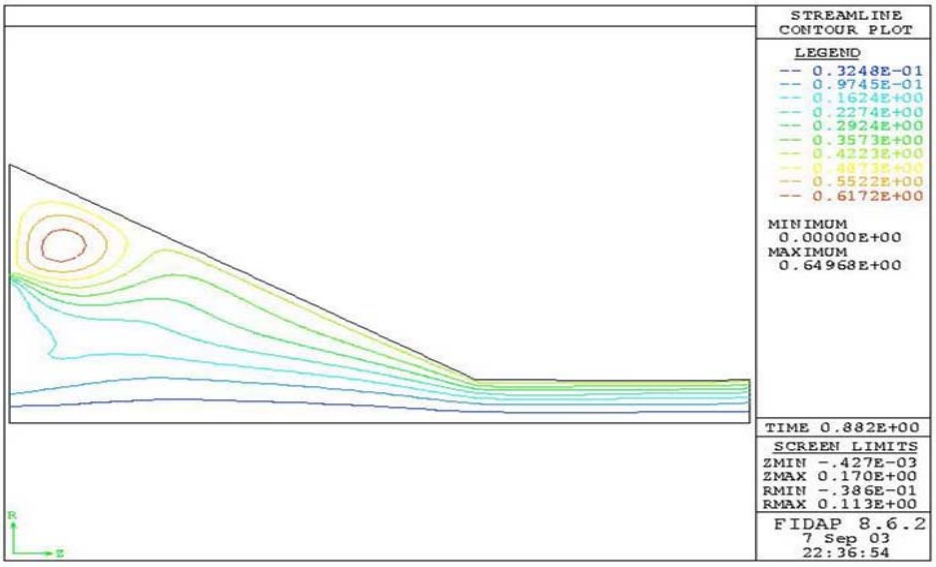

Figure 92: Streamline contour plot for FC-72 (Q = 5.678x 10^{-7} m^3/s, R_2 = 4.0 x 10^{-4} m).

Next, the working fluid was changed to FC-87 and run at the same inlet flow rates. Figure 93 shows the velocity vector plot for the case where the inlet flow rate was 4.416 x 10^{-7} m^3/s. The maximum velocity within the nozzle was found to be 8.79 m/s. The free surface formed by the fluid exiting the nozzle began at a height of 1.250 x 10^{-4} m. It then decreased to 1.218 x 10^{-4} m before it grew to a final height of 1.259 x 10^{-4} m, which produced a cone angle of 2.70 degrees. FC-87 produced the greatest radial height of the free surface for this nozzle geometry, as well as for all other geometries.

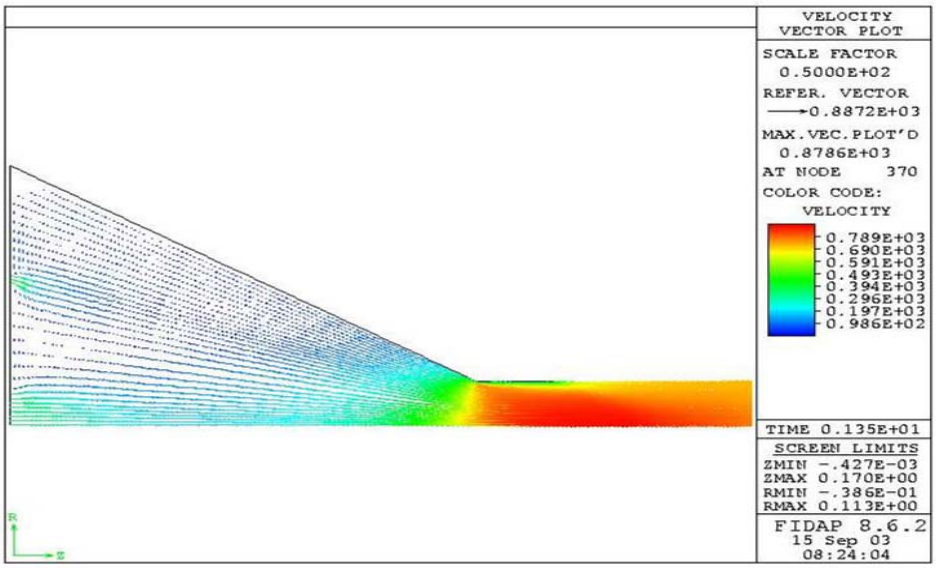

Figure 93: Velocity vector plot for FC-87 (Q = 4.416 x 10^{-7} m^3/s, R_2 = 4.0 x 10^{-4} m). Units are cm/s.

Figure 94 and Figure 95 show the pressure contour plot and the streamline contour plot, respectively. The maximum pressure within the nozzle was found to be 7.44 x 10^4 Pa, whereas the minimum pressure was found to be about -1.44 x 10^4 Pa. The inlet-to-outlet pressure drop was then calculated as approximately 7.53 x 10^4 Pa. The streamline plot shows that the fluid entering through the outer inlet slot must maneuver around a pocket of swirling fluid before it flows to the nozzle wall, while the fluid

entering through the central inlet has almost pure axial motion to the nozzle outlet. Since this geometry has the outer inlet slot further outward in a radial sense, the location of the swirling pocket of fluid is also located further outward in the radial direction.

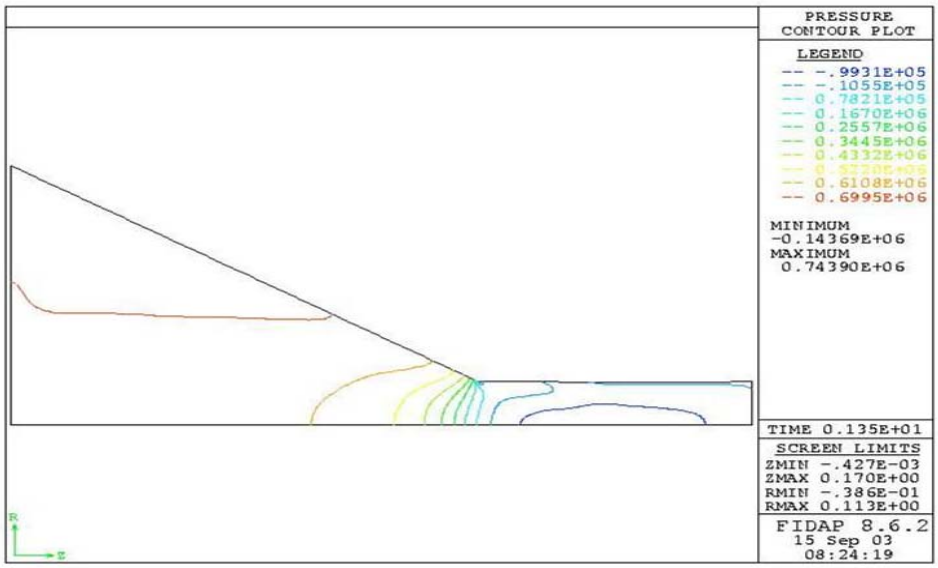

Figure 94: Pressure contour plot for FC-87 ($Q = 4.416 \times 10^{-7}$ m^3/s, $R_2 = 4.0 \times 10^{-4}$ m). Units are gm/cm s^2 ($x10^1$ Pa).

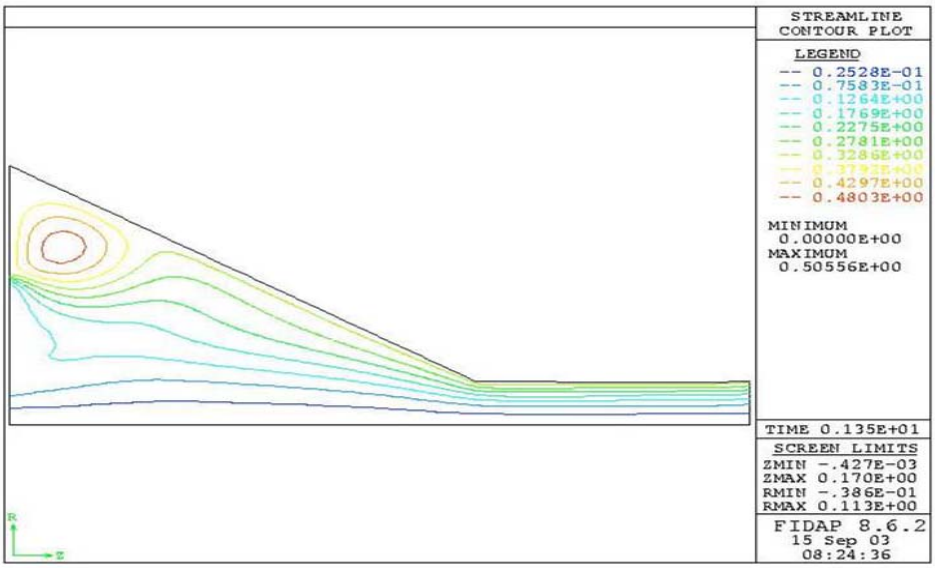

Figure 95: Streamline contour plot for FC-87 ($Q = 4.416 \times 10^{-7}$ m^3/s, $R_2 = 4.0 \times 10^{-4}$ m)

With FC-87 still being used as the working fluid within the nozzle, the flow rate was increased to 5.678 x 10^{-7} m^3/s. The velocity vector plot for this situation is shown in Figure 96. The maximum velocity was again found to be located in the throat of the nozzle and had a magnitude of approximately 11.30 m/s. The free surface began at a height of 1.250 x 10^{-4} m, decreased to 1.218 x 10^{-4} m, and then increased to a final height of 1.261 x 10^{-4} m. The cone angle that resulted from this flow was determined to be about 2.81 degrees. Again, this was the largest radial height for the free surface observed from the studies involving the same nozzle geometry and inlet flow rate.

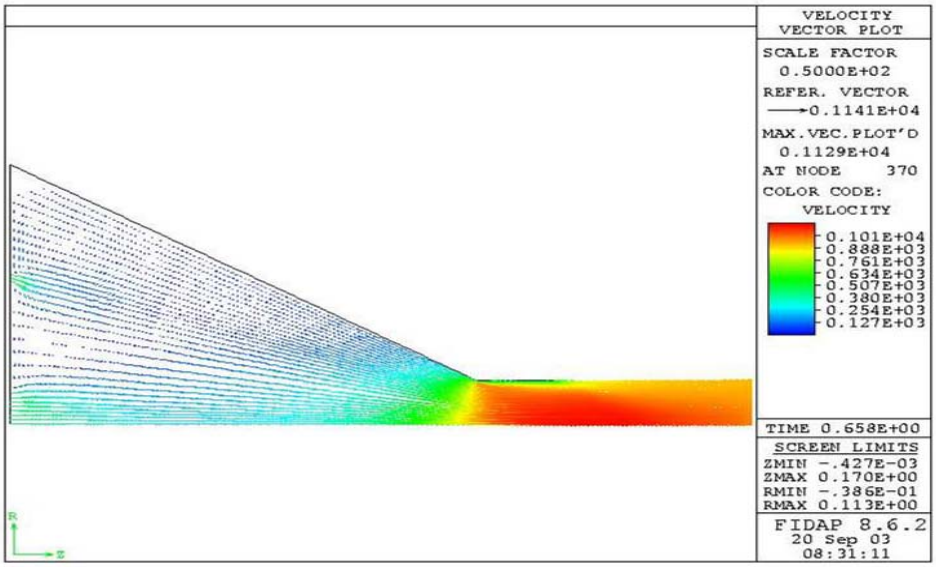

Figure 96: Velocity vector plot for FC-87 (Q = 5.678 x 10^{-7} m^3/s, R_2 = 4.0 x 10^{-4} m). Units are cm/s.

Figure 97 shows the pressure contour plot for this situation. The maximum pressure within the nozzle was found to be 1.23 x 10^5 Pa, while the minimum pressure was found to be -2.46 x 10^4 Pa. The pressure drop from the inlet of the nozzle to the outlet was calculated as approximately 1.25 x 10^5 Pa. The streamline contour plot is shown in Figure 98. This plot shows results that are similar to the other streamline plots

for this nozzle geometry. The fluid entering through the central inlet flowed straight to the nozzle outlet, while the fluid entering through the outer inlet slot flowed toward the nozzle wall before heading toward the outlet. Again, there was a pocket of swirling fluid present near the top of the nozzle outside of where the outer inlet slot was positioned.

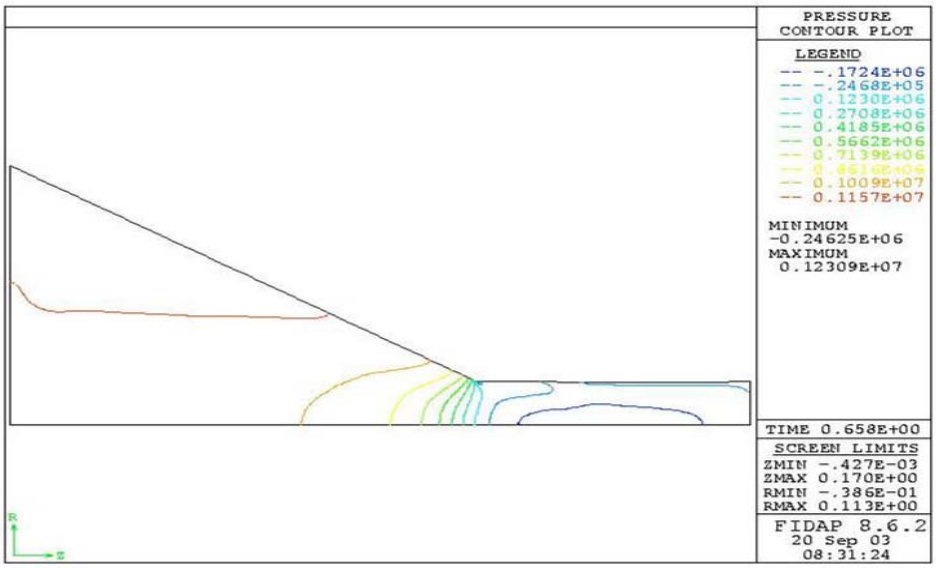

Figure 97: Pressure contour plot for FC-87 ($Q = 5.678 \times 10^{-7}$ m^3/s, $R_2 = 4.0 \times 10^{-4}$ m). Units are gm/cm s^2 ($x10^1$ Pa).

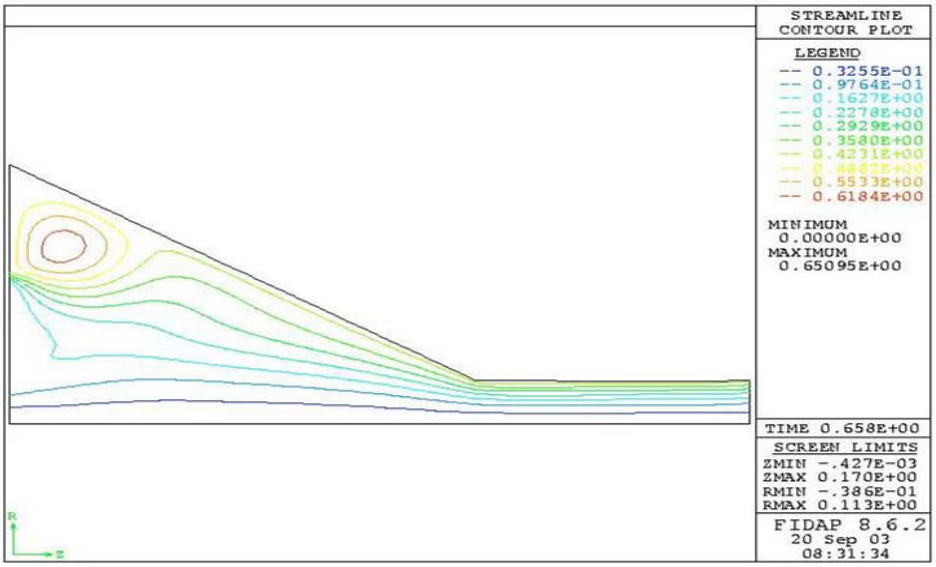

Figure 98: Streamline contour plot for FC-87 ($Q = 5.678 \times 10^{-7}$ m^3/s, $R_2 = 4.0 \times 10^{-4}$ m)

The final variations performed on this nozzle geometry involved using Methanol as the working fluid. Figure 99 shows the velocity vector plot for Methanol with an inlet flow rate of 4.416 x 10^{-7} m^3/s. The maximum velocity for this situation was found to be about 8.82 m/s. The free surface was initially at a height of 1.250 x 10^{-4} m before it decreased to 1.216 x 10^{-4} m. It then increased to a final height 1.247 x 10^{-4} m, which resulted in a cone angle of 1.95 degrees. These values were second only to the values obtained from FC-77 as the lowest free surface radial height and lowest cone angle.

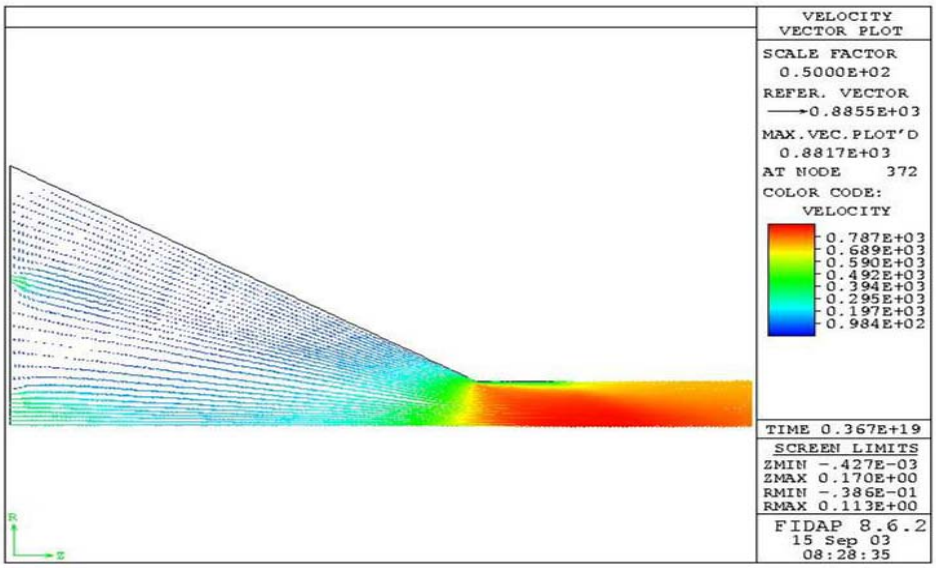

Figure 99: Velocity vector plot for Methanol (Q=4.416 x 10^{-7} m^3/s, R_2 = 4.0 x 10^{-4} m). Units are cm/s.

Figure 100 and Figure 101 show the pressure contour plot and streamline contour plot for this scenario, respectively. The maximum pressure within the nozzle was found to be about 3.59 x 10^4 Pa, while the minimum pressure was determined to be approximately -5.39 x 10^3 Pa. The inlet-to-outlet pressure drop was then calculated as 3.57 x 10^4 Pa which is about half of the pressure drop obtained from the other working fluids. The streamline contour plot shows the fluid entering through the central inlet has

almost a pure axial motion as it flows toward the outlet. It also shows that the fluid entering through the outer inlet slot had to flow around a swirling pocket of fluid to reach the nozzle wall. However, there is a portion of the fluid entering through the outer inlet slot that flows toward the line of symmetry before heading toward the outlet.

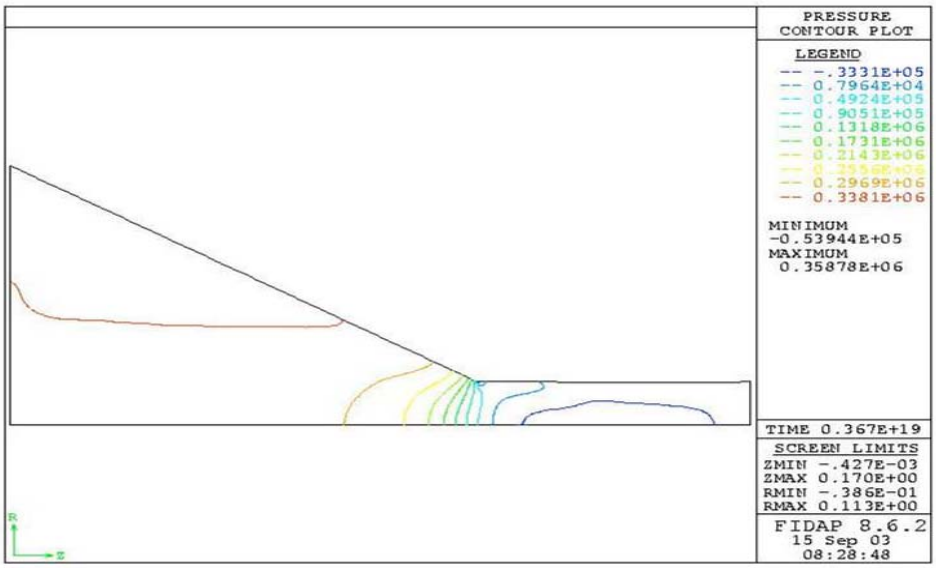

Figure 100: Pressure contour plot for Methanol ($Q = 4.416 \times 10^{-7}$ m^3/s, $R_2 = 4.0 \times 10^{-4}$ m). Units are gm/cm s^2 ($x10^1$ Pa).

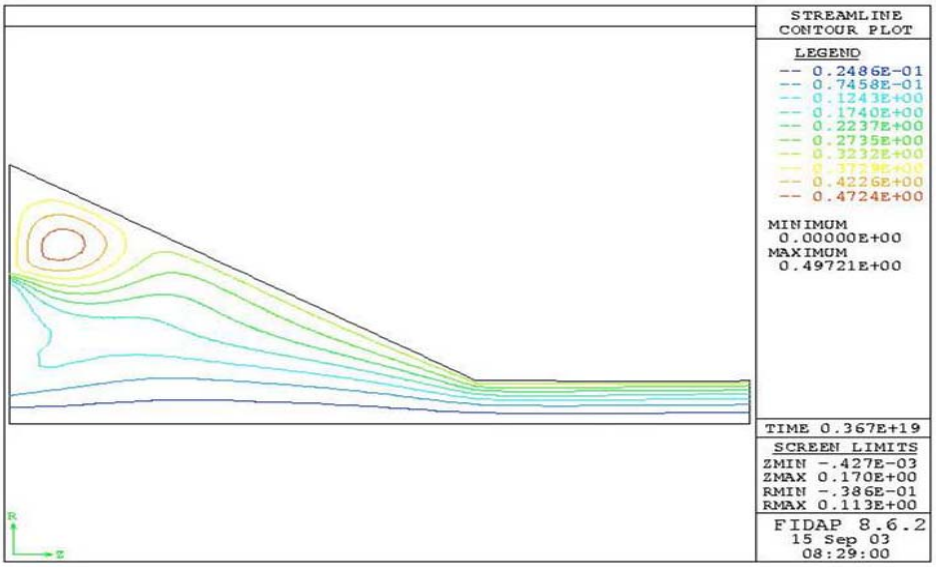

Figure 101: Streamline contour plot for Methanol ($Q = 4.416 \times 10^{-7}$ m^3/s, $R_2 = 4.0 \times 10^{-4}$ m)

Finally, Methanol was used on this nozzle geometry with an inlet flow rate of 5.678 x 10^{-7} m^3/s. The velocity vector plot for these parameters is shown in Figure 102. The maximum velocity was found to be about 11.32 m/s, and was located within the throat of the nozzle. The free surface was originally at a height of 1.250 x 10^{-4} m, and then it decreased to 1.217 x 10^{-4} m before it increased again to a final height of 1.251 x 10^{-4} m. The cone angle was determined to be a mere 2.16 degrees. Again, only FC-77 produced a lower free surface radial height and cone angle.

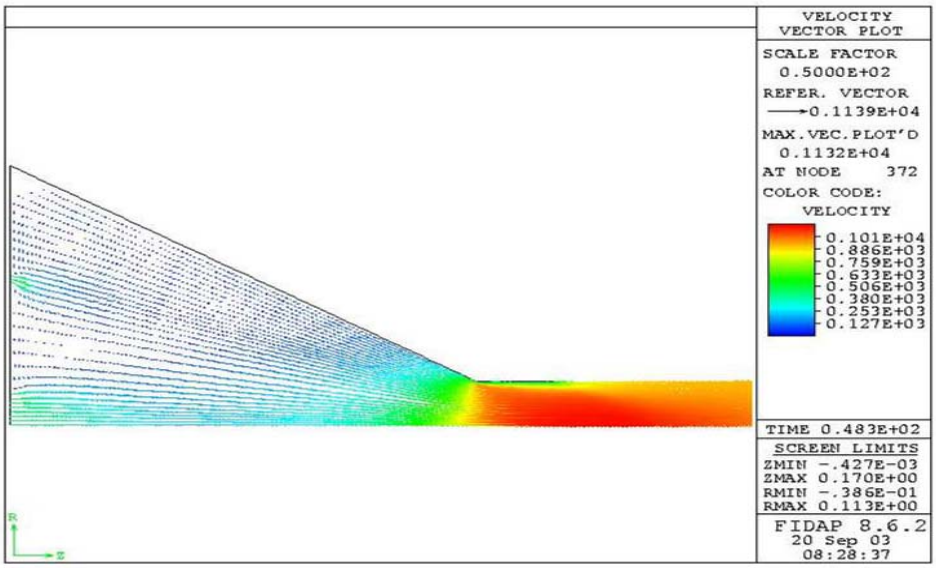

Figure 102: Velocity vector plot for Methanol (Q=5.678 x 10^{-7} m^3/s, R_2=4.0 x 10^{-4} m). Units are cm/s.

The pressure contour plot and streamline contour plot for this situation are shown in Figure 103 and Figure 104. The maximum pressure within the nozzle was found to be about 5.92 x 10^4 Pa, whereas the minimum pressure was found to be -9.78 x 10^3 Pa. The pressure drop from the inlet of the nozzle to the outlet of the nozzle was calculated as 5.90 x 10^4 Pa. The streamline plot shows that as the fluid enters through the outer inlet slot, it must maneuver around a pocket of swirling fluid located at the top of the nozzle

just outside of the where the outer inlet slot is located. The fluid then flows to the outer nozzle wall as it heads toward the outlet. Again, the fluid entering through the central inlet has almost pure axial movement as it flows straight to the outlet of the nozzle.

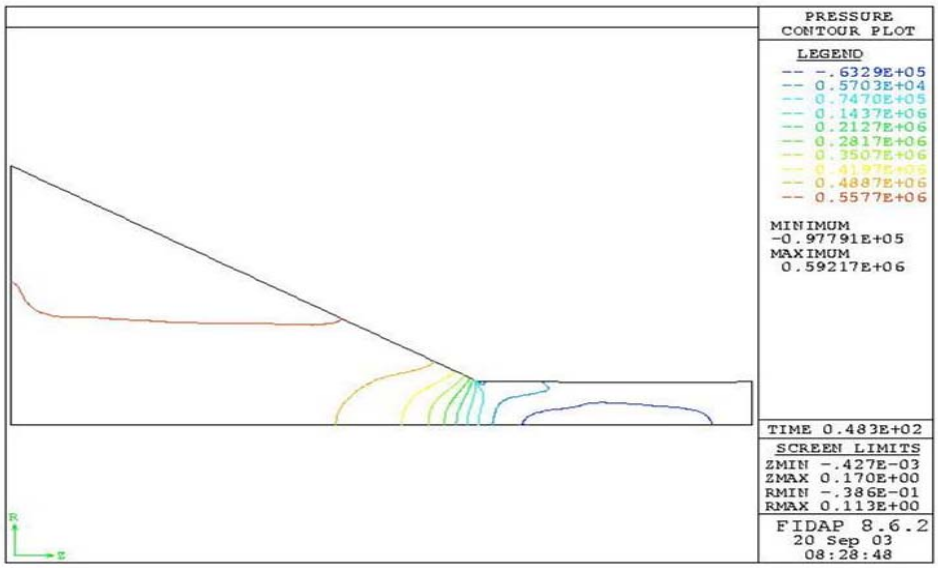

Figure 103: Pressure contour plot for Methanol ($Q = 5.678 \times 10^{-7}$ m^3/s, $R_2 = 4.0 \times 10^{-4}$ m). Units are gm/cm s^2 ($x10^1$ Pa).

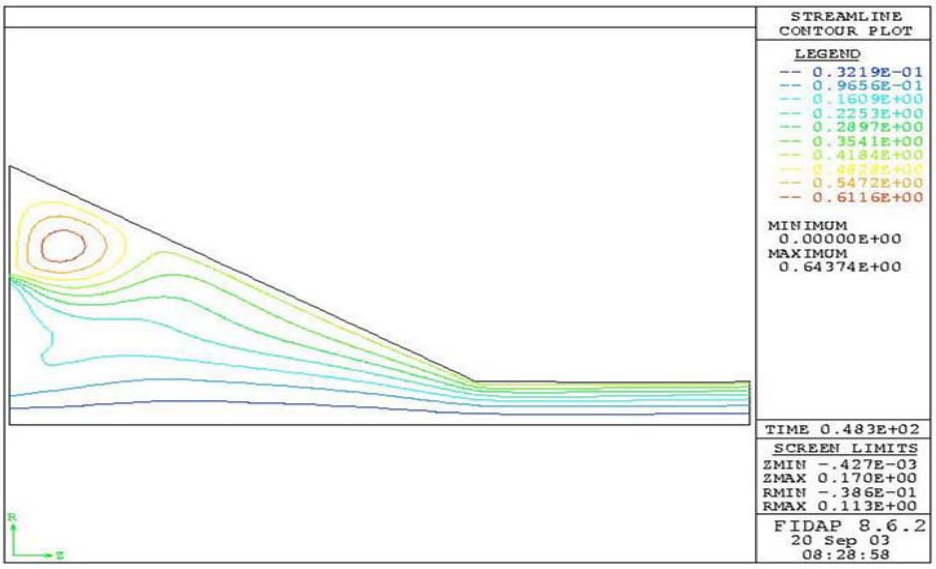

Figure 104: Streamline contour plot for Methanol ($Q = 5.678 \times 10^{-7}$ m^3/s, $R_2 = 4.0 \times 10^{-4}$ m)

Figure 105 and Figure 106 show the free surface profile for this geometry with all of working fluids with an inlet flow rate of 4.416 x 10^{-7} m^3/s. FC-87 resulted in the highest free surface position, with a value of 1.259 x 10^{-4} m.

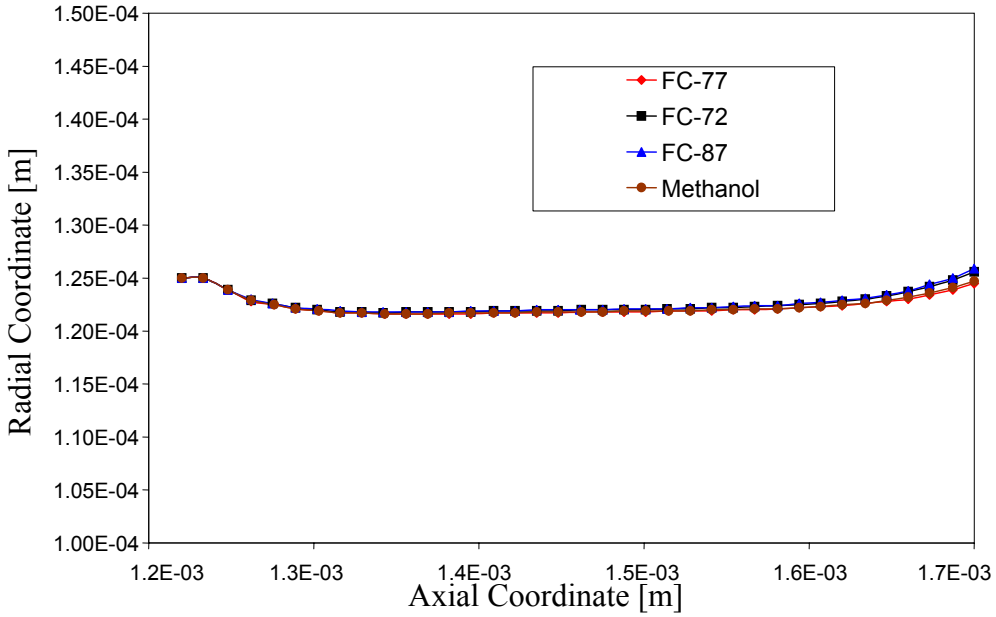

Figure 105: Free surface position for all fluids (Q = 4.416 x 10^{-7} m^3/s, R_2 = 4.0 x 10^{-4} m)

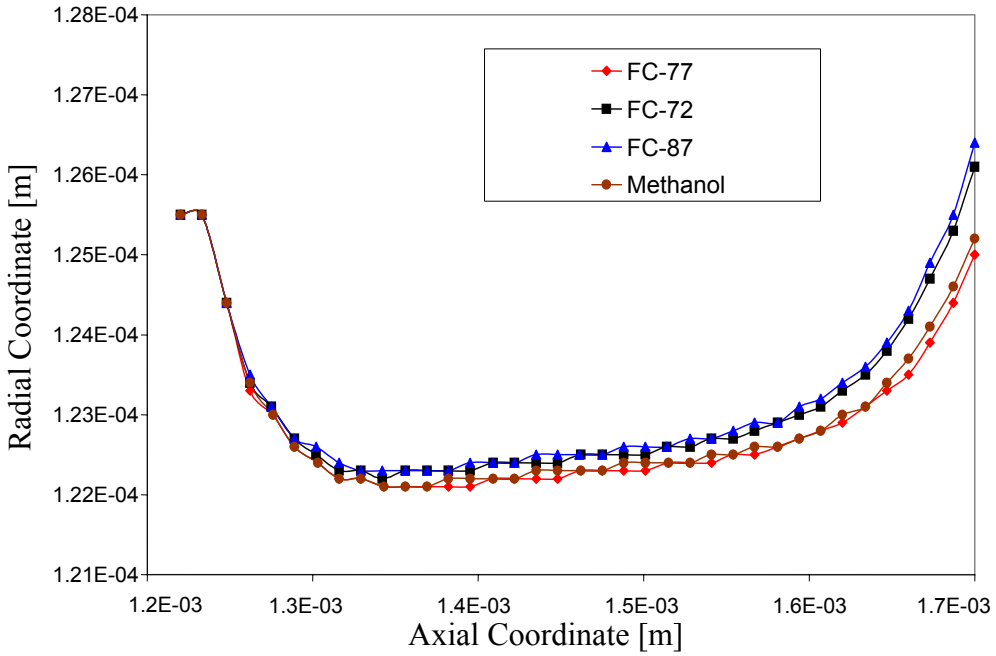

Figure 106: Magnified free surface profile for all fluids (Q = 4.416 x 10^{-7} m^3/s, R_2 = 4.0 x 10^{-4} m)

Figure 107 and Figure 108 show the free surface profile for this geometry with all of working fluids with an inlet flow rate of 5.678 x 10^{-7} m^3/s. Again, it was noted that FC-87 resulted in the highest free surface position, with a value of 1.261 x 10^{-4} m.

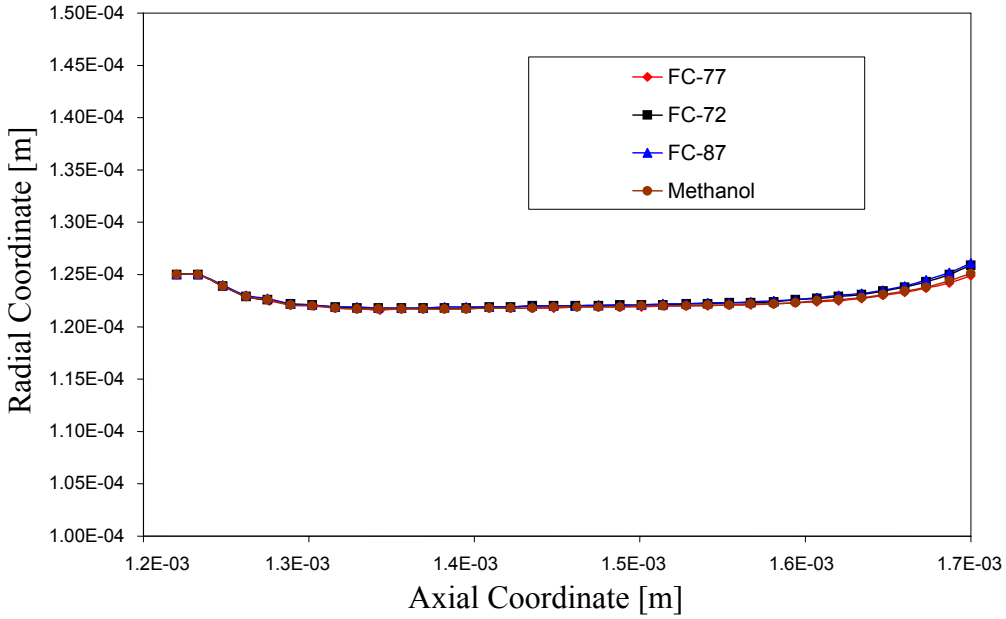

Figure 107: Free surface profile for all fluids (Q = 5.678 x 10^{-7} m^3/s, R_2 = 4.0 x 10^{-4} m)

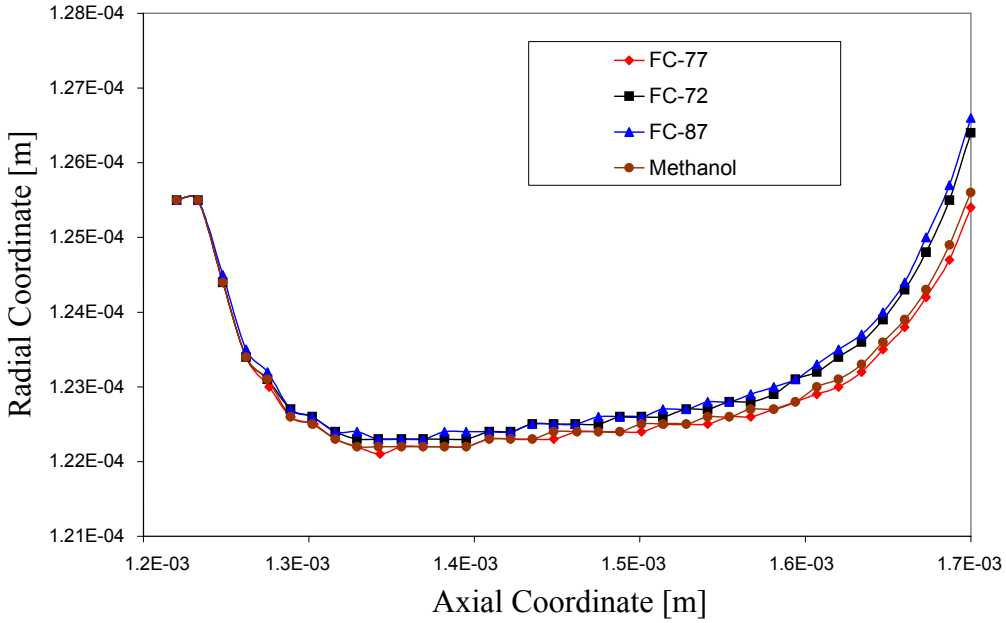

Figure 108: Magnified free surface profile for all fluids (Q = 5.678 x 10^{-7} m^3/s, R_2 = 4.0 x 10^{-4} m)

Figure 109 and 110 show the dimensionless free surface profile for all of the fluids within this nozzle geometry. Once again, a larger Reynolds number produced a larger radial height and cone angle for the free surface of the fluid exiting the nozzle.

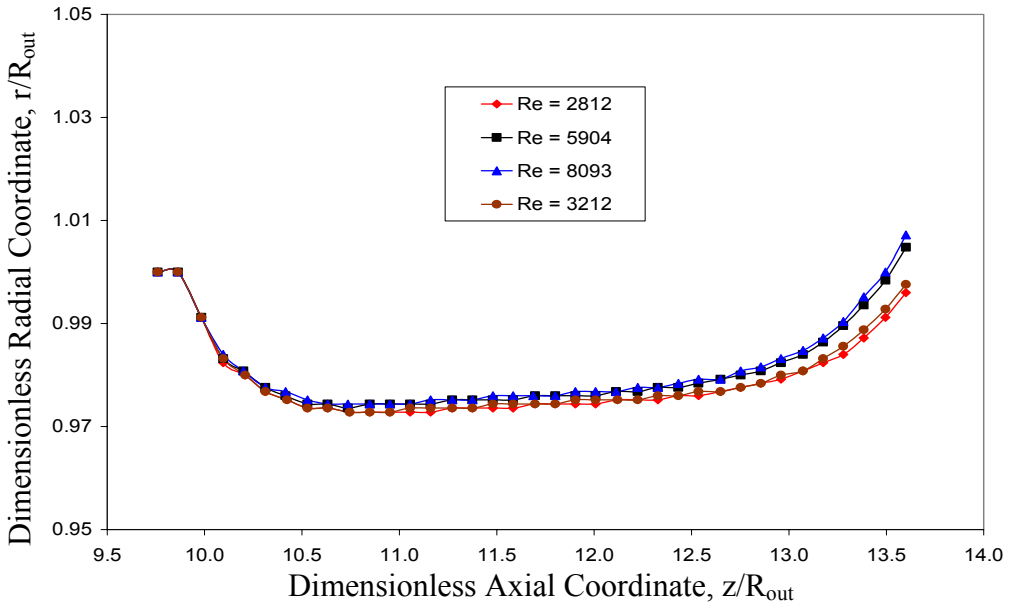

Figure 109: Dimensionless free surface profile for all fluids ($Q = 4.416 \times 10^{-7}$ m^3/s, $R_2 = 4.0 \times 10^{-4}$ m)

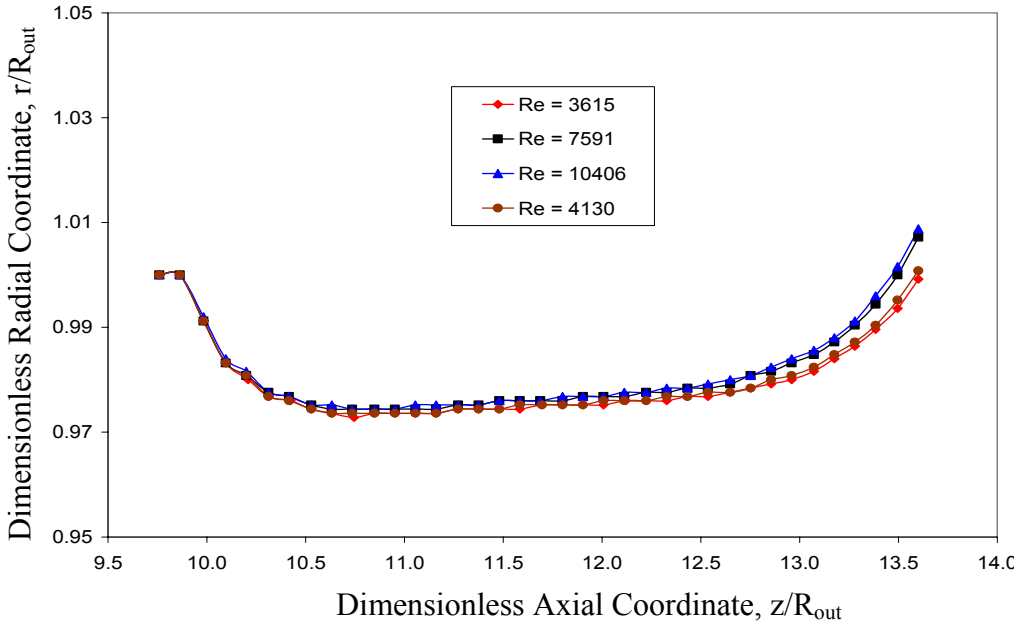

Figure 110: Dimensionless free surface profile for all fluids ($Q = 5.678 \times 10^{-7}$ m^3/s, $R_2 = 4.0 \times 10^{-4}$ m)

5.2.8.3 R_2 Equal to 5.50 x 10^{-4} m

The next geometry that was used was for the nozzle having R_2 equal to 5.50 x 10^{-4} m and R_3 equal to 5.77 x 10^{-4} m. The same fluids were used to investigate their effects on this nozzle geometry. The first situation to be discussed is when FC-77 was used as the working fluid with an inlet flow rate of 4.416 x 10^{-7} m^3/s. Figure 111 shows the velocity vector plot for this instance. The maximum velocity was determined to be 19.77 m/s, which was almost twice as high as this value for the other geometries. The free surface began at 1.250 x 10^{-4} m, declined to 1.219 x 10^{-4} m, then increased again to 1.261 x 10^{-4} m and had a cone angle of about 2.29 degrees. This location of the outer slot provided the most increase in the free surface height of the fluid.

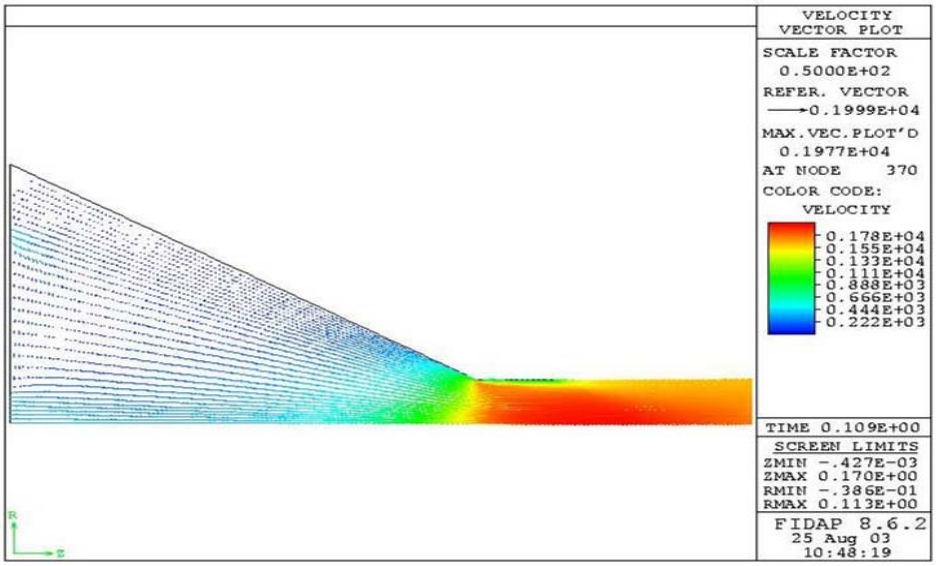

Figure 111: Velocity vector plot for FC-77 (Q = 4.416 x 10^{-7} m^3/s, R_2 = 5.5 x 10^{-4} m). Units are cm/s.

Figure 112 and Figure 113 show the pressure and streamline contour plots for this scenario. The maximum pressure plotted was found to be 3.99 x 10^5 Pa, whereas the minimum pressure was found to be -7.94 x 10^4 Pa. The inlet-to-outlet pressure drop was

calculated as 3.32 x 10^5 Pa. The streamline contour plot shows that most of the fluid that enters through the outer slot flows toward the center of the nozzle as it makes it way towards the outlet, with a portion of the entering fluid swirling in the upper region. The fluid entering through the central inlet has almost purely axial motion.

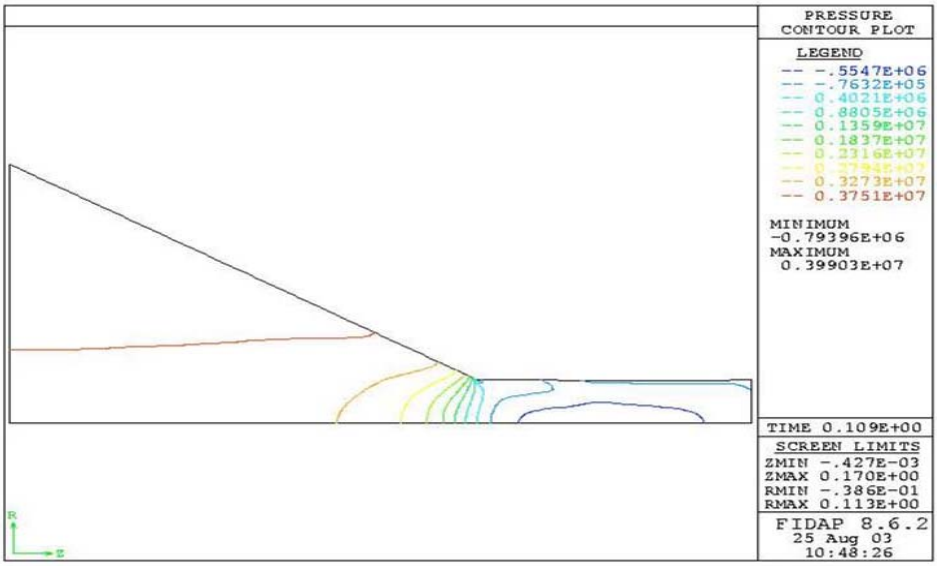

Figure 112: Pressure contour plot for FC-77 (Q = 4.416 x 10^{-7} m^3/s, R_2 = 5.5 x 10^{-4} m). Units are gm/cm s^2 (x10^1 Pa).

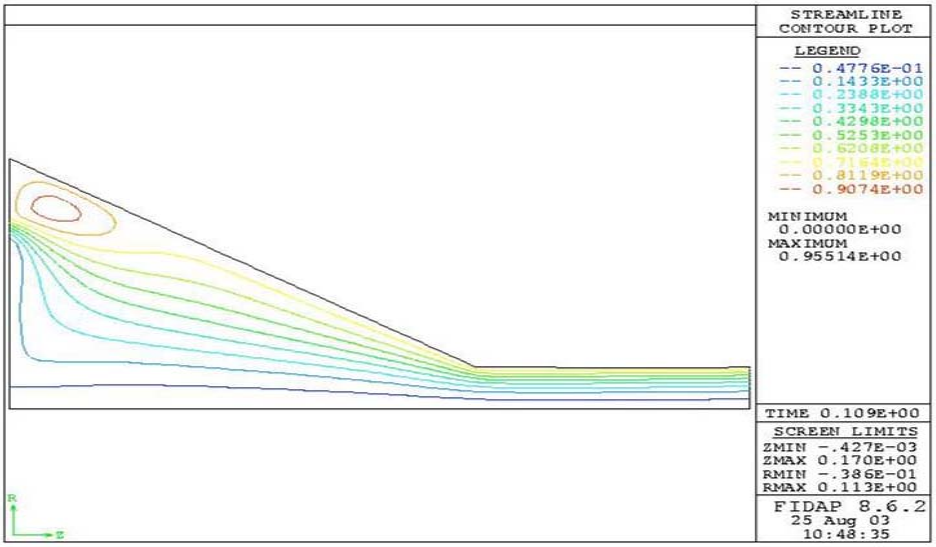

Figure 113: Streamline contour plot for FC-77 (Q = 4.416 x 10^{-7} m^3/s, R_2 = 5.5 x 10^{-4} m)

Next, FC-77 was still being used as the working fluid, but the flow rate was increased to 5.678 x 10^{-7} m^3/s. Figure 114 shows the velocity vector plot for this case. The maximum velocity was found to be about 25.40 m/s within the throat of the nozzle. Again, this value was close to double the value of the maximum velocity for the other nozzle geometries. Similar to the other trials, the free surface decreased in height at first before rising to its final position. For this case, the free surface began at 1.250 x 10^{-4} , decreased to 1.220 x 10^{-4} m, then increased to a height of 1.263 x 10^{-4} m. The cone angle was calculated to be 2.43 degrees, which along with Methanol, was the lowest value.

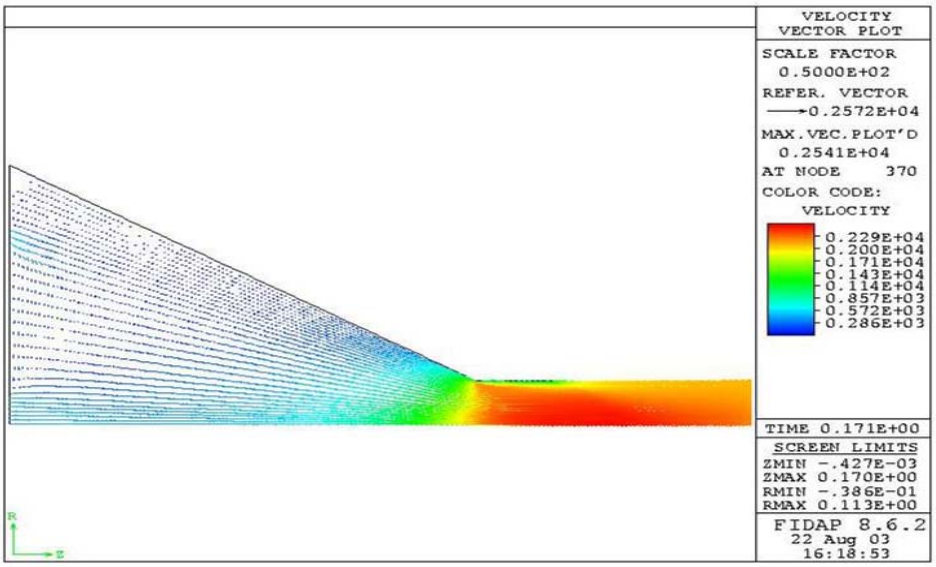

Figure 114: Velocity vector plot for FC-77 (Q = 5.678 x 10^{-7} m^3/s, R_2 = 5.5 x 10^{-4} m). Units are cm/s.

The pressure contour plot for this case is shown in Figure 115. The maximum pressure within the nozzle was found to be 6.59 x 10^5 Pa, and the minimum pressure was found to be -1.38 x 10^5 Pa. The inlet-to-outlet pressure drop was determined to be approximately 5.58 x 10^5 Pa. Figure 116 shows the streamline contour plot for this scenario. This plot is very similar to the streamline plot for the last trial. Most of the

entering fluid flows toward the center of the nozzle as it moves throughout the nozzle. Still, a fraction of the fluid gets caught swirling in an upper region of the nozzle. This region is smaller than the other nozzle geometries because the location of the outer slot is located more toward the outer edge of the nozzle.

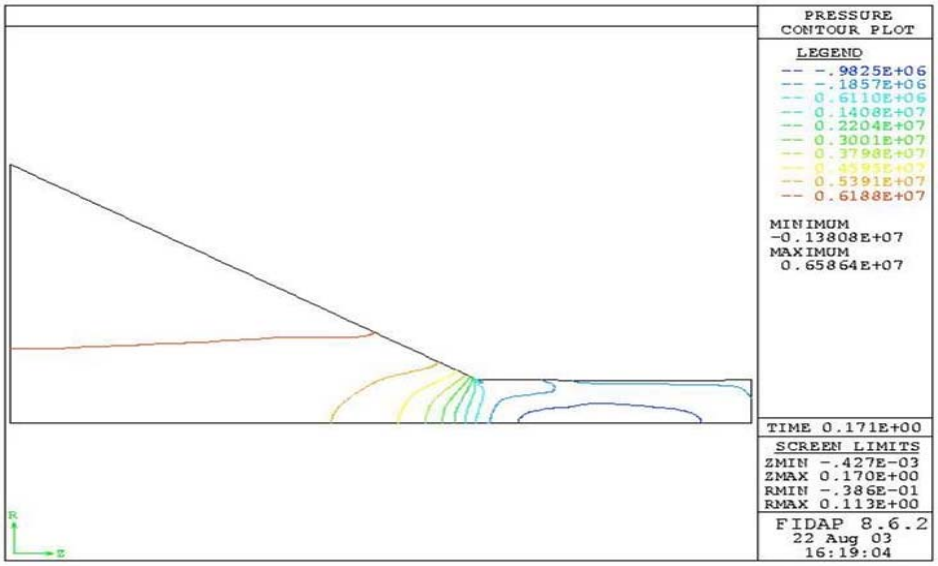

Figure 115: Pressure contour plot for FC-77 ($Q = 5.678 \times 10^{-7}$ m^3/s, $R_2 = 5.5 \times 10^{-4}$ m). Units are gm/cm s^2 ($x10^1$ Pa).

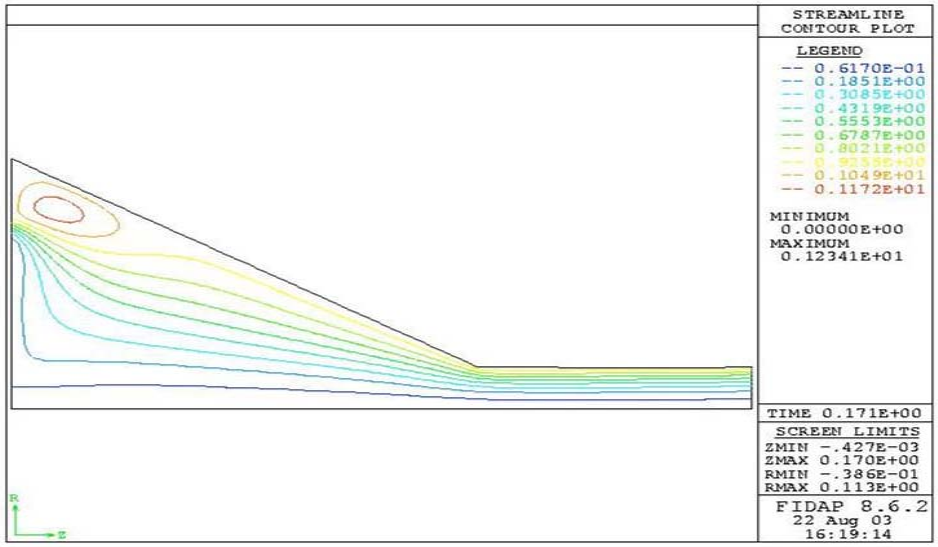

Figure 116: Streamline contour plot for FC-77 ($Q = 5.678 \times 10^{-7}$ m^3/s, $R_2 = 5.5 \times 10^{-4}$ m)

Next, the investigation was continued by changing the working fluid from FC-77 to FC-72. Figure 117 shows the velocity vector plot for the nozzle geometry having R_2 equal to 5.50 x 10^{-4} m, FC-72 as the working fluid, and 4.416 x 10^{-7} m^3/s as the inlet flow rate. The maximum velocity for this scenario was determined to be 19.77 m/s, which is the same maximum velocity that was found when FC-77 was operating under the same circumstances. The free surface height for this case began at 1.250 x 10^{-4} m, gradually dropped to 1.220 x 10^{-4} m, and then rose to a final height of 1.268 x 10^{-4} m and had a cone angle of 2.72 degrees. Overall, this location of the outer inlet slot resulted in the most significant increase in the free surface height for all of the fluids that were analyzed.

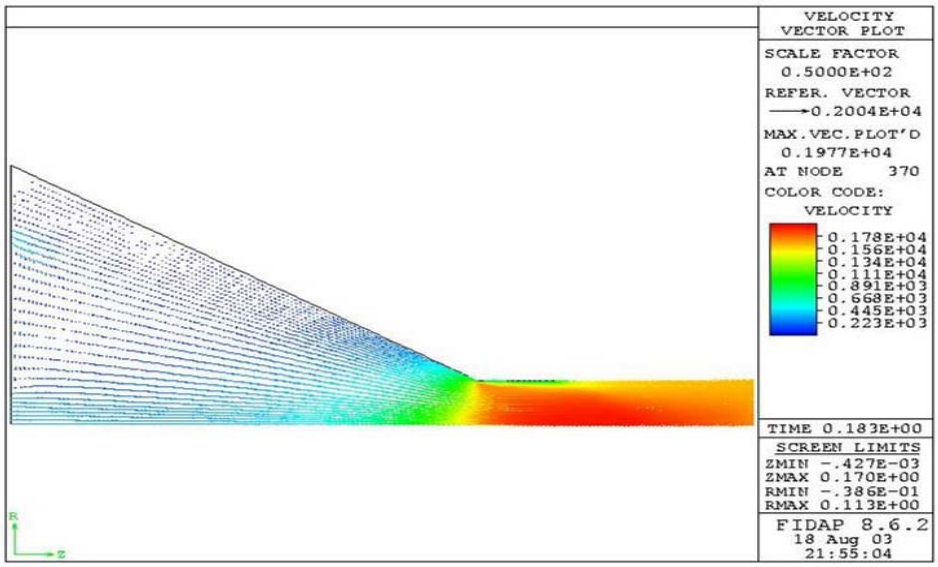

Figure 117: Velocity vector plot for FC-72 (Q = 4.416 x 10^{-7} m^3/s, R_2 = 5.5 x 10^{-4} m). Units are cm/s.

Figure 118 shows the pressure contour plot for this situation. The maximum pressure was found to be 3.75 x 10^5 Pa, while the minimum pressure within the nozzle was -8.46 x 10^4 Pa. The calculated value for the pressure drop from the inlet of the nozzle to the outlet was determined to be 3.39 x 10^5 Pa. The streamline contour plot for

this case is shown in Figure 119. Again, the fluid entering the nozzle through the central inlet has almost pure axial motion throughout. However, most of the fluid entering through the outer slot flows toward the center of the nozzle as it moves toward the outlet.

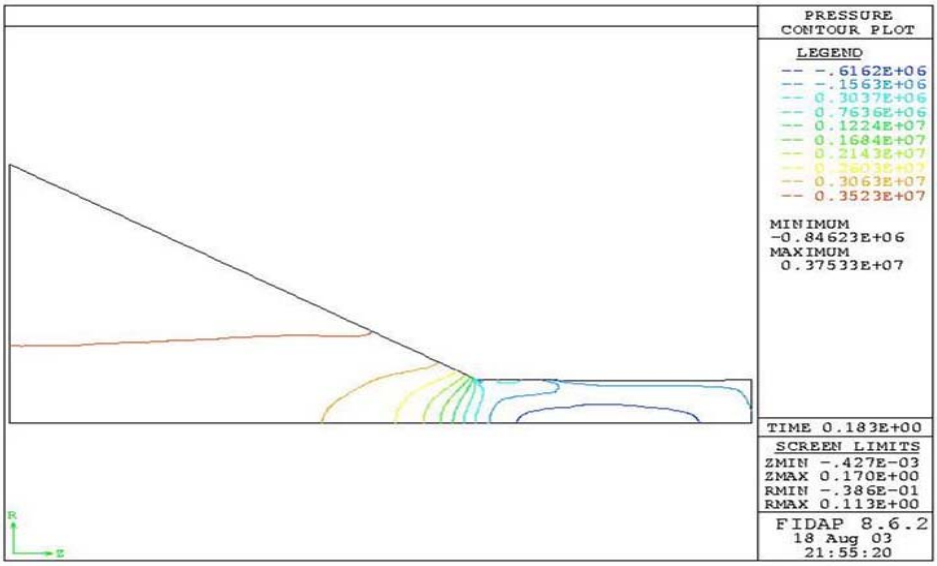

Figure 118: Pressure contour plot for FC-72 ($Q = 4.416 \times 10^{-7}$ m^3/s, $R_2 = 5.5 \times 10^{-4}$ m). Units are gm/cm s^2 ($x10^1$ Pa).

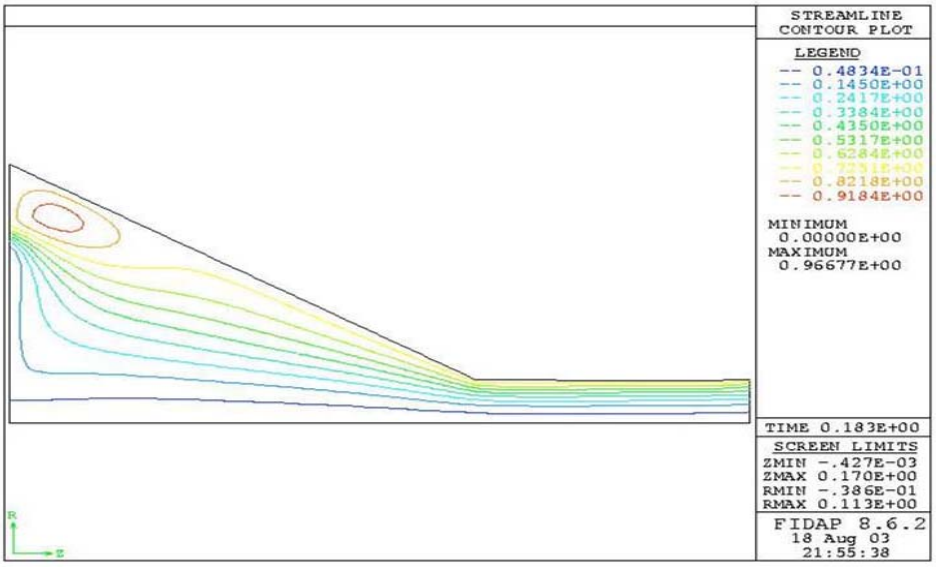

Figure 119: Streamline contour plot for FC-72 ($Q = 4.416 \times 10^{-7}$ m^3/s, $R_2 = 5.5 \times 10^{-4}$ m)

Next, the inlet flow rate for FC-72 was increased to 5.678 x 10^{-7} m^3/s. Figure 120 shows the velocity vector plot for this instance. The maximum velocity, similar to the other trials, was found to be located in the throat of the nozzle and have a value of about 25.40 m/s. This value, again, is much greater than any of the maximum velocity values obtained from the other geometries. The free surface began at height of 1.250 x 10^{-4} m, decreased to 1.220 x 10^{-4} m, and then increased to a final height of 1.269 x 10^{-4} m. The resulting cone angle was calculated to be 2.72 degrees, which is the same value obtained for this fluid traveling at 4.416 x 10^{-7} m^3/s within this same nozzle geometry.

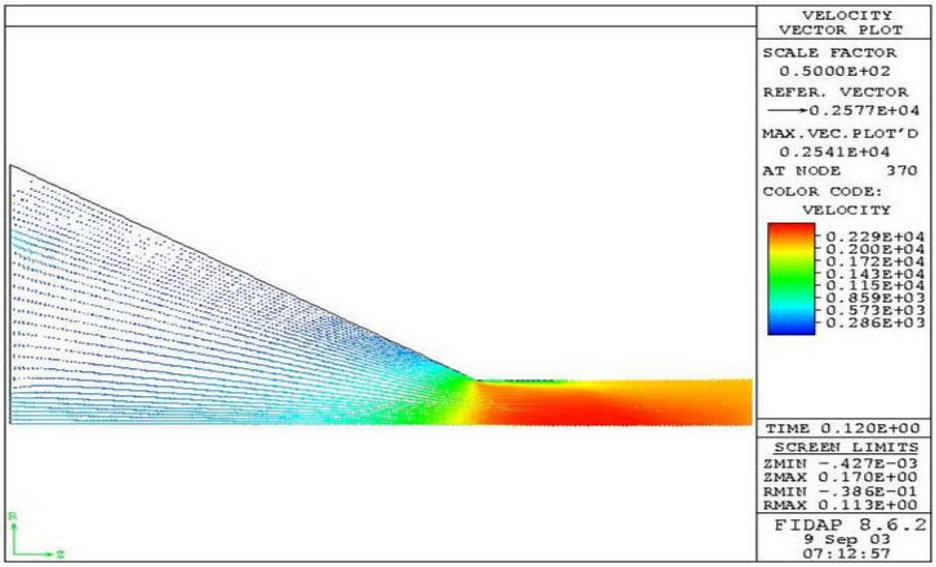

Figure 120: Velocity vector plot for FC-72 (Q = 5.678 x 10^{-7} m^3/s, R_2 = 5.5 x 10^{-4} m). Units are cm/s.

The pressure contour plot and the streamline contour plot are shown in Figure 121 and Figure 122, respectively. The maximum pressure within the nozzle was determined to be about 6.20 x 10^5 Pa, while the minimum pressure was found to be -1.43 x 10^5 Pa. The inlet-to-outlet pressure drop was calculated to be approximately 6.51 x 10^5 Pa. Again, the streamline plot shows that the fluid entering through the central inlet has

almost a pure axial motion as it flows to the nozzle outlet. However, most of the fluid entering through the outer inlet slot flows inward toward the line of symmetry before it heads toward the outlet. Some of the fluid entering through the outer inlet slot must flow around a pocket of swirling fluid as it reaches the nozzle wall.

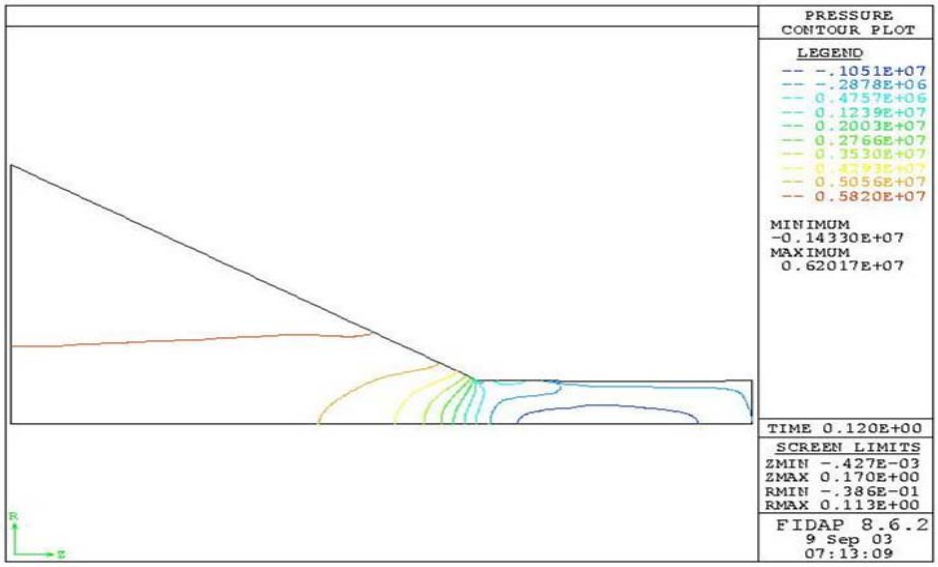

Figure 121: Pressure contour plot for FC-72 ($Q = 5.678 \times 10^{-7}$ m^3/s, $R_2 = 5.5 \times 10^{-4}$ m). Units are gm/cm s^2 ($x10^1$ Pa).

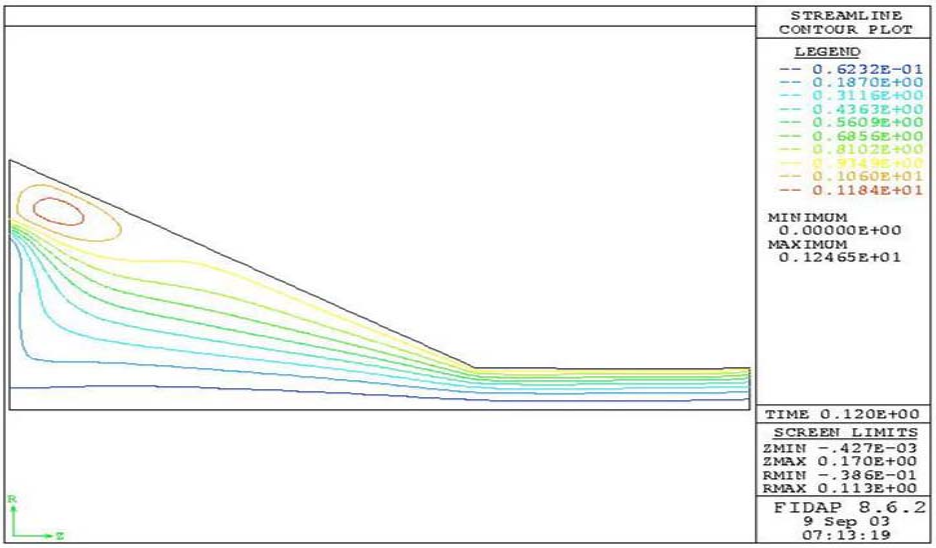

Figure 122: Streamline contour plot for FC-72 ($Q = 5.678 \times 10^{-7}$ m^3/s, $R_2 = 5.5 \times 10^{-4}$ m)

The next variation with this nozzle geometry involved changing the working fluid to FC-87. Figure 123 shows the velocity vector plot of the first case to be analyzed, which was FC-87 entering at 5.678 x 10^{-7} m^3/s. The maximum velocity within the nozzle was found to be 19.77 m/s. The height of the free surface began at 1.250 x 10^{-4} m, decreased to 1.220 x 10^{-4} m, then increased to a height of 1.270 x 10^{-4} m, which resulted in a cone angle of 2.72 degrees. This value for the final free surface height was the largest value produced from any of the fluids that were used.

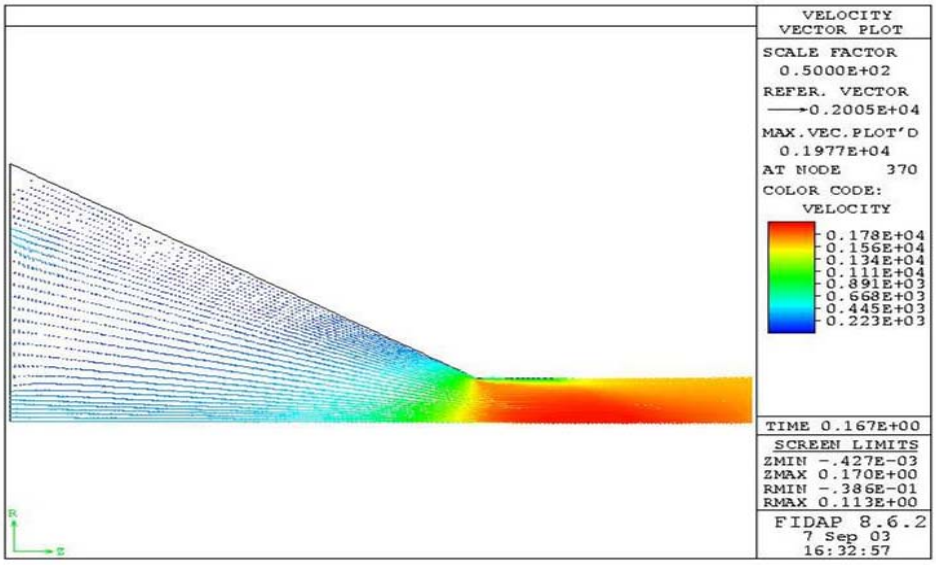

Figure 123: Velocity vector plot for FC-87 (Q = 4.416 x 10^{-7} m^3/s, R_2 = 5.5 x 10^{-4} m). Units are cm/s.

Figure 124 and Figure 125 show the pressure contour plot and the streamline contour plot, respectively. The maximum pressure within the nozzle was found to be about 3.64 x 10^5 Pa, whereas the minimum pressure was found to be -8.45 x 10^4 Pa. The pressure drop from the inlet of the nozzle to the outlet was calculated as 3.82 x 10^5 Pa. The streamline plot shows that some of the fluid entering through the outer slot moves toward the outer wall, while some of the fluid moves toward the center of the nozzle.

Again, the flow entering through the central inlet has almost pure axial movement throughout the nozzle.

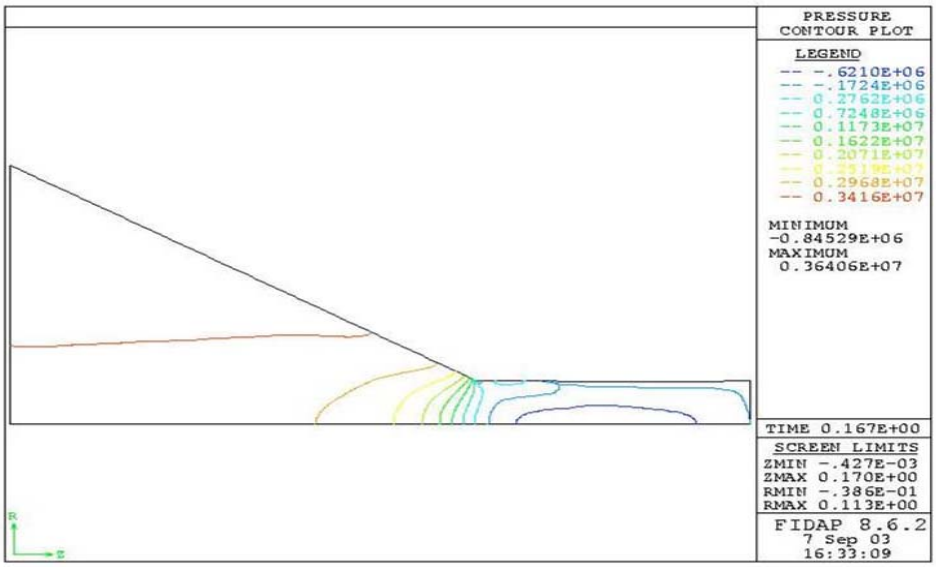

Figure 124: Pressure contour plot for FC-87 ($Q = 4.416 \times 10^{-7}$ m^3/s, $R_2 = 5.5 \times 10^{-4}$ m). Units are gm/cm s^2 ($x10^1$ Pa).

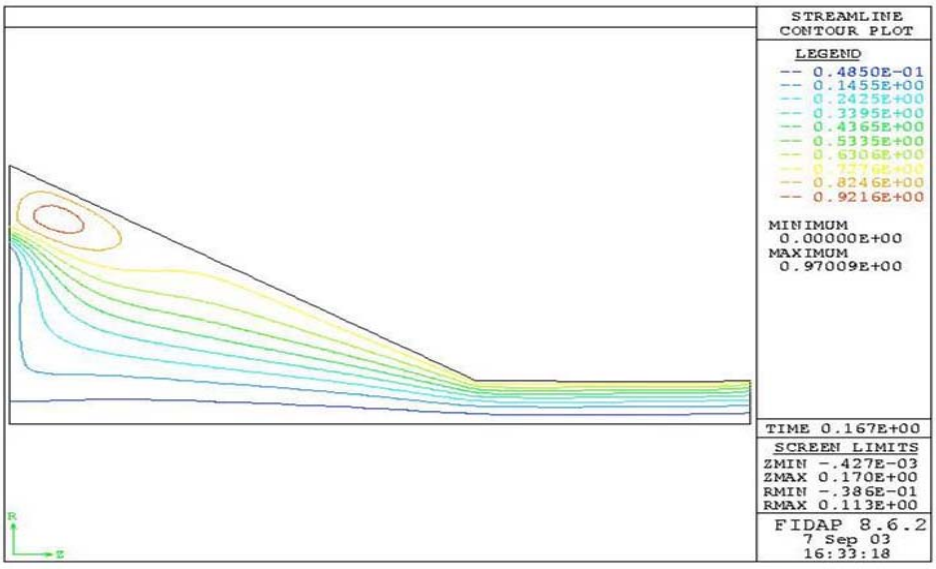

Figure 125: Streamline contour plot for FC-87 ($Q = 4.416 \times 10^{-7}$ m^3/s, $R_2 = 5.5 \times 10^{-4}$ m)

Next, the flow rate of the entering FC-87 for this nozzle geometry was increased to 5.678 x 10^{-7} m^3/s. Figure 126 shows the velocity vector plot for these parameters. The maximum velocity was found at the throat of the nozzle and had a value of approximately 25.40 m/s, which is extremely fast. The free surface began at a height of 1.250 x 10^{-4} m, declined to 1.220 x 10^{-4} m, and then rose to final height of 1.271 x 10^{-4} m. This radial height proved to be the greatest value for any of the trials performed in this study. The cone angle corresponding to the free surface position was determined to be 2.72 degrees.

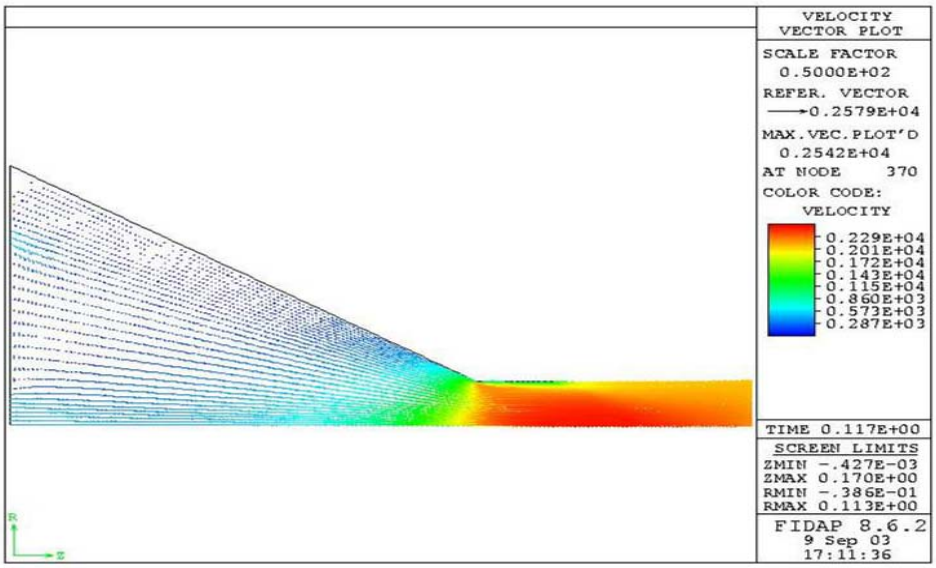

Figure 126: Velocity vector plot for FC-87 (Q = 5.678 x 10^{-7} m^3/s, R_2 = 5.5 x 10^{-4} m). Units are cm/s.

Figure 127 shows the pressure contour plot for this situation. The maximum pressure was found to be about 6.02 x 10^5 Pa, whereas the minimum pressure was found to be about -1.42 x 10^5 Pa. The pressure drop from the inlet of the nozzle to the outlet was calculated as 6.33 x 10^5 Pa. Figure 128 shows the streamline contour plot. It shows results that are similar to the other streamline plots obtained for this nozzle geometry. The fluid entering through the outer inlet slot must maneuver around a pocket of swirling

fluid located at the outer edge of the nozzle near the top plate. Since the location of the outer inlet slot has moved closer to the outer edge of the top plate, the pocket of swirling fluid trapped between it and the nozzle wall has decreased in size.

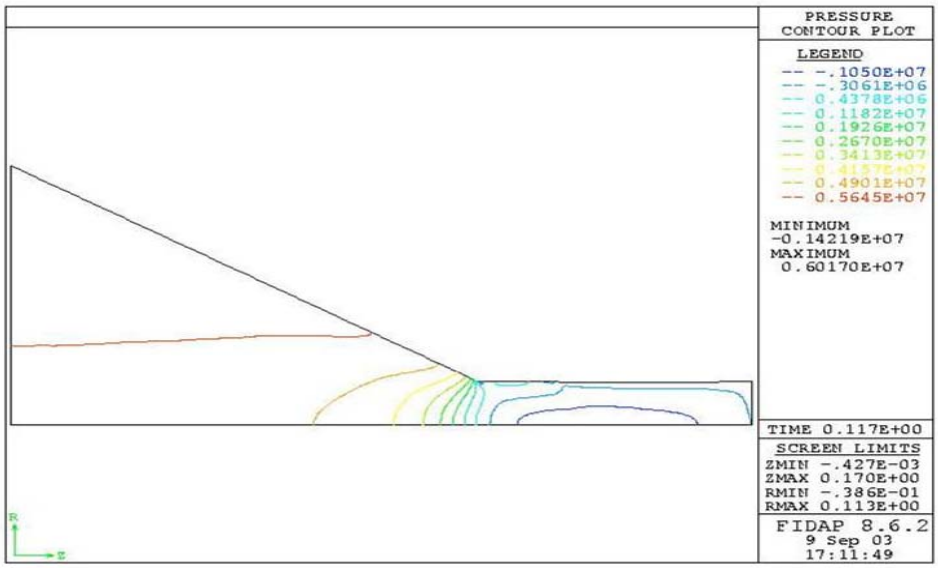

Figure 127: Pressure contour plot for FC-87 ($Q = 5.678 \times 10^{-7}$ m^3/s, $R_2 = 5.5 \times 10^{-4}$ m). Units are gm/cm s^2 ($x10^1$ Pa).

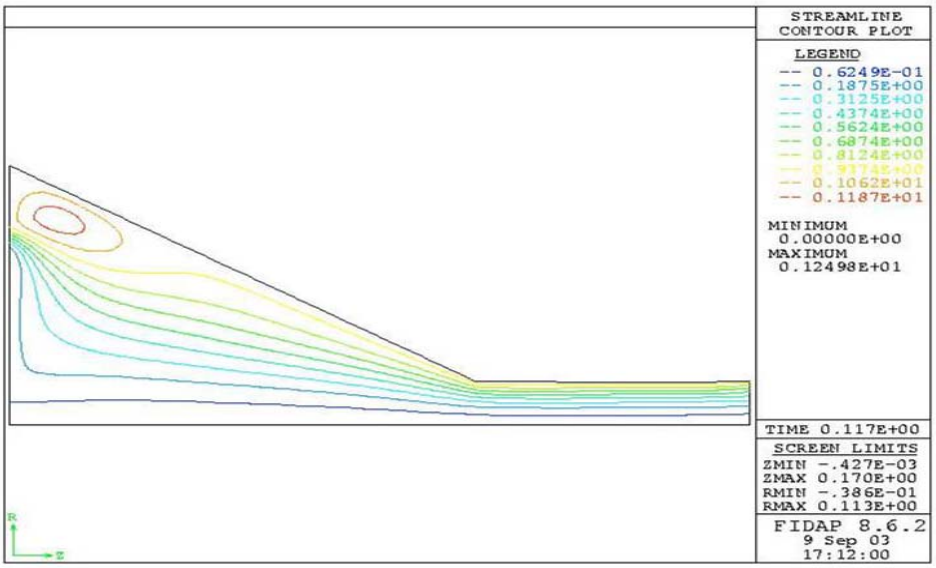

Figure 128: Streamline contour plot for FC-87 ($Q = 5.678 \times 10^{-7}$ m^3/s, $R_2 = 5.5 \times 10^{-4}$ m)

Next, methanol was used as the working fluid entering the nozzle with a flow rate of 4.416 x 10^{-7} m^3/s. Figure 129 shows the velocity vector plot for this situation. The maximum velocity is found to be in the throat of the nozzle with a value of 19.77 m/s. The height of the free surface began at 1.250 x 10^{-4} m, declined gradually to 1.220 x 10^{-4} m, then increased to a height of 1.262 x 10^{-4} m. The cone angle resulting from this trial was calculated as 2.29 degrees. These values were only greater than the values obtained with FC-77 used as the working fluid.

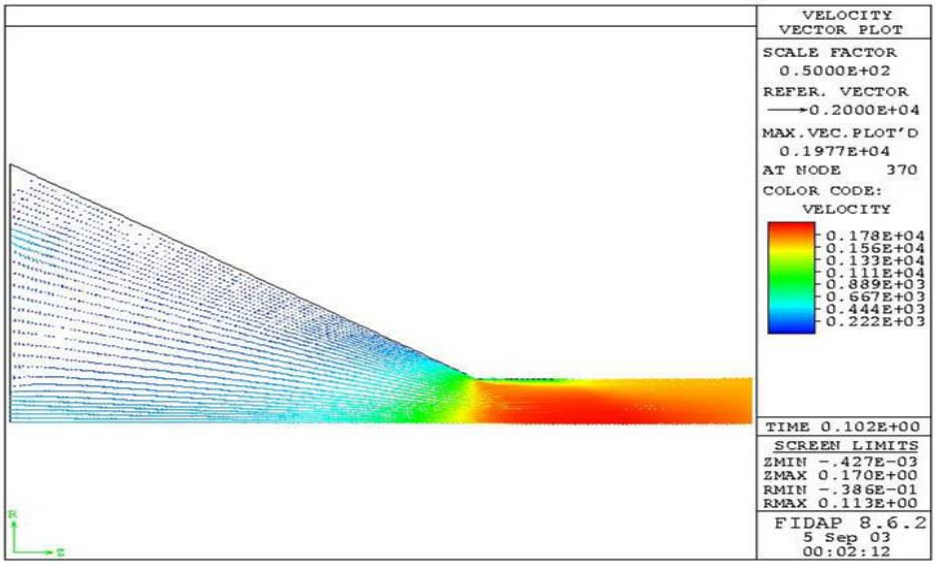

Figure 129: Velocity vector plot for Methanol (Q=4.416 x 10^{-7} m^3/s, R_2=5.5 x 10^{-4} m). Units are cm/s.

The pressure contour plot for this situation is shown in Figure 130. The maximum pressure within the nozzle was found to be 1.76 x 10^5 Pa, and the minimum pressure was -3.61 x 10^4 Pa. The inlet-to-outlet pressure drop was calculated to be about 1.83 x 10^5 Pa, which is one of the lower values found in this investigation. The streamline contour plot is shown in Figure 131. Similar to the other streamline plots, this plot shows that some of the fluid entering through the outer slot moves in the radial

direction toward the outer wall and some moves in the radial direction toward the center of the nozzle as the fluid moves through the nozzle.

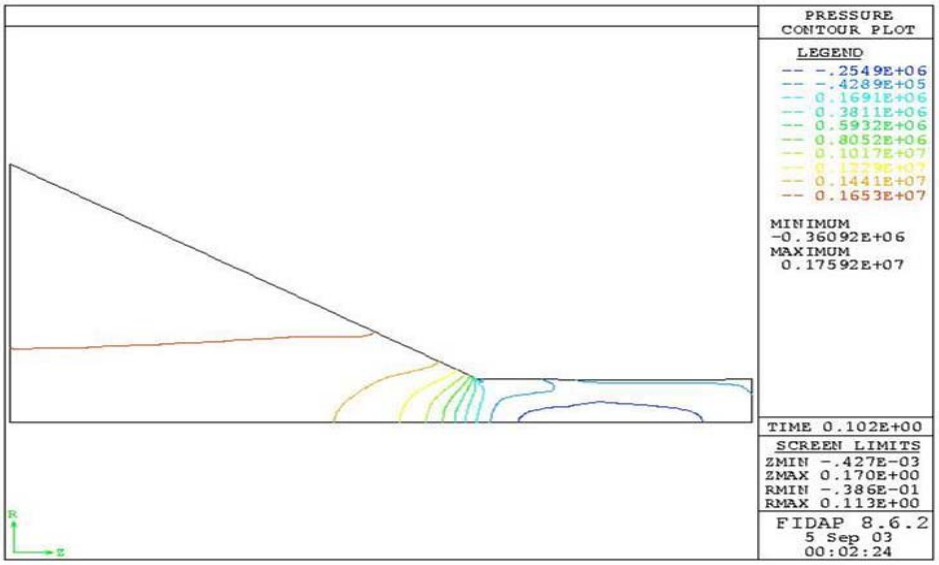

Figure 130: Pressure contour plot for Methanol ($Q = 4.416 \times 10^{-7}$ m^3/s, $R_2 = 5.5 \times 10^{-4}$ m). Units are gm/cm s^2 ($x10^1$ Pa).

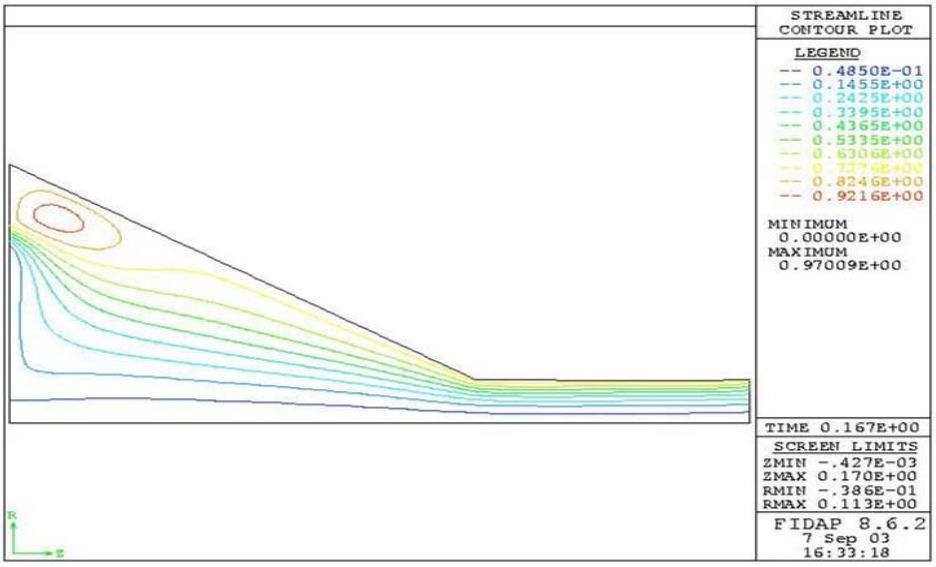

Figure 131: Streamline contour plot for Methanol ($Q = 4.416 \times 10^{-7}$ m^3/s, $R_2 = 5.5 \times 10^{-4}$ m)

The final variation performed with this geometry had Methanol as the working fluid with an inlet flow rate of 5.678 x 10^{-7} m^3/s. Figure 132 shows the results of the velocity vector plot for this scenario. Identical to the other trials performed with this nozzle geometry, the maximum velocity was found to be about 25.40 m/s. The free surface originated at a height of 1.250 x 10^{-4} m, decreased to 1.220 x 10^{-4} m, and then increased to a final height of 1.265 x 10^{-4} m. This free surface position produced a cone angle of approximately 2.43 degrees.

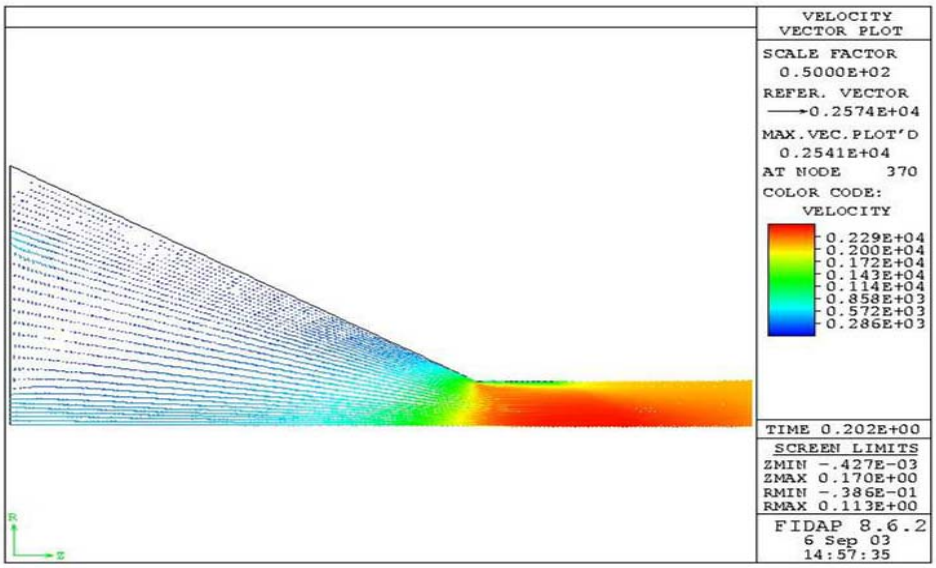

Figure 132: Velocity vector plot for Methanol (Q=5.678 x 10^{-7} m^3/s, R_2=5.5 x 10^{-4} m). Units are cm/s.

The pressure contour plot for this case is shown in Figure 133. The maximum pressure within the nozzle was found to be about 2.90 x 10^5 Pa, whereas the minimum pressure was found to be -6.24 x 10^4 Pa. The inlet-to-outlet pressure drop was calculated to be approximately 3.03 x 10^5 Pa. It was noted that Methanol provided the lowest inlet-to-outlet pressure drops of all of the fluids that were studied. Figure 134 shows the streamline contour plot for this case. Most of the fluid entering the outer inlet slot flows

toward the line of symmetry in the radial direction before it heads toward the nozzle outlet. However, some of the fluid entering from the outer inlet slot flows toward the nozzle wall as it makes it way toward the outlet.

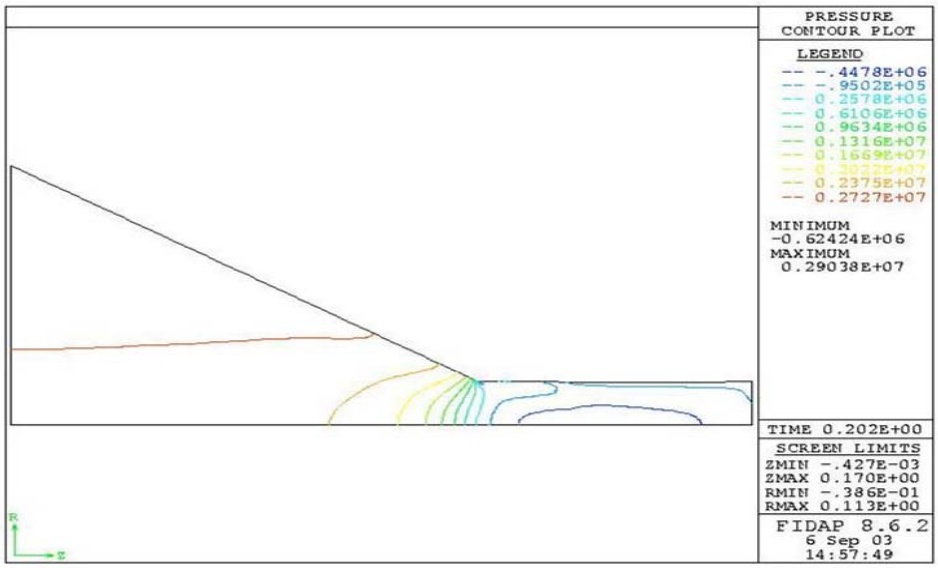

Figure 133: Pressure contour plot for Methanol ($Q = 5.678 \times 10^{-7}$ m^3/s, $R_2 = 5.5 \times 10^{-4}$ m). Units are gm/cm s^2 ($x10^1$ Pa).

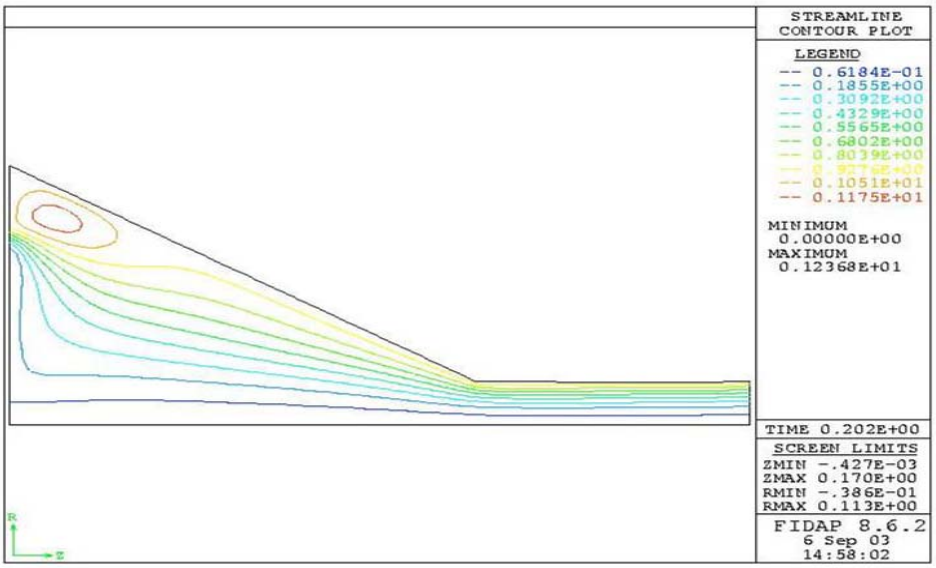

Figure 134: Streamline contour plot for Methanol ($Q = 5.678 \times 10^{-7}$ m^3/s, $R_2 = 5.5 \times 10^{-4}$ m)

Figure 135 and Figure 136 show the free surface profile for all of the fluids that were tested in the nozzle with this geometry. This figure depicts the results obtained solely for the inlet flow rate of 4.416 x 10^{-7} m^3/s. It was observed that FC-87 resulted in the highest free surface, where FC-77 resulted in the lowest.

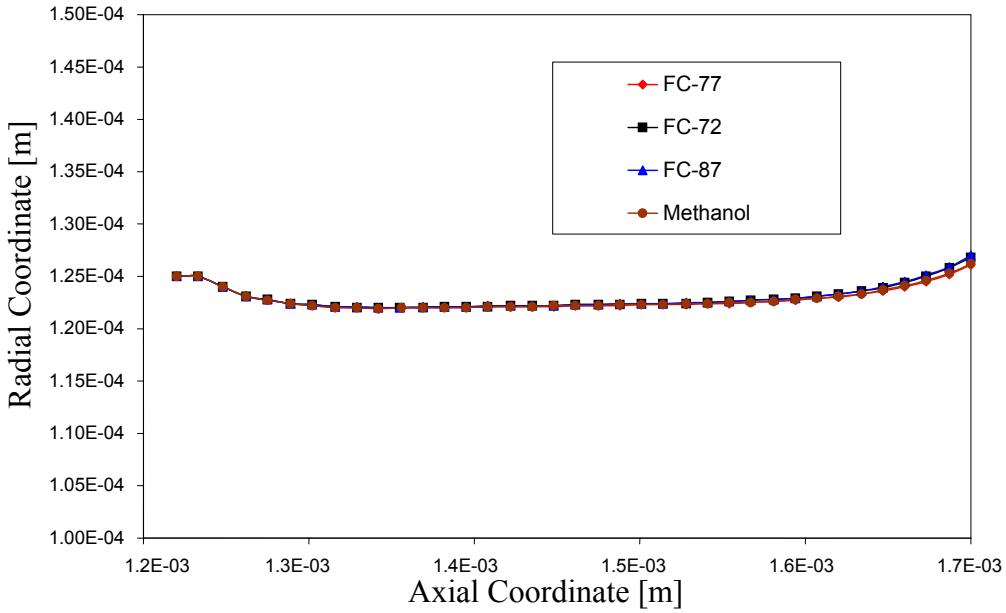

Figure 135: Free surface profile for all of the fluids (Q = 4.416 x 10^{-7} m^3/s, R_2 = 5.5 x 10^{-4} m)

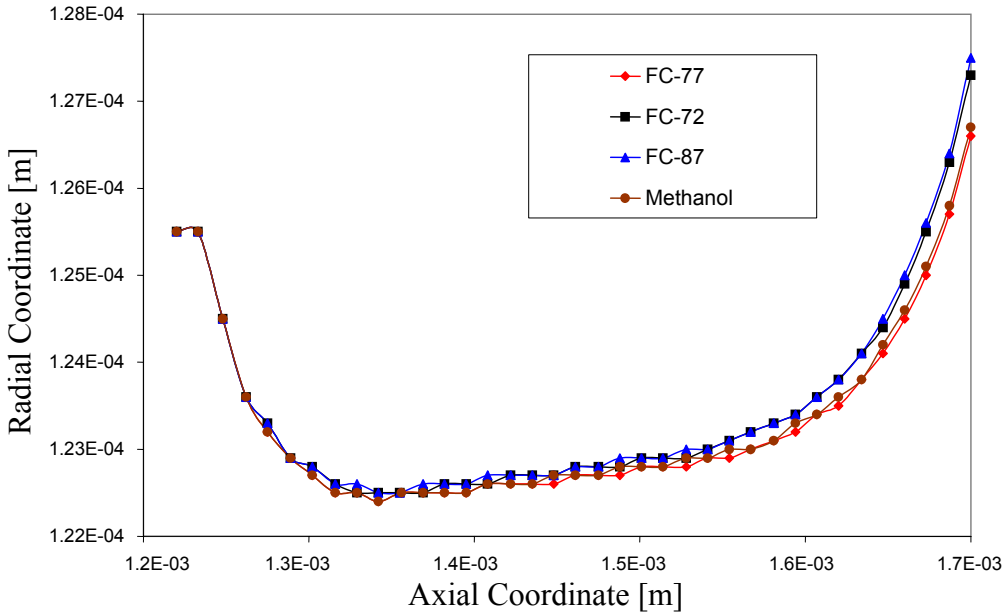

Figure 136: Magnified view of free surface profile for all fluids (Q=4.416 x 10^{-7} m^3/s, R_2=5.5 x 10^{-4} m)

Figure 137 and Figure 138 show the free surface profile for all of the fluids that were tested in the nozzle with this geometry at a flow rate of 5.678 x 10^{-7} m^3/s. It was observed that FC-87 resulted in the highest free surface, where FC-77 had the lowest.

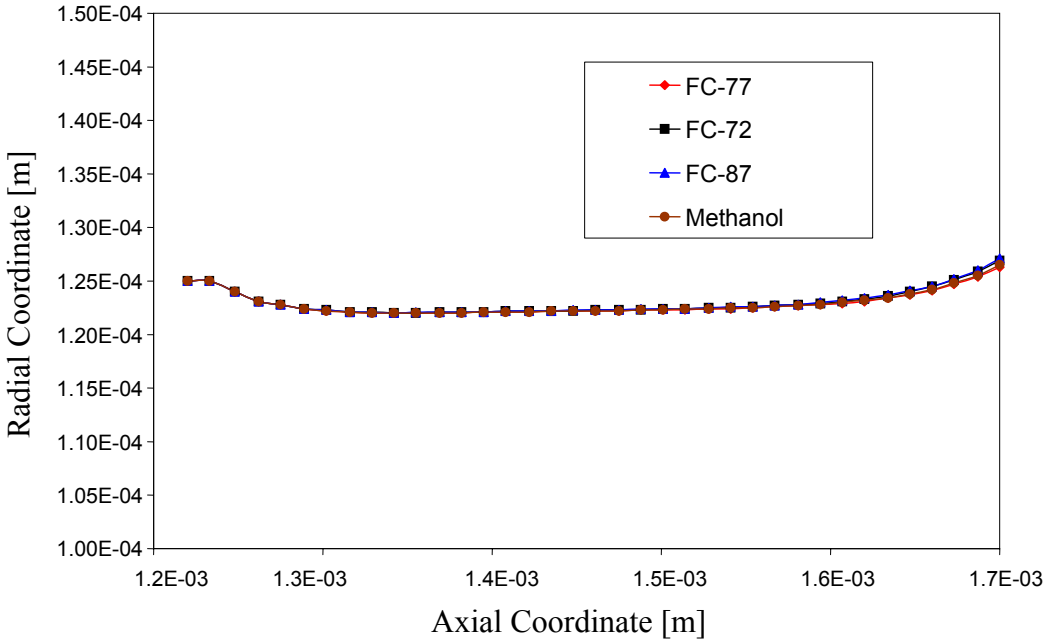

Figure 137: Free surface profile for all fluids (Q = 5.678 x 10^{-7} m^3/s, R_2 = 5.5 x 10^{-4} m)

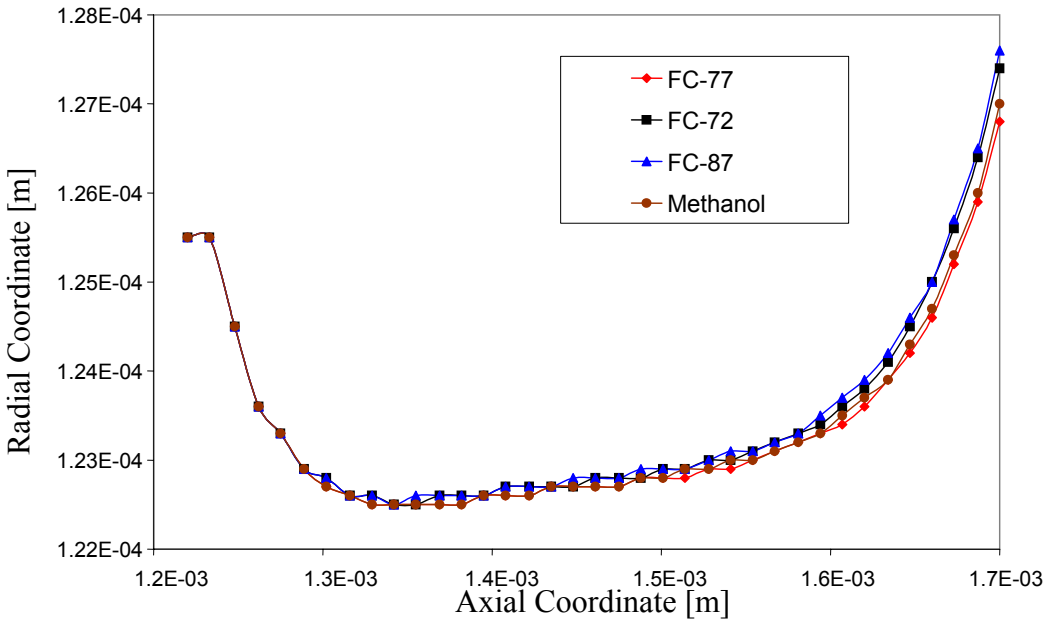

Figure 138: Magnified free surface profile for all fluids (Q = 5.678 x 10^{-7} m^3/s, R_2 = 5.5 x 10^{-4} m)

Figure 139 and Figure 140 each show the dimensionless free surface profile for each fluid flowing in this nozzle geometry. The larger Reynolds number at the nozzle exit produced the larger free surface height; however, the height does not vary too much for the different Reynolds numbers that were evaluated.

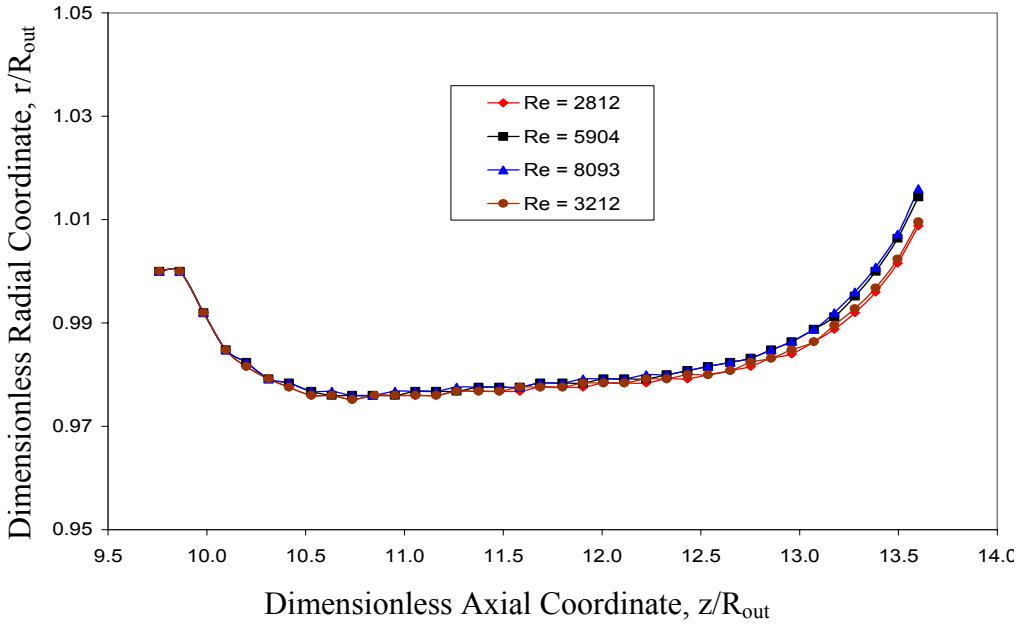

Figure 139: Dimensionless free surface profile for all fluids ($Q = 4.416 \times 10^{-7}$ m^3/s, $R_2 = 5.5 \times 10^{-4}$ m)

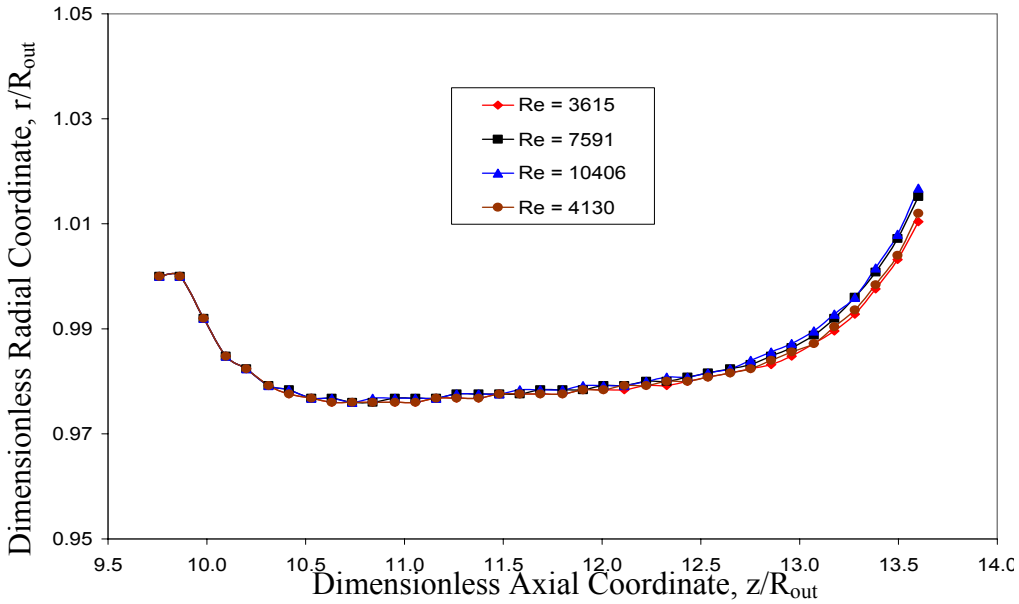

Figure 140: Dimensionless free surface profile for all fluids ($Q = 5.678 \times 10^{-7}$ m^3/s, $R_2 = 5.5 \times 10^{-4}$ m)

5.2.8.4 R_2 Equal to 7.20 x 10^{-4} m

The final variation in nozzle geometry was having R_2 equal to 7.20 x 10^{-4} m, which put R_3 at 7.43 x 10^{-4} m. This location put the outer inlet slot at the very edge of the nozzle. Figure 141 shows the velocity vector plot for FC-77 traveling at 4.416 x 10^{-7} m^3/s. The maximum velocity was found to be about 9.44 m/s within the throat of the nozzle. This is the main reason that the final height of the free surface decreased for this geometry. The free surface height began at 1.250 x 10^{-4} m, decreased to 1.219 x 10^{-4} m, then increased to a final height of 1.244 x 10^{-4} m. This value is almost identical to the height obtained when R_2 was equal to 4.00 x 10^{-4} m. The cone angle for this trial was calculated to be a mere 1.62 degrees.

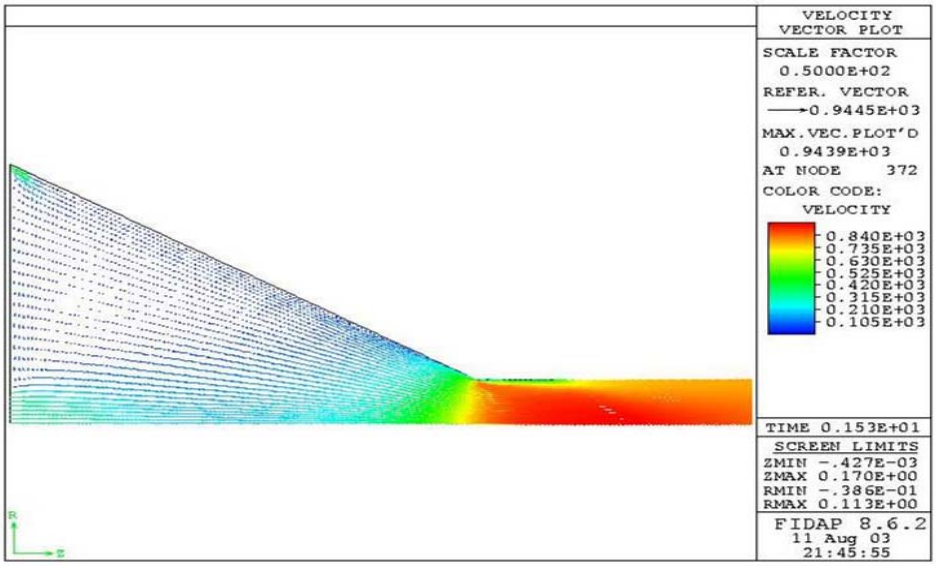

Figure 141: Velocity vector plot for FC-77 (Q = 4.416 x 10^{-7} m^3/s, R_2 = 7.2 x 10^{-4} m). Units are cm/s.

Figure 142 and Figure 143 show the pressure and streamline contour plots. The pressure data revealed that the inlet-to-outlet pressure drop was about 6.87 x 10^4 Pa. The streamline contour plot shows that some of the fluid entering through the outer slot of the

nozzle flows toward the center of the nozzle, then toward the outlet, while some of the fluid flows along the outer wall towards the outlet. The flow entering through the central inlet almost has a pure axial motion. Contrary to the other nozzle geometries, this configuration does not produce a portion of swirling fluid.

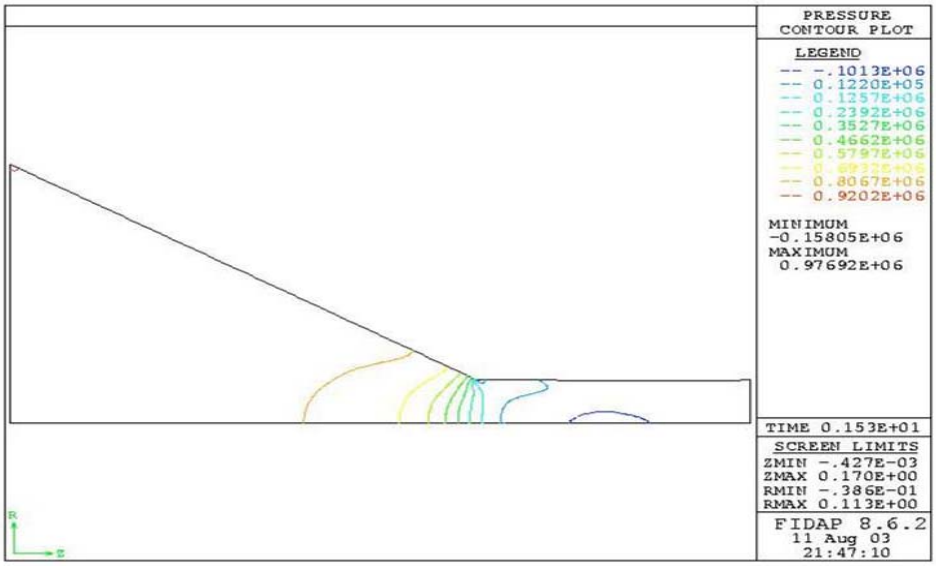

Figure 142: Pressure contour plot for FC-77 ($Q = 4.416 \times 10^{-7}$ m^3/s, $R_2 = 7.2 \times 10^{-4}$ m). Units are $gm/cm\ s^2$ ($x10^1$ Pa).

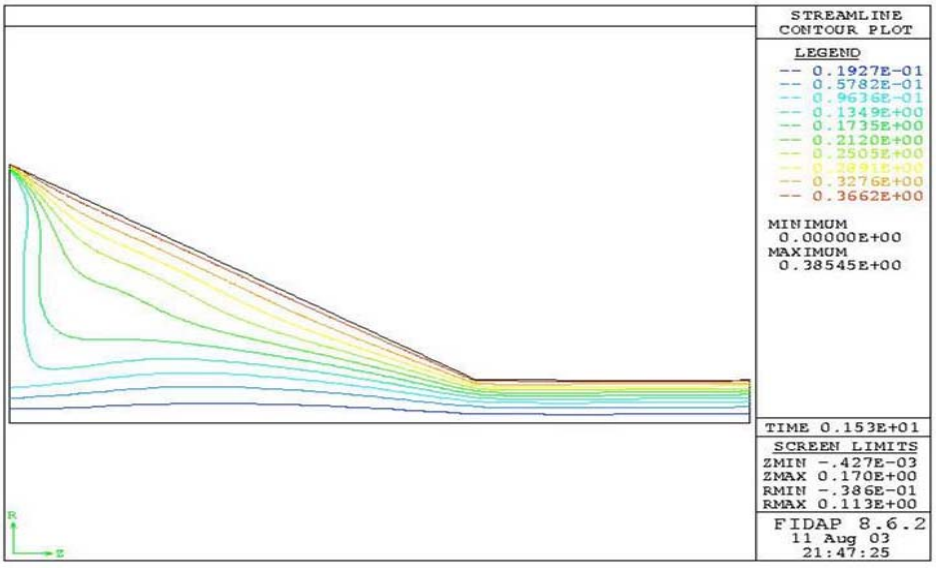

Figure 143: Streamline contour plot for FC-77 ($Q = 4.416 \times 10^{-7}$ m^3/s, $R_2 = 7.2 \times 10^{-4}$ m)

FC-77 was kept as the working fluid as the inlet flow rate increased from 4.416 x 10^{-7} m^3/s to 5.678 x 10^{-7} m^3/s. Figure 144 shows the velocity vector plot for this scenario. The maximum velocity within the nozzle was located in the throat and had a value of 12.16 m/s. The free surface began at a height of 1.250 x 10^{-4} m, gradually declined to 1.220 x 10^{-4} m, before climbing to a final height of 1.250 x 10^{-4} m and had a corresponding cone angle of 1.95 degrees. These values were less than those obtained when R_2 was equal to 5.50 x 10^{-4} m and FC-77 was traveling at 5.678 x 10^{-7} m^3/s.

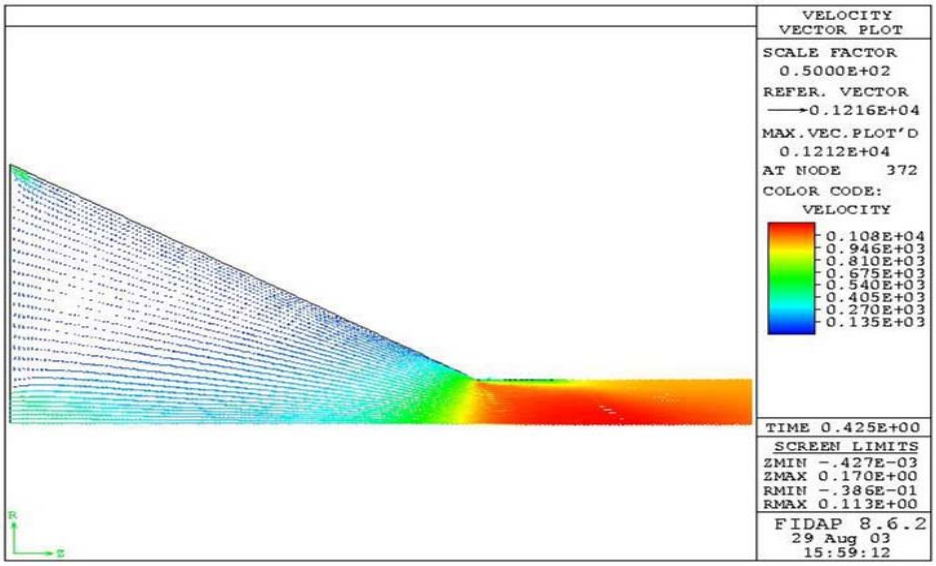

Figure 144: Velocity vector plot for FC-77 (Q = 5.678 x 10^{-7} m^3/s, R_2 = 7.2 x 10^{-4} m). Units are cm/s.

The pressure contour plot for this case can be seen in Figure 145. The maximum pressure that was plotted was 1.61 x 10^5 Pa, whereas the minimum pressure was found to be -2.69 x 10^4 Pa. The pressure drop from the inlet to the outlet of the nozzle was calculated as 1.24 x 10^5 Pa. Figure 146 shows the streamline contour plot. Again, this plot shows that some of the fluid entering the nozzle through the outer inlet slow travels along the top plate of the nozzle toward the center. There, it makes it way toward the

outlet of the nozzle. The other portion of the fluid entering through the outer slot travels along the outer wall toward the outlet. And similar to the other nozzle configurations, the flow entering through the central inlet has almost pure axial motion.

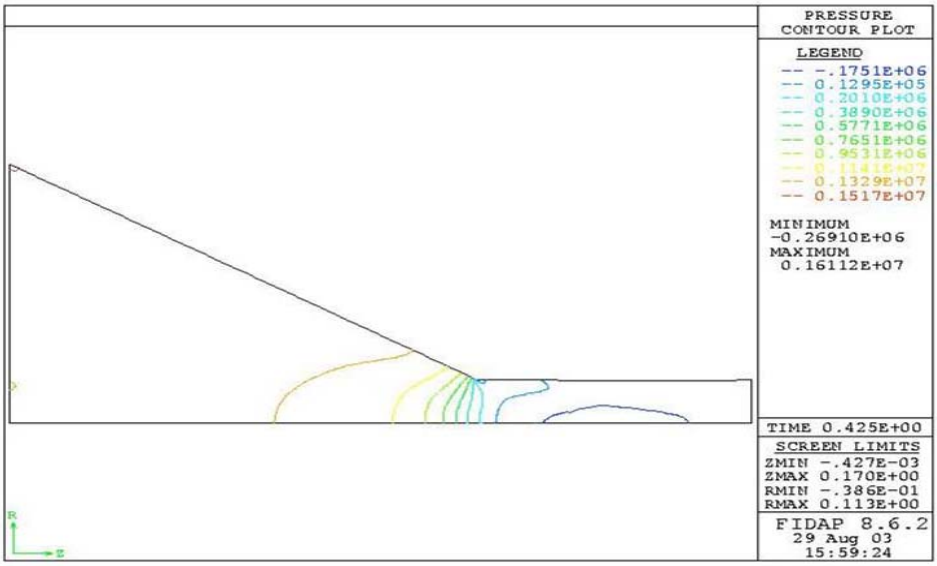

Figure 145: Pressure contour plot for FC-77 ($Q = 5.678 \times 10^{-7}$ m^3/s, $R_2 = 7.2 \times 10^{-4}$ m). Units are gm/cm s^2 ($x10^1$ Pa).

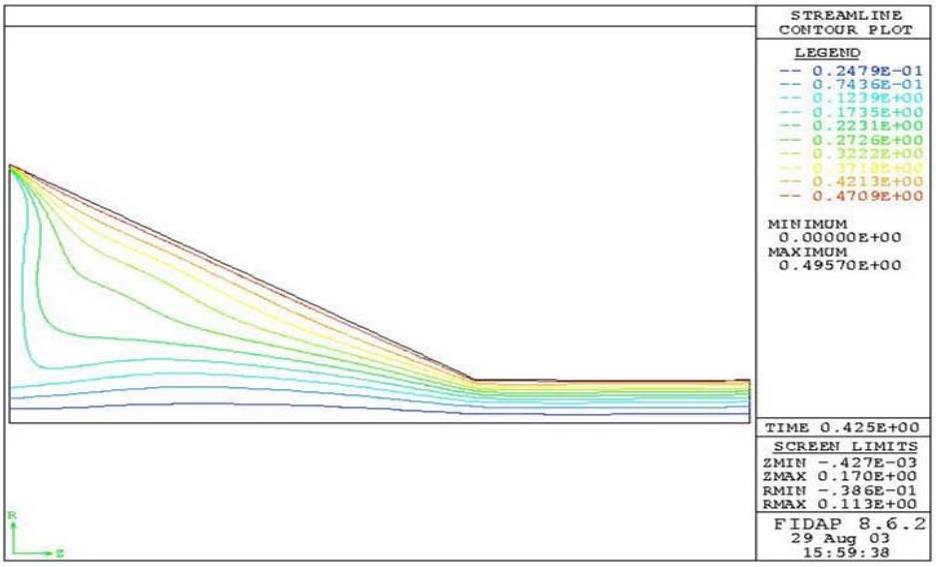

Figure 146: Streamline contour plot for FC-77 ($Q = 5.678 \times 10^{-7}$ m^3/s, $R_2 = 7.2 \times 10^{-4}$ m)

The next variation performed with this nozzle geometry involved changing the working fluid to FC-72 and running the fluid at 4.416 x 10^{-7} m^3 /s. Figure 147 shows the velocity vector plot for this situation. The maximum velocity was found to be about 9.42 m/s. The free surface started out at a height of 1.250 x 10^{-4} m, decreased to a height of 1.221 x 10^{-4} m, and then rose to a final height of 1.260 x 10^{-4} m. The cone angle that resulted from this particular free surface was determined to be 2.59 degrees.

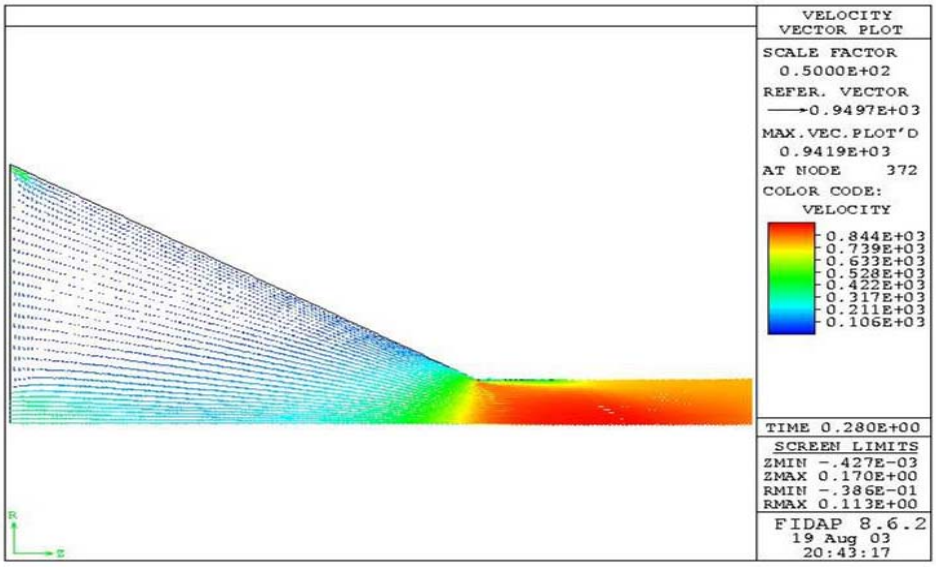

Figure 147: Velocity vector plot for FC-72 (Q = 4.416 x 10^{-7} m^3/s, R_2 = 7.2 x 10^{-4} m). Units are cm/s.

Figure 148 and Figure 149 show the pressure contour plot and the streamline contour plot for this case, respectively. The maximum pressure was found to be 9.22 x 10^4 Pa, while the minimum pressure was found to be -1.62 x 10^4 Pa. The inlet-to-outlet pressure drop was calculated as approximately 6.99 x 10^4 Pa. The streamline plot reveals that the fluid behaves the same way with this nozzle geometry independent of the working fluid. The fluid entering the central inlet has almost pure axial motion, while the fluid entering through the outer slot of the nozzle flows in the radial direction as it moves

toward the outlet. Again, this nozzle geometry does not produce any pockets of swirling fluid. The other nozzle geometries produced swirling on the outer side of the outer inlet slot location. Since this geometry has the outer slot location at the edge of the top plate, there is no place for the fluid to begin to swirl.

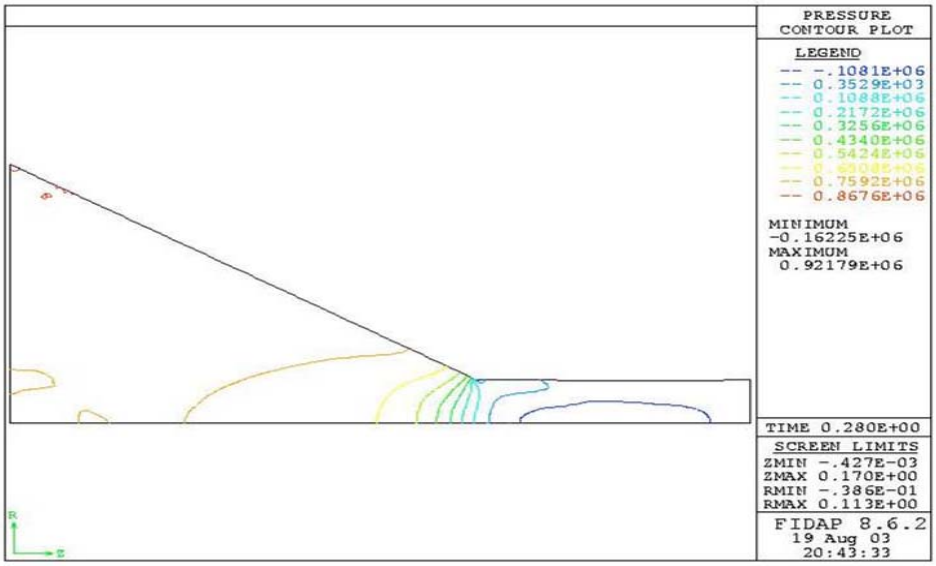

Figure 148: Pressure contour plot for FC-72 ($Q = 4.416 \times 10^{-7}$ m^3/s, $R_2 = 7.2 \times 10^{-4}$ m). Units are $gm/cm\ s^2$ ($x10^1$ Pa).

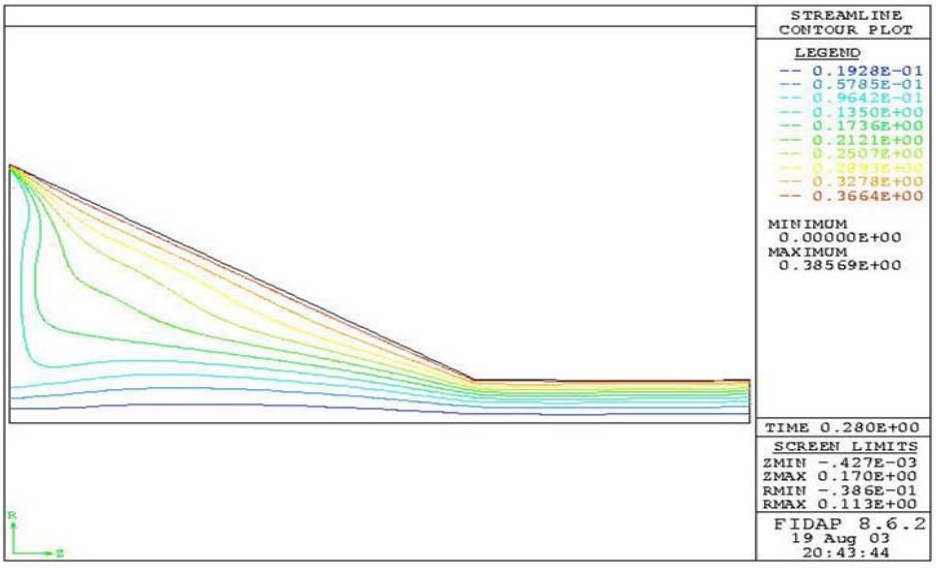

Figure 149: Streamline contour plot for FC-72 ($Q = 4.416 \times 10^{-7}$ m^3/s, $R_2 = 7.2 \times 10^{-4}$ m)

Next, FC-72 was used at an inlet flow rate of 5.678 x 10^{-7} m^3/s. The velocity vector plot for this situation is shown in Figure 150. The maximum velocity was again located within the throat of the nozzle and had a value of about 12.10 m/s, which is the same maximum velocity found for other fluids within this geometry and traveling at this flow rate. The free surface for this case began at a height of 1.250 x 10^{-4} m, decreased to 1.221 x 10^{-4} m, and then increased to a final height of 1.265 x 10^{-4} m. This was the second greatest radial height behind FC-87. The value for the cone angle corresponding to this free surface position was found to be 2.92 degrees.

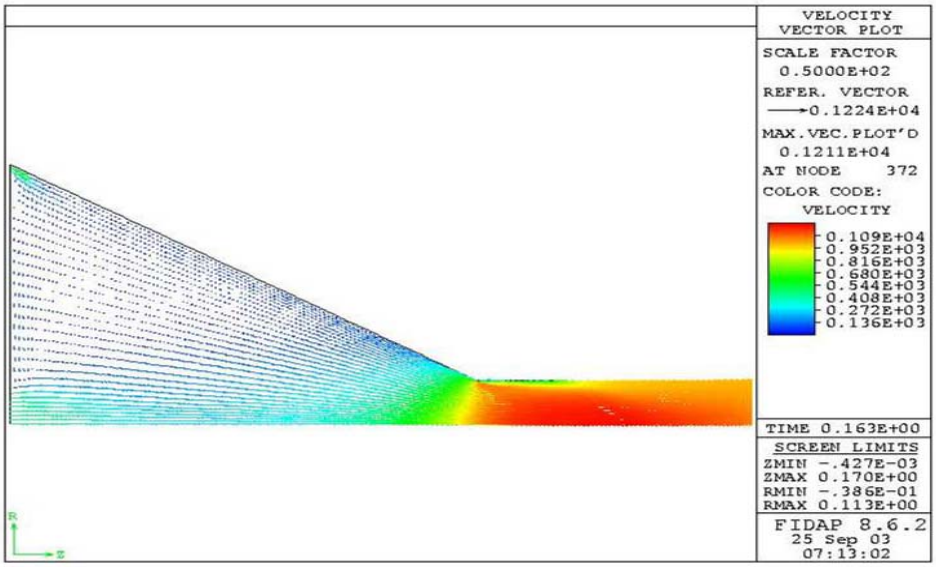

Figure 150: Velocity vector plot for FC-72 (Q = 5.678 x 10^{-7} m^3/s, R_2 = 7.2 x 10^{-4} m). Units are cm/s.

The pressure contour plot for this case is shown in Figure 151. The maximum pressure was determined to be about 1.53 x 10^5 Pa, whereas the minimum pressure was found to be about -2.92 x 10^4 Pa. The inlet-to-outlet pressure drop was calculated to be approximately 1.47 x 10^5 Pa. The streamline contour plot is shown in Figure 152. Some of the fluid entering through the outer inlet slot flows toward the line of symmetry before

flowing toward the nozzle outlet. Still, some of the fluid flows along the nozzle wall toward the outlet. Identical to the other results obtained from this geometry, there are no pockets of swirling fluid present within the nozzle.

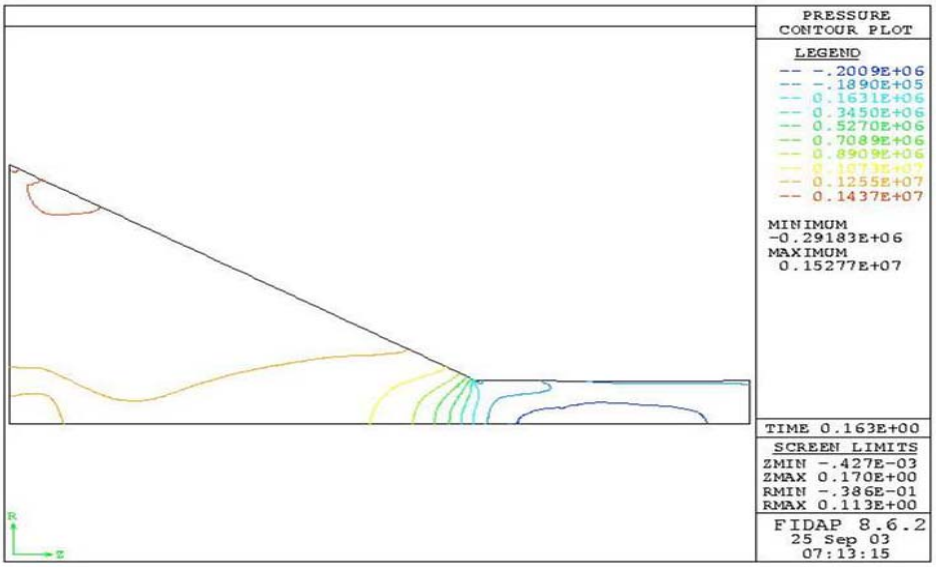

Figure 151: Pressure contour plot for FC-72 ($Q = 5.678 \times 10^{-7}$ m^3/s, $R_2 = 7.2 \times 10^{-4}$ m). Units are gm/cm s^2 ($x10^1$ Pa).

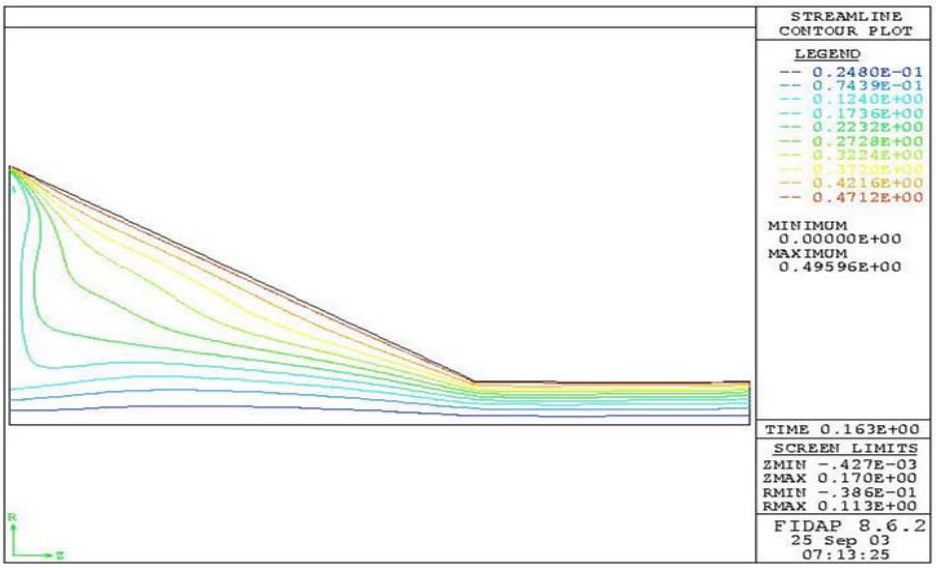

Figure 152: Streamline contour plot for FC-72 ($Q = 5.678 \times 10^{-7}$ m^3/s, $R_2 = 7.2 \times 10^{-4}$ m)

The next working fluid that was used on this nozzle geometry was FC-87. Figure 153 shows the velocity vector plot for the situation where FC-87 is entering the nozzle with a flow rate of 4.416 x 10^{-7} m^3/s. Similar to the other fluids discussed previously, the maximum velocity was found to be about 9.40 m/s. The free surface began at a height of 1.250 x 10^{-4} m, declined to a value of 1.221 x 10^{-4} m, and then inclined to a final height of 1.266 x 10^{-4} m, which formed a cone angle of 2.92 degrees. Again, for this nozzle geometry, FC-87 produced the greatest radial free surface height out of all of the working fluids.

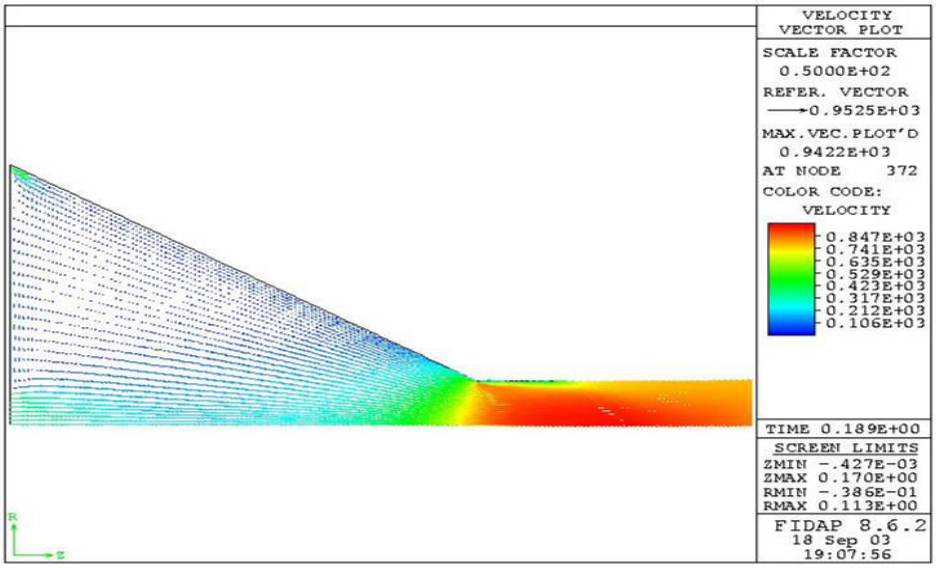

Figure 153: Velocity vector plot for FC-87 (Q = 4.416 x 10^{-7} m^3/s, R_2 = 7.2 x 10^{-4} m). Units are cm/s.

The pressure contour plot and streamline contour plot for this situation are shown in Figure 154 and Figure 155, respectively. The maximum pressure was found to be about 8.97 x 10^4 Pa, while the minimum pressure was found to be about -1.74 x 10^4 Pa. The pressure drop from the inlet to the outlet of the nozzle was calculated to be about 8.66 x 10^4 Pa. The streamline plot shows results that are similar to the other streamline

plots obtained for this nozzle geometry. The fluid entering through the central inlet has almost pure axial motion as it flows through the nozzle, while the fluid entering from the outer inlet slot flows in the radial direction, as well as the axial direction.

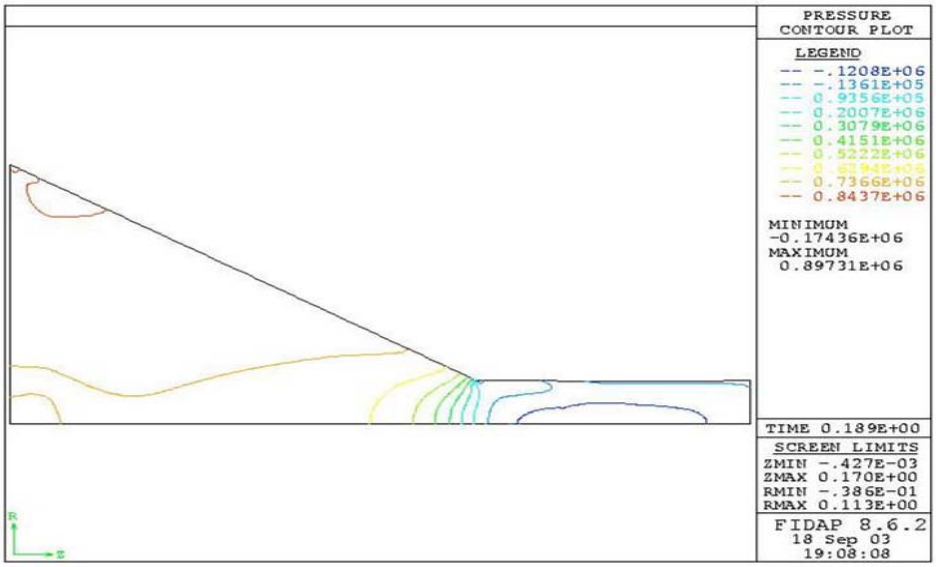

Figure 154: Pressure contour plot for FC-87 (Q = 4.416 x 10^{-7} m^3/s, R_2 = 7.2 x 10^{-4} m). Units are gm/cm s^2 (x10^1 Pa).

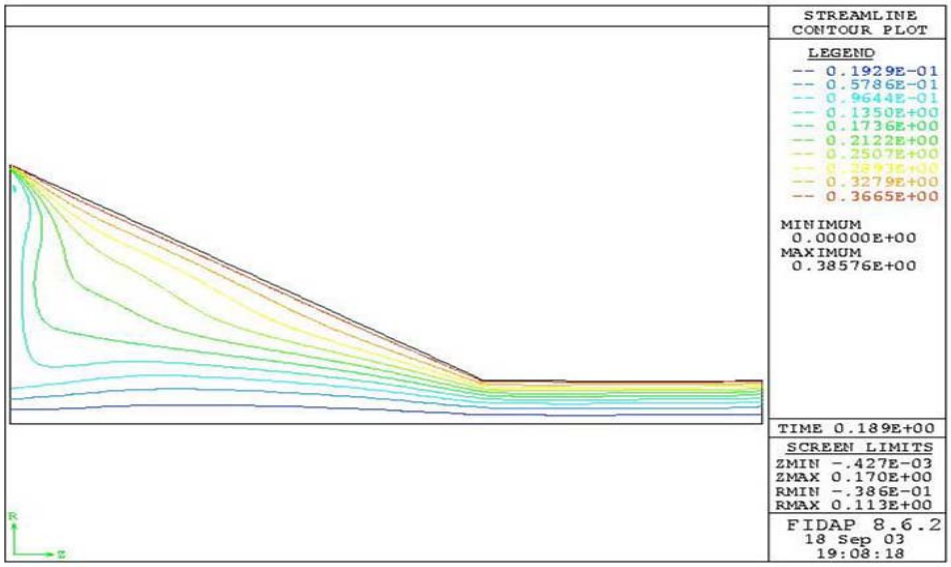

Figure 155: Streamline contour plot for FC-87 (Q = 4.416 x 10^{-7} m^3/s, R_2 = 7.2 x 10^{-4} m)

Next, FC-87 was forced through the inlets of the nozzle at a flow rate of 5.678 x 10^{-7} m^3/s. Figure 156 shows the velocity vector plot for this situation. The maximum velocity within the nozzle was found to be about 12.12 m/s and again was located in the throat. The free surface for this case began at a radial height of 1.250 x 10^{-4} m, declined to a value of 1.221 x 10^{-4} m, before increasing to a final height of 1.270 x 10^{-4} m. The resulting cone angle was determined to be 3.13 degrees. FC-87 once again produced the largest radial height of the free surface and largest cone angle for the given geometry.

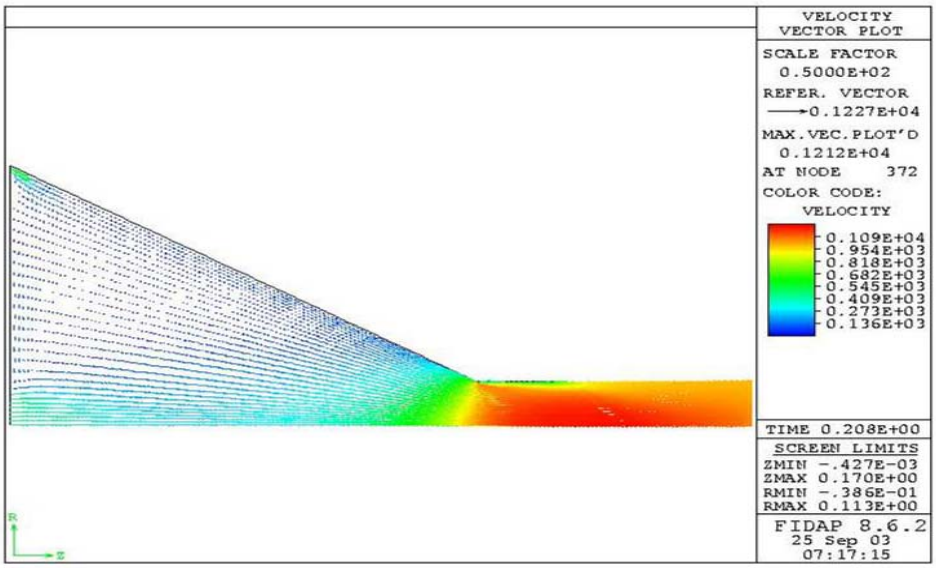

Figure 156: Velocity vector plot for FC-87 (Q = 5.678 x 10^{-7} m^3/s, R_2 = 7.2 x 10^{-4} m). Units are cm/s.

The pressure contour plot for this scenario is depicted in Figure 157. The maximum pressure within the nozzle was determined to be about 1.49 x 10^5 Pa, whereas the minimum pressure was found to be about -3.07 x 10^4 Pa. The pressure drop from the inlet to the outlet of the nozzle was calculated as approximately 1.45 x 10^5 Pa. Figure 158 shows the streamline contour plot for this situation. Some of the fluid entering through the outer inlet slot tended to flow along the top plate of the nozzle toward the

center line before heading toward the outlet. The rest of that fluid followed the nozzle wall to the outlet. It was also observed that the fluid entering through the central inlet flowed through the nozzle in a relatively straight, axial motion.

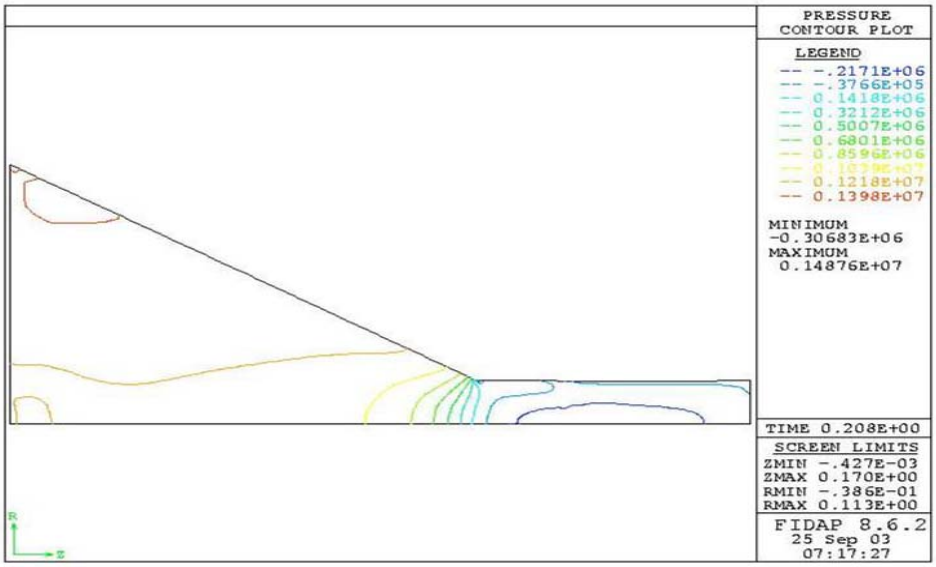

Figure 157: Pressure contour plot for FC-87 ($Q = 5.678 \times 10^{-7}$ m^3/s, $R_2 = 7.2 \times 10^{-4}$ m). Units are gm/cm s^2 ($x10^1$ Pa).

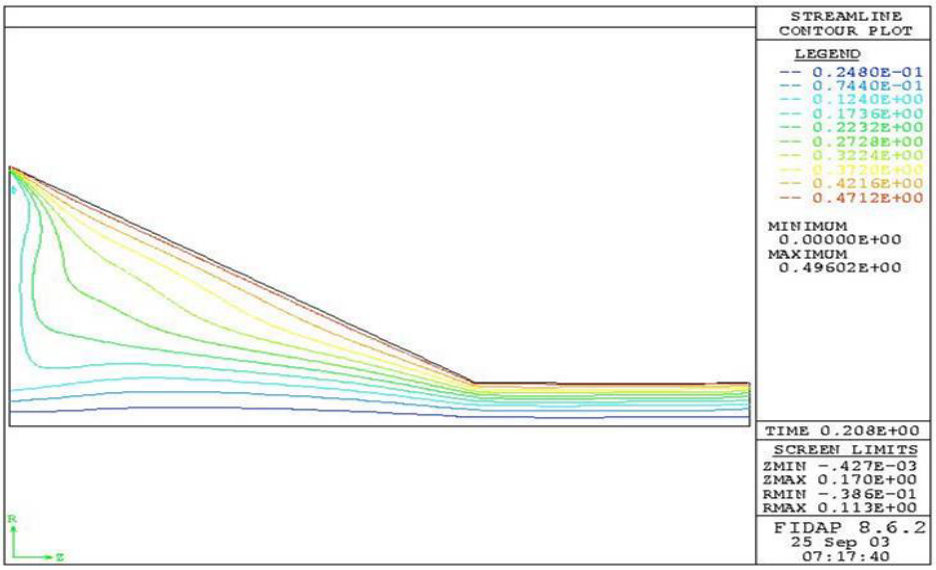

Figure 158: Streamline contour plot for FC-87 ($Q = 5.678 \times 10^{-7}$ m^3/s, $R_2 = 7.2 \times 10^{-4}$ m)

The final working fluid studied on this geometry was Methanol. The velocity vector plot for Methanol flowing at 4.416 x 10^{-7} m^3/s is shown in Figure 159. The maximum velocity was found to be about 9.45 m/s. The free surface height started at 1.250 x 10^{-4} m, decreased to a value of 1.220 x 10^{-4} m, before rising again to a final height of 1.247 x 10^{-4} m. The radial height produced by Methanol was, again, the second lowest behind FC-77. Also second lowest behind FC-77 was the cone angle, which was found to be approximately 1.84 degrees.

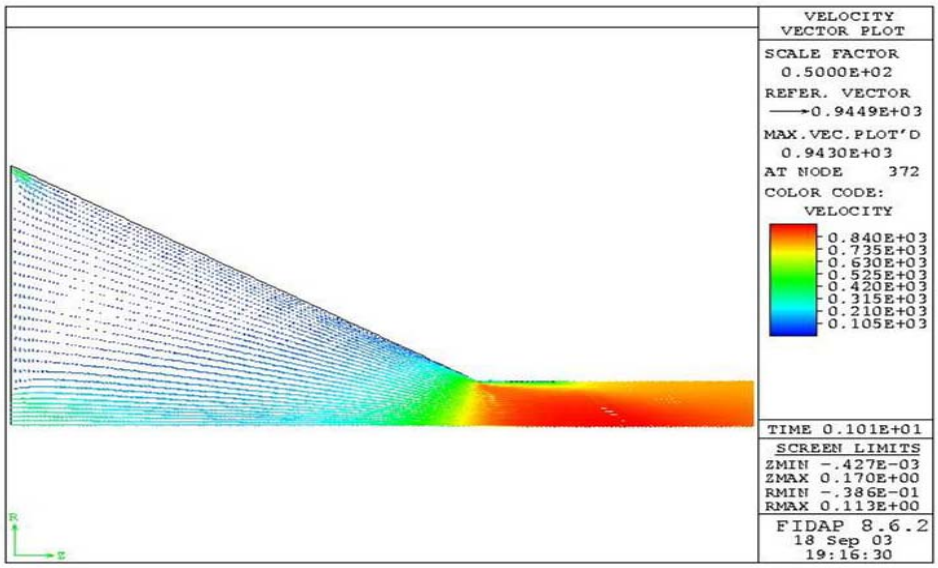

Figure 159: Velocity vector plot for Methanol (Q=4.416 x 10^{-7} m^3/s, R_2=7.2 x 10^{-4} m). Units are cm/s.

Figure 160 shows the pressure contour plot for this scenario. The maximum pressure was found to be about 4.30 x 10^4 Pa, while the minimum pressure was found to be about -7.09 x 10^3 Pa. The inlet-to-outlet pressure was calculated to be approximately 4.00 x 10^4 Pa. This pressure drop was less than half of that value obtained for the other fluids operating in this nozzle geometry. The streamline contour plot is shown in Figure 161. It shows the same results as the previous trials performed on this geometry. Some

of the fluid entering through the outer inlet slot flows in the radial direction toward the line of symmetry before heading axially toward the nozzle outlet, while some of the fluid flows along the wall before heading toward the outlet.

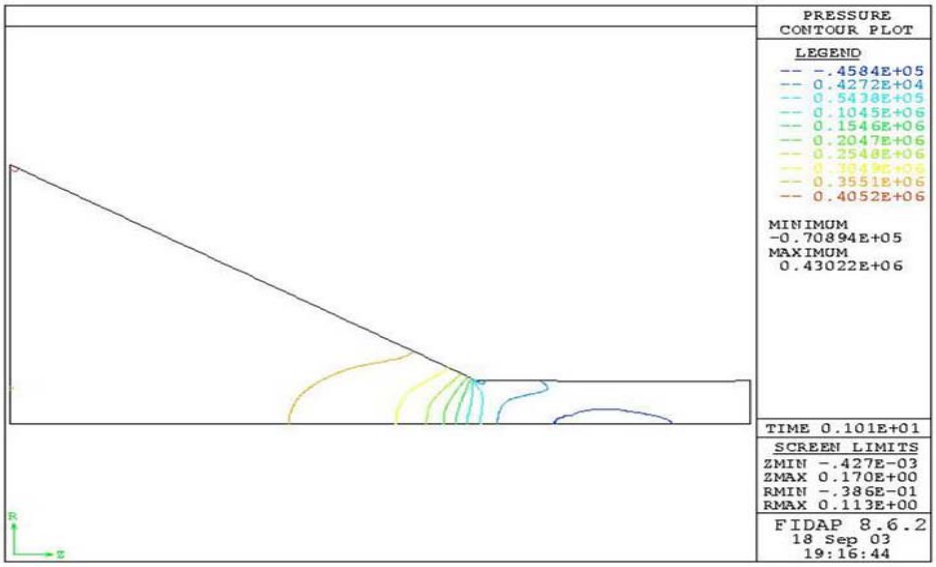

Figure 160: Pressure contour plot for Methanol ($Q = 4.416 \times 10^{-7}$ m^3/s, $R_2 = 7.2 \times 10^{-4}$ m). Units are gm/cm s^2 ($x10^1$ Pa).

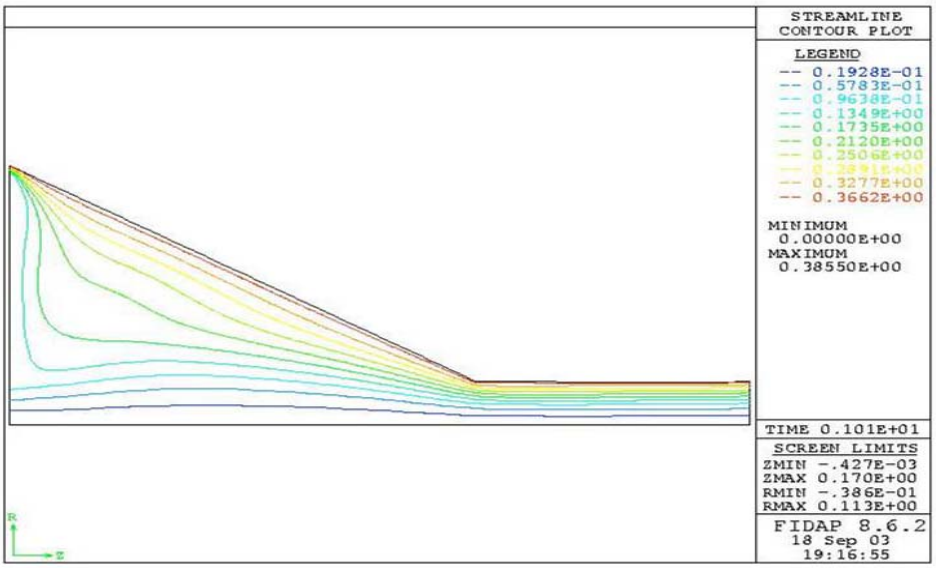

Figure 161: Streamline contour plot for Methanol ($Q = 4.416 \times 10^{-7}$ m^3/s, $R_2 = 7.2 \times 10^{-4}$ m)

The final variation performed on this nozzle geometry had Methanol entering with an inlet flow rate of 5.678 x 10^{-7} m^3/s. Figure 162 shows the velocity vector results for these parameters. Similar to the values obtained from the other fluids operating within this geometry, the maximum velocity was found to be approximately 12.10 m/s. The free surface began at a height of 1.250 x 10^{-4} m, receded to a value of 1.220 x 10^{-4} m, and then increased to a final height of 1.253 x 10^{-4} m. The corresponding cone angle was found to be 2.16 degrees. FC-77 was the only working fluid to produce greater values.

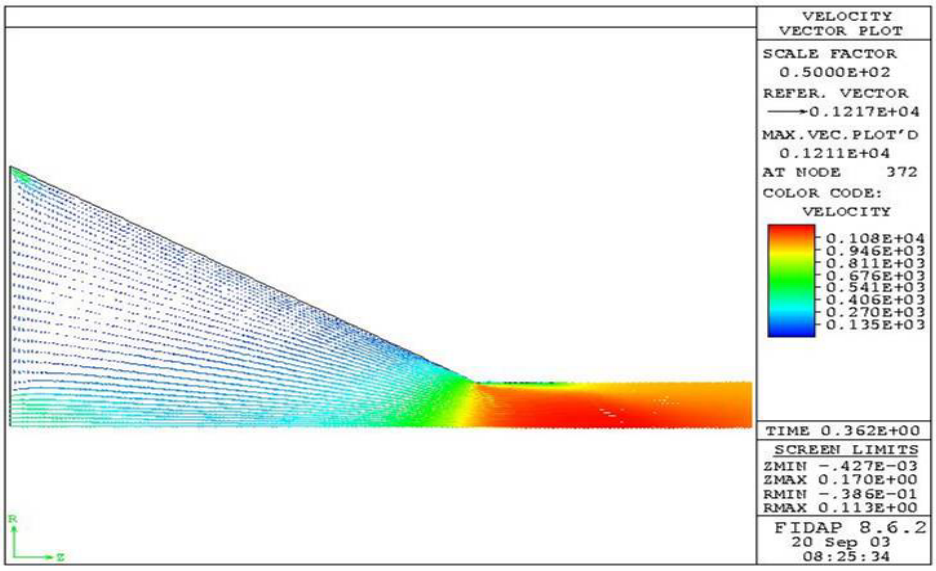

Figure 162: Velocity vector plot for Methanol (Q=5.678 x 10^{-7} m^3/s, R_2=7.2 x 10^{-4} m). Units are cm/s.

Figure 163 and Figure 164 show the pressure and streamline contour plots, respectively. The maximum pressure within the nozzle was found to be approximately 7.11 x 10^4 Pa, whereas the minimum pressure was found to be -1.20 x 10^4 Pa. The inlet-to-outlet pressure drop for this case was determined to be 6.70 x 10^4 Pa. The streamline contour plot shows that the fluid entering through the central inlet has almost pure axial motion as the fluid flows through the nozzle. As previously discussed, this geometry

provided no pockets of swirling fluid. Again, the reason for the absence of the swirling fluid is due to the fact that the location of the outer inlet slot provides no place for a pocket of swirling fluid to form.

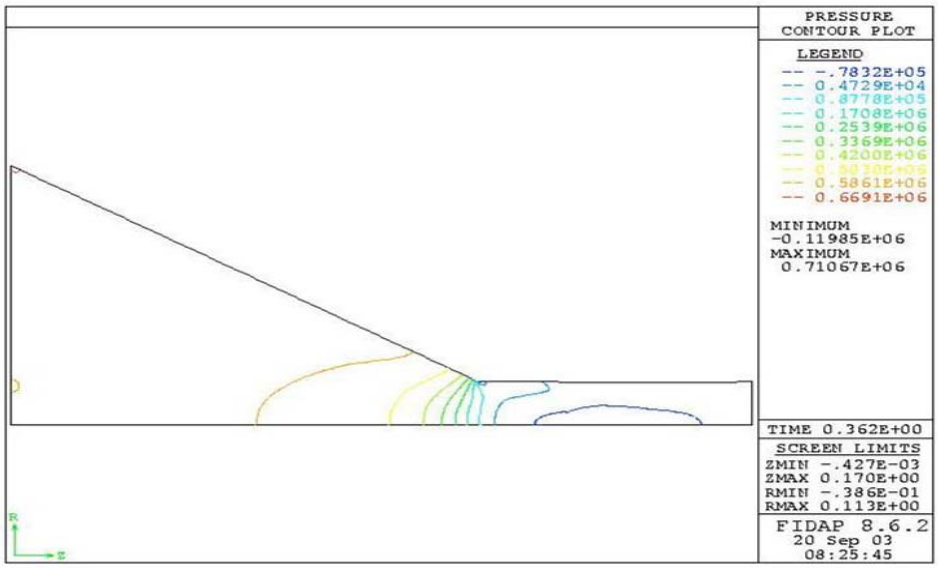

Figure 163: Pressure contour plot for Methanol ($Q = 5.678 \times 10^{-7}$ m^3/s, $R_2 = 7.2 \times 10^{-4}$ m). Units are gm/cm s^2 ($x10^1$ Pa).

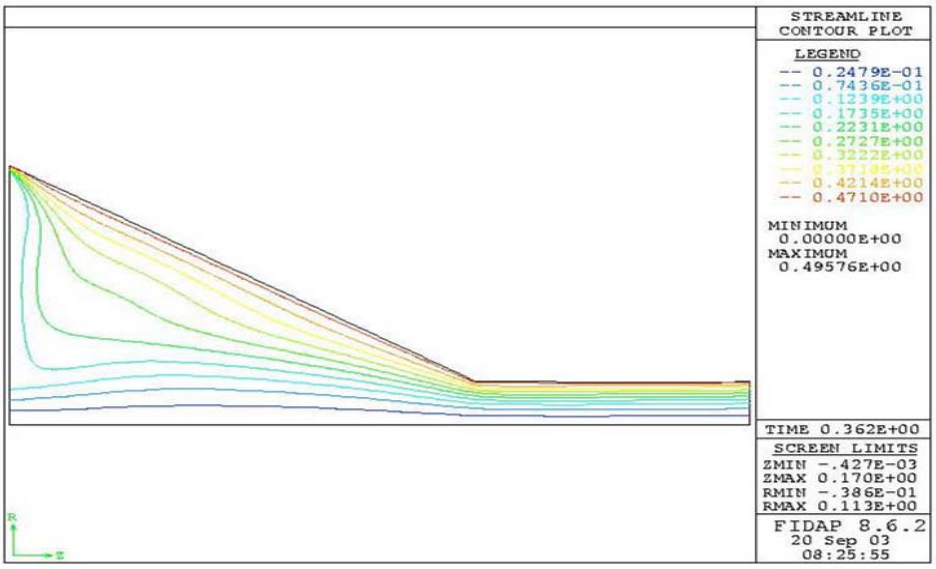

Figure 164: Streamline contour plot for Methanol ($Q = 5.678 \times 10^{-7}$ m^3/s, $R_2 = 7.2 \times 10^{-4}$ m)

Figure 165 and Figure 166 show the free surface profile for the different fluids with an inlet flow rate of 4.416 x 10^{-7} m^3/s in this nozzle geometry. It was noted that FC-87 produced the greatest free surface height, while FC-77 produced the lowest.

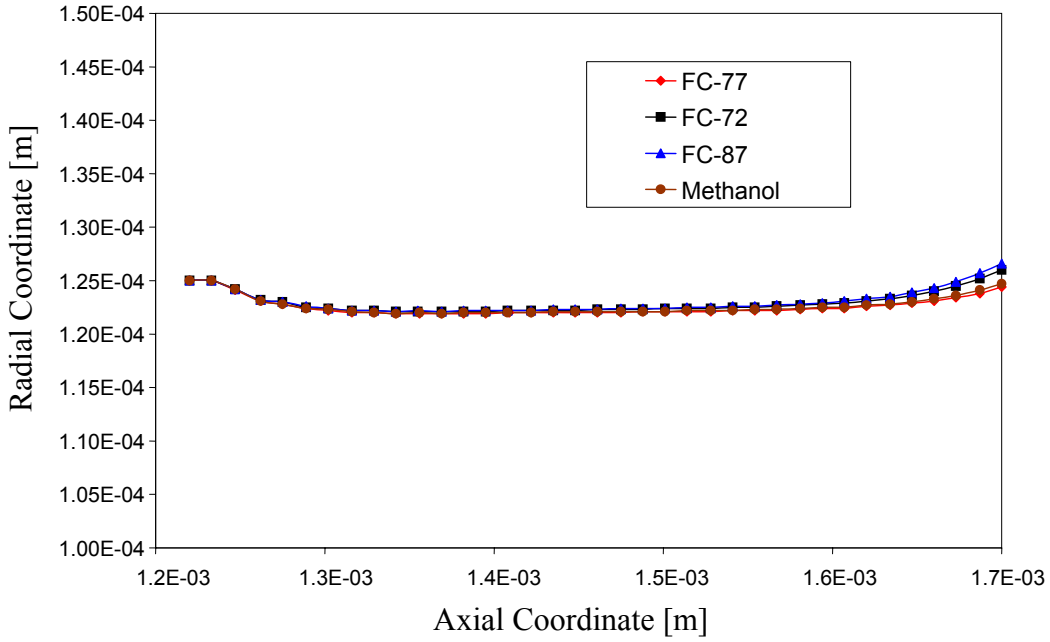

Figure 165: Free surface profile for all fluids (Q = 4.416 x 10^{-7} m^3/s, R_2 = 7.2 x 10^{-4} m).

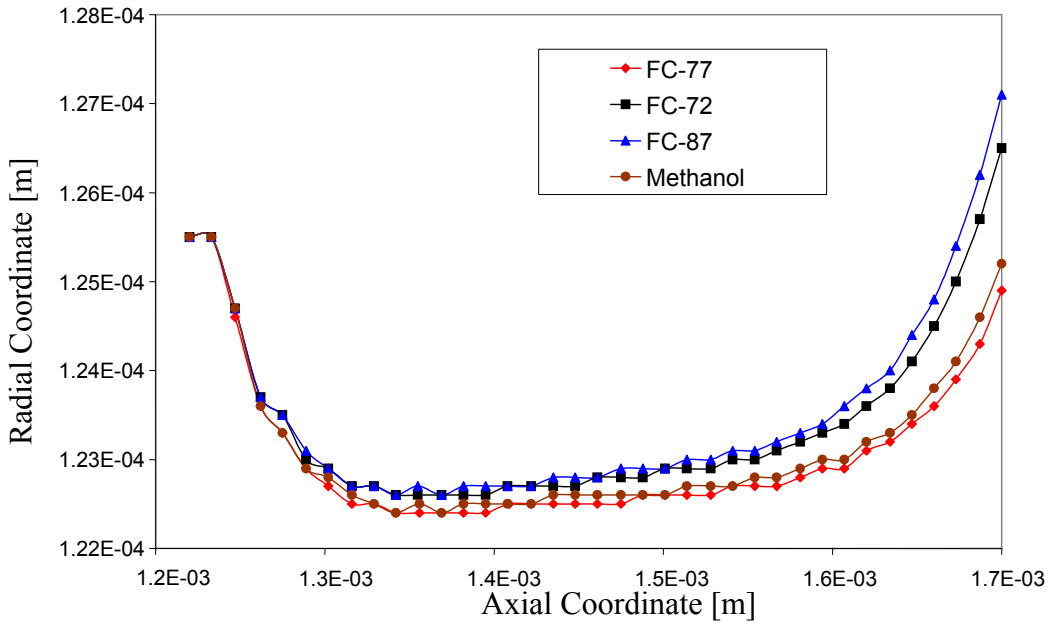

Figure 166: Magnified free surface profile for all fluids (Q = 4.416 x 10^{-7} m^3/s, R_2 = 7.2 x 10^{-4} m).

Figure 167 and Figure 168 show the free surface profile for the different fluids with an inlet flow rate of 5.678 x 10^{-7} m^3/s performed with this nozzle geometry. It was again noted that FC-87 produced the greatest radial height for the free surface

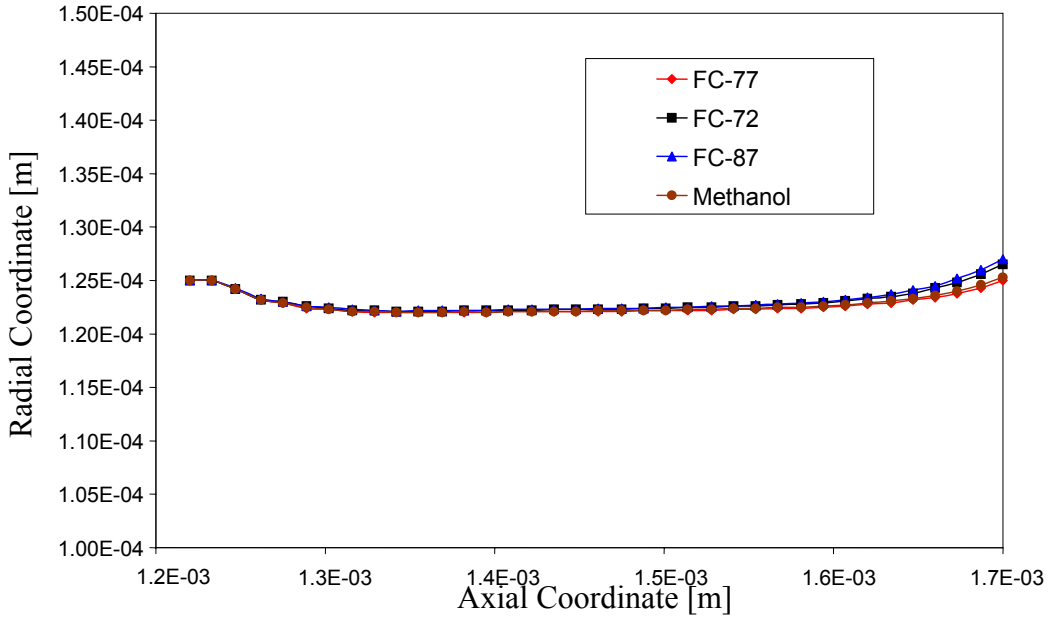

Figure 167: Free surface profile for all fluids (Q = 5.678 x 10^{-7} m^3/s, R_2 = 7.2 x 10^{-4} m).

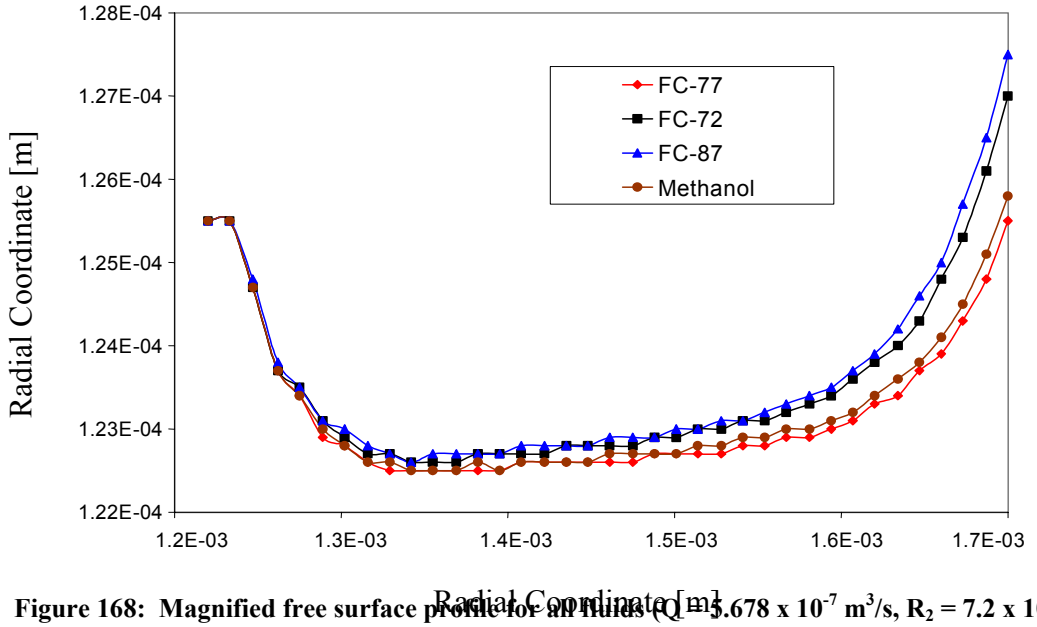

Figure 168: Magnified free surface profile for all fluids (Q = 5.678 x 10^{-7} m^3/s, R_2 = 7.2 x 10^{-4} m)

Figure 169 and Figure 170 show the dimensionless free surface profile for this nozzle geometry based on the Reynolds number at the nozzle exit. Again, the larger Reynolds number produced the greatest free surface height and cone angle for the fluid.

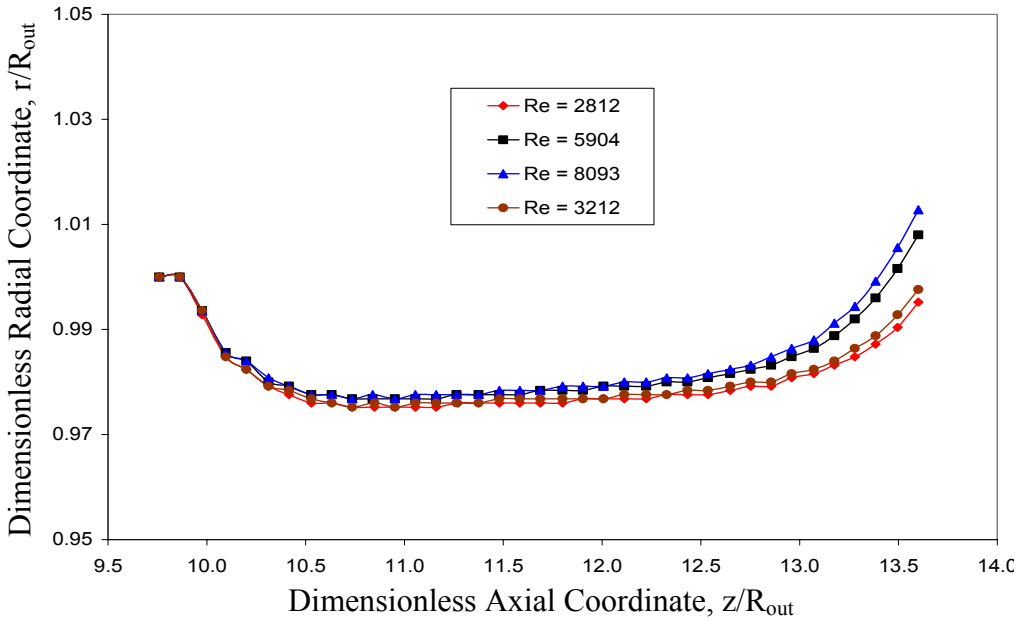

Figure 169: Dimensionless free surface plot for all fluids ($Q = 4.416 \times 10^{-7}$ m^3/s, $R_2 = 7.2 \times 10^{-4}$ m)

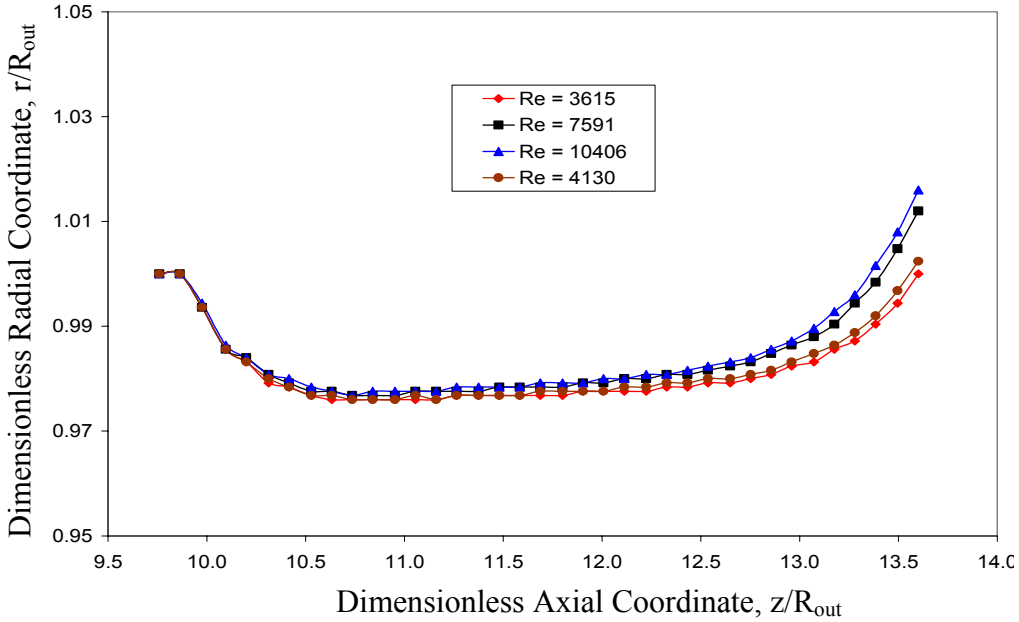

Figure 170: Dimensionless free surface profile for all fluids ($Q = 5.678 \times 10^{-7}$ m^3/s, $R_2 = 7.2 \times 10^{-4}$ m)

Figure 171 and Figure 172 both show the free surface profile for all of the geometries that used FC-77 as the working fluid. These figures show the free surface profile solely for the flow rate of 4.416 x 10^{-7} m^3/s. The results for 5.678 x 10^{-7} m^3/s are identical except for a slight change in the values.

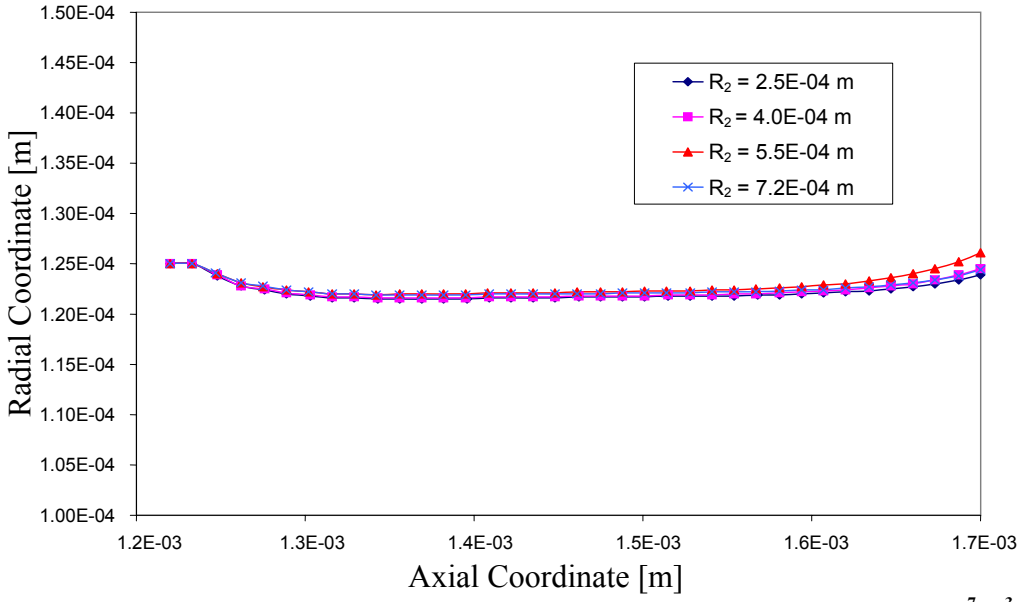

Figure 171: Free surface profile for FC-77 in all nozzle geometries (Q = 4.416 x 10^{-7} m^3/s)

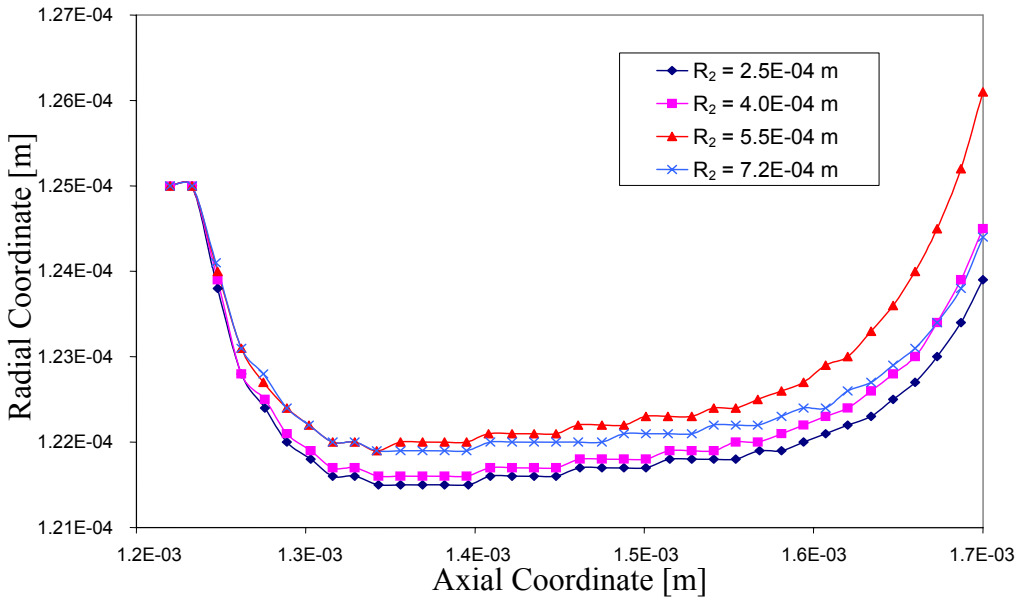

Figure 172: Magnified free surface profile for FC-77 in all nozzle geometries (Q = 4.416 x 10^{-7} m^3/s)

Figure 173 and Figure 174 both show the free surface profile for all of the geometries that used FC-72 as the working fluid. These figures show the free surface profile for the flow rate of 4.416 x 10^{-7} m^3/s. Again, the results for 5.678 x 10^{-7} m^3/s are identical except for a slight change in the values.

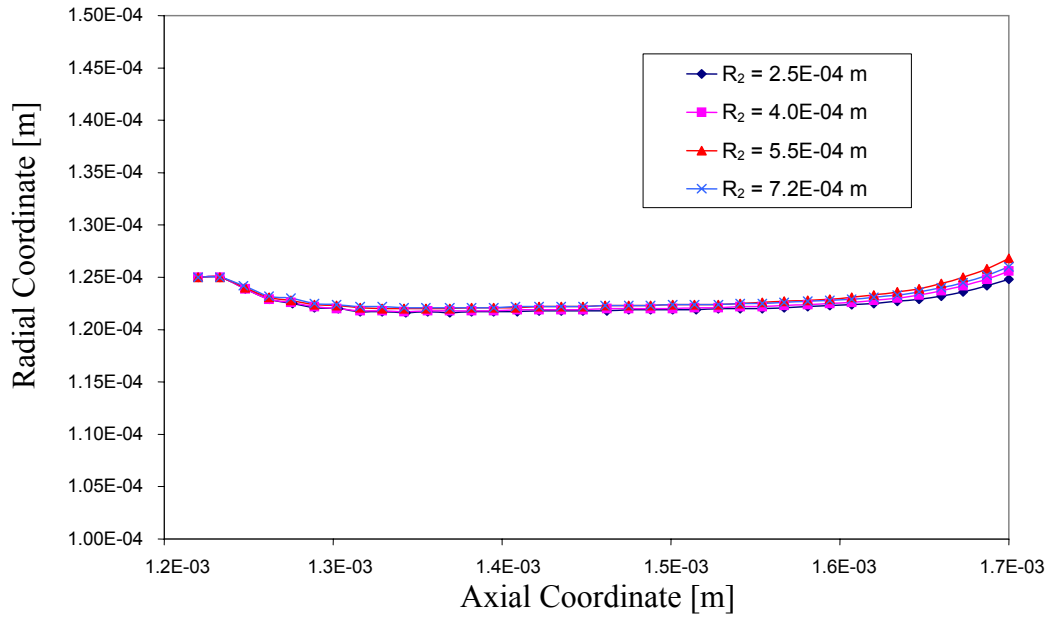

Figure 173: Free surface profile for FC-72 in all nozzle geometries (Q = 4.416 x 10^{-7} m^3/s)

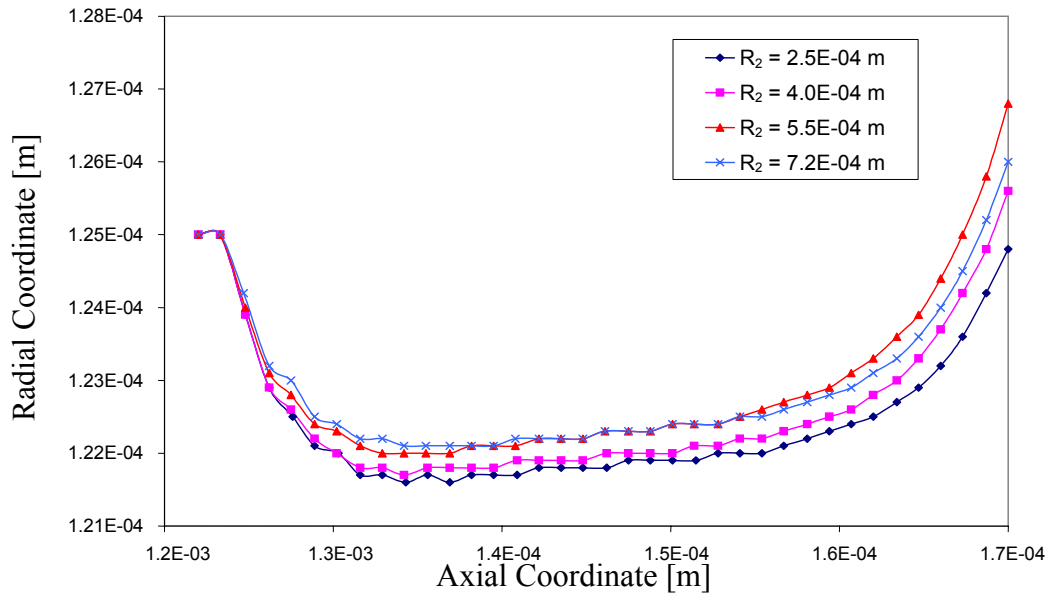

Figure 174: Magnified free surface profile for FC-72 in all nozzle geometries (Q = 4.416 x 10^{-7} m^3/s)

Figure 175 and Figure 176 both show the free surface profile for all of the geometries that used FC-87 as the working fluid. These figures show the free surface profile for the flow rate of 4.416 x 10^{-7} m^3/s. Again, the results for 5.678 x 10^{-7} m^3/s are identical except for a slight change in the values.

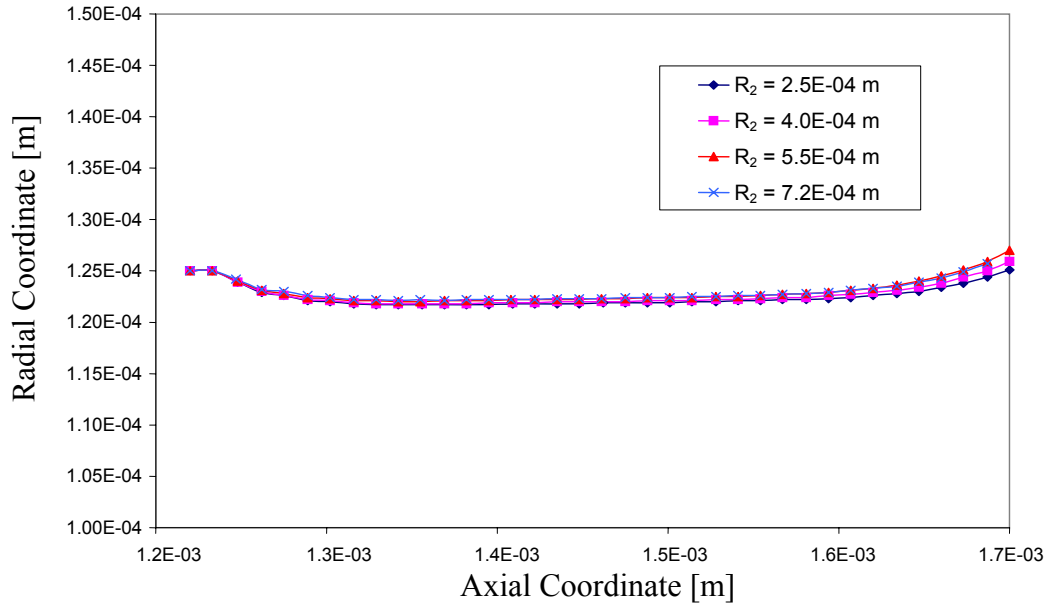

Figure 175: Free surface profile for FC-87 in all nozzle geometries (Q = 4.416 x 10^{-7} m^3/s)

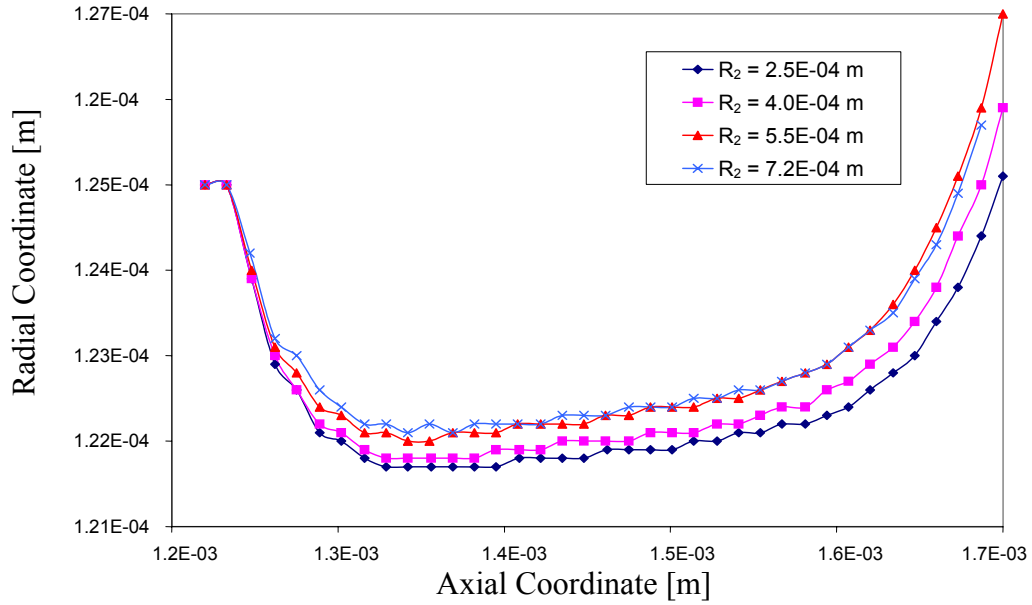

Figure 176: Magnified free surface profile for FC-87 in all nozzle geometries (Q = 4.416 x 10^{-7} m^3/s)

Figure 177 and Figure 178 both show the free surface profile for all of the geometries that used Methanol as the working fluid. These figures show the free surface profile only for the flow rate of 4.416 x 10^{-7} m^3/s. Again, the results for 5.678 x 10^{-7} m^3/s are identical except for a slight change in the values.

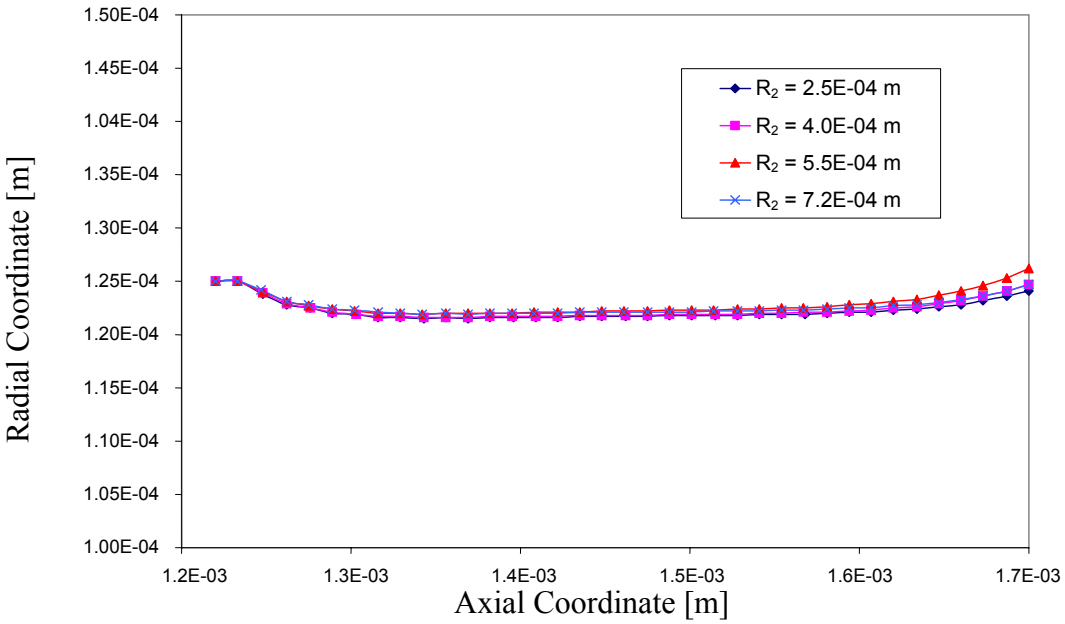

Figure 177: Free surface profile for Methanol in all nozzle geometries (Q = 4.416 x 10^{-7} m^3/s)

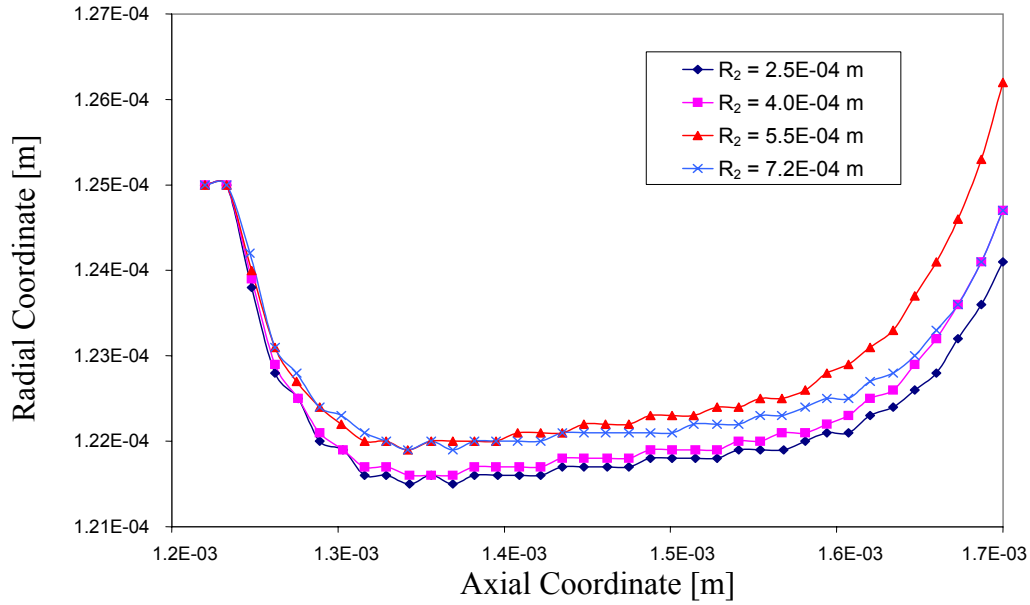

Figure 178: Magnified free surface profile for Methanol in all nozzle geometries (Q=4.416 x $10^{-7}$$m^3/s$)

Table 15 summarizes the final height of the free surface with respect to the nozzle geometry, working fluid, and flow rate. It was expected that for the higher flow rates, an increase in free surface height is evident. Also, as the outer inlet slot was moved outward in the radial direction, it was noted that the free surface height increased until the outer slot was located at the very edge of the nozzle. The maximum velocity within the nozzle for the geometry having R_2 equal to 5.50 x 10^{-4} m was about twice that for any of the other nozzle geometries. Further research is required to determine why this happened.

Table 15: Free surface height for different nozzle geometries, working fluids, and flow rates

Outer Slot Location R_2 [m]	Working Fluid	Free Surface Height	
		4.416 x 10^{-7} m^3/s	5.678 x 10^{-7} m^3/s
2.50 x 10^{-4}	FC-77	1.239 x 10^{-4} m	1.243 x 10^{-4} m
	FC-72	1.248x 10-4 m	1.251 x 10-4 m
	FC-87	1.251 x 10-4 m	1.253 x 10-4 m
	Methanol	1.241 x 10-4 m	1.245x 10-4 m
4.00 x 10^{-4}	FC-77	1.245x 10^{-4} m	1.249 x 10^{-4} m
	FC-72	1.256 x 10^{-4} m	1.259 x 10^{-4} m
	FC-87	1.259 x 10^{-4} m	1.261 x 10^{-4} m
	Methanol	1.247 x 10^{-4} m	1.251 x 10^{-4} m
5.50 x 10^{-4}	FC-77	1.261x 10^{-4} m	1.263 x 10^{-4} m
	FC-72	1.268x 10^{-4} m	1.269 x 10^{-4} m
	FC-87	1.270 x 10^{-4} m	1.271 x 10^{-4} m
	Methanol	1.262 x 10^{-4} m	1.265 x 10^{-4} m
7.20 x 10^{-4}	FC-77	1.244 x 10^{-4} m	1.250 x 10^{-4} m
	FC-72	1.260 x 10^{-4} m	1.265 x 10^{-4} m
	FC-87	1.266 x 10^{-4} m	1.270 x 10^{-4} m
	Methanol	1.247 x 10^{-4} m	1.253 x 10^{-4} m

Figure 179 and Figure 180 show the height of the free surface for each flow rate with respect to fluid and outer inlet slot location. It was observed that a greater Reynolds number produced a greater free surface height. This is easily seen in these figures.

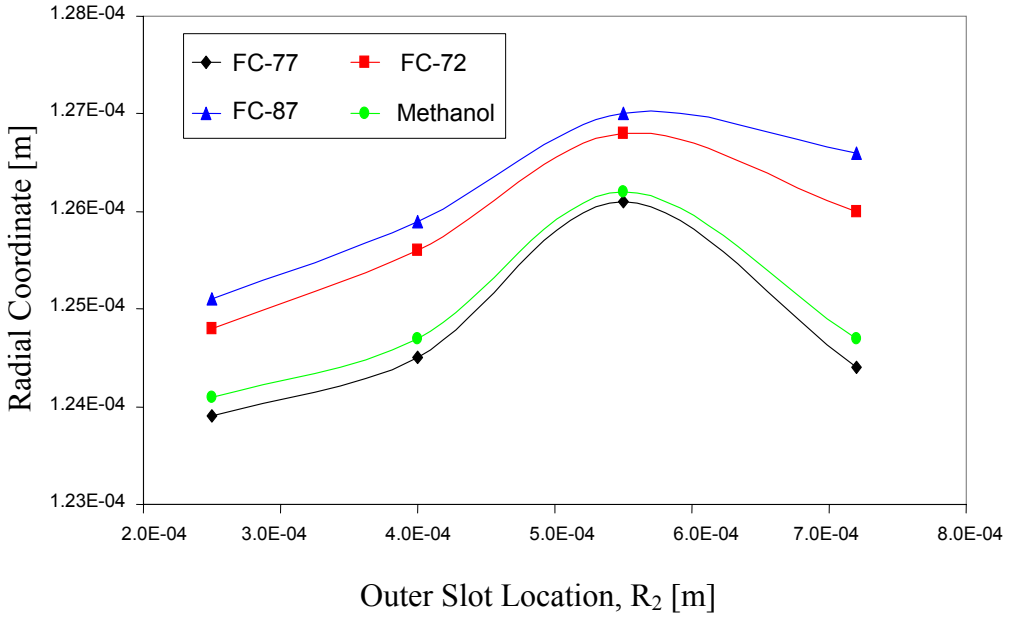

Figure 179: Free surface height for all fluids and all outer slot locations ($Q = 4.416 \times 10^{-7}$ m^3/s)

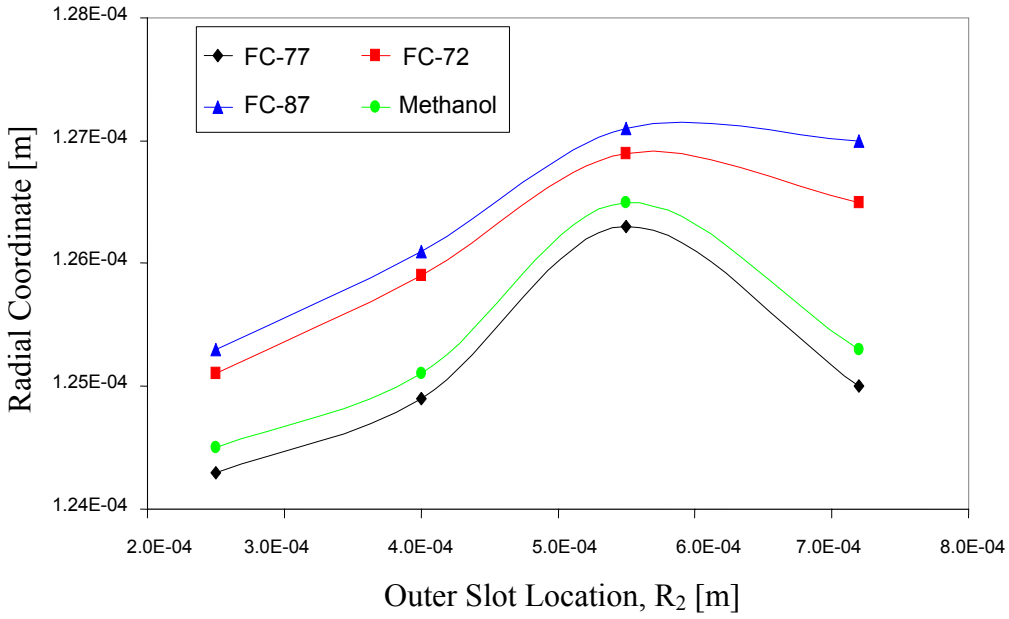

Figure 180: Free surface height for all fluids and all outer slot locations ($Q = 5.678 \times 10^{-7}$ m^3/s)

The cone angle for each of the cases included in the investigation involving the varying outer slot radii is listed in Table 16. It was observed that although the last nozzle geometry (R_2 equal to 7.20 x 10^{-4} m) produced the greatest cone angles for the free surface, the nozzle geometry having R_2 equal to 5.50 x 10^{-4} m produced the greatest radial height of the free surface.

Table 16: Cone angle for different nozzle geometries, working fluids, and flow rates

Outer Slot Location R_2 [m]	Working Fluid	Cone Angle	
		4.416 x 10^{-7} m^3/s	5.678 x 10^{-7} m^3/s
2.50 x 10^{-4}	FC-77	1.51deg	1.73 deg
	FC-72	2.05 deg	2.27 deg
	FC-87	2.27 deg	2.38 deg
	Methanol	1.62 deg	1.95 deg
4.00 x 10^{-4}	FC-77	1.84 deg	2.05 deg
	FC-72	2.48 deg	2.70 deg
	FC-87	2.70 deg	2.81 deg
	Methanol	1.95 deg	2.16 deg
5.50 x 10^{-4}	FC-77	2.29 deg	2.43 deg
	FC-72	2.72 deg	2.72 deg
	FC-87	2.72 deg	2.72 deg
	Methanol	2.29 deg	2.43 deg
7.20 x 10^{-4}	FC-77	1.62 deg	1.95 deg
	FC-72	2.59 deg	2.92 deg
	FC-87	2.92 deg	3.13 deg
	Methanol	1.84 deg	2.16 deg

Figure 181 and 182 show the cone angles produced by the various fluids traveling at both flow rates through all four of the various nozzle geometries. Again, it was seen

that a fluid with a greater Reynolds number produced a greater cone angle. FC-87 produced the largest cone angle of approximately 3.13 degrees when R_2 was equal to 7.20 x 10^{-4} m.

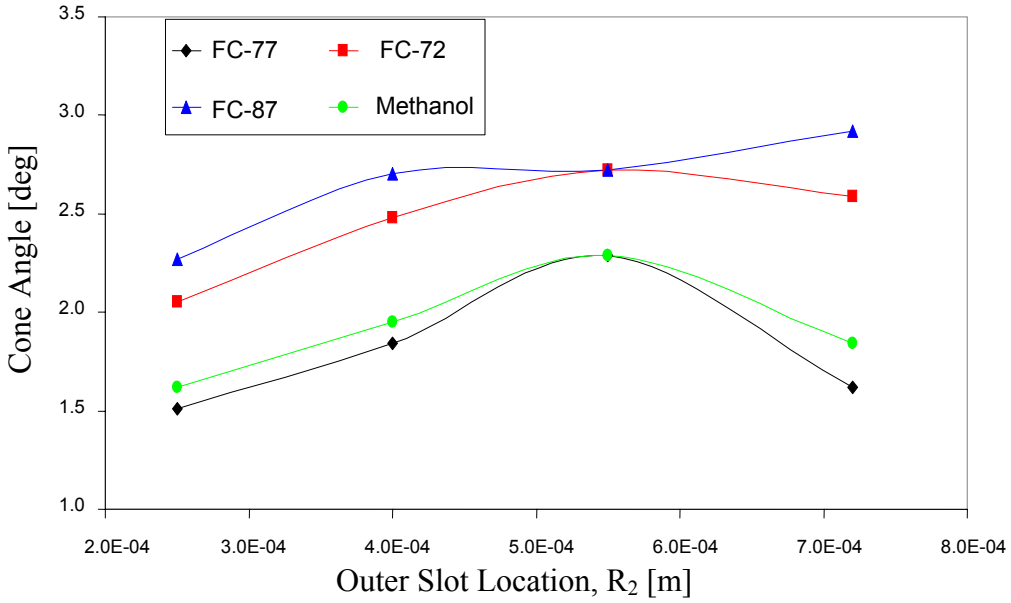

Figure 181: Cone angle for all fluids at all outer slot locations (Q = 4.416 x 10^{-7} m^3/s)

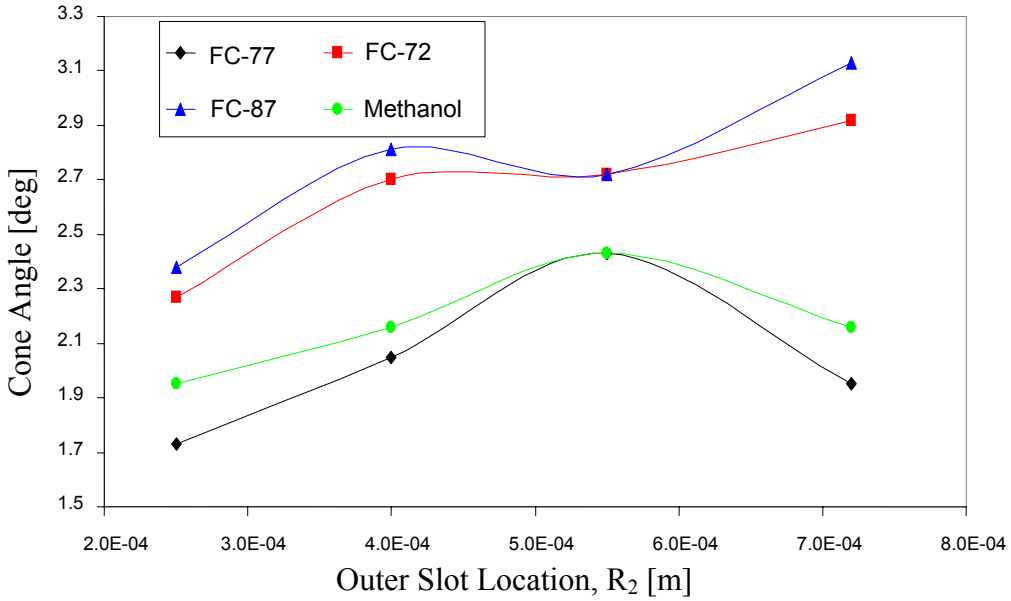

Figure 182: Cone angle for all fluids at all outer slot locations (Q = 5.678 x 10^{-7} m^3/s)

Another important factor is the inlet-to-outlet pressure drop of the nozzle. Table 17 depicts the pressure drop for each of the variations, including nozzle geometry, working fluid, and flow rate. As was expected, an increased flow rate caused an increase in the pressure drop. Also, the pressure drop resulting when FC-72 was the working fluid was less than the pressure drop obtained when FC-77 was used as the working fluid.

Table 17: Pressure drop for different nozzle geometries, working fluids, and flow rates

Outer Slot Location R_2 [m]	Working Fluid	Pressure Drop	
		4.416×10^{-7} m^3/s	5.678×10^{-7} m^3/s
2.50×10^{-4}	FC-77	7.25×10^4 Pa	1.04×10^5 Pa
	FC-72	7.23×10^4 Pa	9.85×10^4 Pa
	FC-87	7.18×10^4 Pa	1.19×10^5 Pa
	Methanol	3.44×10^4 Pa	5.11×10^4 Pa
4.00×10^{-4}	FC-77	7.93×10^4 Pa	1.20×10^5 Pa
	FC-72	7.67×10^4 Pa	1.02×10^5 Pa
	FC-87	7.53×10^4 Pa	1.25×10^5 Pa
	Methanol	3.57×10^4 Pa	5.90×10^4 Pa
5.50×10^{-4}	FC-77	4.07×10^5 Pa	5.58×10^5 Pa
	FC-72	3.39×10^5 Pa	6.51×10^5 Pa
	FC-87	3.82×10^5 Pa	6.33×10^5 Pa
	Methanol	1.83×10^5 Pa	3.03×10^5 Pa
7.20×10^{-4}	FC-77	9.65×10^4 Pa	1.24×10^5 Pa
	FC-72	9.21×10^4 Pa	1.47×10^5 Pa
	FC-87	8.66×10^4 Pa	1.45×10^5 Pa
	Methanol	4.00×10^4 Pa	6.70×10^4 Pa

Figure 183 and Figure 184 show the pressure drop from the inlet of the nozzle to the outlet for both 4.416×10^{-7} m^3/s and 5.678×10^{-7} m^3/s, respectively. It was observed

that the pressure drop peaked when R_2 was set at 5.50 x 10^{-4}. It was also observed that Methanol provided about half of the pressure drop as the other fluids. The pressure drop for the three other fluids were almost identical for the three other nozzle geometries.

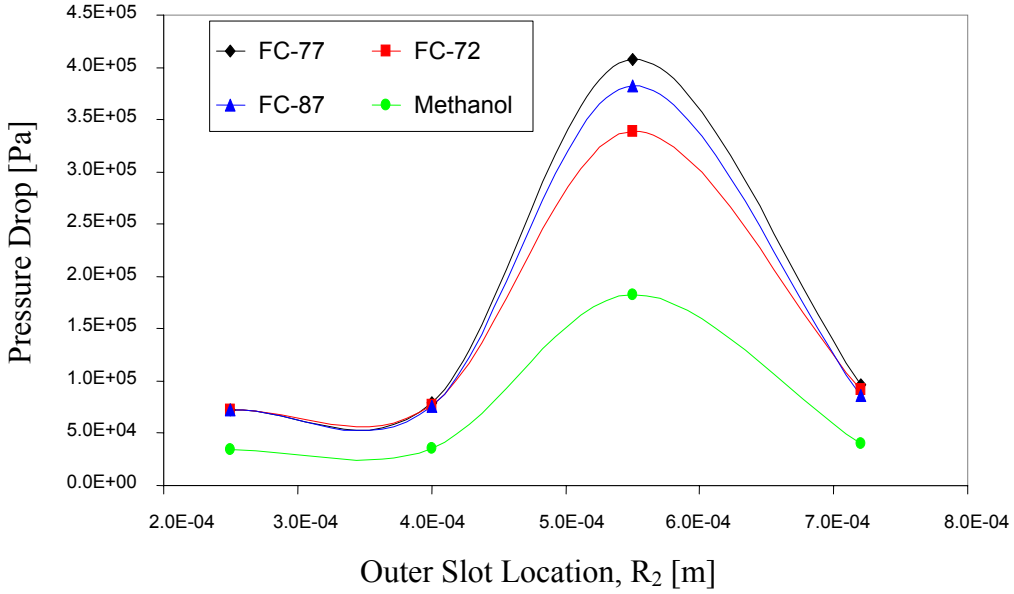

Figure 183: Pressure drop for all fluids at all outer slot locations (Q = 4.416 x 10^{-7} m^3/s)

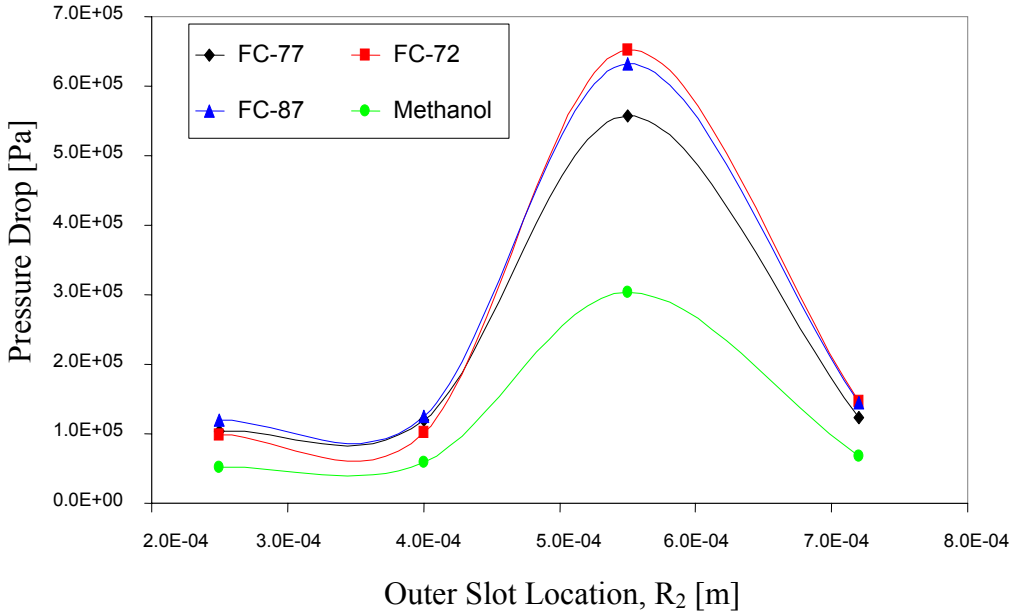

Figure 184: Pressure drop for all fluids at all outer slot locations (Q = 5.678 x 10^{-7} m^3/s)

Figure 185 shows the coefficient of pressure with respect to the Reynolds number for all of the nozzle geometries, fluids, and flow rates involved in this investigation. The plots appear to be somewhat of a sinusoidal wave that dampens out to a relatively constant value at higher Reynolds numbers. The larger nozzle has a higher coefficient of pressure than the smaller nozzle and most of the nozzle geometries where the outer inlet slot location was varied. However, the nozzle geometry having R_2 equal to 5.50 x 10^{-4} m produced the largest coefficient of pressure. This is because the fluid at the outlet of this nozzle was moving almost twice as fast as the other nozzles, which caused the pressure at that location to be low and helped increase the pressure drop.

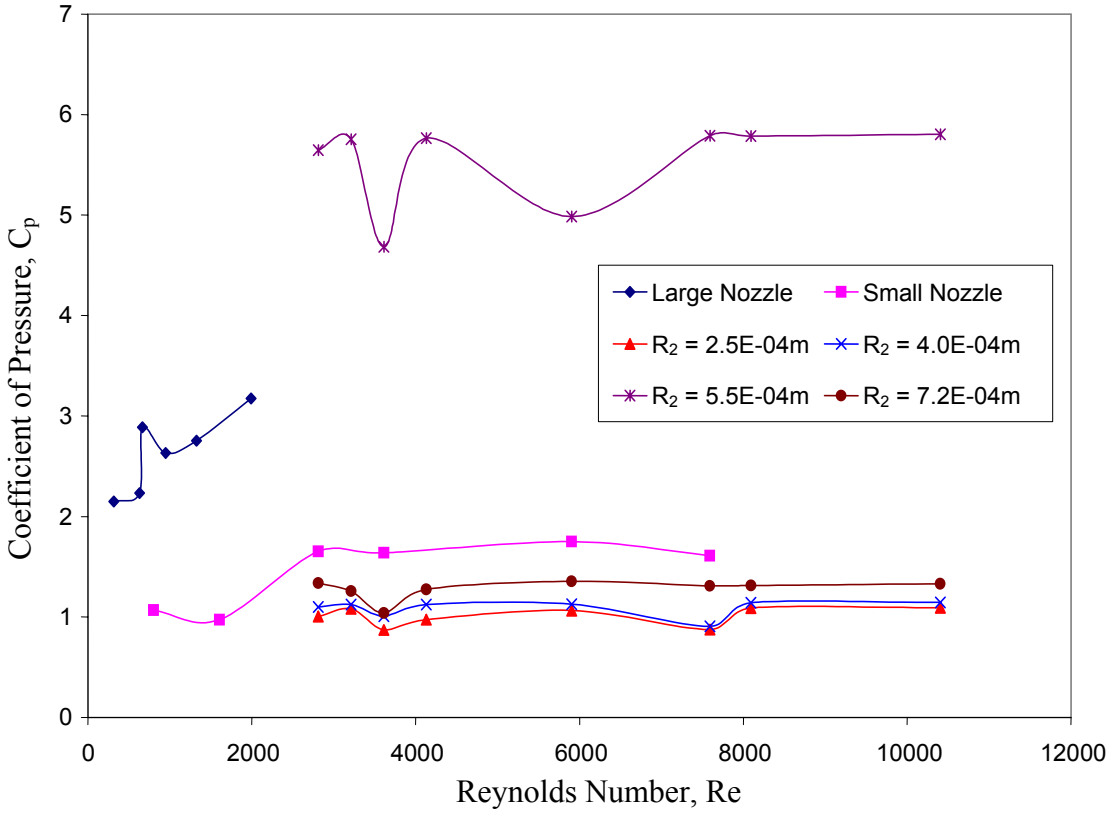

Figure 185: Coefficient of pressure for each nozzle with respect to the Reynolds number

Table 18 shows the inlet flow rate of each fluid, and the corresponding Reynolds number that was calculated at the nozzle exit. It was noted that FC-87 produced a much greater Reynolds number than any of the other fluids. This is because its density is relatively high and its viscosity is fairly low.

Table 18: Reynolds number for each fluid and each flow rate

Inlet Flow Rate Q [m^3/s]	Working Fluid	Reynolds Number at Nozzle Outlet [non-dim]
4.416×10^{-7}	FC-77	2812
	FC-72	5904
	FC-87	8093
	Methanol	3212
5.678×10^{-7}	FC-77	3615
	FC-72	7591
	FC-87	10406
	Methanol	4130

5.2.8.5 Cavitation

Cavitation occurs when the pressure of the liquid falls below the saturated pressure of that liquid corresponding to that temperature. When this happens, the fluid begins to evaporate, which causes tiny bubbles to form at the location where the pressure is below the critical point. These bubbles will eventually erode and destroy the boundary of the nozzle. Table 19 through Table 22 show the values of the cavitation number for each fluid, each flow rate, and each nozzle geometry. It was observed that the nozzle geometry having R_2 equal to 5.50×10^{-4} m had no cavitation present with any of the working fluids. The cavitation number for the trials having R_2 equal to 2.50×10^{-4} m and

4.00 x 10^{-4} m were almost identical, while the case where R_2 was equal to 7.20 x 10^{-4} m produced similar values for the cavitation number. It was noted that FC-77 never produced cavitation within any of the nozzle geometries. FC-87 was the only other fluid beside FC-77 not to have produced cavitation when R_2 was equal to 7.20 x 10^{-4} m.

Table 19: Cavitation number for all fluids at all flow rates (R_2 = 2.50 x 10^{-4} m)

Working Fluid	Saturation Pressure P_{sat} [Pa]	Reynolds Number Re [non-dim]	Minimum Pressure P_{min} [Pa]	Pressure Difference P_{min} - P_{sat} [Pa]	Cavitation Number Ca [non-dim]
FC-77	5.62 x 10^3	2812	12100	6480	0.040
		3615	20300	14680	0.062
FC-72	30.9 x 10^3	5904	12100	-18800	-0.138
		7591	20400	-10500	-0.047
FC-87	81.1 x 10^3	8093	12100	-69000	-0.479
		10406	20700	-60400	-0.254
Methanol	10.0 x 10^3	3212	5340	-4660	-0.034
		4130	9080	-920	-0.004

Table 20: Cavitation number for all fluids at all flow rates (R_2 = 4.00 x 10^{-4} m)

Working Fluid	Saturation Pressure P_{sat} [Pa]	Reynolds Number Re [non-dim]	Minimum Pressure P_{min} [Pa]	Pressure Difference P_{min} - P_{sat} [Pa]	Cavitation Number Ca [non-dim]
FC-77	5.62 x 10^3	2812	13900	8280	0.037
		3615	21100	15480	0.065
FC-72	30.9 x 10^3	5904	13900	-17000	-0.125
		7591	24300	-6600	-0.029
FC-87	81.1 x 10^3	8093	14400	-66700	-0.463
		10406	24600	-56500	-0.237
Methanol	10.0 x 10^3	3212	5390	-4610	-0.034
		4130	9780	-220	-0.001

Table 21: Cavitation number for all fluids at all flow rates ($R_2 = 5.50 \times 10^{-4}$ m)

Working Fluid	Saturation Pressure P_{sat} [Pa]	Reynolds Number Re [non-dim]	Minimum Pressure P_{min} [Pa]	Pressure Difference $P_{min} - P_{sat}$ [Pa]	Cavitation Number Ca [non-dim]
FC-77	5.62×10^3	2812	84600	78980	0.512
		3615	138000	132380	0.556
FC-72	30.9×10^3	5904	84600	53700	0.395
		7591	143000	112100	0.499
FC-87	81.1×10^3	8093	84500	3400	0.024
		10406	142000	60900	0.573
Methanol	10.0×10^3	3212	36100	26100	0.192
		4130	62400	52400	0.140

Table 22: Cavitation number for all fluids at all flow rates ($R_2 = 7.20 \times 10^{-4}$ m)

Working Fluid	Saturation Pressure P_{sat} [Pa]	Reynolds Number Re [non-dim]	Minimum Pressure P_{min} [Pa]	Pressure Difference $P_{min} - P_{sat}$ [Pa]	Cavitation Number Ca [non-dim]
FC-77	5.62×10^3	2812	16200	10580	0.071
		3615	26900	21280	0.089
FC-72	30.9×10^3	5904	16200	-14700	-0.108
		7591	29200	-1700	-0.008
FC-87	81.1×10^3	8093	17400	-63700	0.082
		10406	30700	-50400	0.105
Methanol	10.0×10^3	3212	7090	-2910	-0.175
		4130	12000	2000	-0.084

5.2.8.6 Sectional Velocities for FC-72

Next, the radial velocity component, V_r, the axial velocity component, V_z, and the theta velocity component, V_θ, were all analyzed for the smaller nozzle where the radial

location of the outer inlet slot varied. The three components of velocity were examined for the situation where FC-72 was used as the working fluid and 4.416 x 10^{-7} m^3/s was used as the inlet flow rate. In addition, when the outer inlet slot was located at the position that produced the largest cone angle (R_2 = 5.50 x 10^{-4} m and R_3 = 5.77 x 10^{-4} m), the results for the flow rate of 5.678 x 10^{-7} m^3/s were observed. This was done to observe how the fluid was behaving within the nozzle and compare it to how the fluid was behaving once it exited the nozzle.

The three velocity components were analyzed at seven different locations throughout the nozzle. The first section was located at about 10% of the nozzle length. The second section was located at about 50% of the nozzle length, whereas the third section was at the point where the nozzle converged at the throat. The fourth section was located half way down the throat, while the fifth section was located at the nozzle outlet. The sixth section was located at 1/3 the length of the free surface, and finally, the seventh section was located at 2/3 the length of the free surface. The velocity components were not studied at the end of the free surface, because many numerical assumptions are made at that location, which could jeopardize the accuracy of the numbers. Table 23 shows the sections that were investigated, as well as their axial coordinate.

Table 23: Analyzed sections with corresponding axial coordinate

	Section Planes						
	A	B	C	D	E	F	G
Axial Coordinate [m]	1.00 x 10^{-4}	5.00 x 10^{-4}	1.07 x 10^{-3}	1.15 x 10^{-3}	1.22 x 10^{-3}	1.35 x 10^{-3}	1.54 x 10^{-3}

Figure 186 displays the result for the radial velocity component with FC-72 as the working fluid and the outer inlet slot positioned at R_2 equal to 2.50 x 10^{-4} m, and R_3 equal to 3.04 x 10^{-4} m. The boundary conditions within the problem state that the radial velocity at the line of symmetry, as well as the wall, is equal to zero. This is why all of the radial velocities within the nozzle begin and end at a value of zero. At section A, the radial velocity took on a sinusoidal shape. After Section A, all of the sections within the nozzle produce negative radial velocities. The maximum radial velocity observed was located at section C, which is where the conical shape of the nozzle converges at the throat. Here, the radial velocity was determined to be approximately -2.12 m/s. However, after the fluid exits the nozzle, the radial velocity becomes a positive value. As the fluid moved away from the nozzle outlet, its radial velocity decreased.

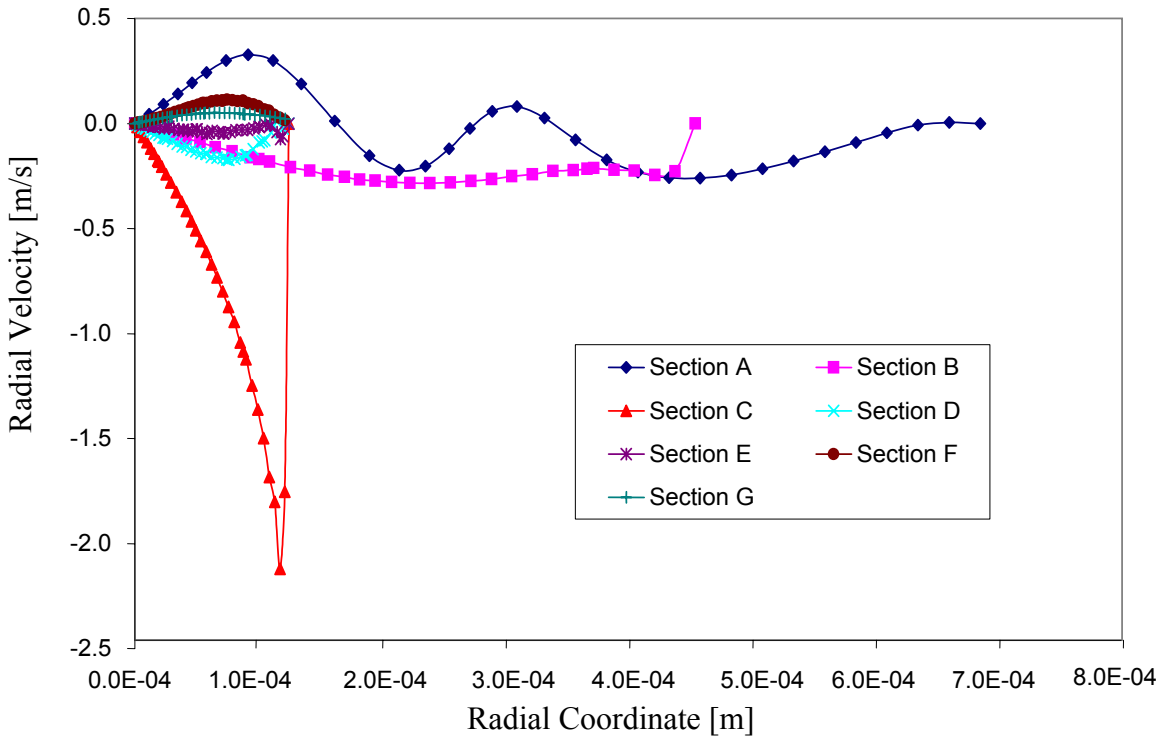

Figure 186: Radial velocity component at various sections (Q = 4.416 x 10^{-7} m^3/s, R_2 = 2.5 x 10^{-4} m)

Figure 187 shows the axial velocity component for the same trial. The values at Sections A and B are the lowest out of the sections that were analyzed. This is because the other sections had a much lower radial height, which forced the fluid to move at a higher speed to provide the same flow rate that had entered the nozzle. At some points towards the outer reaches of Section A where some swirling occurred, the axial velocity became negative. The maximum axial velocity was found to be about 8.60 m/s located just as the fluid exited the nozzle. Where the nozzle converges at the throat, the axial velocity was observed to be fairly even throughout the entire range, before the boundary condition sent the value to zero. Again, the fluid within the nozzle is constrained by the requirement that the velocity along the nozzle wall is equal to zero, which is why the half-parabola shape is depicted in the figure for Sections D and E. However, after the fluid exited the nozzle, the axial velocity decreased gradually, but did not go to zero.

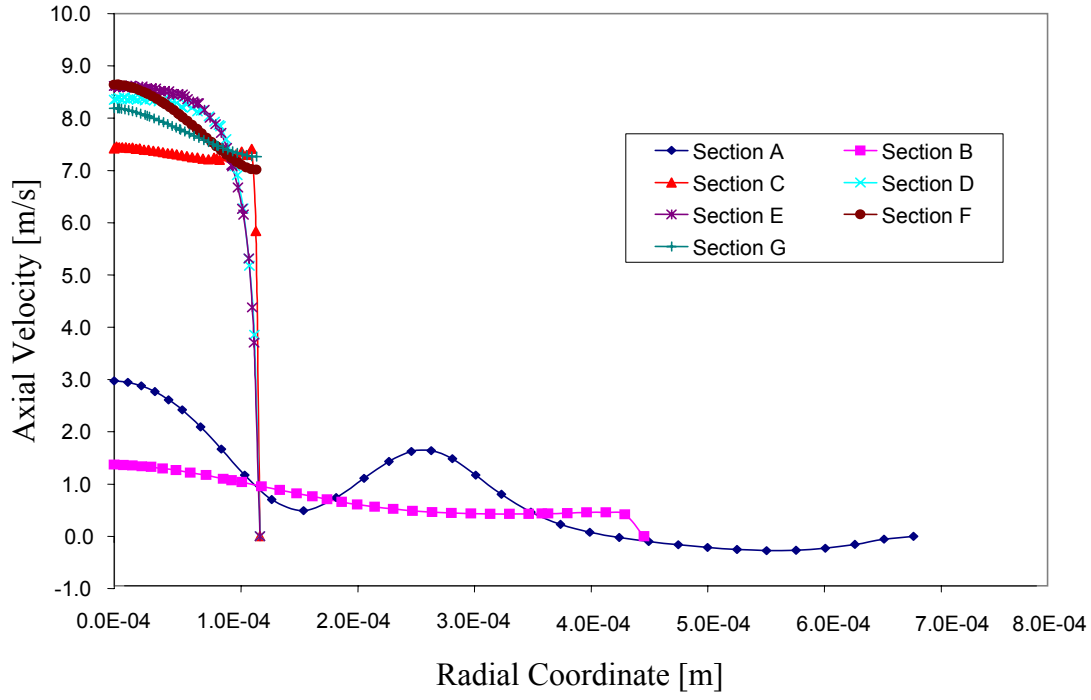

Figure 187: Axial velocity component for various sections ($Q = 4.416 \times 10^{-7}$ m^3/s, $R_2 = 2.5 \times 10^{-4}$ m)

Finally, the values obtained for the theta component of velocity is shown in Figure 188. Again, due to the boundary condition constraining the velocity to zero at the nozzle walls, all of the plots for the sections within the nozzle have a parabolic shape, which begins and ends at zero. After the fluid exited the nozzle, the theta velocity component became more of a linear pattern. Since Section A was close to the inlet of the nozzle, its values peaked when the radial value was 2.50 x 10^{-4} m, which is where the outer inlet slot was located. The value of the theta component had a maximum value of about 3.40 m/s at the location where the nozzle converges, and then it declined minutely as the fluid moved through the throat of the nozzle.

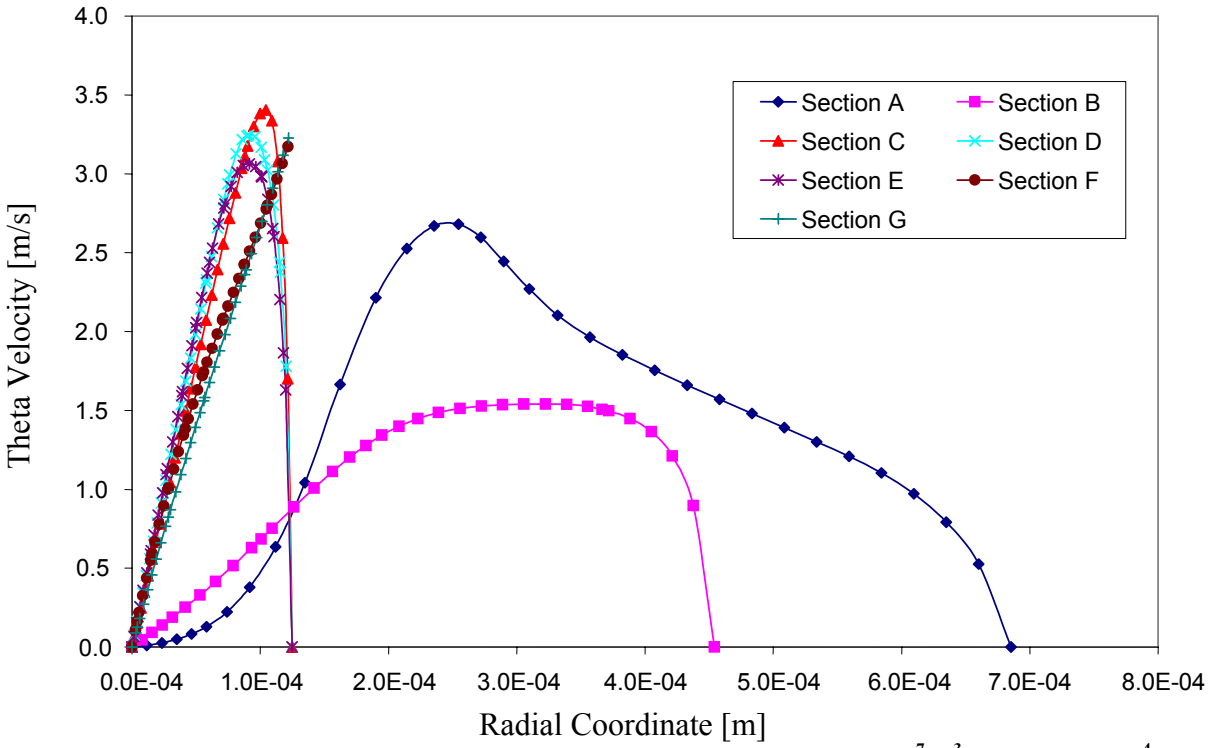

Figure 188: Theta velocity component for various sections (Q = 4.416 x 10^{-7} m^3/s, R_2 = 2.5 x 10^{-4} m)

The next variation that was investigated continued to utilize FC-72 as the working fluid with a flow rate of 4.416 x 10^{-7} m^3/s. However, the location of the outer inlet slot

was positioned so that R_2 was equal to 4.00 x 10^{-4} m and R_3 was equal to 4.36 x 10^{-4} m. Figure 189 shows the radial velocity values for this situation. Similar to the previous trial, the results for Section A provided somewhat of a sinusoidal wave. Again, all of the values for the radial velocity within the nozzle were negative. At Section C, where the nozzle converges to form the throat, the radial velocity reached its maximum value in the study. At that section, the value dipped down to about -2.10 m/s, which is quite large compared to the other observed locations. Once again, as the fluid exited the nozzle, the radial velocity became positive and slowly decreased as the distance from the nozzle increased.

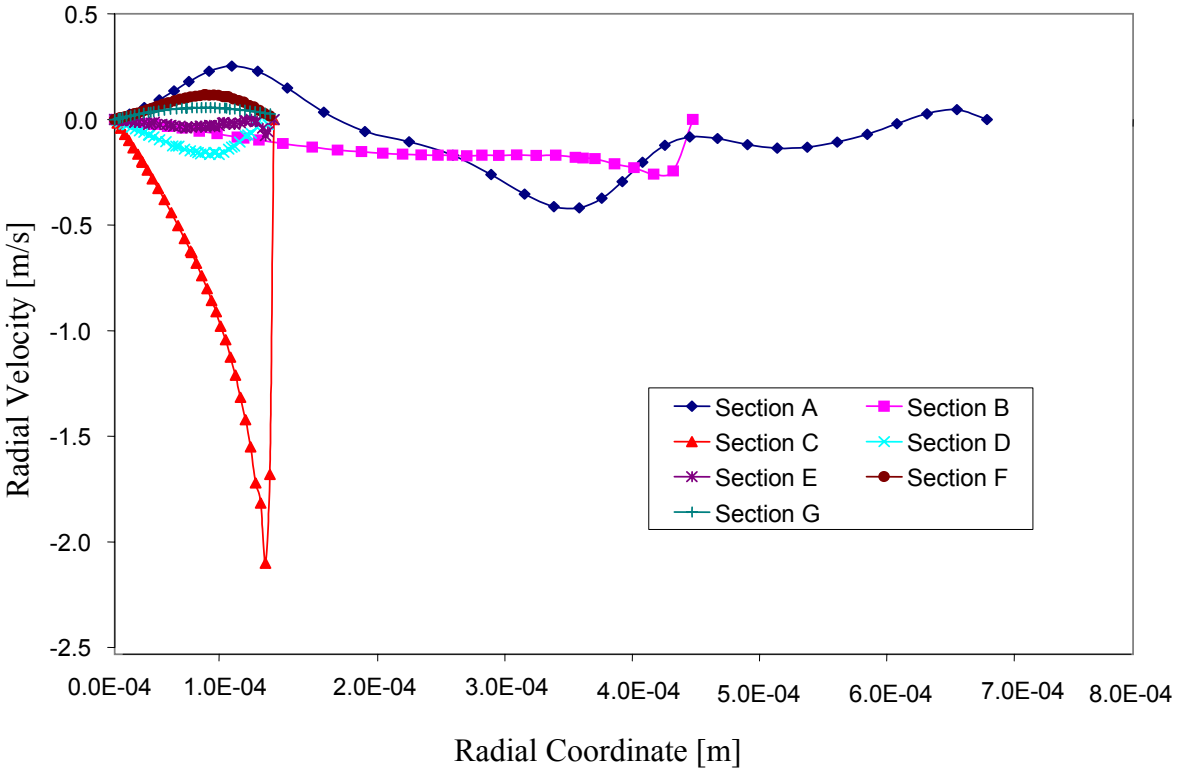

Figure 189: Radial velocity component for various sections (Q = 4.416 x 10^{-7} m^3/s, R_2 = 4.0 x 10^{-4} m)

Figure 190 shows the axial velocity component values obtained for the various sections. Similar to the radial velocity component, the axial velocity at Section A

resembled a sinusoidal wave. Again, the maximum axial velocity obtained was determined to be approximately 8.70 m/s located just as the fluid exited the nozzle. The axial velocity of the fluid in Section C is about the same throughout its extent before it drops off to zero, whereas the axial velocity of the fluid in the throat of the nozzle is a maximum at the line of symmetry and then declines gradually to zero at the nozzle wall. After the fluid exited the nozzle, it was observed that the axial velocity decreased as the axial distance from the nozzle increased. It was also noted that as the radial distance from the line of symmetry increased, the axial velocity decreased.

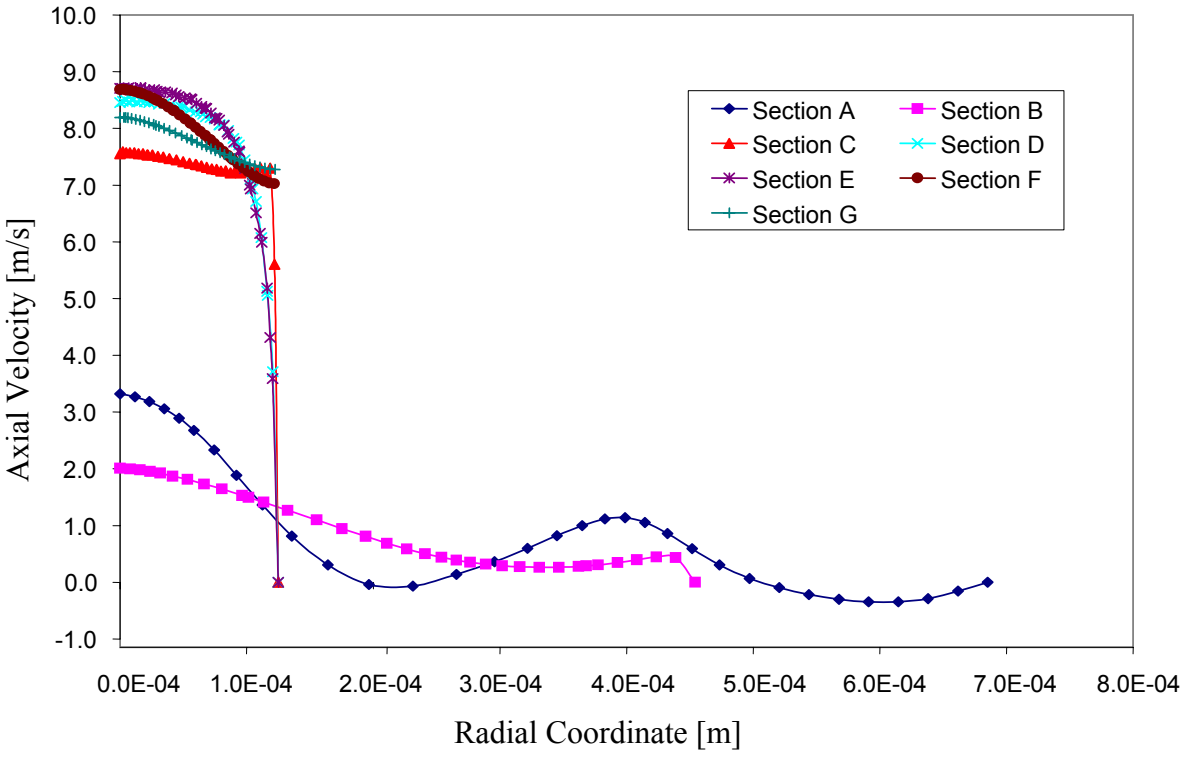

Figure 190: Axial velocity component for various sections ($Q = 4.416 \times 10^{-7}$ m^3/s, $R_2 = 4.0 \times 10^{-4}$ m)

Figure 191 reveals the values for the theta velocity component for this scenario. Again, the values for all of the sections within the nozzle form parabolas due to the boundary conditions. However, after the fluid exited the nozzle, it was observed that the

theta velocity values formed a linear model. The maximum value was again located at Section C, where the nozzle converges to form the throat. This value was determined to be about 8.75 m/s. As the fluid moved through the throat of the nozzle, this maximum value decreased slightly. For this case, the theta velocity values at Section A and Section B both peaked at the approximate location of the outer inlet slot.

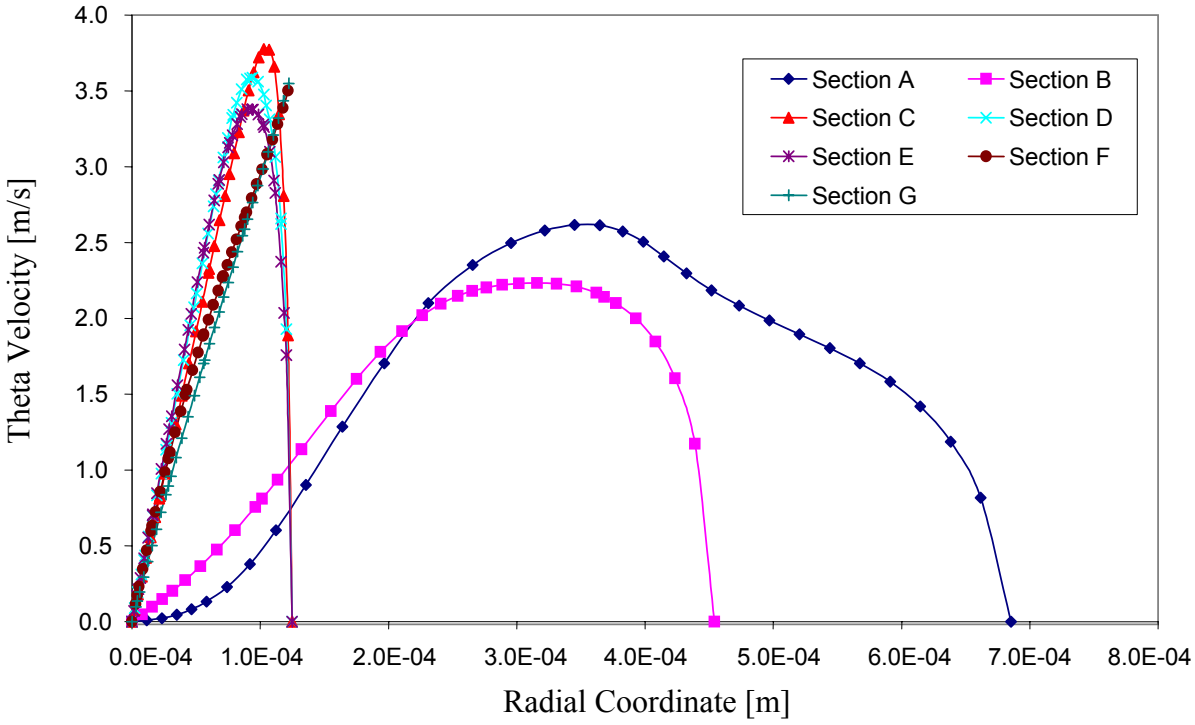

Figure 191: Theta velocity component for various sections ($Q = 4.416 \times 10^{-7}$ m^3/s, $R_2 = 4.0 \times 10^{-4}$ m)

Next, the nozzle geometry with R_2 equal to 5.50×10^{-4} m and R_3 equal to 5.77×10^{-4} m was used to analyze the three components of velocity. Since this particular geometry produced the greatest cone angle, the velocity values were investigated for both of the flow rates used – 4.416×10^{-7} m^3/s and 5.678×10^{-7} m^3/s. The first flow rate to be studied was 4.416×10^{-7} m^3/s. Figure 192 shows the radial velocity component for this scenario with FC-72 as the working fluid. Again, Section A took on a sinusoidal pattern.

It was noted that the radial velocity for this geometry was greater than that for the other geometries. The radial velocity at Section C was more than double that of the other geometries. It was at this location where the radial velocity component was a maximum with a value of nearly -4.66 m/s. The other nozzle geometries produced a maximum radial velocity of roughly -2.10 m/s. As with the other nozzles, all of the radial velocity values within the nozzle were negative, while they became positive once the fluid exited the nozzle.

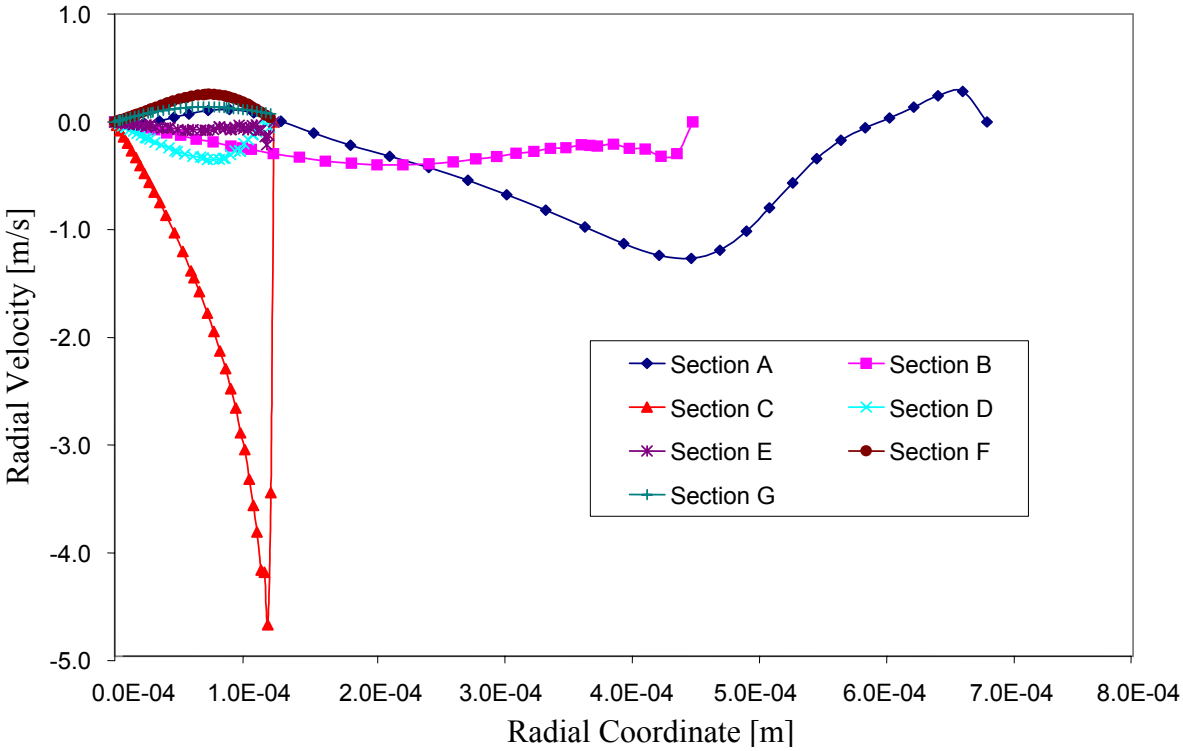

Figure 192: Radial velocity component for various sections ($Q = 4.416 \times 10^{-7}$ m^3/s, $R_2 = 5.5 \times 10^{-4}$ m)

Figure 193 shows the axial velocity component for the different sections with 4.416×10^{-7} m^3/s as the inlet flow rate. Because the nozzle is larger at Sections A and B, their respective axial velocities are smaller than the other sections. However, it was observed that all three components of velocity were much larger than the same results

found in the other nozzles. The maximum axial velocity for this geometry was found at the nozzle outlet and had a value of about 19.60 m/s. This value is a little over 10.00 m/s faster than the maximum axial velocity for the other geometries. This is the reason for this nozzle geometry producing the largest radial free surface height. The patterns of the axial velocity throughout the different sections for this geometry are almost identical to the patterns observed for the other geometries. In this case, however, the values are much greater.

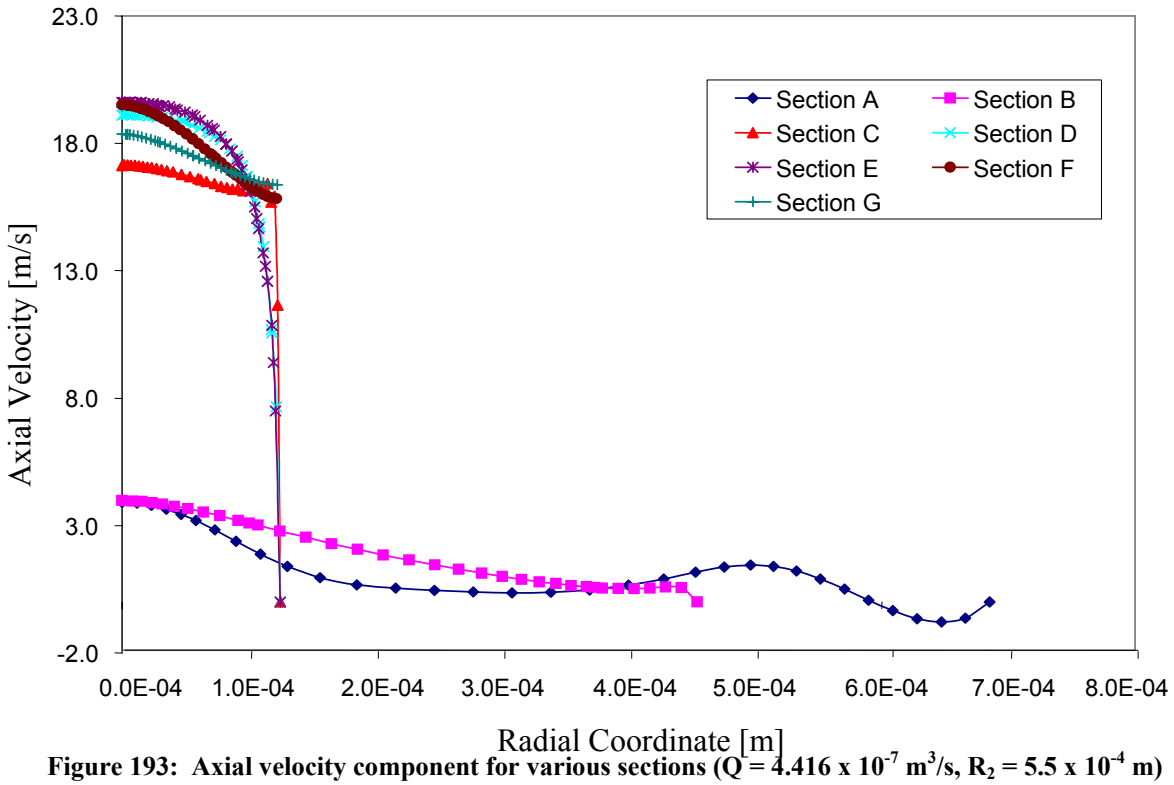

Figure 193: Axial velocity component for various sections ($Q = 4.416 \times 10^{-7}$ m^3/s, $R_2 = 5.5 \times 10^{-4}$ m)

The theta velocity component is shown in Figure 194. Comparable to the other velocity components for this geometry, the theta velocity component was much larger than those for the other nozzle geometries. The theta velocity for all of the sections within the nozzle produced a parabolic shape due to the no slip condition at the nozzle

wall, and the boundary conditions at the line of symmetry. However, after the fluid exited the nozzle, it was noted that the theta velocity component formed a linear pattern with its value increasing as the radial distance increased. The maximum value was about 9.30 m/s located at Section C. The theta velocity value decreased slightly from the maximum value as the fluid moved through the throat of the nozzle.

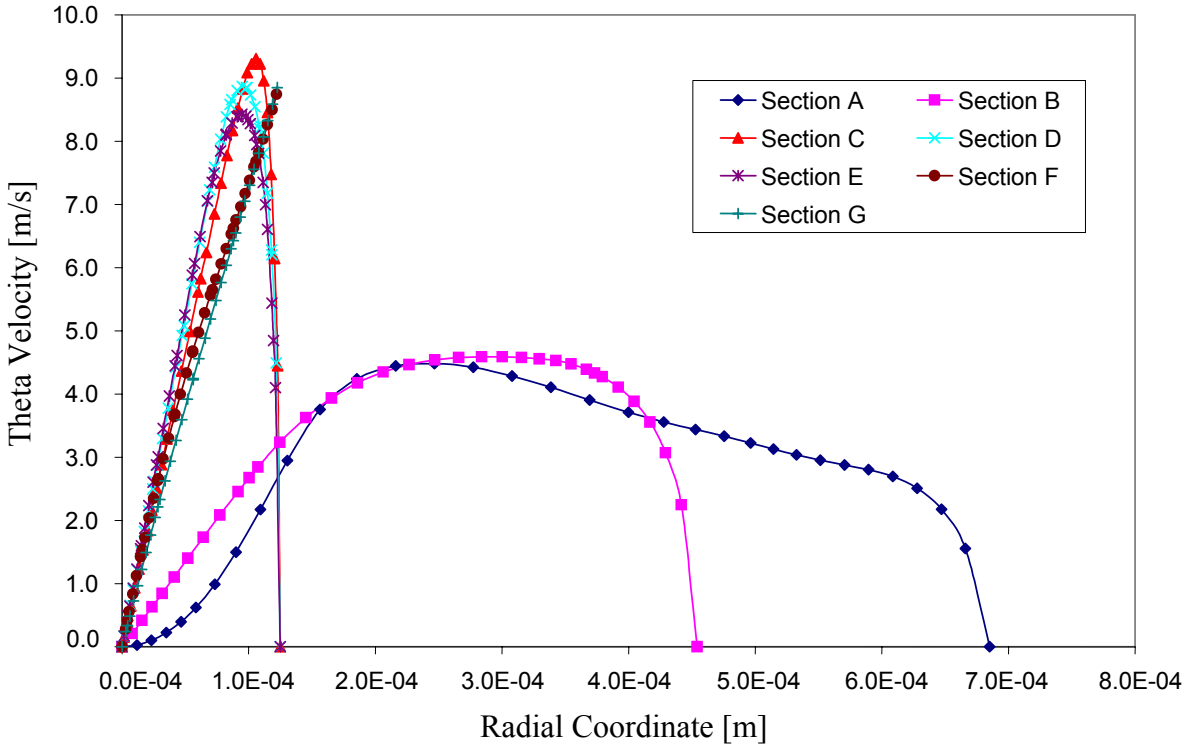

Figure 194: Theta velocity component for various sections ($Q = 4.416 \times 10^{-7}$ m^3/s, $R_2 = 5.5 \times 10^{-4}$ m)

This same nozzle geometry ($R_2 = 5.50 \times 10^{-4}$ m and $R_3 = 5.77 \times 10^{-4}$ m) was analyzed with higher flow rate of 5.678×10^{-7} m^3/s. Figure 195 shows the radial velocity component for this situation. As expected, the values for all three velocity components were greater than the other cases that were studied. This is primarily due to the increased flow rate, as well as the nozzle geometry. For the radial velocity component, the patterns for each section appeared the same as the other trials, only this trial produced larger

values. For this case, the maximum radial velocity was again located at Section C where the nozzle converges to form the throat. This value was determined to be about -6.00 m/s. Once more, the radial velocities within the nozzle initiate and terminate at zero because of the no slip condition on the nozzle walls, and the boundary condition of zero radial velocity along the line of symmetry. However, as the fluid exits the nozzle, it is no longer in contact with the nozzle wall. This is why the radial velocity outside of the nozzle does not terminate at zero. It was also noted that the region outside of the nozzle is the only region to produce all positive values for the radial velocity component.

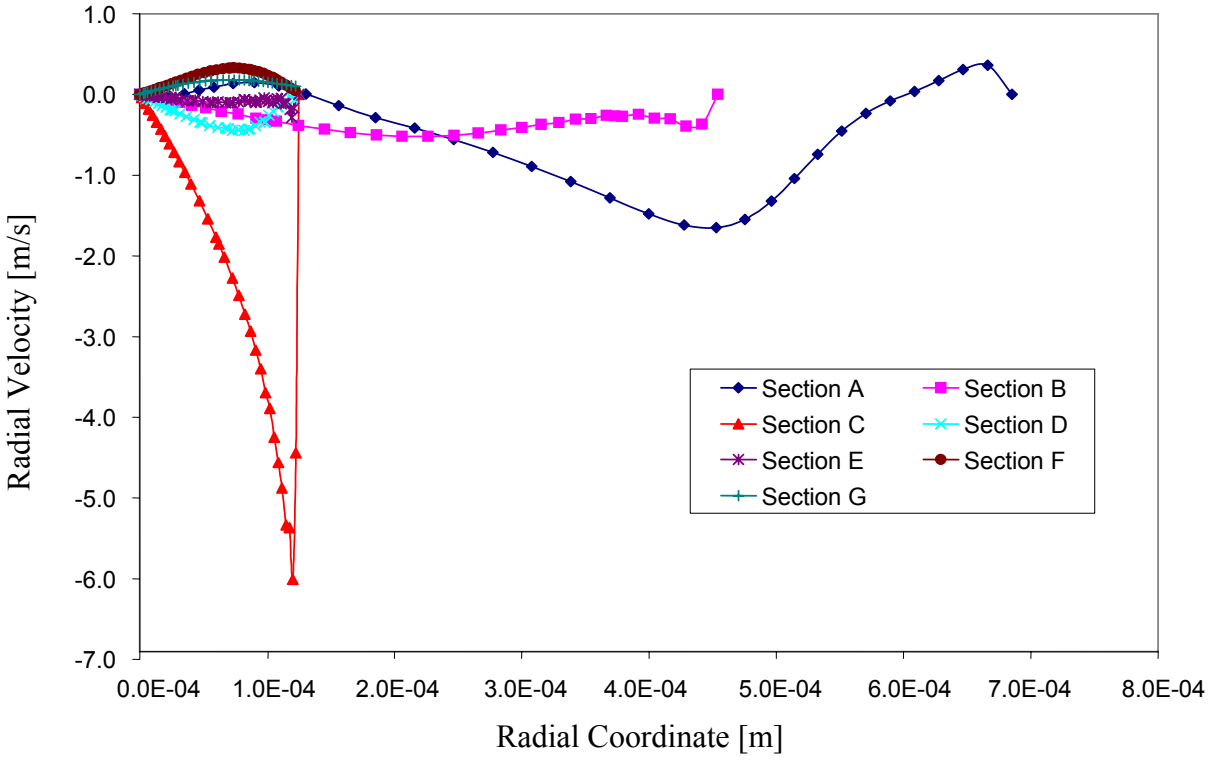

Figure 195: Radial velocity component for various sections ($Q = 5.678 \times 10^{-7}$ m^3/s, $R_2 = 5.5 \times 10^{-4}$ m)

The axial velocity component for this case is shown in Figure 196. The values for Section A and Section B were the lowest. From the streamline contour plot, a portion near the outer nozzle wall along Section A tends to swirl, which causes the value for the

axial velocity to temporarily become negative. The maximum axial velocity was found to be where the fluid exited the nozzle and maintained a value of about 25.25 m/s. After the fluid exited the nozzle, the axial velocity decreased slightly, but remained at about 20.00 m/s. However, the axial velocity of the fluid within the throat of the nozzle decreased to a value of zero along the nozzle wall to form the shape of half of a parabola. The fluid converging from the conical nozzle shape to the throat of the nozzle remained at a fairly constant axial velocity throughout the range.

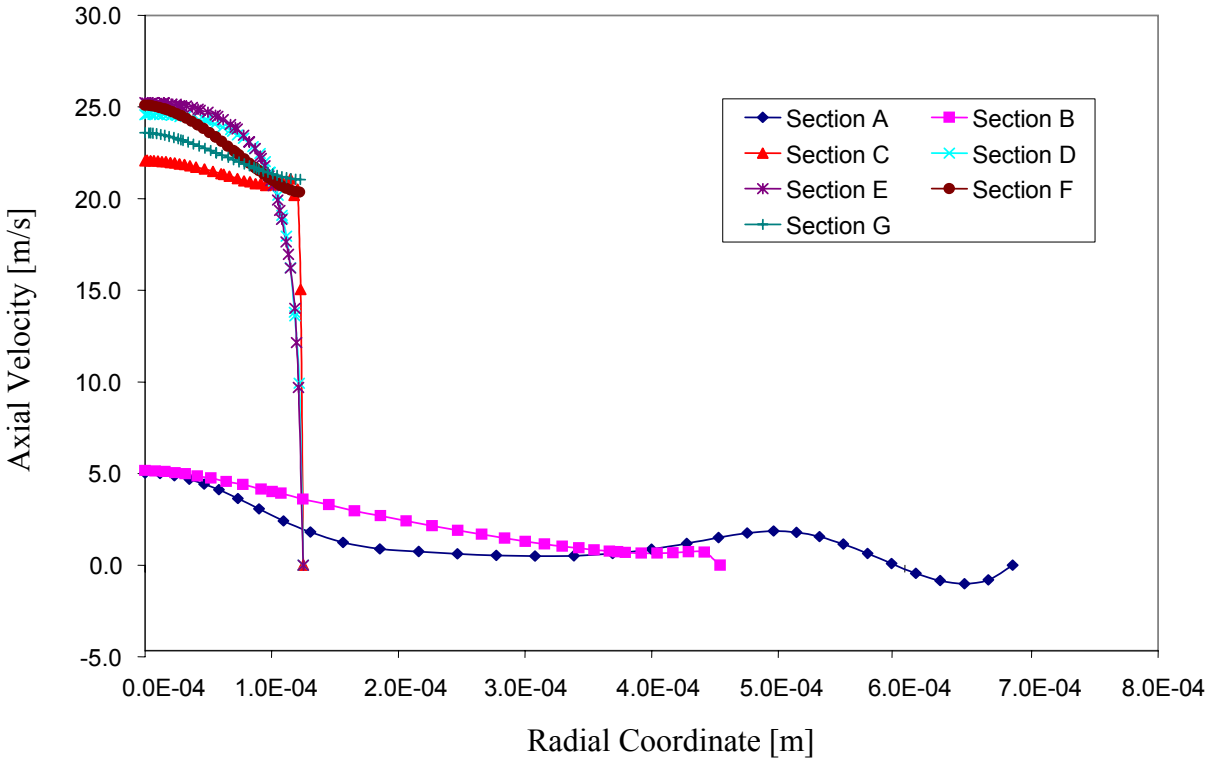

Figure 196: Axial velocity component for various sections ($Q = 5.678 \times 10^{-7}$ m^3/s, $R_2 = 5.5 \times 10^{-4}$ m)

Finally for this geometry, the theta velocity component is shown in Figure 197. Again, Sections A and B produce the lowest values for the velocity component. The value for section A peaked at a radial distance of about 2.00×10^{-4} m, whereas the value for Section B peaked at a radial distance of about 4.00×10^{-4} m. The maximum theta

velocity value was found at Section C with a magnitude of about 12.10 m/s. Similar to the other trials, this maximum value decreased slightly as the fluid moved through the throat of the nozzle – through Sections D and E. Once the fluid exited the nozzle, it was no longer bound by the nozzle wall, and therefore, no longer bound by the no-slip condition. This is why the pattern of the theta velocity component for the fluid outside of the nozzle is in the shape of a line rather than a parabola.

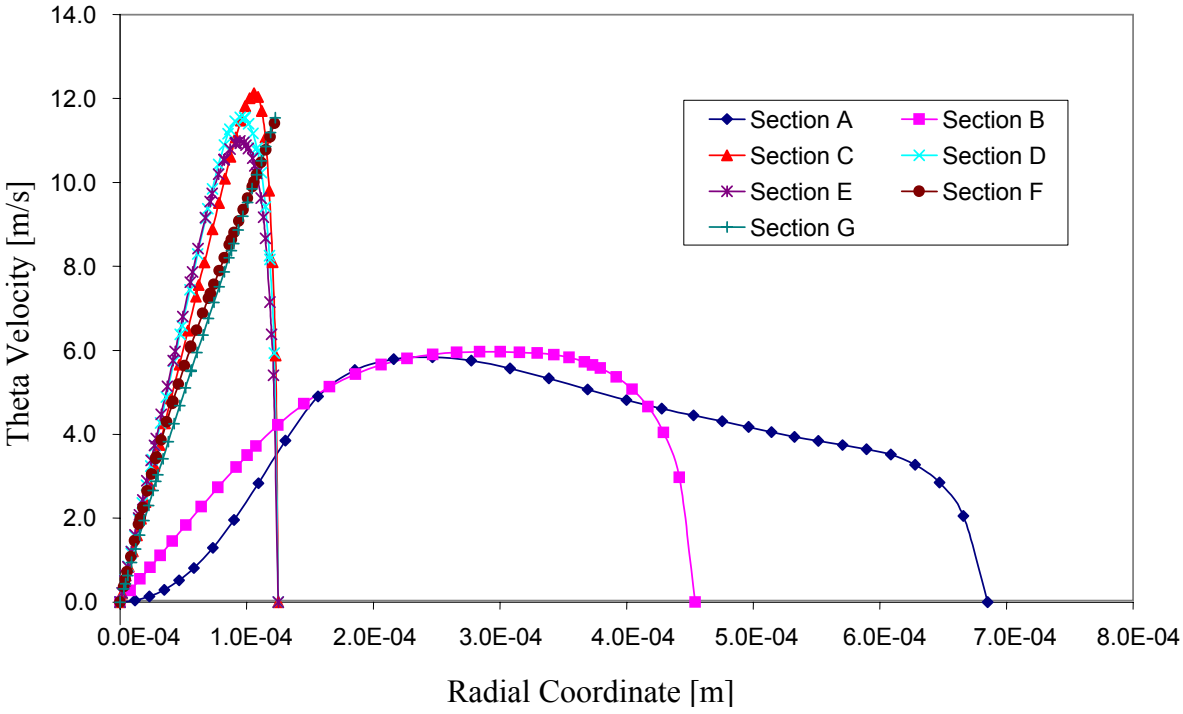

Figure 197: Theta velocity component for various sections ($Q = 5.678 \times 10^{-7}$ m^3/s, $R_2 = 5.5 \times 10^{-4}$ m)

The final nozzle geometry that was investigated had the outer inlet slot positioned so that R_2 was equal to 7.20×10^{-4} m and R_3 was equal to 7.43×10^{-4} m. For this case, FC-72 was still used as the working fluid, and the only inlet flow rate was 4.416×10^{-7} m^3/s. Figure 198 shows the radial velocity results obtained for this case. It was again noted that most of the values for the radial velocity component within the nozzle were negative, whereas the values were all positive after the fluid exited the nozzle. From the

positive and negative values observed along Section A, it was noted that the fluid entering from the central inlet flowed outward in the radial direction toward the nozzle wall. However, the fluid entering from the outer inlet slot began to flow toward the symmetry line as it moved toward the nozzle outlet. The radial velocity reached a maximum value of approximately -2.50 m/s at Section C, before it decreased as it went through the throat of the nozzle.

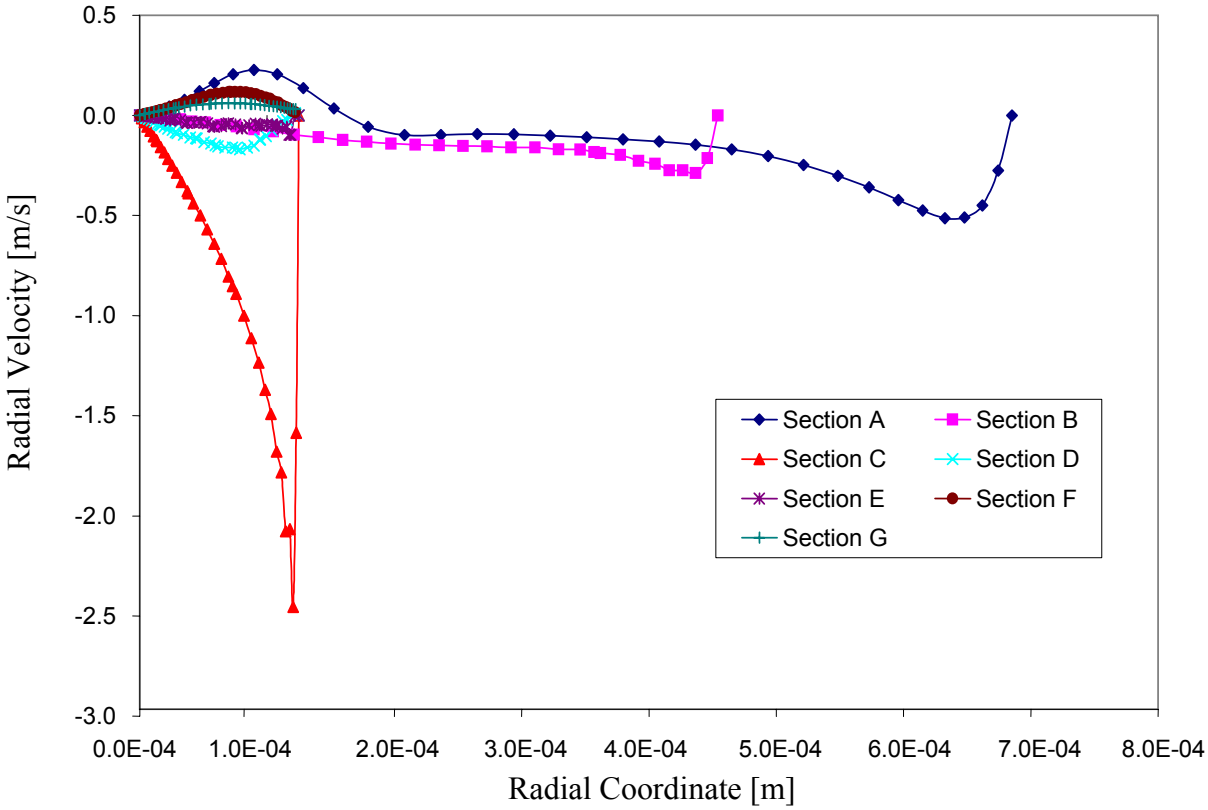

Figure 198: Radial velocity component for various sections ($Q = 4.416 \times 10^{-7}$ m^3/s, $R_2 = 7.2 \times 10^{-4}$ m)

Figure 199 shows the axial velocity component for this situation. It was noted that for this geometry, all of the velocity components have decreased from the values provided by the geometry having R_2 equal to 5.50×10^{-4} m to the same order of magnitude of the values for the first two geometries. Unlike the other geometries, the

axial velocity for a very small portion of the fluid along Section A becomes negative. This is because the outer inlet slot is position at the edge of the top plate, which provides no means for the fluid to swirl. This can be confirmed from viewing the streamline contour plot for these parameters. The maximum axial velocity had a value of about 3.85 m/s at the location where the fluid exited the nozzle. The fluid within the nozzle declined gradually to a value of zero due to the boundary conditions placed on the system. The axial velocity of the fluid outside of the nozzle also decreased gradually, but never went below 7.50 m/s.

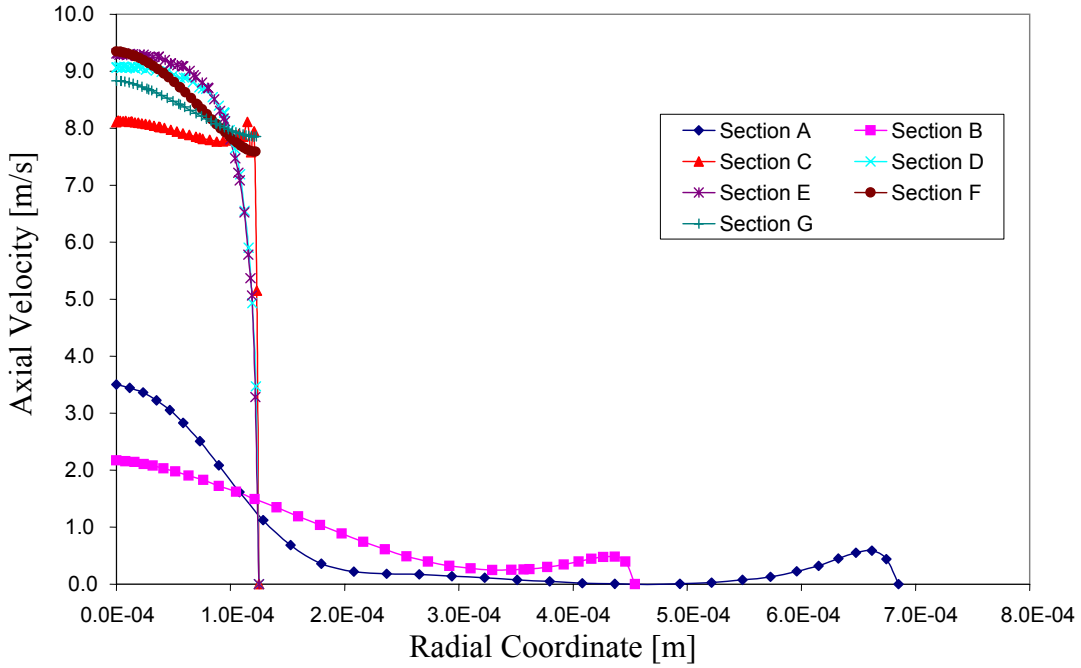

Figure 199: Axial velocity component for various sections ($Q = 4.416 \times 10^{-7}$ m^3/s, $R_2 = 7.2 \times 10^{-4}$ m)

The last case that was studied involved the theta velocity component for the various sections, which is shown in Figure 200. Again, the theta velocity value for all of the sections within the nozzle form a parabola because of the boundary conditions placed on the system. Section A and Section B provided the lowest values with Section A

peaking at a radial distance of about 2.00 x 10^{-4} m, and Section B peaking at a radial distance of about 3.00 x 10^{-4} m. The maximum theta velocity value was approximately 4.10 m/s located at Section C. Similar to the other trials, this value decreased insignificantly as the fluid moved through the throat of the nozzle. Once the fluid exited the nozzle, it was free of conditional requirements along the nozzle wall, which allowed the theta velocity to take on a linear form. For these sections, the theta velocity component increased as the radial distance increased.

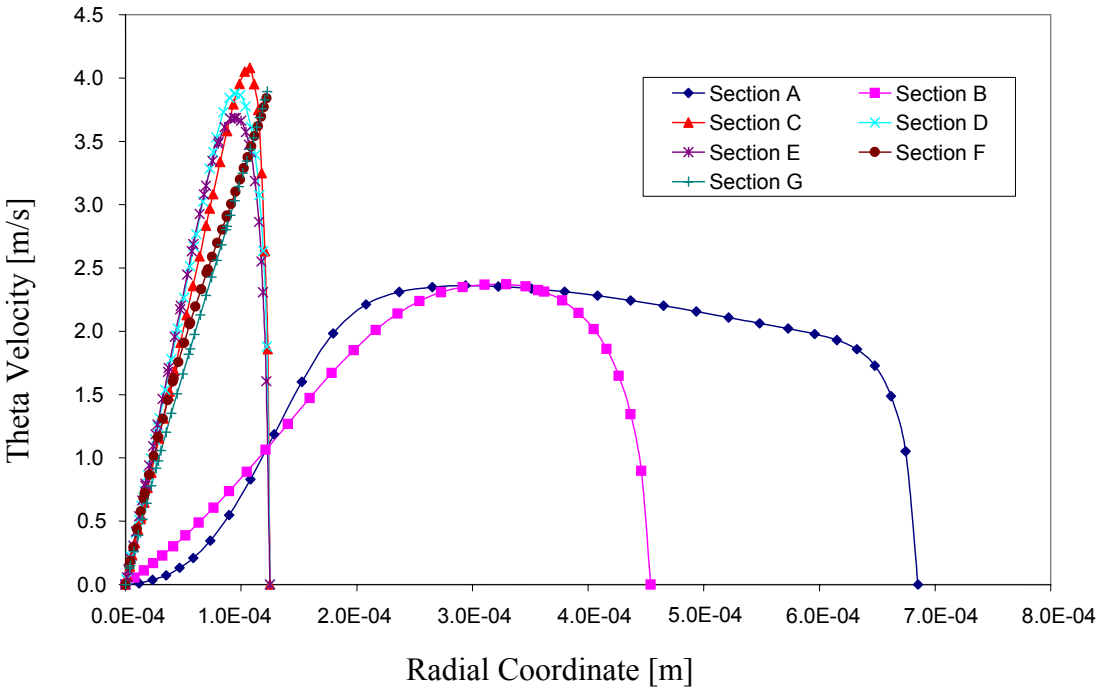

Figure 200: Theta velocity component for various sections (Q = 4.416 x 10^{-7} m^3/s, R_2 = 7.2 x 10^{-4} m)

Compounding on the previous plots, it is desired to obtain a magnified view of the velocity component plots for the outlet of the nozzle and the exiting liquid sheet. Therefore, each velocity component at Sections E, F, and G were plotted in dimensionless form in Figure 201 through Figure 209. These plots simply provide a clearer view of what is occurring at these particular sections of the nozzle, and it is for

this reason that a description of the occurrences has previously been discussed. These descriptions can be referenced from the previous pages. However, it can be easily seen that the all of the velocities al all of the sections were at a maximum when the ratio of the outer slot location to the top plate radius was equal to 0.74 (R_2 equal to 5.50 x 10^{-4} m).

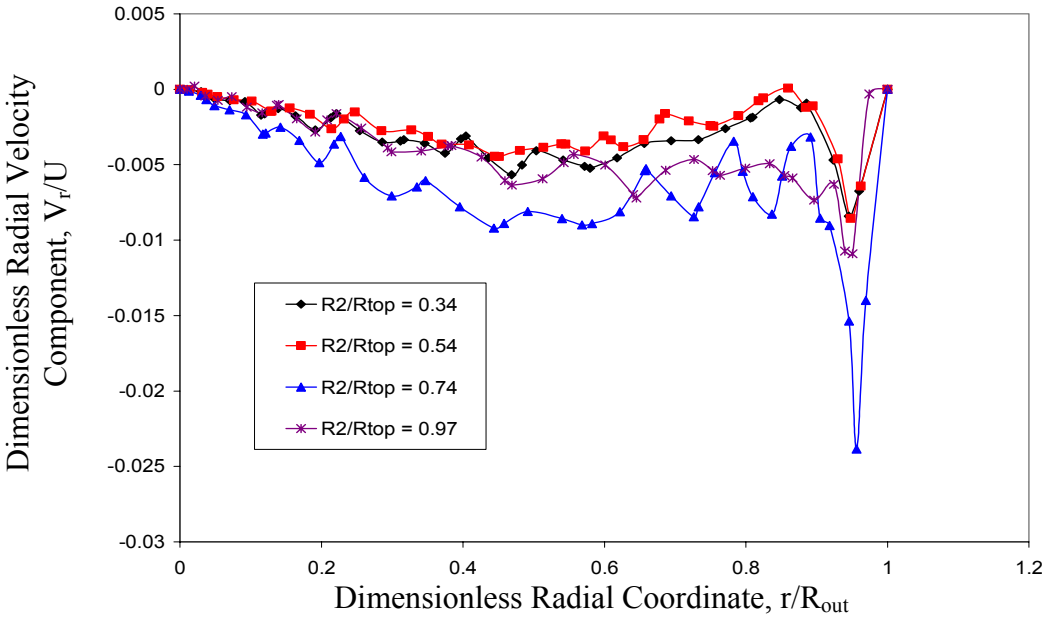

Figure 201: Dimensionless radial velocity component at Section E (FC-72, Q = 4.416 x 10^{-7} m^3/s)

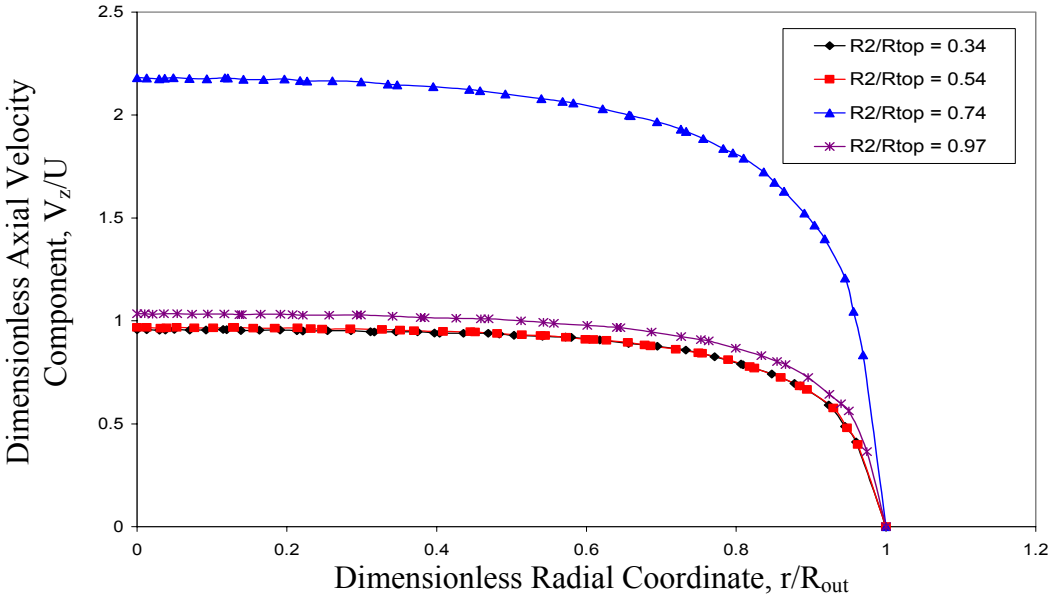

Figure 202: Dimensionless axial velocity component at Section E (FC-72, Q = 4.416 x 10^{-7} m^3/s)

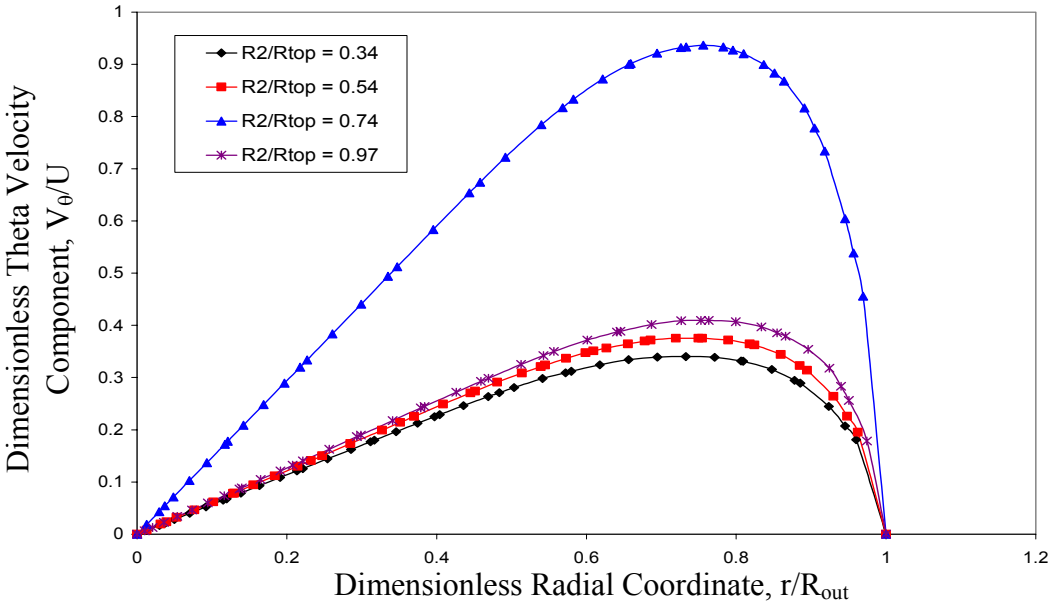

Figure 203: Dimensionless theta velocity component at Section E (FC-72, Q = 4.416 x 10^{-7} m^3/s)

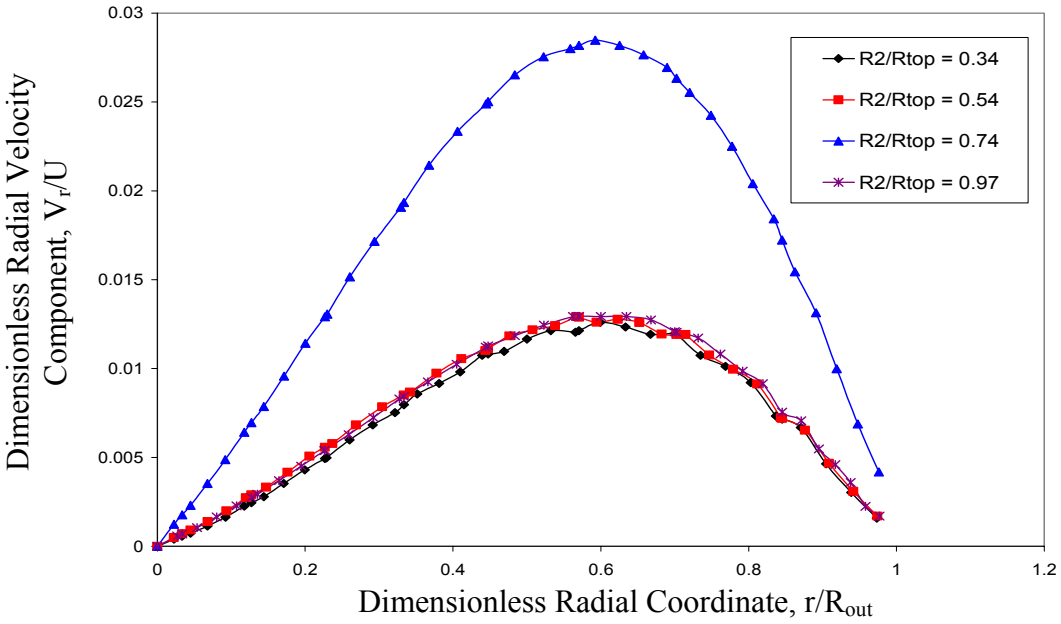

Figure 204: Dimensionless radial velocity component at Section F (FC-72, Q = 4.416 x 10^{-7} m^3/s)

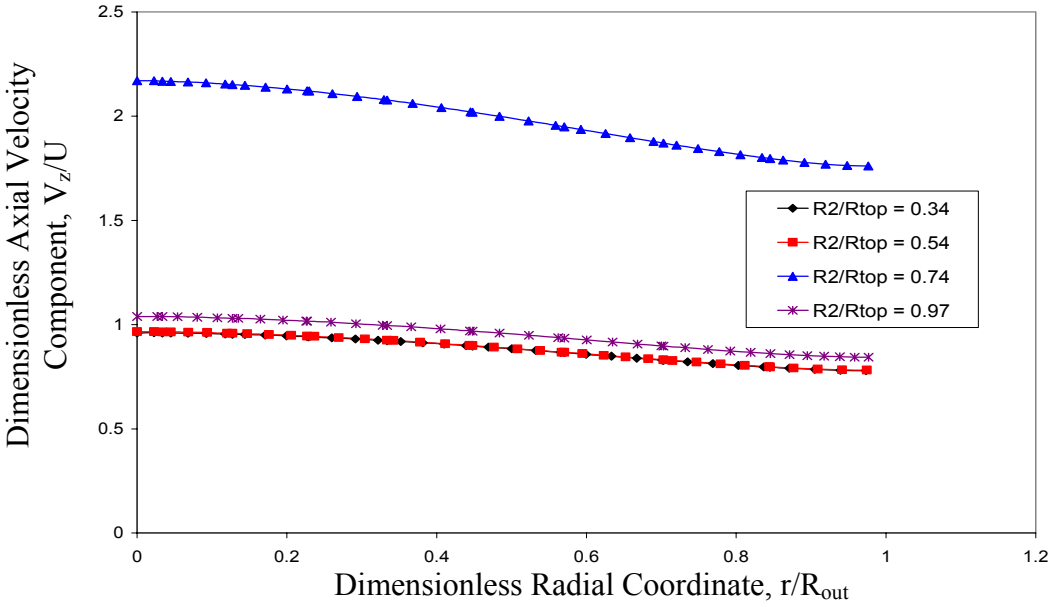

Figure 205: Dimensionless axial velocity component at Section F (FC-72, Q = 4.416 x 10^{-7} m^3/s)

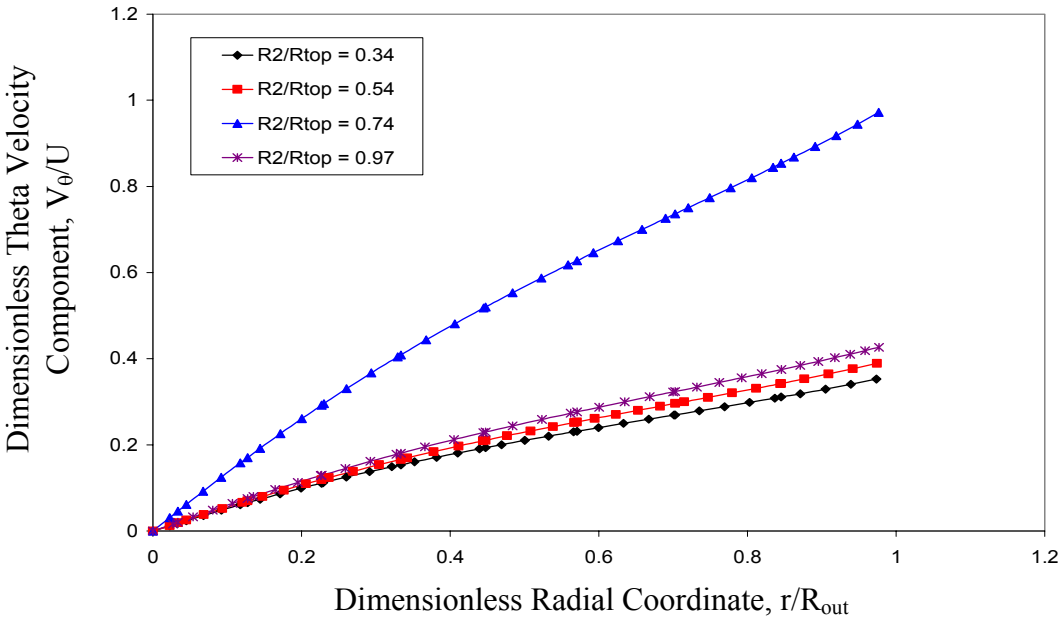

Figure 206: Dimensionless theta velocity component at Section F (FC-72, Q = 4.416 x 10^{-7} m^3/s)

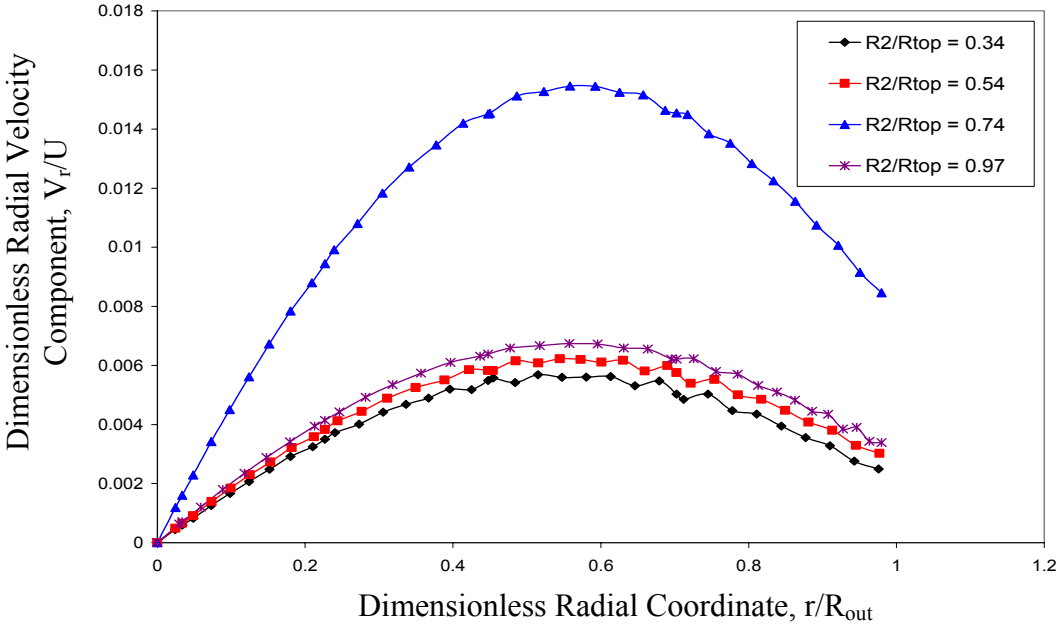

Figure 207: Dimensionless radial velocity component at Section G (FC-72, Q = 4.416 x 10^{-7} m^3/s)

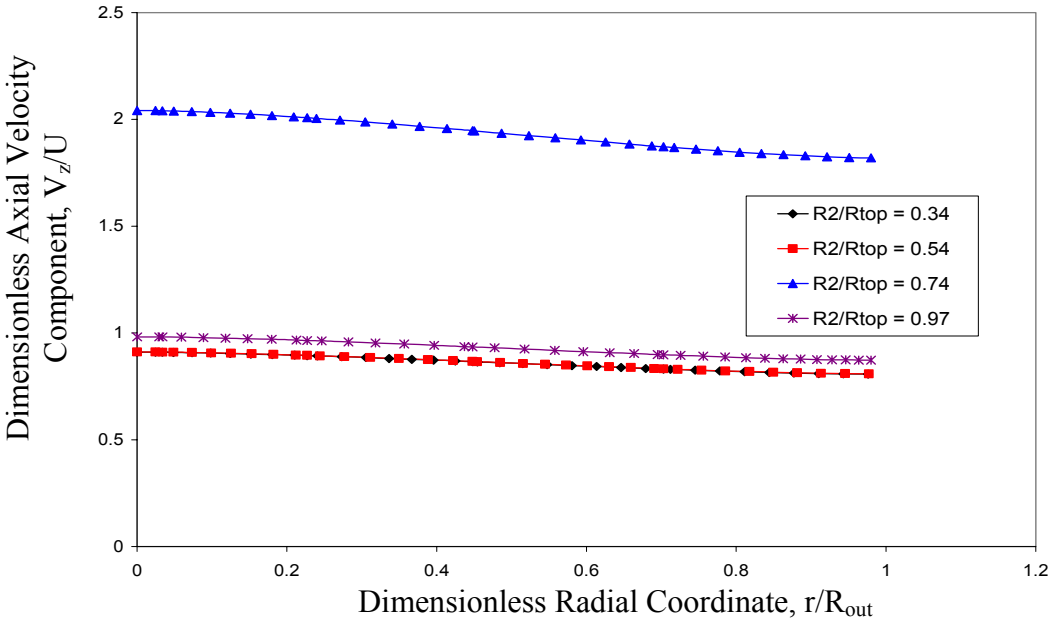

Figure 208: Dimensionless axial velocity component at Section G (FC-72, Q = 4.416 x 10^{-7} m^3/s)

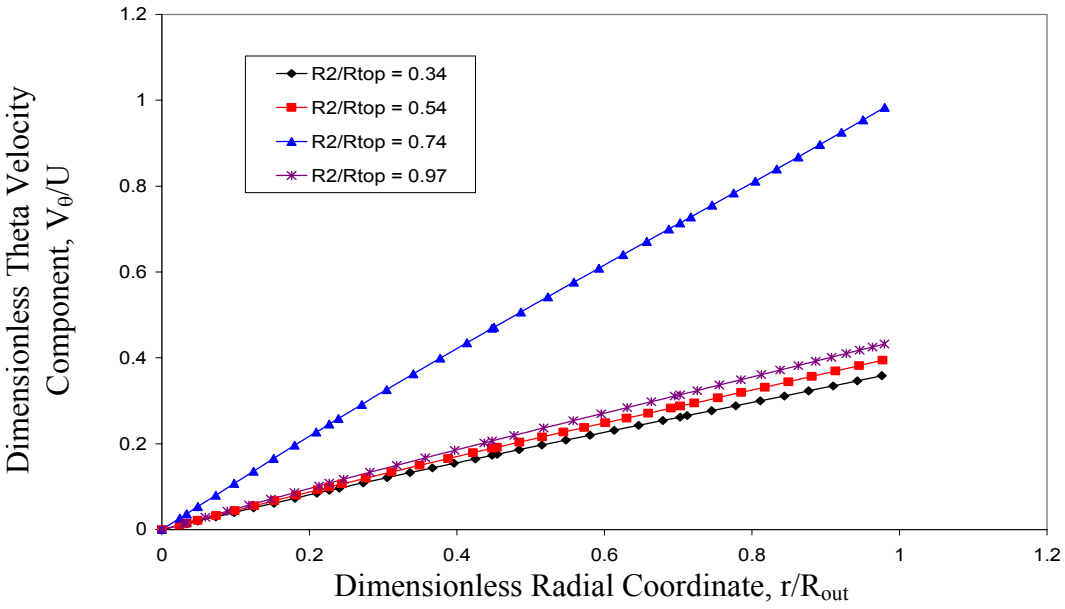

Figure 209: Dimensionless theta velocity component at Section G (FC-72, Q = 4.416 x 10^{-7} m^3/s)

Figure 210 through Figure 221 are dimensionless plots that compare each component of velocity at each section for FC-72 in all of the various nozzle geometries. Again, these plots were obtained to acquire a more understandable view of how the fluid is behaving at certain sections for the various nozzle geometries. As was previously mentioned, the zero-velocity boundary conditions along the nozzle wall do not apply to the fluid after it has exited the nozzle. This is why the velocities at Sections F and G do not have a value of zero at its outermost radial node. It was also noted that as the fluid moved further away from the nozzle outlet, its associated velocities became more linear in nature. The following twelve figures depict each velocity component for each of the different nozzle geometries.

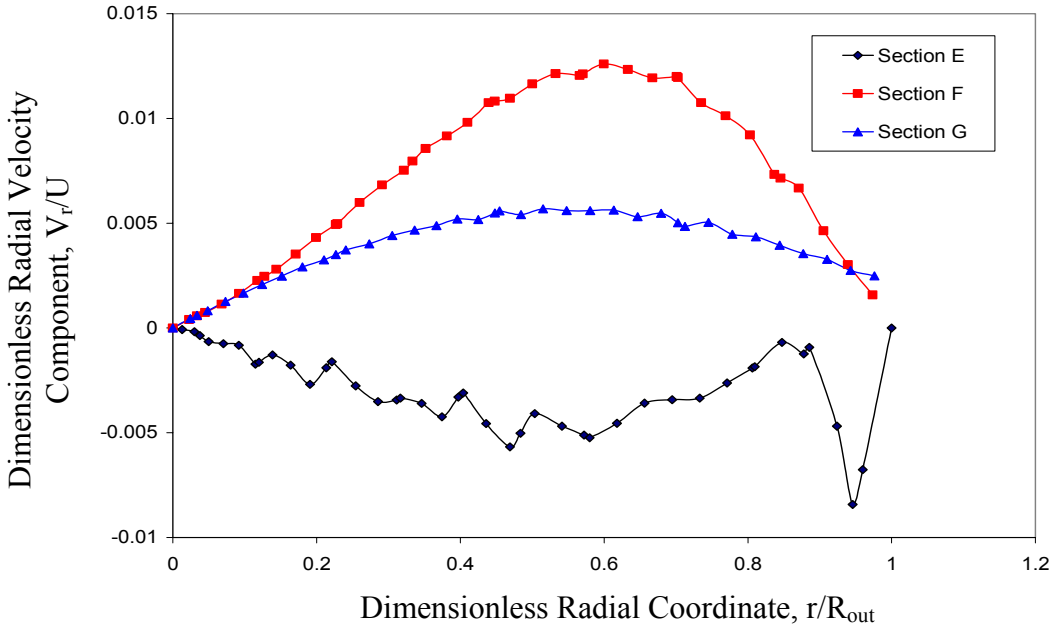

Figure 210: Dimensionless radial velocity component at various sections ($R_2 = 2.5 \times 10^{-4}$ m)

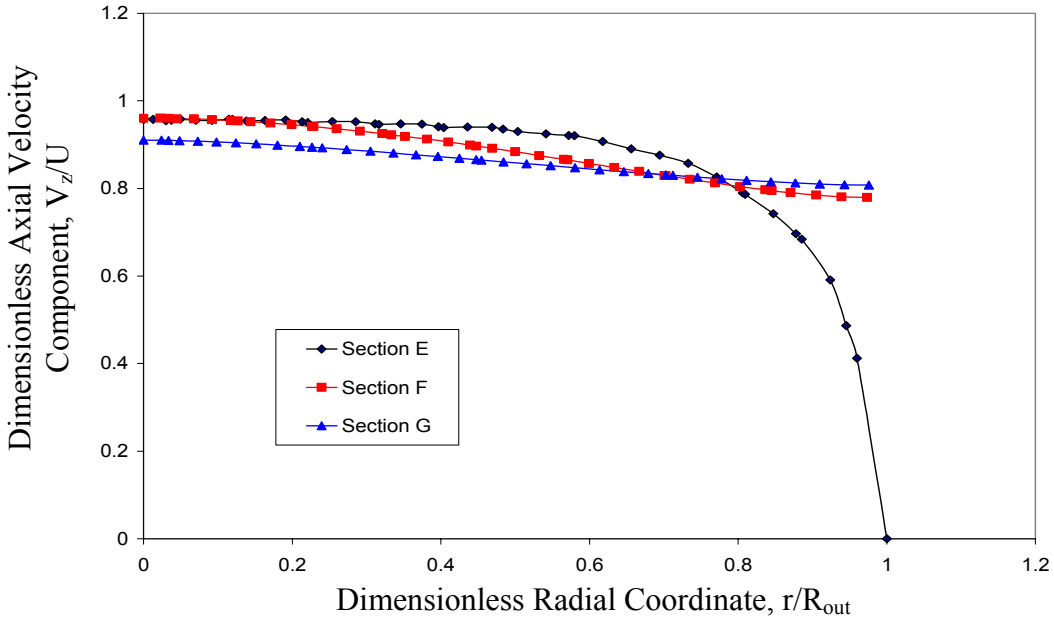

Figure 211: Dimensionless axial velocity component at various sections ($R_2 = 2.5 \times 10^{-4}$ m)

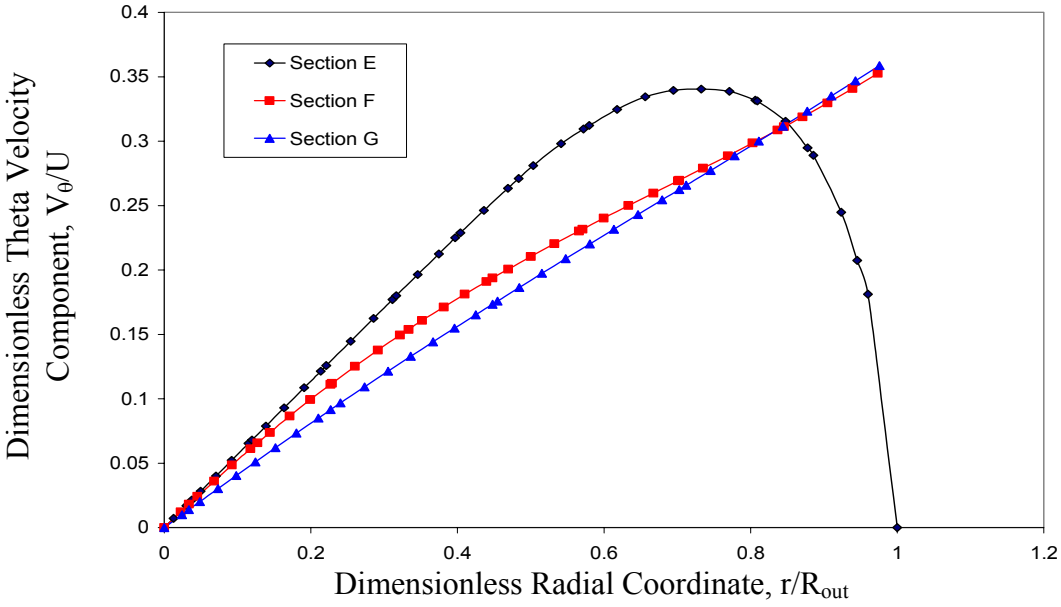

Figure 212: Dimensionless theta velocity component at various sections ($R_2 = 2.5 \times 10^{-4}$ m)

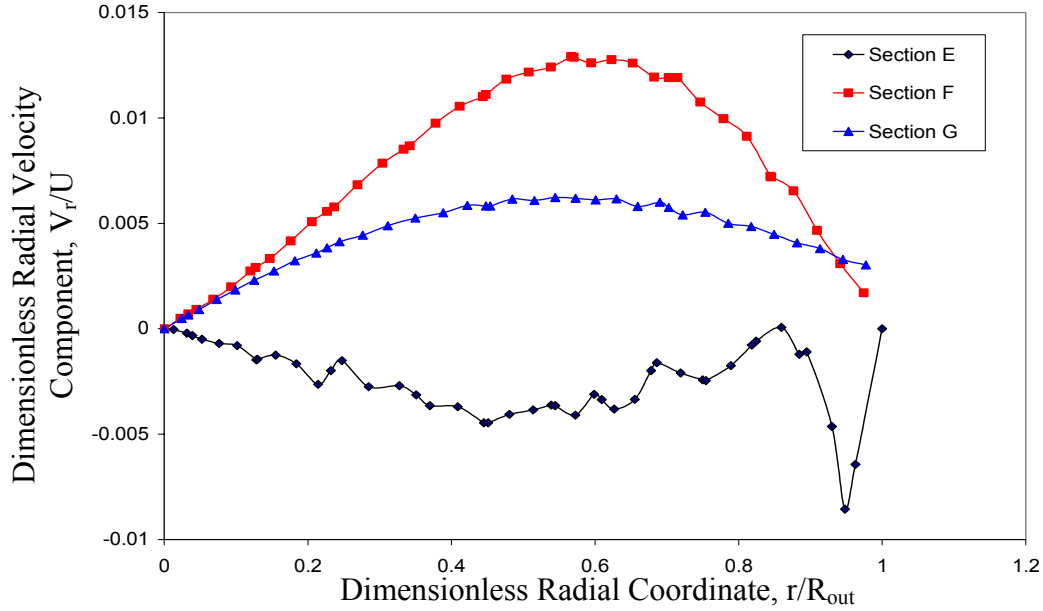

Figure 213: Dimensionless radial velocity at various sections ($R_2 = 4.0 \times 10^{-4}$ m)

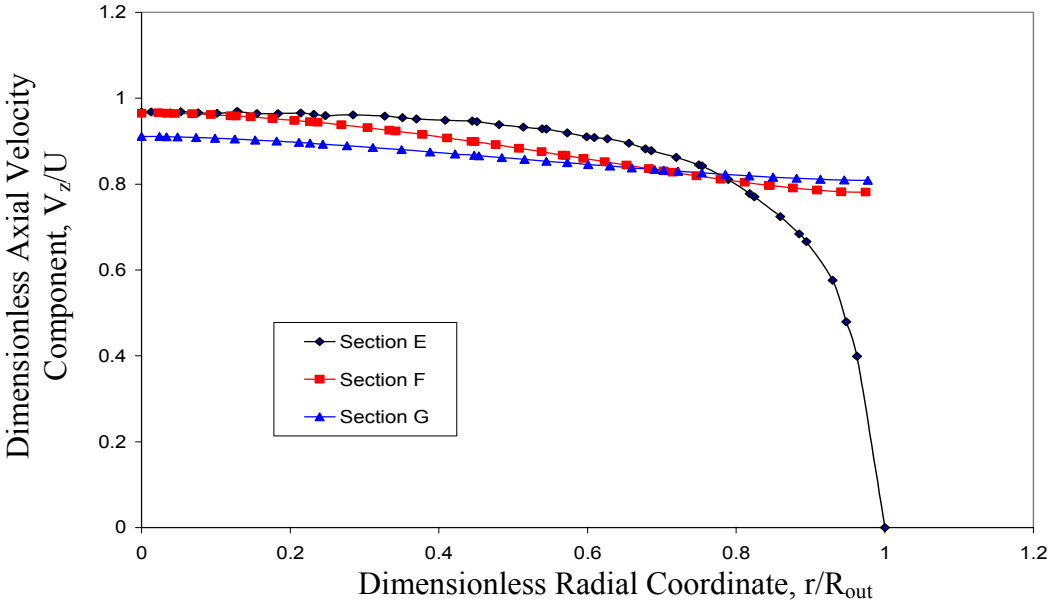

Figure 214: Dimensionless axial velocity component at various sections ($R_2 = 4.0 \times 10^{-4}$ m)

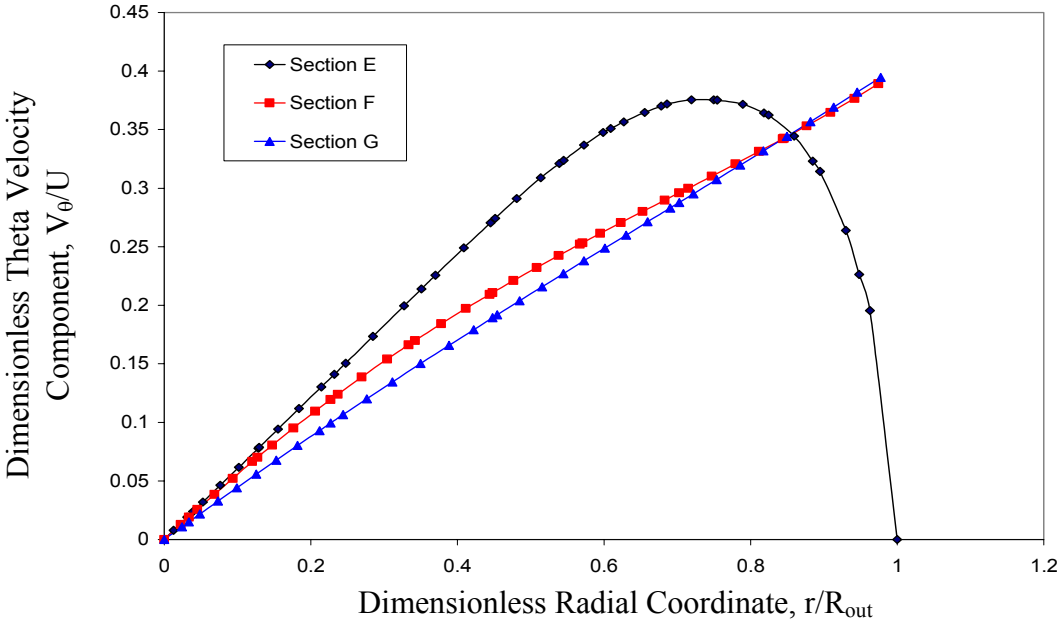

Figure 215: Dimensionless theta velocity component at various sections ($R_2 = 4.0 \times 10^{-4}$ m)

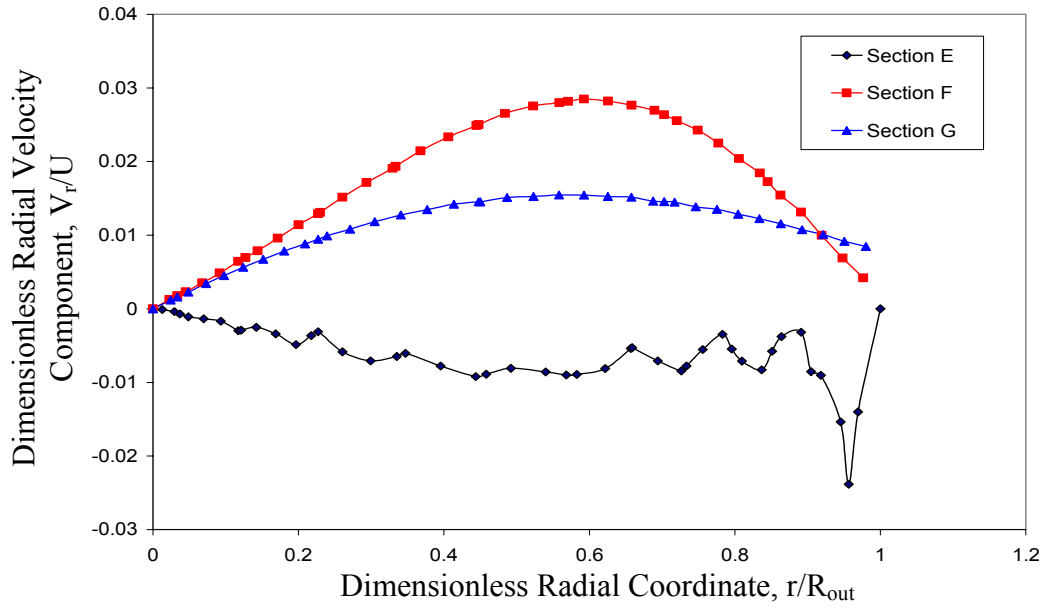

Figure 216: Dimensionless radial velocity component at various sections (R_2 = 5.5 x 10^{-4} m)

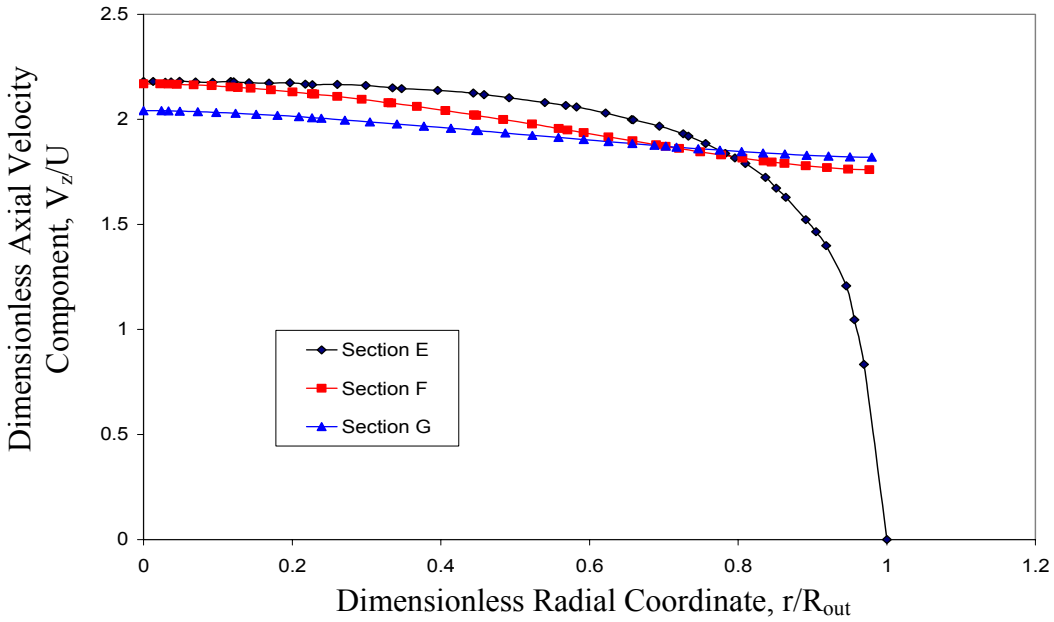

Figure 217: Dimensionless axial velocity component at various sections (R_2 = 5.5 x 10^{-4} m)

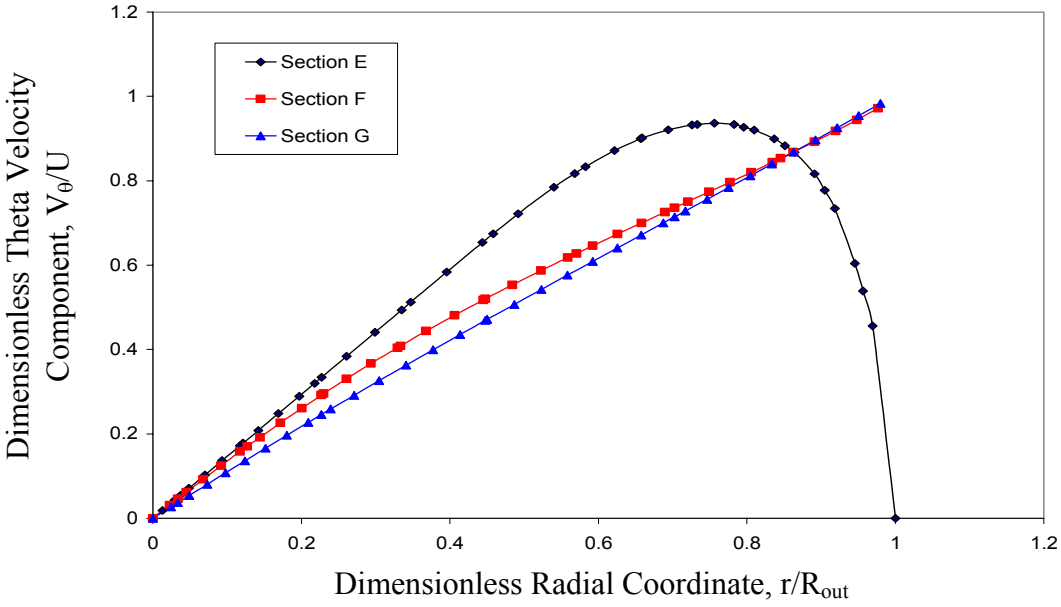

Figure 218: Theta velocity component at various sections (R_2 = 5.5 x 10^{-4} m)

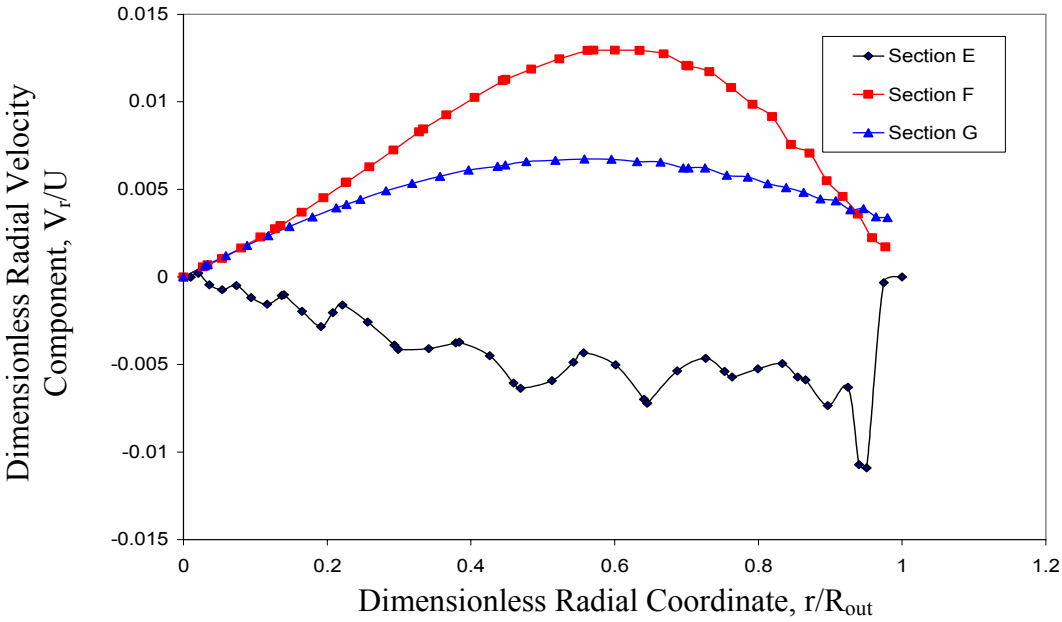

Figure 219: Dimensionless radial velocity component at various sections (R_2 = 7.2 x 10^{-4} m)

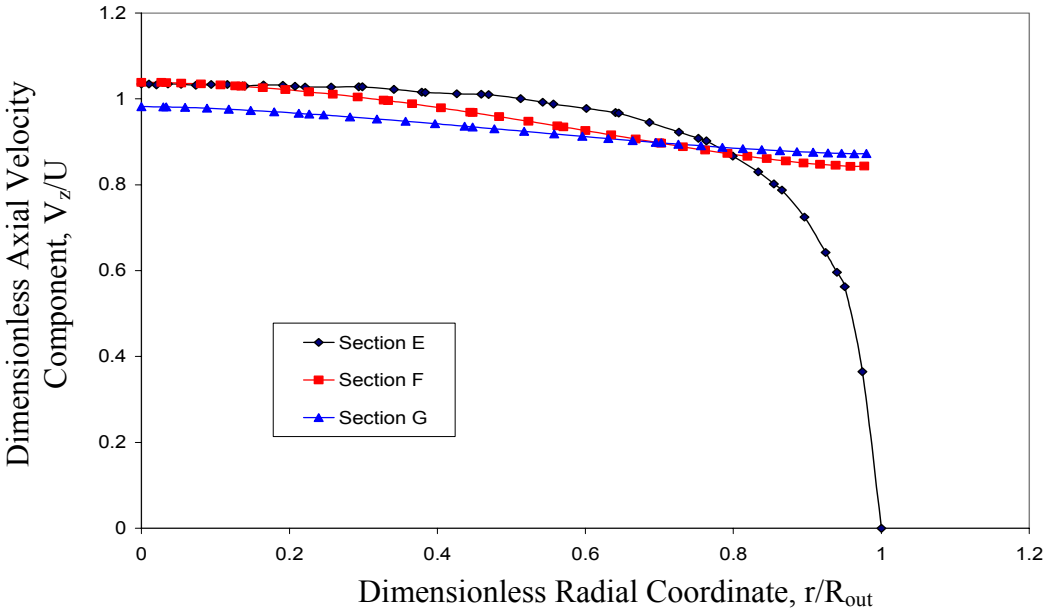

Figure 220: Dimensionless axial velocity component at various sections ($R_2 = 7.2 \times 10^{-4}$ m)

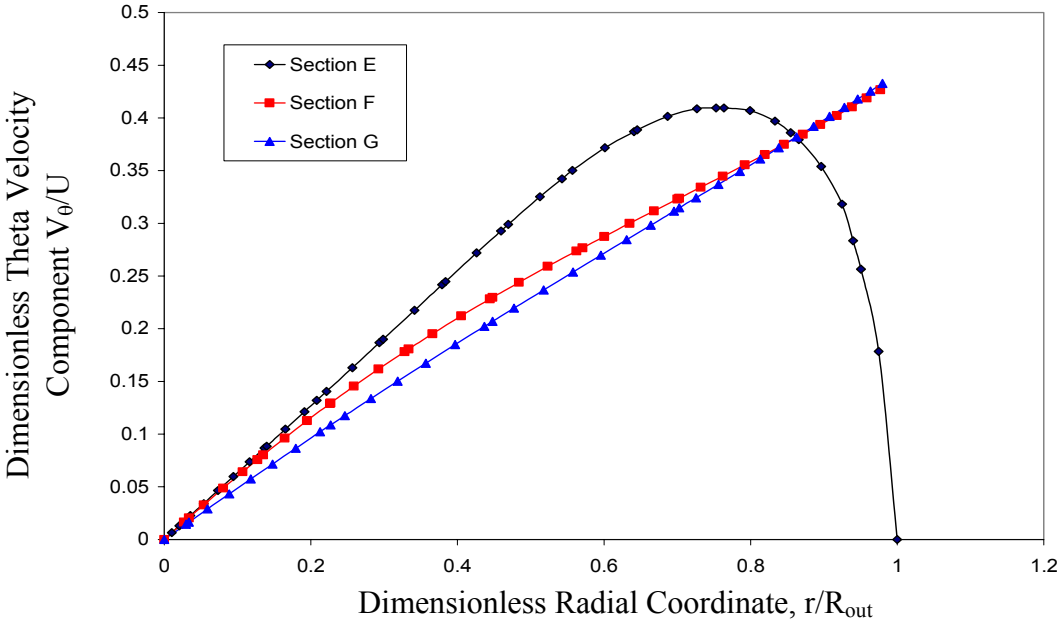

Figure 221: Dimensionless theta velocity component at various sections ($R_2 = 7.2 \times 10^{-4}$ m)

It is also important to know the average for each velocity component at each section throughout the nozzle. Tables 24-28 depict the average velocity components at each of the nozzle sections that were investigated. From these averages, the average component of momentum can be found at each section. It was observed that both the average velocity component and the average momentum component peaked at Section F, which is just after the fluid exited the nozzle. These tables confirm the previous graphs in the sense that the values calculated for the nozzle having R_2 equal to 5.50 x 10^{-4} m are almost twice as much as the values obtained for the other outer slot location geometries. This could explain why that particular nozzle geometry produced the greatest radial free surface height during this investigation.

Table 24: Average velocity and momentum components at each section (R_2=2.50 x 10^{-4} m, Re=5904)

Section	$V_{r,\,avg}$ [m/s]	$V_{z,\,avg}$ [m/s]	$V_{\theta,\,avg}$ [m/s]	$\dot{M}_{r,avg}$ [kg m/s^2]	$\dot{M}_{z,avg}$ [kg m/s^2]	$\dot{M}_{\theta,avg}$ [kg m/s^2]	$\dot{M}$ [kg m/s^2]
Inlet	0.000	0.433	0.433	0.000	3.21 x 10^{-4}	3.21 x 10^{-4}	4.54 x 10^{-4}
A	-0.125	0.270	1.430	-9.24 x 10^{-5}	2.00 x 10^{-4}	1.06 x 10^{-3}	1.08 x 10^{-3}
B	-0.216	0.524	0.662	-1.60 x 10^{-4}	3.88 x 10^{-4}	4.91 x 10^{-4}	6.46 x 10^{-4}
C	-1.024	6.677	2.361	-7.60 x 10^{-4}	4.95 x 10^{-3}	1.75x 10^{-3}	5.31 x 10^{-3}
D	-0.509	3.248	2.441	-3.78 x 10^{-5}	2.41 x 10^{-3}	1.81 x 10^{-3}	3.01 x 10^{-3}
E	-0.459	6.971	2.298	-3.41 x 10^{-5}	5.17 x 10^{-3}	1.70 x 10^{-3}	5.45 x 10^{-3}
F	0.267	7.645	2.263	1.98 x 10^{-5}	5.67 x 10^{-3}	1.68 x 10^{-3}	5.92 x 10^{-3}
G	0.398	7.559	2.193	2.95 x 10^{-5}	5.61 x 10^{-3}	1.63 x 10^{-3}	5.84 x 10^{-3}

Table 25: Average velocity and momentum components at each section (R_2=4.00 x 10^{-4} m, Re=5904)

Section	$V_{r,avg}$ [m/s]	$V_{z,avg}$ [m/s]	$V_{\theta,avg}$ [m/s]	$\dot{M}_{r,avg}$ [kg m/s^2]	$\dot{M}_{z,avg}$ [kg m/s^2]	$\dot{M}_{\theta,avg}$ [kg m/s^2]	$\dot{M}$ [kg m/s^2]
Inlet	0.000	0.680	0.680	0.00	5.04 x 10^{-4}	5.04 x 10^{-4}	7.13 x 10^{-4}
A	-0.122	0.314	1.822	-9.04 x 10^{-5}	2.33 x 10^{-4}	1.35 x 10^{-3}	1.37 x 10^{-3}
B	-0.163	0.518	1.761	-1.21 x 10^{-4}	3.84 x 10^{-4}	1.31 x 10^{-3}	1.37 x 10^{-3}
C	-1.014	6.753	2.677	-7.52 x 10^{-4}	5.01 x 10^{-3}	1.99 x 10^{-3}	5.44 x 10^{-3}
D	-0.994	7.093	2.723	-7.37 x 10^{-5}	5.26 x 10^{-3}	2.02 x 10^{-3}	5.64 x 10^{-3}
E	-0.259	7.136	2.650	-1.92 x 10^{-5}	5.29 x 10^{-3}	1.97 x 10^{-3}	5.64 x 10^{-3}
F	0.808	7.615	2.483	5.99 x 10^{-5}	5.65 x 10^{-3}	1.84 x 10^{-3}	5.94 x 10^{-3}
G	0.450	7.568	2.404	3.34 x 10^{-5}	5.62 x 10^{-3}	1.78 x 10^{-3}	5.89 x 10^{-3}

Table 26: Average velocity and momentum components at each section (R_2=5.50 x 10^{-4} m, Re=5904)

Section	$V_{r,avg}$ [m/s]	$V_{z,avg}$ [m/s]	$V_{\theta,avg}$ [m/s]	$\dot{M}_{r,avg}$ [kg m/s^2]	$\dot{M}_{z,avg}$ [kg m/s^2]	$\dot{M}_{\theta,avg}$ [kg m/s^2]	$\dot{M}$ [kg m/s^2]
Inlet	0.000	0.846	0.846	0.00	6.28 x 10^{-4}	6.28 x 10^{-4}	8.88 x 10^{-4}
A	-0.526	0.634	1.290	-3.90 x 10^{-4}	4.70 x 10^{-4}	9.57 x 10^{-4}	1.14 x 10^{-3}
B	-0.280	1.145	4.234	-2.07 x 10^{-4}	8.50x 10^{-4}	3.14 x 10^{-3}	3.26x 10^{-3}
C	-2.314	15.88	6.799	-1.72 x 10^{-3}	1.78 x 10^{-2}	5.04 x 10^{-3}	1.86 x 10^{-2}
D	-0.222	14.88	6.925	-1.65 x 10^{-4}	1.10 x 10^{-2}	5.14 x 10^{-3}	1.22 x 10^{-2}
E	-0.664	16.89	6.670	-4.93 x 10^{-5}	1.25 x 10^{-2}	4.95 x 10^{-3}	1.35 x 10^{-2}
F	0.182	17.14	6.178	1.35 x 10^{-4}	1.27 x 10^{-2}	4.58 x 10^{-3}	1.35 x 10^{-2}
G	0.115	17.02	5.990	8.50 x 10^{-5}	1.26 x 10^{-2}	4.44 x 10^{-3}	1.34 x 10^{-2}

Table 27: Average velocity and momentum components at each section (R_2=5.50 x 10^{-4} m, Re=7591)

Section	$V_{r,avg}$ [m/s]	$V_{z,avg}$ [m/s]	$V_{\theta,avg}$ [m/s]	$\dot{M}_{r,avg}$ [kg m/s^2]	$\dot{M}_{z,avg}$ [kg m/s^2]	$\dot{M}_{\theta,avg}$ [kg m/s^2]	$\dot{M}$ [kg m/s^2]
Inlet	0.000	1.088	1.088	0.00	8.07 x 10^{-4}	8.07 x 10^{-4}	1.14 x 10^{-3}
A	-0.688	0.814	4.082	-5.10 x 10^{-4}	6.04 x 10^{-4}	3.03 x 10^{-3}	3.13 x 10^{-3}
B	-0.351	1.524	5.104	-2.61 x 10^{-4}	1.13 x 10^{-3}	3.79 x 10^{-3}	3.96 x 10^{-3}
C	-2.965	20.41	8.847	-2.20 x 10^{-3}	1.51 x 10^{-2}	6.56 x 10^{-3}	1.67 x 10^{-2}
D	-0.282	16.38	9.023	-2.09 x 10^{-4}	1.22 x 10^{-2}	6.69 x 10^{-3}	1.39 x 10^{-2}
E	-0.885	16.62	8.694	-6.57 x 10^{-5}	1.23 x 10^{-2}	6.45 x 10^{-3}	1.39 x 10^{-2}
F	0.233	22.02	8.051	1.73 x 10^{-4}	1.63 x 10^{-2}	5.97 x 10^{-3}	1.74x 10^{-2}
G	0.150	21.86	7.805	1.11 x 10^{-4}	1.62 x 10^{-2}	5.79 x 10^{-3}	1.72 x 10^{-2}

Table 28: Average velocity and momentum components at each section (R_2=7.20 x 10^{-4} m, Re=5904)

Section	$V_{r,avg}$ [m/s]	$V_{z,avg}$ [m/s]	$V_{\theta,avg}$ [m/s]	$\dot{M}_{r,avg}$ [kg m/s^2]	$\dot{M}_{z,avg}$ [kg m/s^2]	$\dot{M}_{\theta,avg}$ [kg m/s^2]	$\dot{M}$ [kg m/s^2]
Inlet	0.000	0.568	0.568	0.00	4.21 x 10^{-4}	4.21 x 10^{-4}	5.96 x 10^{-4}
A	-0.217	0.250	1.953	-1.61 x 10^{-4}	1.86 x 10^{-4}	1.45 x 10^{-3}	1.47 x 10^{-3}
B	-0.170	0.563	1.892	-1.26 x 10^{-4}	4.17 x 10^{-4}	1.40 x 10^{-3}	1.47 x 10^{-3}
C	-1.185	7.748	2.939	-8.79 x 10^{-4}	5.75 x 10^{-3}	2.18 x 10^{-3}	6321 x 10^{-3}
D	-0.981	7.577	2.881	-7.28 x 10^{-5}	5.62 x 10^{-3}	2.14 x 10^{-3}	6.01 x 10^{-3}
E	-0.474	7.667	2.810	-3.52 x 10^{-5}	5.69 x 10^{-3}	2.08 x 10^{-3}	6.06 x 10^{-3}
F	0.811	8.208	2.719	6.02 x 10^{-5}	6.09 x 10^{-3}	2.02 x 10^{-3}	6.42 x 10^{-3}
G	0.488	8.111	2.638	3.62 x 10^{-5}	6.02 x 10^{-3}	1.96 x 10^{-3}	6.33 x 10^{-3}

Next, the pressure drop obtained from FIDAP for this scenario was compared to the calculated pressure drop according to Bernoulli's equation. It was known that the pressure drop obtained from FIDAP must be larger than the value calculated using Bernoulli's equation. Table 29 shows the pressure drop obtained from the program, as well as the calculated pressure drop. It was noted that, in fact, all of the trials obeyed the requirement by having the pressure drop from the program greater than the calculated pressure drop.

Table 29: Pressure drop comparison for various outer slot locations

Outer Slot Location R_2 [m]	Inlet Flow Rate Q [m^3/s]	FIDAP Pressure Drop [Pa]	Calculated Pressure Drop [Pa]
2.50×10^{-4}	4.416×10^{-7}	7.25×10^{4}	5.45×10^{4}
4.00×10^{-4}	4.416×10^{-7}	7.67×10^{4}	5.77×10^{4}
5.50×10^{-4}	4.416×10^{-7}	3.39×10^{5}	3.29×10^{5}
	5.678×10^{-7}	6.51×10^{5}	3.38×10^{5}
7.20×10^{-4}	4.416×10^{-7}	9.21×10^{4}	6.64×10^{4}

6

Conclusion

The conclusions gathered from the results of this investigation can be summarized as follows:

1. The larger nozzle produced a greater radial height of the free surface and a greater cone angle.
2. The radial height of the free surface increased as the Reynolds number increased.
3. The cone angle produced by the fluid exiting the nozzle became larger as the Reynolds number became larger.
4. The cone angle increased as the radial value of the outer inlet slot also increased.
5. Increasing the radial distance of the outer inlet slot resulted in an increase in free surface height for all of the fluids that were investigated. However, the last scenario where the outer inlet slot was position on the edge of the nozzle resulted in a lower free surface height than the previous position.
6. The pressure drop from the inlet of the nozzle to the outlet increased with an increase in the flow rate.
7. The pressure drop also increased as the radial distance of the outer inlet slot increased. However, the pressure drop decreased when the location of the outer inlet slot reached the edge of the nozzle.
8. Overall, all of the variations produced small changes in the free surface position.

References

Burmeister, L.C., *Convective Heat Transfer*, Wiley, New York, 1993.

Ciofalo, M., DiPiazza, I., Brucato, V., "Investigation of Cooling of Hot Walls by Liquid Water Sprays," *International Journal of Heat and Mass Transfer*, Vol. 42, No. 7, 1999, pp. 1157-1175.

Datta, A., and Som, S.K., "Numerical Prediction of Air Core Diameter Coefficient of Discharge and Spray Cone Angle of a Swirl Spray Pressure Nozzle," *International Journal of Heat and Fluid Flow*, Vol. 21, No. 4, 2000, pp. 412-419.

Dumouchel, C., Blook, M. I. G., Dimbrowski, N., Ingham, D. B., and Ledoux, M., "Viscous Flow in a Swirl Atomizer," *Chemical Engineering Science*, Vol. 48, No. 1, 1993, pp. 81-87.

Gavaises, M., Arcoumane, C., "Modeling of Sprays from High-Pressure Swirl Atomizers," *International Journal of Engine Research*, Vol. 2, No. 2, 2001, pp. 95-117.

Jeng, S. M., Jog, M. A., and Benjamin, M. A., "Computation and Experimental Study of Liquid Sheet Emanating from Simplex Fuel Nozzle," *AIAA Journal*, Vol. 36, No. 2, 1998, pp. 201-207.

Miller, P.C.H., and Ellis, M.C. Butler, "Effects of Formulation of Spray Nozzle Performance for Applications from Ground-Based Boom Sprayers," *Crop Protection*, Vol. 19, No. 8-10, 2000, pp. 609-615.

Rothe, P.H., and Block, J.A., "Aerodynamic Behavior of Liquid Sprays," *International Journal of Multiphase Flow*, Vol. 3, No. 3, 1977, pp. 263-272.

Sakman, A. T., Jog, M. A., Jeng, S. M., and Benjamin, M. A., "Parametric Study of Simplex Fuel Nozzle Internal Flow and Performance," *AIAA Journal*, Vol. 38, No. 7, 2000, pp. 1214-1218.

Som, S.K., and Biswas, G., "Dispersion of Spray from Swirl Nozzles," *Chemical Engineering and Processing*, Vol. 20, No. 4, 1986, pp. 191-200.

White, Frank M. *Fluid Mechanics: Fourth Edition*, Boston, McGraw-Hill, 1999.

Appendices

Appendix I: GAMBIT File for Large Nozzle

```
solver select "FIDAP"

undo begingroup
vertex create coordinates 0 0 0
undo endgroup
undo begingroup
vertex create coordinates 4.2 0 0
undo endgroup
undo begingroup
vertex create coordinates 4.2 0.3175 0
undo endgroup
undo begingroup
vertex create coordinates 3.0988 0.3175 0
undo endgroup
undo begingroup
vertex create coordinates 2.7178 0.3175 0
undo endgroup
undo begingroup
vertex create coordinates 0 1.88722 0
undo endgroup
undo begingroup
vertex create coordinates 0 1.68656 0
undo endgroup
undo begingroup
vertex create coordinates 0 0.10033 0
undo endgroup
undo begingroup
vertex create coordinates -1 2.4648 0
undo endgroup
undo begingroup
vertex create coordinates -1 0 0
undo endgroup

edge create straight "vertex.1" "vertex.2"
edge create straight "vertex.2" "vertex.3"
edge create straight "vertex.3" "vertex.4"
edge create straight "vertex.4" "vertex.5"
edge create straight "vertex.5" "vertex.6"
edge create straight "vertex.6" "vertex.7"
edge create straight "vertex.7" "vertex.8"
```

Appendix I: (Continued)

```
edge create straight "vertex.8" "vertex.1"
edge create straight "vertex.6" "vertex.9"
edge create straight "vertex.9" "vertex.10"
edge create straight "vertex.10" "vertex.1"

face create wireframe "edge.1" "edge.2" "edge.3" "edge.4" "edge.5" "edge.6" "edge.7"
"edge.8" real

face create wireframe "edge.9" "edge.10" "edge.11" "edge.8" "edge.7" "edge.6" real

undo begingroup
edge picklink "edge.1"
edge mesh "edge.1" successive ratio1 1 intervals 110
undo endgroup
undo begingroup
edge picklink "edge.2"
edge mesh "edge.2" successive ratio1 1 intervals 28
undo endgroup
undo begingroup
edge picklink "edge.3"
edge mesh "edge.3" successive ratio1 1 intervals 30
undo endgroup
undo begingroup
edge picklink "edge.4"
edge mesh "edge.4" successive ratio1 1 intervals 10
undo endgroup
undo begingroup
edge picklink "edge.5"
edge mesh "edge.5" successive ratio1 1 intervals 70
undo endgroup
undo begingroup
edge picklink "edge.6"
edge mesh "edge.6" successive ratio1 1 intervals 6
undo endgroup
undo begingroup
edge picklink "edge.7"
edge mesh "edge.7" successive ratio1 1 intervals 16
undo endgroup
undo begingroup
edge picklink "edge.8"
edge mesh "edge.8" successive ratio1 1 intervals 6
undo endgroup
```

Appendix I: (Continued)

```
undo begingroup
edge picklink "edge.9"
edge mesh "edge.9" successive ratio1 1 intervals 20
undo endgroup
undo begingroup
edge picklink "edge.10"
edge mesh "edge.10" successive ratio1 1 intervals 28
undo endgroup
undo begingroup
edge picklink "edge.11"
edge mesh "edge.11" successive ratio1 1 intervals 20
undo endgroup

face mesh "face.1" map size 1

face mesh "face.2" map size 1

physics create "symmetry" btype "PLOT" edge "edge.1"
physics create "outlet" btype "PLOT" edge "edge.2"
physics create "free" btype "SURFACE" edge "edge.3"
physics create "wall1" btype "PLOT" edge "edge.4"
physics create "wall2" btype "PLOT" edge "edge.5"
physics create "inlet1" btype "PLOT" edge "edge.6"
physics create "top" btype "PLOT" edge "edge.7"
physics create "inlet2" btype "PLOT" edge "edge.8"
physics create "wall3" btype "PLOT" edge "edge.9"
physics create "inlet" btype "PLOT" edge "edge.10"
physics create "symm" btype "PLOT" edge "edge.11"
physics create "fluid" ctype "FLUID" face "face.1" "face.2"

export fidap “large.FDNEUT”
```

Appendix II: FIJOUR File for Large Nozzle

```
FICONV( NEUT, INPU, RESU )
INPUTFILE( FILE = large.FDNEUT" )
OUTPUTFILE( FILE, DELE )
END(  )

FIPREP( )

PROBLEM( ADD, CYLI, INCO, TRANS, LAMI, NONL, NEWT, MOME, ISOT,
FREE, SING )
EXECUTION( ADD, NEWJ )

ENTITY( ADD, NAME = "fluid", FLUI, PROP = "fc77" )
ENTITY( ADD, NAME = "wall1", PLOT )
ENTITY( ADD, NAME = "wall2", PLOT )
ENTITY( ADD, NAME = "symmetry", PLOT )
ENTITY( ADD, NAME = "inlet1", PLOT )
ENTITY( ADD, NAME = "inlet2", PLOT )
ENTITY( ADD, NAME = "outlet", PLOT )
ENTITY( ADD, NAME = "top", PLOT )
ENTITY( ADD, NAME = "free", SURFACE, DEPTH = 0, SPINES, STRAIGHT )

SOLUTION( ADD, N.R. = 70, KINE = 25, VELC = 0.00001, RESC = 0.001, SURF =
0.0001 )
BODYFORCE( ADD, CONS, FZC = 981, FRC = 0, FTHETA = 0 )
DATAPRINT( ADD, CONT )
OPTIONS( ADD, UPWINDING )
UPWINDING( ADD, STREAMLINE )
RELAXATION( )
 0.65, 0.65, 0.65, 0, 0, 0.4

PRESSURE( ADD, MIXED = 1E-11, DISC )
DENSITY( ADD, SET = "fc77", CONS = 1.78 )
/Density for FC-72
/DENSITY(ADD, SET = “fc72”, CONS = 1.68)
VISCOSITY( ADD, SET = "fc77", CONS = 0.01424 )
/Viscosity for FC-72
/VISCOSITY( ADD, SET = “fc72”, CONS = 0.0064)
SURFACETENSION( ADD, SET = "fc77", CONS = 15 )
/Surface Tension for FC-72
/SURFACETENSION( ADD, SET = “fc72”, CONS = 10 )
```

Appendix II: (Continued)

TIMEINTEGRATION(ADD, BACK, NSTEPS = 2000, TSTART = 0, DT = 0.000001, VARI, NOFIXED = 10, WIND = 0.90)

/For an inlet flow rate of 1.262 x 10^{-6} m^3/s
ICNODE(ADD, URC, ENTI = "inlet1", CONS = -5.35)
ICNODE(ADD, UZC, ENTI = "inlet1", CONS = 5.35)
ICNODE(ADD, URC, ENTI = "inlet2", CONS = 0)
ICNODE(ADD, UZC, ENTI = "inlet2", CONS = 7.566)
BCNODE(ADD, URC, ENTI = "inlet1", CONS = -5.35)
BCNODE(ADD, UZC, ENTI = "inlet1", CONS = 5.35)
BCNODE(ADD, URC, ENTI = "inlet2", CONS = 0)
BCNODE(ADD, UZC, ENTI = "inlet2", CONS = 7.566)

/For an inlet flow rate of 2.524 x 10^{-6} m^3/s
/ICNODE(ADD, URC, ENTI = "inlet1", CONS = -10.7)
/ICNODE(ADD, UZC, ENTI = "inlet1", CONS = 10.7)
/ICNODE(ADD, URC, ENTI = "inlet2", CONS = 0)
/ICNODE(ADD, UZC, ENTI = "inlet2", CONS = 15.132)
/BCNODE(ADD, URC, ENTI = "inlet1", CONS = -10.7)
/BCNODE(ADD, UZC, ENTI = "inlet1", CONS = 10.7)
/BCNODE(ADD, URC, ENTI = "inlet2", CONS = 0)
/BCNODE(ADD, UZC, ENTI = "inlet2", CONS = 15.132)

/For an inlet flow rate of 3.785 x 10^{-6} m^3/s
/ICNODE(ADD, URC, ENTI = "inlet1", CONS = -16.05)
/ICNODE(ADD, UZC, ENTI = "inlet1", CONS = 16.05)
/ICNODE(ADD, URC, ENTI = "inlet2", CONS = 0)
/ICNODE(ADD, UZC, ENTI = "inlet2", CONS = 22.698)
/BCNODE(ADD, URC, ENTI = "inlet1", CONS = -16.05)
/BCNODE(ADD, UZC, ENTI = "inlet1", CONS = 16.05)
/BCNODE(ADD, URC, ENTI = "inlet2", CONS = 0)
/BCNODE(ADD, UZC, ENTI = "inlet2", CONS = 22.698)

/Boundary Conditions for all flow rates
BCNODE(ADD, VELO, ENTI = "wall1", CONS = 0, X, Y, Z)
BCNODE(ADD, VELO, ENTI = "wall2", CONS = 0, X, Y, Z)
BCNODE(ADD, URC, ENTI = "symmetry", CONS = 0)
BCNODE(ADD, URC, ENTI = "top", CONS = 0)
BCNODE(ADD, UZC, ENTI = "top", CONS = 0)
BCNODE(SURFACE, ZERO, NODE = 146)
BCNODE(SURFACE, ZERO, NODE = 213)
BCNODE(COORDINATE, NODE = 213)

BCNODE(COORDINATE, NODE = 170)

/Initial Conditions for the top plate for an inlet flow rate of 1.262 x 10^{-6} m^3/s
ICNODE(ADD, UTHETA, NODE = 10, CONS = 5.297)
ICNODE(ADD, UTHETA, NODE = 11, CONS = 4.968)
ICNODE(ADD, UTHETA, NODE = 12, CONS = 4.639)
ICNODE(ADD, UTHETA, NODE = 13, CONS = 4.309)
ICNODE(ADD, UTHETA, NODE = 14, CONS = 3.980)
ICNODE(ADD, UTHETA, NODE = 15, CONS = 3.651)
ICNODE(ADD, UTHETA, NODE = 16, CONS = 3.321)
ICNODE(ADD, UTHETA, NODE = 17, CONS = 2.992)
ICNODE(ADD, UTHETA, NODE = 18, CONS = 2.663)
ICNODE(ADD, UTHETA, NODE = 19, CONS = 2.333)
ICNODE(ADD, UTHETA, NODE = 20, CONS = 2.004)
ICNODE(ADD, UTHETA, NODE = 21, CONS = 1.675)
ICNODE(ADD, UTHETA, NODE = 22, CONS = 1.346)
ICNODE(ADD, UTHETA, NODE = 23, CONS = 1.016)
ICNODE(ADD, UTHETA, NODE = 24, CONS = 0.387)
ICNODE(ADD, UTHETA, NODE = 25, CONS = 0.358)

/Initial conditions for the top plate for an inlet flow rate of 2.524 x 10^{-6} m^3/s
/ICNODE(ADD, UTHE, NODE = 10, CONS = 10.594)
/ICNODE(ADD, UTHE, NODE = 11, CONS = 9.936)
/ICNODE(ADD, UTHE, NODE = 12, CONS = 9.277)
/ICNODE(ADD, UTHE, NODE = 13, CONS = 8.618)
/ICNODE(ADD, UTHE, NODE = 14, CONS = 7.96)
/ICNODE(ADD, UTHE, NODE = 15, CONS = 7.301)
/ICNODE(ADD, UTHE, NODE = 16, CONS = 6.643)
/ICNODE(ADD, UTHE, NODE = 17, CONS = 5.984)
/ICNODE(ADD, UTHE, NODE = 18, CONS = 5.326)
/ICNODE(ADD, UTHE, NODE = 19, CONS = 4.667)
/ICNODE(ADD, UTHE, NODE = 20, CONS = 4.008)
/ICNODE(ADD, UTHE, NODE = 21, CONS = 3.35)
/ICNODE(ADD, UTHE, NODE = 22, CONS = 2.691)
/ICNODE(ADD, UTHE, NODE = 23, CONS = 2.033)
/ICNODE(ADD, UTHE, NODE = 24, CONS = 1.374)
/ICNODE(ADD, UTHE, NODE = 25, CONS = 0.715)

/Initial conditions for the top plate for an inlet flow rate of 3.785 x 10^{-6} m^3/s
/ICNODE(ADD, UTHE, NODE = 10, CONS = 15.893)
/ICNODE(ADD, UTHE, NODE = 11, CONS = 14.905)
/ICNODE(ADD, UTHE, NODE = 12, CONS = 13.917)

Appendix II: (Continued)

/ICNODE(ADD, UTHE, NODE = 13, CONS = 12.929)
/ICNODE(ADD, UTHE, NODE = 14, CONS = 11.941)
/ICNODE(ADD, UTHE, NODE = 15, CONS = 10.953)
/ICNODE(ADD, UTHE, NODE = 16, CONS = 9.965)
/ICNODE(ADD, UTHE, NODE = 17, CONS = 8.977)
/ICNODE(ADD, UTHE, NODE = 18, CONS = 7.989)
/ICNODE(ADD, UTHE, NODE = 19, CONS = 7.001)
/ICNODE(ADD, UTHE, NODE = 20, CONS = 6.013)
/ICNODE(ADD, UTHE, NODE = 21, CONS = 5.025)
/ICNODE(ADD, UTHE, NODE = 22, CONS = 4.037)
/ICNODE(ADD, UTHE, NODE = 23, CONS = 3.049)
/ICNODE(ADD, UTHE, NODE = 24, CONS = 2.061)
/ICNODE(ADD, UTHE, NODE = 25, CONS = 1.073)

/Boundary conditions for the top plate for an inlet flow rate 1.262 x 10^{-6} m^3/s
BCNODE(ADD, UTHETA, NODE = 10, CONS = 5.297)
BCNODE(ADD, UTHETA, NODE = 11, CONS = 4.968)
BCNODE(ADD, UTHETA, NODE = 12, CONS = 4.639)
BCNODE(ADD, UTHETA, NODE = 13, CONS = 4.309)
BCNODE(ADD, UTHETA, NODE = 14, CONS = 3.980)
BCNODE(ADD, UTHETA, NODE = 15, CONS = 3.651)
BCNODE(ADD, UTHETA, NODE = 16, CONS = 3.321)
BCNODE(ADD, UTHETA, NODE = 17, CONS = 2.992)
BCNODE(ADD, UTHETA, NODE = 18, CONS = 2.663)
BCNODE(ADD, UTHETA, NODE = 19, CONS = 2.333)
BCNODE(ADD, UTHETA, NODE = 20, CONS = 2.004)
BCNODE(ADD, UTHETA, NODE = 21, CONS = 1.675)
BCNODE(ADD, UTHETA, NODE = 22, CONS = 1.346)
BCNODE(ADD, UTHETA, NODE = 23, CONS = 1.016)
BCNODE(ADD, UTHETA, NODE = 24, CONS = 0.387)
BCNODE(ADD, UTHETA, NODE = 25, CONS = 0.358)

/Boundary conditions for the top plate for an inlet flow rate of 2.524 x 10^{-6} m^3/s
/BCNODE(ADD, UTHE, NODE = 10, CONS = 10.594)
/BCNODE(ADD, UTHE, NODE = 11, CONS = 9.936)
/BCNODE(ADD, UTHE, NODE = 12, CONS = 9.277)
/BCNODE(ADD, UTHE, NODE = 13, CONS = 8.618)
/BCNODE(ADD, UTHE, NODE = 14, CONS = 7.96)
/BCNODE(ADD, UTHE, NODE = 15, CONS = 7.301)
/BCNODE(ADD, UTHE, NODE = 16, CONS = 6.643)
/BCNODE(ADD, UTHE, NODE = 17, CONS = 5.984)
/BCNODE(ADD, UTHE, NODE = 18, CONS = 5.326)

Appendix II: (Continued)

/BCNODE(ADD, UTHE, NODE = 19, CONS = 4.667)
/BCNODE(ADD, UTHE, NODE = 20, CONS = 4.008)
/BCNODE(ADD, UTHE, NODE = 21, CONS = 3.35)
/BCNODE(ADD, UTHE, NODE = 22, CONS = 2.691)
/BCNODE(ADD, UTHE, NODE = 23, CONS = 2.033)
/BCNODE(ADD, UTHE, NODE = 24, CONS = 1.374)
/BCNODE(ADD, UTHE, NODE = 25, CONS = 0.715)

/Boundary conditions for the top plate for an inlet flow rate of 3.785×10^{-6} m^3/s
/BCNODE(ADD, UTHE, NODE = 10, CONS = 15.893)
/BCNODE(ADD, UTHE, NODE = 11, CONS = 14.905)
/BCNODE(ADD, UTHE, NODE = 12, CONS = 13.917)
/BCNODE(ADD, UTHE, NODE = 13, CONS = 12.929)
/BCNODE(ADD, UTHE, NODE = 14, CONS = 11.941)
/BCNODE(ADD, UTHE, NODE = 15, CONS = 10.953)
/BCNODE(ADD, UTHE, NODE = 16, CONS = 9.965)
/BCNODE(ADD, UTHE, NODE = 17, CONS = 8.977)
/BCNODE(ADD, UTHE, NODE = 18, CONS = 7.989)
/BCNODE(ADD, UTHE, NODE = 19, CONS = 7.001)
/BCNODE(ADD, UTHE, NODE = 20, CONS = 6.013)
/BCNODE(ADD, UTHE, NODE = 21, CONS = 5.025)
/BCNODE(ADD, UTHE, NODE = 22, CONS = 4.037)
/BCNODE(ADD, UTHE, NODE = 23, CONS = 3.049)
/BCNODE(ADD, UTHE, NODE = 24, CONS = 2.061)
/BCNODE(ADD, UTHE, NODE = 25, CONS = 1.073)

END( )

Appendix III: GAMBIT File for Small Nozzle

```
solver select "FIDAP"

undo begingroup
vertex create coordinates 0 0 0
undo endgroup
undo begingroup
vertex create coordinates 0.17 0 0
undo endgroup
undo begingroup
vertex create coordinates 0.17 0.0125 0
undo endgroup
undo begingroup
vertex create coordinates 0.122 0.0125 0
undo endgroup
undo begingroup
vertex create coordinates 0.107 0.0125 0
undo endgroup
undo begingroup
vertex create coordinates 0 0.0743 0
undo endgroup
undo begingroup
vertex create coordinates 0 0.0543 0
undo endgroup
undo begingroup
vertex create coordinates 0 0.01 0
undo endgroup

edge create straight "vertex.1" "vertex.2"
edge create straight "vertex.2" "vertex.3"
edge create straight "vertex.3" "vertex.4"
edge create straight "vertex.4" "vertex.5"
edge create straight "vertex.5" "vertex.6"
edge create straight "vertex.6" "vertex.7"
edge create straight "vertex.7" "vertex.8"
edge create straight "vertex.8" "vertex.1"

face create wireframe "edge.1" "edge.2" "edge.3" "edge.4" "edge.5" "edge.6" "edge.7"
"edge.8" real
```

Appendix III: (Continued)

```
undo begingroup
edge picklink "edge.1"
edge mesh "edge.1" successive ratio1 1 intervals 172
undo endgroup
undo begingroup
edge picklink "edge.2"
edge mesh "edge.2" successive ratio1 1 ratio2 1.1 intervals 32
undo endgroup
undo begingroup
edge picklink "edge.3"
edge mesh "edge.3" successive ratio1 1 intervals 36
undo endgroup
undo begingroup
edge picklink "edge.4"
edge mesh "edge.4" successive ratio1 1 intervals 24
undo endgroup
undo begingroup
edge picklink "edge.5"
edge mesh "edge.5" successive ratio1 1 intervals 112
undo endgroup
undo begingroup
edge picklink "edge.6"
edge mesh "edge.6" successive ratio1 1 intervals 8
undo endgroup
undo begingroup
edge picklink "edge.7"
edge mesh "edge.7" successive ratio1 1 intervals 16
undo endgroup
undo begingroup
edge picklink "edge.8"
edge mesh "edge.8" successive ratio1 1 intervals 8
undo endgroup
/Mesh the face
face mesh "face.1" map size 1

physics create "symmetry" btype "PLOT" edge "edge.1"
physics create "outlet" btype "PLOT" edge "edge.2"
physics create "free" btype "SURFACE" edge "edge.3"
physics create "wall1" btype "PLOT" edge "edge.4"
physics create "wall2" btype "PLOT" edge "edge.5"
physics create "inlet1" btype "PLOT" edge "edge.6"
physics create "top" btype "PLOT" edge "edge.7"
```

physics create "inlet2" btype "PLOT" edge "edge.8"
physics create "fluid" ctype "FLUID" face "face.1"

export fidap “small.FDNEUT”

Appendix IV: FIJOUR File for Small Nozzle (1.262×10^{-7} m^3/s and 2.524×10^{-7} m^3/s)

```
FICONV( NEUT, INPU, RESU )
INPUTFILE( FILE = small.FDNEUT" )
OUTPUTFILE( FILE, DELE )
END(  )

FIPREP( )

PROBLEM( ADD, CYLI, INCO, TRANS, LAMI, NONL, NEWT, MOME, ISOT,
FREE, SING )
EXECUTION( ADD, NEWJ )

ENTITY( ADD, NAME = "fluid", FLUI, PROP = "fc77" )
ENTITY( ADD, NAME = "wall1", PLOT )
ENTITY( ADD, NAME = "wall2", PLOT )
ENTITY( ADD, NAME = "symmetry", PLOT )
ENTITY( ADD, NAME = "inlet1", PLOT )
ENTITY( ADD, NAME = "inlet2", PLOT )
ENTITY( ADD, NAME = "outlet", PLOT )
ENTITY( ADD, NAME = "top", PLOT )
ENTITY( ADD, NAME = "free", SURFACE, DEPTH = 0, SPINES, STRAIGHT )

SOLUTION( ADD, N.R. = 70, KINE = 25, VELC = 0.0001, RESC = 0.01, SURF =
0.001 )
BODYFORCE( ADD, CONS, FZC = 981, FRC = 0, FTHETA = 0 )
DATAPRINT( ADD, CONT )
OPTIONS( ADD, UPWINDING )
UPWINDING( ADD, STREAMLINE )
RELAXATION( )
 0.6, 0.6, 0.6, 0, 0, 0.1

PRESSURE( ADD, MIXED = 1E-18, DISC )
DENSITY( ADD, SET = "fc77", CONS = 1.78 )
VISCOSITY( ADD, SET = "fc77", CONS = 0.01424 )
SURFACETENSION( ADD, SET = "fc77", CONS = 15 )

POSTPROCESS( ADD, NBLOCK = 2 )
 1 401 400
 402 800 1
```

```
PRINTOUT( ADD, NBLOCK = 2 )
 1 401 400
 402 800 1

TIMEINTEGRATION( ADD, BACK, NSTEPS = 800, TSTART = 0, DT = 0.0000001,
VARI, NOFIXED = 10, WIND = 0.90 )

/Initial conditions for an inlet flow rate of 1.262 x 10-7 m3/s
ICNODE( ADD, URC, ENTI = "inlet1", CONS = -17.362 )
ICNODE( ADD, UZC, ENTI = "inlet1", CONS = 17.362 )
ICNODE( ADD, URC, ENTI = "inlet2", CONS = 0 )
ICNODE( ADD, UZC, ENTI = "inlet2", CONS = 24.553 )
ICNODE( ADD, UTHETA, NODE = 10, CONS = 12.688 )
ICNODE( ADD, UTHETA, NODE = 11, CONS = 12.041 )
ICNODE( ADD, UTHETA, NODE = 12, CONS = 11.394 )
ICNODE( ADD, UTHETA, NODE = 13, CONS = 10.747 )
ICNODE( ADD, UTHETA, NODE = 14, CONS = 10.100 )
ICNODE( ADD, UTHETA, NODE = 15, CONS = 9.453 )
ICNODE( ADD, UTHETA, NODE = 16, CONS = 8.806 )
ICNODE( ADD, UTHETA, NODE = 17, CONS = 8.159 )
ICNODE( ADD, UTHETA, NODE = 18, CONS = 7.512 )
ICNODE( ADD, UTHETA, NODE = 19, CONS = 6.866 )
ICNODE( ADD, UTHETA, NODE = 20, CONS = 6.219 )
ICNODE( ADD, UTHETA, NODE = 21, CONS = 5.572 )
ICNODE( ADD, UTHETA, NODE = 22, CONS = 4.915 )
ICNODE( ADD, UTHETA, NODE = 23, CONS = 4.278 )
ICNODE( ADD, UTHETA, NODE = 24, CONS = 3.631 )
ICNODE( ADD, UTHETA, NODE = 25, CONS = 2.984 )

/Initial conditions for an inlet flow rate of 2.524 x 10-7 m3/s
/ICNODE( ADD, URC, ENTI = "inlet1", CONS = -34.723 )
/ICNODE( ADD, UZC, ENTI = "inlet1", CONS = 34.723 )
/ICNODE( ADD, URC, ENTI = "inlet2", CONS = 0 )
/ICNODE( ADD, UZC, ENTI = "inlet2", CONS = 49.106 )
/ICNODE( ADD, UTHE, NODE = 10, CONS = 25.377 )
/ICNODE( ADD, UTHE, NODE = 11, CONS = 24.083 )
/ICNODE( ADD, UTHE, NODE = 12, CONS = 22.789 )
/ICNODE( ADD, UTHE, NODE = 13, CONS = 21.495 )
/ICNODE( ADD, UTHE, NODE = 14, CONS = 20.201 )
/ICNODE( ADD, UTHE, NODE = 15, CONS = 18.907 )
/ICNODE( ADD, UTHE, NODE = 16, CONS = 17.613 )
/ICNODE( ADD, UTHE, NODE = 17, CONS = 16.319 )
```

Appendix IV: (Continued)

```
/ICNODE( ADD, UTHE, NODE = 18, CONS = 15.025 )
/ICNODE( ADD, UTHE, NODE = 19, CONS = 13.731 )
/ICNODE( ADD, UTHE, NODE = 20, CONS = 12.437 )
/ICNODE( ADD, UTHE, NODE = 21, CONS = 11.143 )
/ICNODE( ADD, UTHE, NODE = 22, CONS = 9.849 )
/ICNODE( ADD, UTHE, NODE = 23, CONS = 8.555 )
/ICNODE( ADD, UTHE, NODE = 24, CONS = 7.261 )
/ICNODE( ADD, UTHE, NODE = 25, CONS = 5.967 )

/Boundary conditions for an inlet flow rate of 1.262 x 10^-7 m^3/s
BCNODE( ADD, URC, ENTI = "inlet1", CONS = -17.362 )
BCNODE( ADD, UZC, ENTI = "inlet1", CONS = 17.362 )
BCNODE( ADD, URC, ENTI = "inlet2", CONS = 0 )
BCNODE( ADD, UZC, ENTI = "inlet2", CONS = 24.553 )
BCNODE( ADD, VELO, ENTI = "wall1", CONS = 0, X, Y, Z )
BCNODE( ADD, VELO, ENTI = "wall2", CONS = 0, X, Y, Z )
BCNODE( ADD, URC, ENTI = "symmetry", CONS = 0 )
BCNODE( ADD, URC, ENTI = "top", CONS = 0 )
BCNODE( ADD, UZC, ENTI = "top", CONS = 0 )
BCNODE( SURFACE, ZERO, NODE = 146 )
BCNODE( SURFACE, ZERO, NODE = 205 )
BCNODE( COORDINATE, NODE = 205 )
BCNODE( COORDINATE, NODE = 170 )
BCNODE( ADD, UTHETA, NODE = 10, CONS = 12.688 )
BCNODE( ADD, UTHETA, NODE = 11, CONS = 12.041 )
BCNODE( ADD, UTHETA, NODE = 12, CONS = 11.394 )
BCNODE( ADD, UTHETA, NODE = 13, CONS = 10.747 )
BCNODE( ADD, UTHETA, NODE = 14, CONS = 10.100 )
BCNODE( ADD, UTHETA, NODE = 15, CONS = 9.453 )
BCNODE( ADD, UTHETA, NODE = 16, CONS = 8.806 )
BCNODE( ADD, UTHETA, NODE = 17, CONS = 8.159 )
BCNODE( ADD, UTHETA, NODE = 18, CONS = 7.512 )
BCNODE( ADD, UTHETA, NODE = 19, CONS = 6.866 )
BCNODE( ADD, UTHETA, NODE = 20, CONS = 6.219 )
BCNODE( ADD, UTHETA, NODE = 21, CONS = 5.572 )
BCNODE( ADD, UTHETA, NODE = 22, CONS = 4.915 )
BCNODE( ADD, UTHETA, NODE = 23, CONS = 4.278 )
BCNODE( ADD, UTHETA, NODE = 24, CONS = 3.631 )
BCNODE( ADD, UTHETA, NODE = 25, CONS = 2.984 )

/Boundary conditions for an inlet flow rate of 2.524 x 10^-7 m^3/s
/BCNODE( ADD, URC, ENTI = "inlet1", CONS = -34.723 )
```

Appendix IV: (Continued)

```
/BCNODE( ADD, UZC, ENTI = "inlet1", CONS = 34.723 )
/BCNODE( ADD, URC, ENTI = "inlet2", CONS = 0 )
/BCNODE( ADD, UZC, ENTI = "inlet2", CONS = 49.106 )
/BCNODE( ADD, VELO, ENTI = "wall1", CONS = 0, X, Y, Z )
/BCNODE( ADD, VELO, ENTI = "wall2", CONS = 0, X, Y, Z )
/BCNODE( ADD, URC, ENTI = "symmetry", CONS = 0 )
/BCNODE( ADD, URC, ENTI = "top", CONS = 0 )
/BCNODE( ADD, UZC, ENTI = "top", CONS = 0 )
/BCNODE( SURF, ZERO, NODE = 146 )
/BCNODE( SURF, ZERO, NODE = 205 )
/BCNODE( COOR, NODE = 205 )
/BCNODE( COOR, NODE = 170 )
/BCNODE( ADD, UTHE, NODE = 10, CONS = 25.377 )
/BCNODE( ADD, UTHE, NODE = 11, CONS = 24.083 )
/BCNODE( ADD, UTHE, NODE = 12, CONS = 22.789 )
/BCNODE( ADD, UTHE, NODE = 13, CONS = 21.495 )
/BCNODE( ADD, UTHE, NODE = 40, CONS = 20.201 )
/BCNODE( ADD, UTHE, NODE = 15, CONS = 18.907 )
/BCNODE( ADD, UTHE, NODE = 16, CONS = 17.613 )
/BCNODE( ADD, UTHE, NODE = 17, CONS = 16.319 )
/BCNODE( ADD, UTHE, NODE = 18, CONS = 15.025 )
/BCNODE( ADD, UTHE, NODE = 19, CONS = 13.731 )
/BCNODE( ADD, UTHE, NODE = 20, CONS = 12.437 )
/BCNODE( ADD, UTHE, NODE = 21, CONS = 11.143 )
/BCNODE( ADD, UTHE, NODE = 22, CONS = 9.849 )
/BCNODE( ADD, UTHE, NODE = 23, CONS = 8.555 )
/BCNODE( ADD, UTHE, NODE = 24, CONS = 7.261 )
/BCNODE( ADD, UTHE, NODE = 25, CONS = 5.967 )

END( )
```

Appendix V: FIJOUR File for Small Nozzle (4.416 x 10^{-7} m^3/s and 5.678 x 10^{-7} m^3/s)

```
FICONV( NEUT, INPU, RESU )
INPUTFILE( FILE = small.FDNEUT" )
OUTPUTFILE( FILE, DELE )
END(  )

FIPREP(  )

PROBLEM( ADD, CYLI, INCO, TRAN, TURB, NONL, NEWT, MOME, ISOT, FREE,
SING )
EXECUTION( ADD, NEWJ )

ENTITY( ADD, NAME = "fluid", FLUI, PROP = "fc77" )
ENTITY( ADD, NAME = "wall1", WALL )
ENTITY( ADD, NAME = "wall2", WALL )
ENTITY( ADD, NAME = "symmetry", PLOT )
ENTITY( ADD, NAME = "inlet1", PLOT )
ENTITY( ADD, NAME = "inlet2", PLOT )
ENTITY( ADD, NAME = "outlet", PLOT )
ENTITY( ADD, NAME = "top", PLOT )
ENTITY( ADD, NAME = "free", SURF, DEPT = 0, SPIN, STRA )
SOLUTION( ADD, N.R. = 70, KINE = 25, VELC = 0.0001, RESC = 0.01, SURF =
0.001 )
BODYFORCE( ADD, CONS, FZC = 981, FRC = 0, FTHE = 0 )
DATAPRINT( ADD, CONT )
OPTIONS( ADD, UPWI )
UPWINDING( ADD, STRE )
RELAXATION(  )
  0.6,   0.6,   0.6,     0,     0,   0.1

PRESSURE( ADD, MIXE = 1e-16, DISC )
DENSITY( ADD, SET = "fc77", CONS = 1.78 )
/Density for FC-72
/DENSITY( ADD, SET = “fc72”, CONS = 1.68 )
VISCOSITY( ADD, SET = "fc77", MIXL, CONS = 0.01424 )
/Viscosity for FC-72
/VISCOSITY( ADD, SET = “fc72”, CONS = 0.0064 )
SURFACETENSION( ADD, SET = "fc77", CONS = 15 )
/Surface Tension for FC-72
/SURFACETENSION( ADD, SET = “fc72”, CONS = 10 )
```

Appendix V: (Continued)

```
POSTPROCESS( ADD, NBLO = 2 )
   1,  301,  300
 302,  600,    1
PRINTOUT( NBLO = 2 )
   1,  301,  300
 302,  600,    1

TIMEINTEGRATION( ADD, BACK, NSTE = 600, TSTA = 0, DT = 1e-07, VARI,
NOFI = 10, WIND = 0.9 )
RENUMBER( ADD, PROF )
EDDYVISCOSITY( ADD, SPEZ )

/Initial conditions for 4.416 x 10^-7 m^3/s
ICNODE( ADD, URC, ENTI = "inlet1", CONS = -60.765 )
ICNODE( ADD, UZC, ENTI = "inlet1", CONS = 60.765 )
ICNODE( ADD, URC, ENTI = "inlet2", CONS = 0 )
ICNODE( ADD, UZC, ENTI = "inlet2", CONS = 85.935 )
ICNODE( ADD, UTHE, NODE = 10, CONS = 44.409 )
ICNODE( ADD, UTHE, NODE = 11, CONS = 42.145 )
ICNODE( ADD, UTHE, NODE = 12, CONS = 39.88 )
ICNODE( ADD, UTHE, NODE = 13, CONS = 37.616 )
ICNODE( ADD, UTHE, NODE = 14, CONS = 35.351 )
ICNODE( ADD, UTHE, NODE = 15, CONS = 33.087 )
ICNODE( ADD, UTHE, NODE = 16, CONS = 30.822 )
ICNODE( ADD, UTHE, NODE = 17, CONS = 28.558 )
ICNODE( ADD, UTHE, NODE = 18, CONS = 26.296 )
ICNODE( ADD, UTHE, NODE = 19, CONS = 24.029 )
ICNODE( ADD, UTHE, NODE = 20, CONS = 21.765 )
ICNODE( ADD, UTHE, NODE = 21, CONS = 19.5 )
ICNODE( ADD, UTHE, NODE = 22, CONS = 17.236 )
ICNODE( ADD, UTHE, NODE = 23, CONS = 14.972 )
ICNODE( ADD, UTHE, NODE = 24, CONS = 12.707 )
ICNODE( ADD, UTHE, NODE = 25, CONS = 10.443 )

/Initial conditions for an inlet flow rate of 5.678 x 10^-7 m^3/s
/ICNODE( ADD, URC, ENTI = "inlet1", CONS = -78.127 )
/ICNODE( ADD, UZC, ENTI = "inlet1", CONS = 78.127 )
/ICNODE( ADD, URC, ENTI = "inlet2", CONS = 0 )
/ICNODE( ADD, UZC, ENTI = "inlet2", CONS = 110.488 )
/ICNODE( ADD, UTHE, NODE = 10, CONS = 57.096 )
/ICNODE( ADD, UTHE, NODE = 11, CONS = 54.185 )
/ICNODE( ADD, UTHE, NODE = 12, CONS = 51.274 )
```

```
/ICNODE( ADD, UTHE, NODE = 13, CONS = 48.362 )
/ICNODE( ADD, UTHE, NODE = 14, CONS = 45.451 )
/ICNODE( ADD, UTHE, NODE = 15, CONS = 42.54 )
/ICNODE( ADD, UTHE, NODE = 16, CONS = 39.628 )
/ICNODE( ADD, UTHE, NODE = 17, CONS = 36.717 )
/ICNODE( ADD, UTHE, NODE = 18, CONS = 33.806 )
/ICNODE( ADD, UTHE, NODE = 19, CONS = 30.894 )
/ICNODE( ADD, UTHE, NODE = 20, CONS = 27.983 )
/ICNODE( ADD, UTHE, NODE = 21, CONS = 25.072 )
/ICNODE( ADD, UTHE, NODE = 22, CONS = 22.16 )
/ICNODE( ADD, UTHE, NODE = 23, CONS = 19.249 )
/ICNODE( ADD, UTHE, NODE = 24, CONS = 16.338 )
/ICNODE( ADD, UTHE, NODE = 25, CONS = 13.426 )

/Boundary conditions for an inlet flow rate of 4.416 x 10-7 m3/s
BCNODE( ADD, URC, ENTI = "inlet1", CONS = -60.765 )
BCNODE( ADD, UZC, ENTI = "inlet1", CONS = 60.765 )
BCNODE( ADD, URC, ENTI = "inlet2", CONS = 0 )
BCNODE( ADD, UZC, ENTI = "inlet2", CONS = 85.935 )
BCNODE( ADD, VELO, ENTI = "wall1", CONS = 0, X, Y, Z )
BCNODE( ADD, VELO, ENTI = "wall2", CONS = 0, X, Y, Z )
BCNODE( ADD, URC, ENTI = "symmetry", CONS = 0 )
BCNODE( ADD, URC, ENTI = "top", CONS = 0 )
BCNODE( ADD, UZC, ENTI = "top", CONS = 0 )
BCNODE( SURF, CONS = 0, NODE = 146 )
BCNODE( SURF, CONS = 0, NODE = 205 )
BCNODE( COOR, NODE = 146 )
BCNODE( COOR, NODE = 170 )
BCNODE( ADD, UTHE, NODE = 10, CONS = 44.409 )
BCNODE( ADD, UTHE, NODE = 11, CONS = 42.145 )
BCNODE( ADD, UTHE, NODE = 12, CONS = 39.88 )
BCNODE( ADD, UTHE, NODE = 13, CONS = 37.616 )
BCNODE( ADD, UTHE, NODE = 14, CONS = 35.351 )
BCNODE( ADD, UTHE, NODE = 15, CONS = 33.087 )
BCNODE( ADD, UTHE, NODE = 16, CONS = 30.822 )
BCNODE( ADD, UTHE, NODE = 17, CONS = 28.558 )
BCNODE( ADD, UTHE, NODE = 18, CONS = 26.296 )
BCNODE( ADD, UTHE, NODE = 19, CONS = 24.029 )
BCNODE( ADD, UTHE, NODE = 20, CONS = 21.765 )
BCNODE( ADD, UTHE, NODE = 21, CONS = 19.5 )
BCNODE( ADD, UTHE, NODE = 22, CONS = 17.236 )
BCNODE( ADD, UTHE, NODE = 23, CONS = 14.972 )
```

Appendix V: (Continued)

```
BCNODE( ADD, UTHE, NODE = 24, CONS = 12.707 )
BCNODE( ADD, UTHE, NODE = 25, CONS = 10.443 )

/Boundary conditions for an inlet flow rate of 5.678 x 10-7 m3/s
/BCNODE( ADD, URC, ENTI = "inlet1", CONS = -78.127 )
/BCNODE( ADD, UZC, ENTI = "inlet1", CONS = 78.127 )
/BCNODE( ADD, URC, ENTI = "inlet2", CONS = 0 )
/BCNODE( ADD, UZC, ENTI = "inlet2", CONS = 110.488 )
/BCNODE( ADD, VELO, ENTI = "wall1", CONS = 0, X, Y, Z )
/BCNODE( ADD, VELO, ENTI = "wall2", CONS = 0, X, Y, Z )
/BCNODE( ADD, URC, ENTI = "symmetry", CONS = 0 )
/BCNODE( ADD, URC, ENTI = "top", CONS = 0 )
/BCNODE( ADD, UZC, ENTI = "top", CONS = 0 )
/BCNODE( SURF, CONS = 0, NODE = 146 )
/BCNODE( SURF, CONS = 0, NODE = 205 )
/BCNODE( COOR, NODE = 146 )
/BCNODE( COOR, NODE = 170 )
/BCNODE( ADD, UTHE, NODE = 10, CONS = 57.096 )
/BCNODE( ADD, UTHE, NODE = 11, CONS = 54.185 )
/BCNODE( ADD, UTHE, NODE = 12, CONS = 51.274 )
/BCNODE( ADD, UTHE, NODE = 13, CONS = 48.362 )
/BCNODE( ADD, UTHE, NODE = 14, CONS = 45.451 )
/BCNODE( ADD, UTHE, NODE = 15, CONS = 42.54 )
/BCNODE( ADD, UTHE, NODE = 16, CONS = 39.628 )
/BCNODE( ADD, UTHE, NODE = 17, CONS = 36.717 )
/BCNODE( ADD, UTHE, NODE = 18, CONS = 33.806 )
/BCNODE( ADD, UTHE, NODE = 19, CONS = 30.894 )
/BCNODE( ADD, UTHE, NODE = 20, CONS = 27.983 )
/BCNODE( ADD, UTHE, NODE = 21, CONS = 25.072 )
/BCNODE( ADD, UTHE, NODE = 22, CONS = 22.16 )
/BCNODE( ADD, UTHE, NODE = 23, CONS = 19.249 )
/BCNODE( ADD, UTHE, NODE = 24, CONS = 16.338 )
/BCNODE( ADD, UTHE, NODE = 25, CONS = 13.426 )

END( )
```

Appendix VI: GAMBIT File for Varying Outer Slot Location

solver select "FIDAP"

undo begingroup
vertex create coordinates 0 0 0
undo endgroup
undo begingroup
vertex create coordinates 0.17 0 0
undo endgroup
undo begingroup
vertex create coordinates 0.17 0.0125 0
undo endgroup
undo begingroup
vertex create coordinates 0.122 0.0125 0
undo endgroup
undo begingroup
vertex create coordinates 0.107 0.0125 0
undo endgroup
undo begingroup
vertex create coordinates 0 0.0743 0
undo endgroup
undo begingroup
vertex create coordinates 0 0.0304 0
/For R_3 equal to 4.36×10^{-4} m
/vertex create coordinates 0 0.0436 0
/For R_3 equal to 5.77×10^{-4} m
/vertex create coordinates 0 0.0577 0
/Omit this command for R_3 equal to 7.43×10^{-4} m
undo endgroup
undo begingroup
vertex create coordinates 0 0.025 0
/For R_2 equal to 4.00×10^{-4} m
/vertex create coordinates 0 0.04 0
/For R_2 equal to 5.50×10^{-4} m
/vertex create coordinates 0 0.055 0
/For R_2 equal to 7.20×10^{-4} m
/vertex create coordinates 0 0.072 0
undo endgroup
undo begingroup
vertex create coordinates 0 0.01 0
undo endgroup

Appendix VI: (Continued)

edge create straight "vertex.1" "vertex.2"
edge create straight "vertex.2" "vertex.3"
edge create straight "vertex.3" "vertex.4"
edge create straight "vertex.4" "vertex.5"
edge create straight "vertex.5" "vertex.6"
edge create straight "vertex.6" "vertex.7"
edge create straight "vertex.7" "vertex.8"
edge create straight "vertex.8" "vertex.9"
edge create straight “vertex.9” “vertex.10”
/Omit previous command for R_2 equal to 7.20 x 10^{-4} m

face create wireframe "edge.1" "edge.2" "edge.3" "edge.4" "edge.5" "edge.6" "edge.7" "edge.8" “edge.9” real
undo begingroup
edge picklink "edge.1"
edge mesh "edge.1" successive ratio1 1 intervals 172
undo endgroup
undo begingroup
edge picklink "edge.2"
edge mesh "edge.2" successive ratio1 1 ratio2 1.1 intervals 32
undo endgroup
undo begingroup
edge picklink "edge.3"
edge mesh "edge.3" successive ratio1 1 intervals 36
undo endgroup
undo begingroup
edge picklink "edge.4"
edge mesh "edge.4" successive ratio1 1 intervals 24
undo endgroup
undo begingroup
edge picklink "edge.5"
edge mesh "edge.5" successive ratio1 1 intervals 112
undo endgroup
undo begingroup
edge picklink "edge.6"
edge mesh "edge.6" successive ratio1 1 intervals 20
/For R_2 equal to 4.00 x 10^{-4} m
/edge mesh “edge.6” successive ratio1 1 intervals 16
/For R_2 equal to 5.50 x 10^{-4} m
/edge mesh “edge.6” successive ratio1 1 intervals 12

Appendix VI: (Continued)

/For R_2 equal to 7.20 x 10^{-4} m
/edge mesh “edge.6” successive ratio1 1 intervals 4
undo endgroup
undo begingroup
edge picklink "edge.7"
edge mesh "edge.7" successive ratio1 1 intervals 4
/For R_2 equal to 7.20 x 10^{-4} m
/edge mesh “edge.8” successive ratio1 1 intervals 24
undo endgroup
undo begingroup
edge picklink "edge.8"
edge mesh "edge.8" successive ratio1 1 intervals 4
/For R_2 equal to 4.00 x 10^{-4} m
/edge mesh “edge.8” successive ratio1 1 intervals 8
/For R_2 equal to 5.50 x 10^{-4} m
/edge mesh “edge.8” successive ratio1 1 intervals 12
/For R_2 equal to 7.20 x 10^{-4} m
/edge mesh “edge.8” successive ratio1 1 intervals 4
undo endgroup
undo begingroup
edge mesh “edge.9” successive ratio1 1 intervals 4
/Omit for R_2 equal to 7.20 x 10^{-4} m
undo endgroup
face mesh "face.1" map size 1

physics create "symmetry" btype "PLOT" edge "edge.1"
physics create "outlet" btype "PLOT" edge "edge.2"
physics create "free" btype "SURFACE" edge "edge.3"
physics create "wall1" btype "PLOT" edge "edge.4"
physics create "wall2" btype "PLOT" edge "edge.5"
physics create "inlet1" btype "PLOT" edge "edge.6"
physics create "top" btype "PLOT" edge "edge.7"
physics create "inlet2" btype "PLOT" edge "edge.8"
physics create "fluid" ctype "FLUID" face "face.1"

export fidap “025.FDNEUT”
/For R_2 equal to 4.00x 10^{-4} m
/export fidap “04.FDNEUT”
/For R_2 equal to 5.50 x 10^{-4} m
/export fidap “055.FDNEUT”
/For R_2 equal to 7.20 x 10^{-4} m
/export fidap “072.FDNEUT”

Appendix VII: FIJOUR File for Varying Outer Slot Location

```
FICONV( NEUT, INPU, RESU )
INPUTFILE( FILE = small.FDNEUT" )
OUTPUTFILE( FILE, DELE )
END(  )

FIPREP(  )

PROBLEM( ADD, CYLI, INCO, TRAN, TURB, NONL, NEWT, MOME, ISOT, FREE,
SING )
EXECUTION( ADD, NEWJ )

ENTITY( ADD, NAME = "fluid", FLUI, PROP = "fc77" )
ENTITY( ADD, NAME = "wall1", WALL )
ENTITY( ADD, NAME = "wall2", WALL )
ENTITY( ADD, NAME = "symmetry", PLOT )
ENTITY( ADD, NAME = "inlet1", PLOT )
ENTITY( ADD, NAME = "inlet2", PLOT )
ENTITY( ADD, NAME = "outlet", PLOT )
ENTITY( ADD, NAME = "top1", WALL )
ENTITY( ADD, NAME = "top2", WALL )
ENTITY( ADD, NAME = "free", SURF, DEPT = 0, SPIN, STRA )

SOLUTION( ADD, N.R. = 70, KINE = 25, VELC = 0.0001, RESC = 0.01, SURF =
0.001 )
BODYFORCE( ADD, CONS, FZC = 981, FRC = 0, FTHE = 0 )
DATAPRINT( ADD, CONT )
OPTIONS( ADD, UPWI )
UPWINDING( ADD, STRE )
RELAXATION(  )
  0.6,   0.6,   0.6,     0,     0,   0.1

PRESSURE( ADD, MIXE = 1e-16, DISC )
DENSITY( ADD, SET = "fc77", CONS = 1.78 )
/Density for FC-72
/DENSITY( ADD, SET = “fc72”, CONS = 1.68 )
/Density for FC-87
/DENSITY( ADD, SET = “fc87”, CONS = 1.63 )
/Density for Methanol
/DENSITY( ADD, SET = “methanol”, CONS = 0.7855 )
VISCOSITY( ADD, SET = "fc77", MIXL, CONS = 0.01424 )
```

Appendix VII: (Continued)

```
/Viscosity for FC-72
/VISCOSITY( ADD, SET = “fc72”, MIXL, CONS = 0.0064 )
/Viscosity for FC-87
/VISCOSITY( ADD, SET = “fc87”, MIXL, CONS = 0.00453 )
/Viscosity for Methanol
/VISCOSITY( ADD, SET = “methanol”, MIXL, CONS = 0.0055 )
SURFACETENSION( ADD, SET = "fc77", CONS = 15 )
/Surface Tension for FC-72
/SURFACETENSION( ADD, SET = “fc72”, CONS = 10 )
/Surface Tension for FC-87
/SURFACETENSION( ADD, SET = “fc87”, CONS = 9.5 )
/Surface Tension for Methanol
/SURFACETENSION( ADD, SET = “methanol”, CONS = 22.2 )

POSTPROCESS( ADD, NBLO = 2 )
   1,  351,  350
 352, 4000,    1
PRINTOUT( NBLO = 2 )
   1,  351,  350
 352, 4000,    1
TIMEINTEGRATION( ADD, BACK, NSTE = 4000, TSTA = 0, DT = 1e-07, VARI,
NOFI = 10,WIND = 0.9 )
RENUMBER( ADD, PROF )
EDDYVISCOSITY( ADD, SPEZ )

/Initial conditions for an inlet flow rate of 1.262 x 10-7 m3/s
ICNODE( ADD, UZC, ENTI = "inlet1", CONS = 351.439 )
ICNODE( ADD, UTHE, ENTI = "inlet1", CONS = 351.439 )
ICNODE( ADD, UZC, ENTI = "inlet2", CONS = 351.439 )

/Inlet conditions for an inlet flow rate of 5.678 x 10-7 m3/s
/ICNODE( ADD, UZC, ENTI = "inlet1", CONS = 451.85 )
/ICNODE( ADD, UTHE, ENTI = "inlet1", CONS = 451.85 )
/ICNODE( ADD, UZC, ENTI = "inlet2", CONS = 451.85 )

/Boundary conditions for an inlet flow rate of 1.262 x 10-7 m3/s
BCNODE( ADD, UZC, ENTI = "inlet1", CONS = 351.439 )
BCNODE( ADD, UTHE, ENTI = "inlet1", CONS = 351.439 )
BCNODE( ADD, UZC, ENTI = "inlet2", CONS = 351.439 )
BCNODE( ADD, VELO, ENTI = "wall1", CONS = 0, X, Y, Z )
BCNODE( ADD, VELO, ENTI = "wall2", CONS = 0, X, Y, Z )
BCNODE( ADD, VELO, ENTI = "top1", CONS = 0, X, Y, Z )
```

Appendix VII: (Continued)

```
BCNODE( ADD, VELO, ENTI = "top2", CONS = 0, X, Y, Z )
BCNODE( ADD, URC, ENTI = "symmetry", CONS = 0 )
BCNODE( SURF, CONS = 0, NODE = 205 )
BCNODE( SURF, CONS = 0, NODE = 146 )
BCNODE( COOR, NODE = 146 )
BCNODE( COOR, NODE = 170 )
/Boundary conditions for an inlet flow rate of 5.678 x 10-7 m3/s
/BCNODE( ADD, UZC, ENTI = "inlet1", CONS = 451.85 )
/BCNODE( ADD, UTHE, ENTI = "inlet1", CONS = 451.85)
/BCNODE( ADD, UZC, ENTI = "inlet2", CONS = 451.85 )
/BCNODE( ADD, VELO, ENTI = "wall1", CONS = 0, X, Y, Z )
/BCNODE( ADD, VELO, ENTI = "wall2", CONS = 0, X, Y, Z )
/BCNODE( ADD, VELO, ENTI = "top1", CONS = 0, X, Y, Z )
/BCNODE( ADD, VELO, ENTI = "top2", CONS = 0, X, Y, Z )
/BCNODE( ADD, URC, ENTI = "symmetry", CONS = 0 )
/BCNODE( SURF, CONS = 0, NODE = 205 )
/BCNODE( SURF, CONS = 0, NODE = 146 )
/BCNODE( COOR, NODE = 146 )
/BCNODE( COOR, NODE = 170 )

END(  )
```

Appendix VIII – Fluid Properties

FC-77

Density:	1780 kg/m^3
Viscosity:	0.001424 kg/m s
Surface Tension:	0.015 N/m

FC-72

Density:	1680 kg/m^3
Viscosity:	0.00064 kg/m s
Surface Tension:	0.010 N/m

FC-87

Density:	1630 kg/m^3
Viscosity:	0.000453 kg/m s
Surface Tension:	0.0095 N/m

Methanol

Density:	785.5 kg/m^3
Viscosity:	0.00055 kg/m s
Surface Tension:	0.0222 N/m